POLITECNICO DI MILANO

Facoltà di Ingegneria Edile - Architettura
Corso di laurea magistrale in Ingegneria dei Sistemi Edilizi

Seismic performance of bridges during Canterbury earthquakes

Relatori: Prof. Alberto FRANCHI
Prof. Alessandro PALERMO

Tesi di Laurea di:

Maria BRANDO Matr. 751083

Anno Accademico 2010 – 2011

TABLE OF CONTENTS

TABLE OF FIGURES

ABSTRACT

On February 22nd, 2011 a M6.3 Earthquake occurred with an epicentre near the town of Lyttelton, 10 km South of the Christchurch CBD. Compared with the 2010 Darfield Earthquake, despite the magnitude was lower and the localized effects induced by this earthquake were similar, PGA ranged between 0.5 and 2.2g, reaching therefore values much higher than the level adopted in the design of NZ road highway bridges. After the event, the bridges were inspected by the network consultants and researchers to establish safety conditions and repairs that were required to enable traffic flow and to document damage. A summary of observations from the field is herein proposed, highlighting the main damage typologies shown by the bridges with respect to each structural component.

The observations made in the visual inspections were biased towards a subset of bridges which the Bridge Group knew were damaged. To avoid this bias a complete database is put together of all 223 bridges within the Christchurch area. The database compiles information to identify, locate and describe each bridge and the severity and type of damage that occurred on or at the bridge site. A statistical analysis is done using the database, to describe the city bridges, to quantify the overall damage, and to analyse trends leading to the damage of bridges. A comparison between the field observation and the results of impact assessment obtained using the Earthquake Loss Estimation (ELE) tool MAEviz.

The second part of the work aims to focus on the seismic performance of three concrete bridges: two highways, Port Hills and Horotane Valley Overpass, and one road bridge, Moorhouse Avenue Overbridge. The assessment involves site investigations and numerical modelling: static push-over analysis is used to determine the displacement capacity, which is compared then with the demand obtained from the registered spectra. Then time-history analyses are performed using accelerograms from the nearest ground motion record stations. To properly capture the seismic performance of the bridges, shear and axial bending interaction for the piers and soil structure interaction, resulting in slope failure, are considered.

PREFAZIONE

Il 22 Febbraio 2011 la regione di Canterbury, in Nuova Zelanda, è stata colpita da un terremoto di magnitudo 6.3, con epicentro in Lyttelton, 10 km a sud di Christchurch. Facendo un confronto tra detto evento e il precedente terremoto di Darfield, nonostante la potenza dell'ultimo evento fosse minore con effetti localizzati derivanti molto simili, le accelerazioni registrate hanno raggiunto valori compresi tra 0.5 e 2.2g, molto più elevati rispetto ai valori limite previsti dalla normativa neozelandese per i ponti.

Il presente lavoro, nato dalla collaborazione tra il Politecnico di Milano e l'University of Canterbury in Nuova Zelanda, tratta della performance dei ponti nell'area di Christchurch a seguito degli ultimi due eventi sismici. L'obiettivo è quello di valutare, attraverso analisi numeriche, la capacità residua di alcuni dei ponti danneggiati e di istituire un confronto tra i risultati ottenuti e le osservazioni condotte sul campo.

Innanzitutto, nel primo capitolo, viene presentata una panoramica dei danni più tipici riscontrati nei ponti a seguito dei più recenti terremoti di una certa intensità. I danni vengono catalogati in base alle varie parti strutturali componenti il ponte . La stessa impostazione viene mantenuta nel secondo capitolo dove però l'attenzione viene focalizzata sull'area di Christchurch, descrivendo i danni osservati durante le ispezioni a seguito dei due terremoti di cui sopra.

Sebbene utile per capire l'importanza dell'ultimo terremoto rispetto al precedente, la panoramica offerta non permette di cogliere quelli che sono stati gli effetti su una scala più ampia. Infatti concentrando l'attenzione solo sui ponti danneggiati, il risultato che si ottiene è quello di fornire un quadro certamente più negativo rispetto a quanto accaduto nella realtà. Per ovviare a questo inconveniente, analisi statistiche sui livelli di danno rilevati sull'intero stock di ponti nell'area di Christchurch, comprendente 223 ponti, sono state condotte grazie all'utilizzo del Database dell'University of Canterbury. I livelli di danno, quattro in totale, sono stati stabiliti seguendo la classificazione offerta da Hazus, un software utilizzato per l'analisi del rischio per predire e quindi prevenire le conseguenze di catastrofi naturali. A ciascuna parte strutturale e non del ponte viene quindi assegnato il valore numerico indicante il livello di danno. Analisi di tipo statistico sono ottenute considerando l'indice di danno globale, dato dalla somma dei valori numerici del livello di danno delle varie parti della struttura. I risultati vengono poi confrontati con la previsione di danno ottenuta dalle analisi con il software MAEviz, utilizzato, così come HAZUS, per valutare l'impatto di fenomeni naturali.

La seconda parte del lavoro focalizza l'attenzione sul comportamento sismico di tre ponti in c.a. estrapolati dallo stock analizzato: due ponti autostradali, Port Hills e Horotane Valley, e un ponte stradale, Moorhouse Avenue. La valutazione comprende indagini sia visive che numeriche: analisi statiche pushover vengono effettuate per determinare la capacità della struttura che viene poi

confrontata con la “demand” durante gli eventi sismici. Una prima previsione di quest’ultima viene fornita da un’analisi spettrale in cui, noto il periodo naturale della struttura, gli spettri di risposta per ciascun terremoto vengono confrontati con lo spettro di progetto. L’effettiva performance dei ponti studiati viene infine valutata con analisi non lineari time history, usando gli accelerogrammi registrati nelle stazioni più vicine.

Le differenti tipologie di danno osservate sui tre ponti hanno portato a considerare, nella fase di modellazione numerica, accorgimenti che permettessero una migliore valutazione dell’effettiva risposta delle strutture. In particolare per Port Hills importante è stato considerare l’interazione tra l’azione assiale e il momento mentre per Moorhouse Avenue quella tra taglio e momento. Nel caso di Horotane Valley Overpass il contributo di danno maggiore è derivato dallo “slope failure” in corrispondenza delle spalle del ponte, e per questo motivo accorgimenti e assunzioni progettuali sono stati adottati per modellare l’interazione tra terreno e struttura.

1 DAMAGE TO BRIDGES IN PAST AND RECENT EARTHQUAKES

1.1 Introduction

Bridges give the impression of being rather simple structural system. Indeed, they have always occupied a special place in the affections of structural designers because their structural forms tends to be a simple expression of their functional requirement. Despite or because their structural simplicity bridge, in particular prestressed or reinforced concrete bridges, have not performed as well as might be expected in under the recent seismic attacks. In fact in recent earthquakes in California, Japan and Central and South America, modern bridges designed specifically for seismic resistance have collapsed or have been severely damaged when subjected to ground shaking of an intensity that has frequently been less than corresponding to current code intensities.

This unexpected poor performance can be attributed to the design philosophy adopted at the time of the construction along with a lack in the care of design and execution of details.

Typically, unlike buildings, bridges have a little or no redundancy in structural system so that the failure of one structural element or connection can cause the collapse of the whole structure. For this reason the structural simplicity may be sometimes a disadvantage.

Moreover bridges are more sensitive to soil-structure interaction effects than buildings. In fact the no synchronous seismic input at different supports due to travelling wave effects make the response of bridges to ground motion less predictable than other structures, proportionally with the length of the bridge. Also the conditions of construction site have an important role in the performance of the bridge: difficult ground condition such as river and estuary crossing will not infrequently be over sandy or silty soils with a potential for liquefaction; where roads or railroads cross active faults, the local geography will be contorted as result of earlier fault movement and bridging of the fault will be necessary. As a result, large relative displacements of supports could occur due to fault dislocation in a future earthquake.

In order to be able to design new bridges or to retrofit existing bridges, a clear understanding of potential problem areas is essential. A good way to develop this understanding is learning from failures and damages that have occurred to bridges in earlier earthquakes. It is worth thus presenting an overview of past earthquake damage.

1.2 Damage to Bridges in Recent Earthquakes

The design deficiency that can be identified by analysing bridge damages caused by earthquake, tend to be a direct consequence of the elastic design philosophy almost uniformly adopted for seismic design of bridges prior to 1970. The consequences of this seismic design approach were:

1. seismic deflections, based on the specified lateral force levels, were underestimated;

2. the ratio of gravity load to seismic force adopted for design was incorrect, since seismic force levels were artificially low;

3. structural actions and associated concepts of ductility ad capacity design are crucial to the survival of inelastic system under seismic response and were not considered in the elastic design process.

As will be seen in the following examples, most of the observed damage can be attributed to one, or a combination, of these three different deficiencies.

1.2.1 Seismic Displacement

The underestimation of seismic displacements, based on elastic theory, gross-section stiffness and low lateral force levels, affected the length of seating provided at movement joints, unrealistically short and the lateral separation between adjacent structures, inadequate. This lack resulted in pounding.

1.2.1.1 Span failures due to unseating at movement joints

Expansion joints introduce a structural irregularity that can have catastrophic consequences. Adjacent frames separated by movement joints may move out of phase, increasing the relative displacement across the joint. Such joints are commonly provided in bridges to alleviate stresses associated with volume changes that occur as a bridge ages and as the temperature changes. These joints can occur within a span (inspan hinges), or they can occur at the supports, as is the case for simply supported bridges. Earthquake ground shaking, or transient or permanent ground deformations resulting from the earthquake, can induce superstructure movements that cause the supported span to unseat. Unseating is especially a problem with the shorter seats that were common in older construction and for multi-span bridges with tall columns [1-5].

There have been many examples of bridge failure caused by relative movement of spans in the longitudinal direction exceeding seating widths, resulting in unseating at unrestrained movement joints. In much of the United States and in many other areas of the world, bridges often comprise a series of simple spans supported on bents. These spans are prone to being toppled from their supporting substructures due to either shaking or differential support movement associated with ground deformation. Unseating of simple spans was observed in California in earlier earthquakes, leading in recent decades to development of bridge construction practices based on monolithic box-girder substructure construction. Problems of unseating still occur with older bridge construction and with new bridges in regions where simple spans are still common. For example, during the 1991 Costa Rica earthquake, widespread liquefaction led to abutment and internal bent rotations, resulting in the collapse of no fewer than four bridges with simple supports [4].

The collapse of the Showa Bridge in the 1964 Niigata earthquake demonstrates one result of the unseating of simple spans (Figure 1.1).

Figure 1.1. ***Showa Bridge collapse in 1964 Niigata earthquake.***

Figure 1.2 shows two examples damage from the 1971 San Fernando earthquake [6]. In Figure 1.2a is shown a span collapse: although linkage restrainer bolts were provided a cross the movement joints in this bridge, they had insufficient strength to restrain the longitudinal relative movement. In the case shown in Figure 1.2b a simply supported span has unseated due to excessive relative displacement between adjacent bents. The support lines are skewed to the bridge axis, and it has been observed that skewed spans develop larger displacements than right spans, as a consequence of a tendency for the skew span to rotate in the direction of decreasing skew, thus tending to drop off the supports at the acute corners. In Figure 1.3, Figure 1.4 and Figure 1.5 are shown other examples of span failure in recent famous earthquakes.

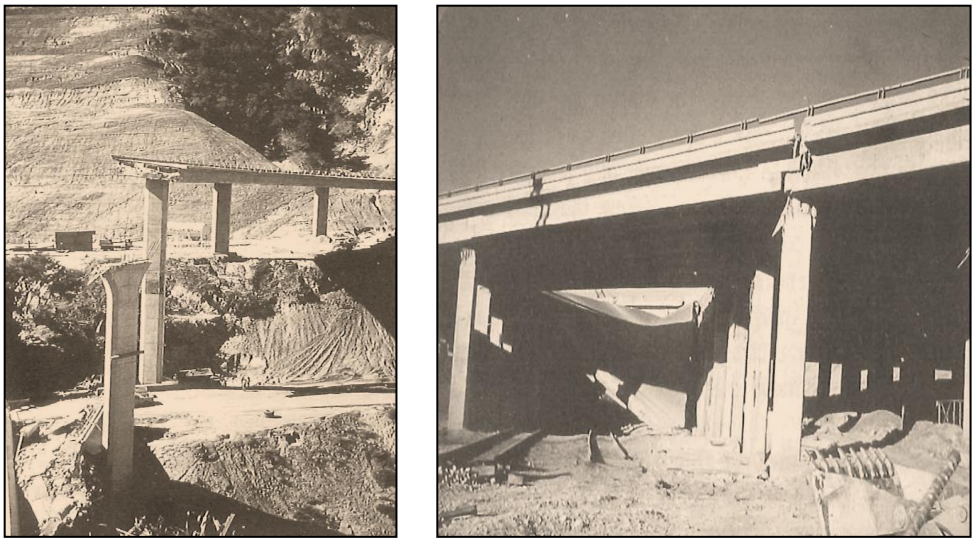

(a) **(b)**

Figure 1.2. ***Damage from 1971 San Fernando earthquake: a) Span Collapse; b) Unseating (simple span, screw) [7]***

(a) **(b)**

Figure 1.3. ***a) Span collapses at the Golden State-Antelope Valley interchange collectors, 1994 Northridge earthquake [8],*** **b)** ***Fallen Beam due to Superstructure Movement in the Longitudinal Direction in Taiwan Chi Chi Earthquake, 1999 [9]***

Figure 1.4. ***Example of collapsed span as a result of insufficient support length, 1995 Kobe earthquake [10]***

Figure 1.5. ***Example of damaged bearing and collapsed span, 1995 Kobe earthquake [10]***

The combination of longitudinal and transverse response caused this behaviour, schematically illustrated in Figure 1.6.

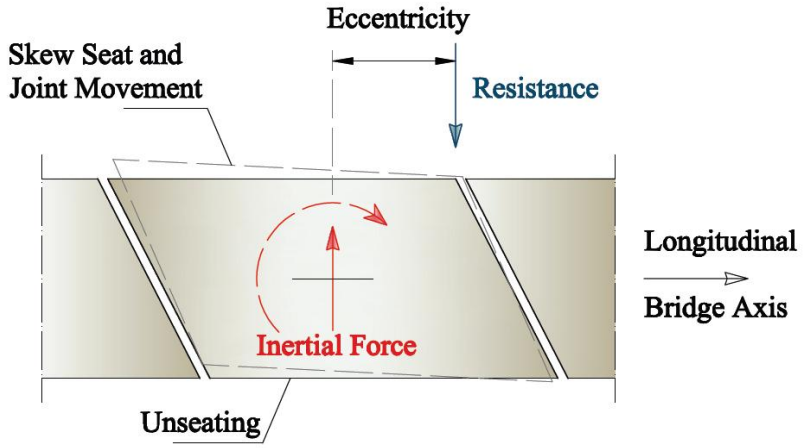

Figure 1.6. ***Unseating due to bridge skew***

1.2.1.2 Amplification of Displacement Due to Soil Effects

Soft soils will generally result in amplification of structural vibration response, increasing the probability of unseating. Liquefaction of the soil may occur also when bridges are supported by piles in saturated sandy silts or silty sands, causing a loss of support to the piles.

Bridges with simply supported spans are particularly susceptible to span failure resulting from liquefaction, an example is shown in Figure 1.7 a-b from the 1990 Costa Rica earthquake. The supports of the bridge were skewed at about 30° to the transverse axis, and the spans were thrown off the internal support in the direction of decreasing skew.

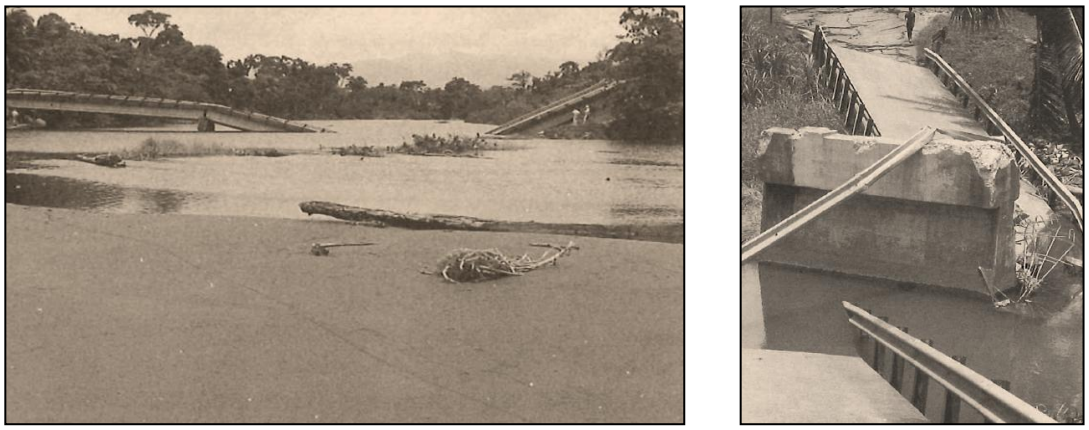

(a) **(b)**

Figure 1.7. ***a) Liquefaction failure, Rio Viscaya bridge, 1990 Costa Rica earthquake b) Liquefaction failure, Rio Viscaya bridge, 1990 Costa Rica earthquake [7]***

Another example is the unseating of simply supported link span, from the 1995 Kobe earthquake, shown in Figure 1.8, caused from the failure of the tension-link restrainers connecting the link span to the arch support. Slumping and liquefaction at the site caused large movements of the arch bridge support resulting in unseating of the span.

Lateral spreading of the soil caused also the failure of Gaoyuan Bridge span in 2008 Wenchuan earthquake (Figure 1.9).

Figure 1.8. ***Unseating of simply supported link span, Nishinomiya-ko bridge, Kobe earthquake***

Figure 1.9. ***Gaoyuan Bridge nearby fault trace, 2008 Wenchuan earthquake [11]***

1.2.1.3 Pounding of Bridge Structures

Impact forces from pounding of bridge components can be very high, causing amplification of member shear forces with increased probability of brittle shear failure, as shown in Figure 1.10. In the 1989 Loma Prieta earthquake at the China Basin/Southern viaduct section of I-280 in San Francisco, there was a 150 mm separation between the lower roadway and columns independently supporting an upper-level deck proved inadequate.

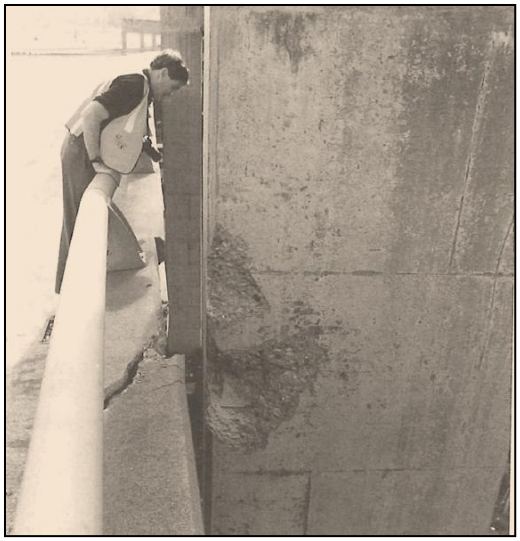

Figure 1.10. ***Pounding of I-280 China Basin/Southern viaduct, 1989 Loma Prieta earthquake [7]***

Other minor pounding damage resulting in spalling of concrete and possible bucking of steel bars are shown in Figure 1.11.

(a) **(b)**

Figure 1.11. ***Pounding damage: (a) between adjacent spans at the Interstate-5 at Santa Clara River in Los Angeles County during the 1994 Northridge earthquake and (b) at the abutment of a bridge near Nishinomiya Port in the 1995 Kobe earthquake [8]***

1.2.2 Abutment Slumping

Related to response of soft soil and incompletely consolidated abutment fill, slumping of abutment fill and rotation of abutments have been widespread in recent earthquakes. Seismic acceleration increase the earth pressure on the abutments under longitudinal response.

Impact of the bridge with the abutment may generate high passive pressure, causing a further increase in lateral pressures. Inadequately compacted natural or fill soils tend to slump toward the moving soli. The contact between the top of the abutment and the superstructure leads to the rotation of the abutment, as shown in Figure 1.12, which typically brings to damages to the top of the abutment backwall and to the pile support system (if abutment rotation are high).

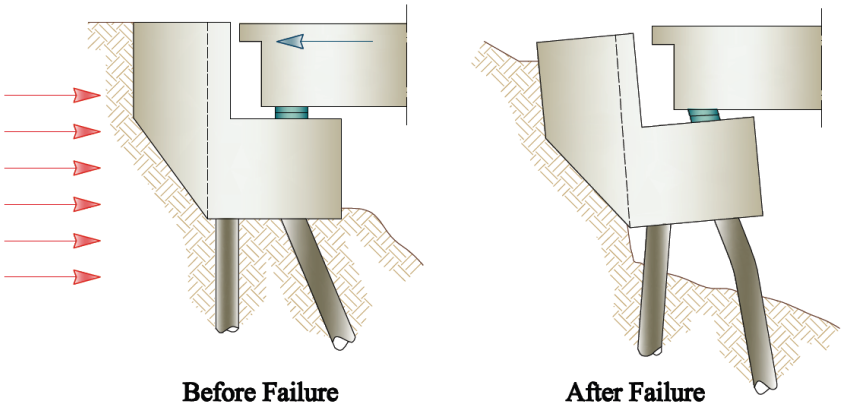

Figure 1.12. ***Abutment slumping and rotation***

Figure 1.13 show examples of abutment failure from the 1990 Costa Rica earthquake. The bridge shown in Figure 1.13a had severe slumping and a 9° rotation of one abutment, resulting in a lateral and shear displacement of the pile tops of about 660 mm and in flexural and shear failure of the supporting piles. An extreme case of abutment back wall damage is shown in Figure 1.13b: this bridge pushed its end span through and over the abutment, when an internal pier collapsed and rotated, because of liquefying sand. Total collapse is uncommon and generally related to other causes.

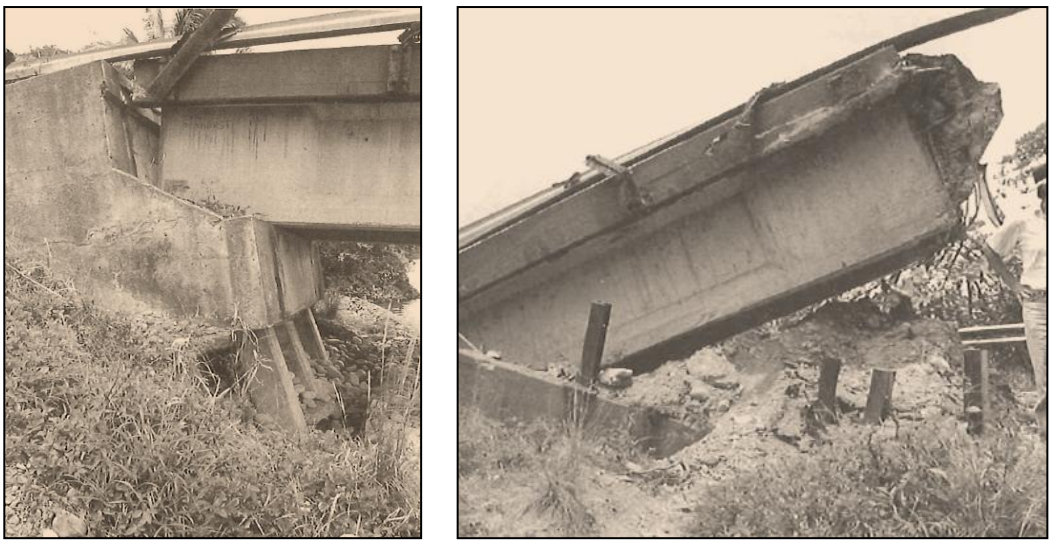

(a) **(b)**

Figure 1.13. ***Damage to the abutment in 1990 Costa Rica Earthquake: a) abutment slumping and rotation, Rio Banano Bridge; b) abutment failure due to passive pressure, Rio Vascaya bridge [7]***

1.2.3 Column Failures

Another direct consequence of the elastic design philosophy identified at the beginning of this chapter as a philosophy adopted for seismic design of bridges prior to 1970, is the failure of the columns of bridge. This can happen as result of a number of deficiencies herein presented.

1.2.3.1 Flexural Strength and Ductility Failures

The lack of the concept of ductility capacity in the design of bridges until the 1970s is translate in four particular deficiencies.

1.2.3.1.1 Undependable column flexural strength

Column longitudinal reinforcement was often lap spliced immediately above the foundation. Tests indicate that lap-splice length as short as 20 bar diameters, commonly used for Californian bridges designed prior 1971, is insufficient to enable the flexural strength of the column [12]. Figure 1.14a shows damage to the base of a column, attributable to lap-slice bond failure, which occurred in the 1989 Loma Prieta earthquake [3]. Inadequate flexural strength may also occur as result of butt welding of longitudinal reinforcement close to maximum moment locations (at the base of the piers). An example is given in Figure 1.14b where is shown flexural failure of a column of the Hanshin expressway in the 1995 Kobe earthquake [13], caused by failure of a large number of butt welds at the same location, dose to the column base.

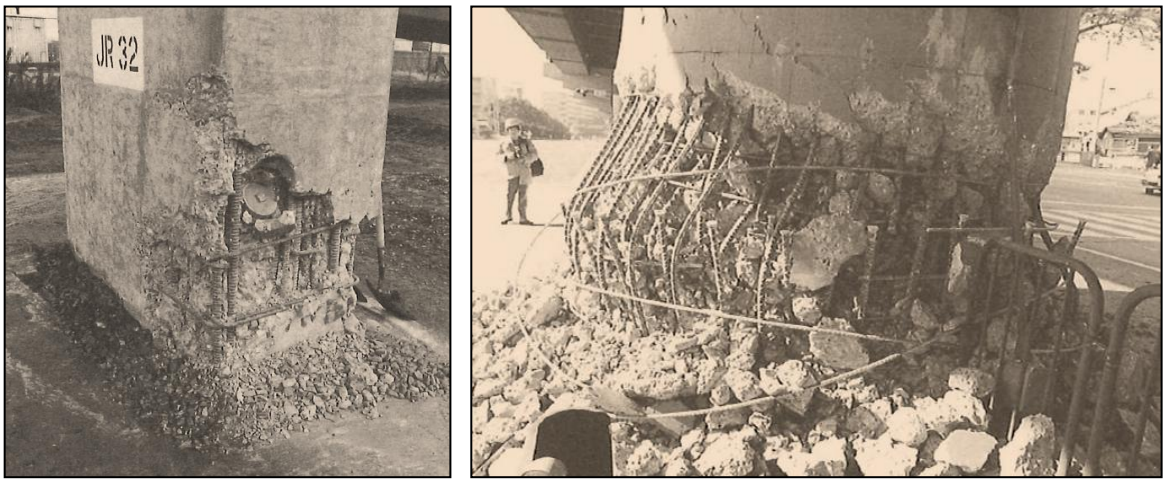

(a) **(b)**

Figure 1.14. ***Bond failure of lap splices at column base, 1989 Loma Prieta earthquake [7]***

1.2.3.1.2 Inadequate Flexural Ductility

To survive intense seismic attack, structures must possess ductility, that is the property of being able to deform through several cycles of displacements much larger than the yield displacement, without significant strength degradation. At displacement ductility levels of about 2 to 3, concrete compression strains in the plastic hinge regions exceed the unconfined compression strain capacity, and spalling of the cover concrete occurs. Unless the core concrete is well confined by close-spaced transverse hoops or spirals, crushing rapidly extends into the core, the longitudinal reinforcement buckles, and rapid strength degradation occurs, resulting eventually in an inability to support gravity load. This behavior may be accelerated when transverse reinforcement is lap spliced in the cover concrete, as is common with older bridges. Figure 1.15 shows an example of flexural plastic hinge failures in Kobe earthquake, 1995.

Figure 1.15. ***Two examples of flexural failure due to lack of confinement at bottom of reinforced concrete piers supporting a steel superstructure, 1995 Kobe Earthquake [10]***

1.2.3.1.3 Premature Termination of Column Reinforcement

A number of bridge in Japan developed flexure-shear failures at column midheight during 1982 Urahawa-ohi [14] and 1995 Kobe [13] earthquakes, as result of premature termination of the column longitudinal reinforcement. Bar termination was based on the design moment envelope, without accounting for the effects of tension shift due to diagonal shear cracking and this deficiency was exacerbated by the provision of a short development length of bars lap spliced at this location. Failure of the 18 columns of the collapsed section of the Hanshin expressway in the 1995 Kobe earthquake (Figure 1.16) was initiated by premature termination of 33% of the column longitudinal reinforcement at 20% of the column height. This forced the plastic hinge to form above the base, where it could not benefit from confinement provided by the strong footing, which was essential for survival of the columns, since very little confinement was provided.

Figure 1.16. ***Flexural failure above column base of columns of the Hanshin expressway, due to premature termination of longitudinal reinforcement and inadequate confinement in the 1995 Kobe earthquake [8]***

1.2.3.2 Column Shear Failures

Shear mechanism interact in a complex way, resulting from the combination of concrete compression shear transfer, aggregate interlock along inclined flexure-shear cracks, arching action sustained by axial forces, and truss mechanisms utilizing horizontal ties provided by transverse reinforcement. If the transverse reinforcement of the truss mechanism yields, flexure-shear crack widths increase rapidly, reducing the strength of the concrete shear-resisting mechanisms utilizing aggregate interlock. As a consequence, shear failure is brittle and involves rapid strength degradation. Inelastic shear deformation is thus unsuitable for ductile seismic response. Shear strength equations for column design is generally less conservative than flexural design equations in older bridges. Prior to 1970, there was a lack of appreciation of the need to ensure that actual shear strength exceeded actual flexural strength and as a consequence it is not uncommon to find bridge columns where flexural strength may be two to three times the shear strength. Shear failures occurred extensively in the 1971 San Fernando [15], 1994 Northridge [2] and 1999 Taiwan earthquake [9].

In Figure 1.17 damage from San Fernando Earthquake are presented. Figure 1.17a shows the typical brittle failure when flexural strength exceeds shear strength. No indication that the plastic hinging developed at the base of the pier is noticed. On the other hand, in the pier in Figure 1.17b no damage occurred in the mid region, but at the top developed a plastic hinge giving rise to shear failure within the hinge region. This leads to an important observation: as a consequence of a reduction in aggregate interlock shear transfer in plastic hinges, shear strength in plastic hinge regions is less than in other part of the element.

The cause of failure of six of the seven bridge structures that failed in 1994 Northridge earthquake has been attributed to column shear failures [16]. The rupture of transverse reinforcement cause the loss of the structural integrity of the column, that thus fail under gravity loads. Examples of column collapse caused by shear failures are shown in Figure 1.18.

After the Chi-Chi earthquake, Wushi bridge was severely damaged and the road was closed [9]. Under horizontal vibration, substantial shear cracks showed on the southbound hammerhead concrete pier (Figure 1.19).

The sudden and the brittle nature of the shear failure must be considered and special efforts has to be taken the design and construction of the details.

(a) **(b)**

Figure 1.17. ***Shear failure within (a) and outside (b) the plastic hinge region in San Fernando Mission Blvd-Gothic Avenue Bridge and I-10 Freeway at Venice Blvd, respectively, during the 1994 Northridge earthquake [8]***

Figure 1.18. ***Confinement failure at bridge pier top, 1994 Northridge earthquake [8]***

Figure 1.19. Wushi Bridge, shear failure of piers P2S and P3N, 1999 Taiwan earthquake [9]

1.2.4 Cap Beam Failures

Cap beam failures and subsequent seismic assessments indicate significant deficiencies in three areas:

- Shear capacity, especially where seismic and gravity shears are additive;
- Premature termination of cap beam negative moment reinforcement;
- Insufficient anchorage of cap bean reinforcement into the end regions.

Figure 1.20 shows two examples of damage to cap beam during the1989 Loma Prieta earthquake. In Figure 1.20a is illustrated the damage to outrigger cap beams: the flexural cracks resulting from negative moments under combined gravity load and seismic force, were steeply inclined under the influence of shear. Figure 1.20b shows the growth of a flexural crack formed at the inner face of a column as a results of the inadequate anchorage provided by the 900-mm development length of 18 bars into the joint region.

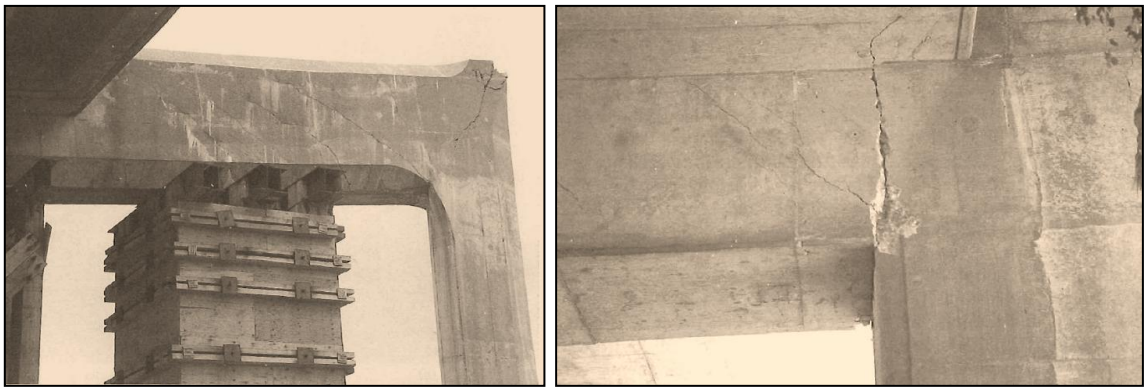

(a) **(b)**

Figure 1.20. ***a) Abutment slumping and rotation failure, Rio Bananito bridge, 1990 Costa Rica earthquake[4]; b) Cap beam positive moment cracks at inner column face, 1989 Loma Prieta earthquake [7]***

Figure 1.21. ***Sliding shear at top columns of the Cypress viaduct in the 1989 Loma Prieta earthquake [8]***

1.2.5 Joint Failures

Shear failure may strike also the connections. in fact the transfer of forces through connections results in horizontal and vertical join shear forces. This problem was taken under consideration specially after the 1989 Loma Prieta earthquake which caused shear problems in the connection between cap beams and columns. It has been uncommon for these shear forces to be considered in bridge design, and until recently properly design joint shear reinforcement was almost never provided. Without this reinforcement joint shear failure may occur, as evidenced by the diagonal cracking of the joint region if a Cypress viaduct bent and by the crack pattern in the joint region of a bent of the Embarcadero viaduct depicted in Figure 1.22.

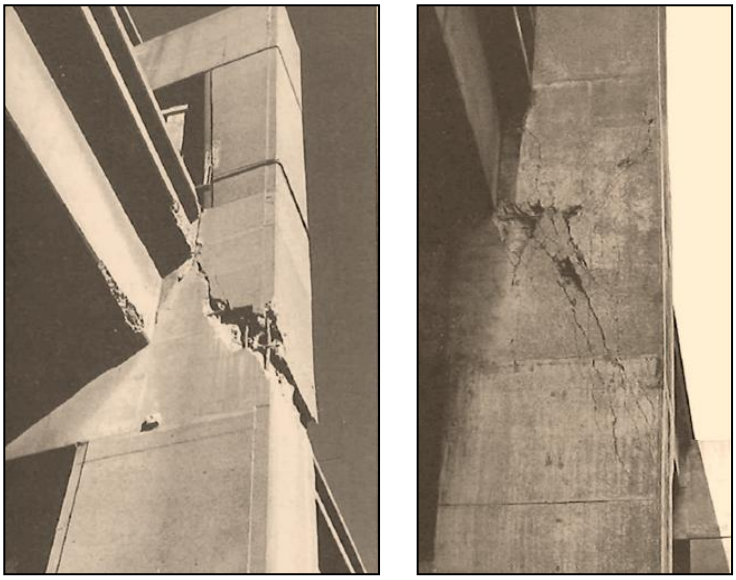

(a) **(b)**

Figure 1.22. ***Joint shear failure, 1989 Loma Prieta earthquake, I-480 viaduct and Embarcadero viaduct [7]***

1.2.6 Footing Failures

Few examples of footing failures caused by seismic actions have been reported after the recent earthquakes. The reasons of the low frequency of damage in this part of the bridge structure may be the following ones:

1. The premature shear or flexible failure of columns can prevent the development of the maximum footing forces;

2. Rocking of the footing may protect it from excessive seismic forces;

3. Footing can’t be easily inspected to assess damage after earthquakes

Although the rarity of this kind of damage, the most common deficiencies discovered are presented below:

a. Footing flexure and shear strength;

b. Joint shear strength at the connection between the footing and the column, where shear forces are maximum;

c. Increase of shear problems due to anchorage and development of column reinforcement, which were provided by straight bar extended down into the footing by 90° hooks bent out away from the column axis. An example of the consequences of inadequate development of column longitudinal reinforcement is provided by Figure 1.23. This bridge bent, failed in 1971 San Fernando earthquake, had straight-bar anchorage of column reinforcement in a footing reinforced solely with a bottom two-way flexural mat of reinforcement.

d. Inappropriate connection between tension piles and footing.

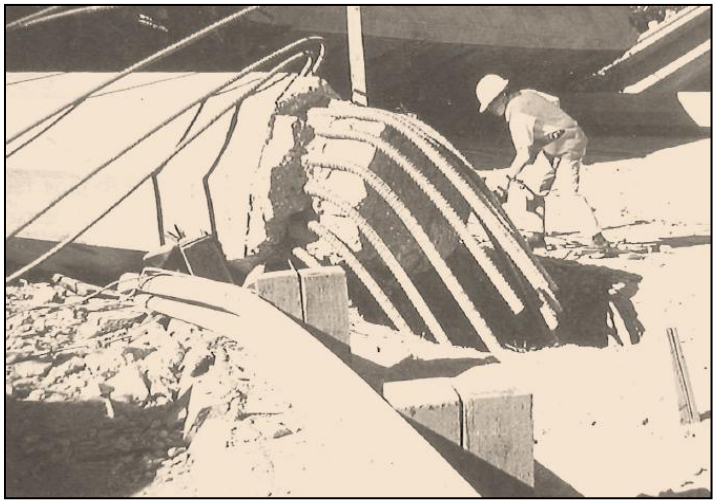

Figure 1.23. ***Pullout failure, 1971 San Fernando earthquake [7]***

2 OVERVIEW OF DAMAGES AFTER CANTERBURY EARTHQUAKES

2.1 Introduction

The region in and around Christchurch, comprising Christchurch City, Selwyn and Waimakariri Districts, contains over 800 road, rail and pedestrian bridges. Most of these bridges are integral reinforced concrete or hybrid, i.e. precast concrete deck and cast in place substructure (piers, foundations). All bridges have symmetric characteristics, with small to moderate total spans between ten and thirty meters, and very stiff decking systems. Most of the damage to these bridges from the recent earthquake events (Darfield, September 4, 2010 and Christchurch, February 22, 2011) coincided with areas highly susceptible to liquefaction. In fact, for Christchurch City, damage was mainly confined to the bridges in the central and eastern regions, with lateral spreading affecting bridges spanning both the Avon and Heathcote Rivers, while in the Waimakariri district the town of Kaiapoi sustained massive damage due to liquefaction during the Darfield earthquake (Figure 2.1). Very few bridges developed significant damage on non-liquefiable sites. Abutments, approaches and piers suffered varying levels of damage, with very little damage observed in bridge superstructures. In this chapter field observations and preliminary investigations undertaken after both events [17, 18] are summarized, presenting an overview of the damage to the bridge inventory in the Canterbury region. A joint University of Canterbury / University of Auckland research group and international overseas bridge experts inspected several bridges, collaborating with designers engaged by Christchurch City Council and New Zealand Transportation Agency (NZTA) to perform post-earthquake visual assessments. Observations will mainly comprise Christchurch City Council road bridges, pedestrian and highway bridges. Particular attention is also given to non-structural components, i.e. damaged pipelines running along bridges and approaches, highlighting the need for an integrated design approach of structures and utilities.

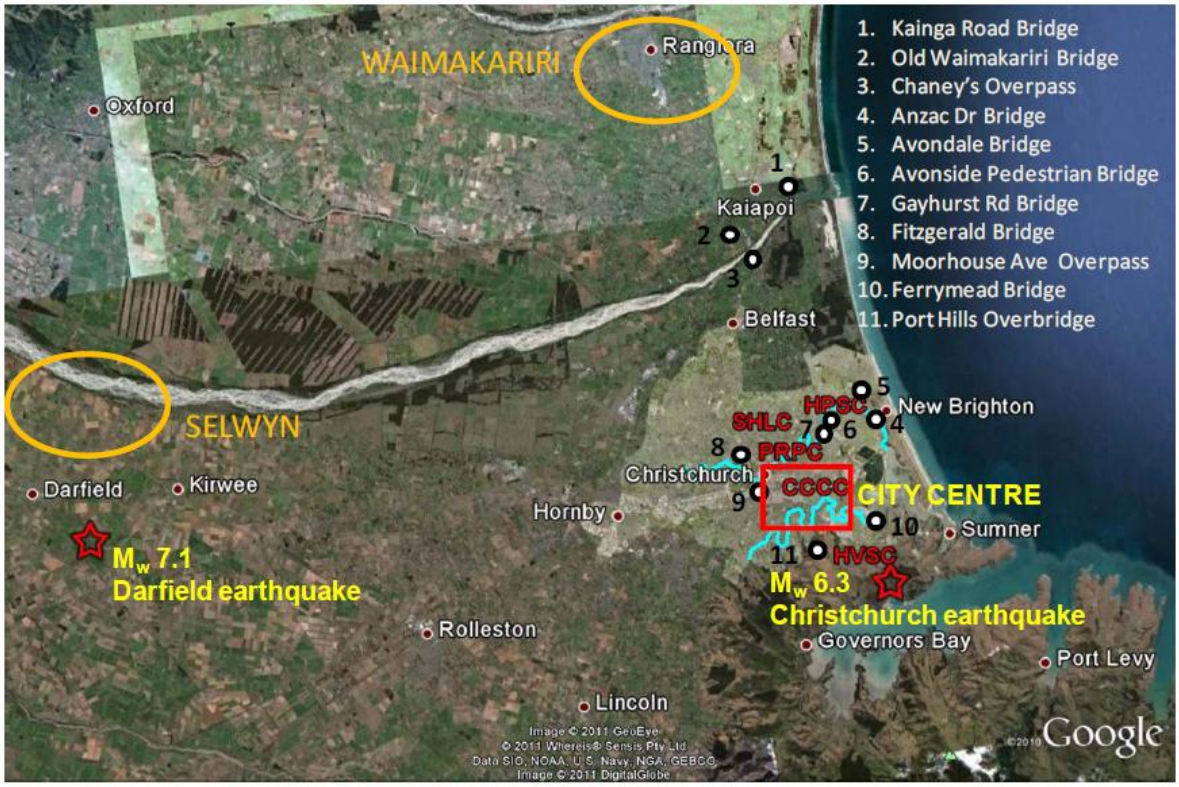

Figure 2.1. ***Overview of Christchurch and the surrounding region, indicating locations of a selection of damaged bridges, strong motion stations and the epicenters of the major earthquakes (Google Inc. 2011).***

2.2 Seismic demand

At 4.35am on the 4 September 2010 a fault ruptured with an epicentre 30-40km from the New Zealand city of Christchurch. The resulting magnitude 7.1 earthquake would cause widespread damage to three districts within the vicinity of strong shaking, and would cost the country NZ$5billion [Wilson & Williams, 2011]. Fortunately however no lives were lost. The duration of strong shaking of this event was relatively short at only 15 seconds compared to what has been observed in other major events such as the 2003 Hokkaido earthquake which lasted 45 seconds [Galloway, Hare & Bull, 2011]. The earthquake yielded New Zealand's richest set of strong motion data since recordings began in the 1960's. The peak recorded horizontal acceleration was 0.82g and similarly the peak velocity was found to be over 1m/s. Interestingly at one site near the fault there was a recorded vertical acceleration of 1.26g. For the Christchurch CBD, below a period of 2.0s, it was found to have a return period of 400-500 years; for the longer periods it was found to be in the order of a 1000-3000 return period event. [19]

The M_w 6.1 February 22, 2011 Christchurch earthquake, considered part of the aftershock sequence of the 2010 Darfield event, had an epicenter less than 10km from the Christchurch CBD between Lyttelton and the south eastern edge of the city [17]. The close proximity and shallow depth of this event caused higher intensity shaking in Christchurch relative to the Darfield event. Despite the short duration (15-20 seconds) the February 22, 2011 event recorded one of the highest maximum Peak Ground Acceleration (PGA_{max}=2.1g, close to epicenter) in the world experienced close to an

important city. In the CBD, ground motions were characterized by large vertical accelerations as well, resulting from a reverse-thrust faulting mechanism. Further aftershocks occurred during the following months, one of the strongest was the M_w 6.0 on June 13, 2011, with an epicenter again on the south eastern edge of the city (Table 2.1).

Table 2.1. ***Table comparing peak ground accelerations in the vicinity of Christchurch for the Darfield, Christchurch and Sumner earthquakes (geometric mean of horizontal PGA)***

Event	M_w	PGA	
		Maximum Horizontal	Maximum Vertical
Darfield, September 4, 2010	7.1	0.8g	1.3g
Christchurch, February 22, 2011	6.2	1.7g	2.2g
Sumner, June 13, 2011	6.0	2.0g	1.1g

In respects to the geological nature of this fault, seismologists could not have asked for a more complete set of information to describe the fault with. Aside from the extensive strong motion data already mentioned above in which there were 7 strong-motion detectors within 10km of the fault, there was also: a very visible and clear 30km length fault rupture; clear InSAR images (Interferometric synthetic aperture radar); and a well mapped area in which a GPS coseismic displacement vector field could be made. The conclusion of all the modelling undertaken was that the sequence of events initiated with a reverse fault which is named the Charing Cross Fault. Models predicted that this fault should rupture the surface, but it did not due dissipation of strain in the deep layer of gravels of the Canterbury plains. This rupture triggered the Greendale Fault, which was the main source of the earthquake energy. This fault had dextral east-west strike-slip movement. This main fault then triggered at least two more faults: one at the reverse Hororata Fault at the west end of the Greendale Fault; the other, a complex formation at the east end of the Greendale Fault. It is expected that there are likely to be more blind unknown faults, as fault models made of the rupture sequence under predict the magnitude observed in reality. [20]

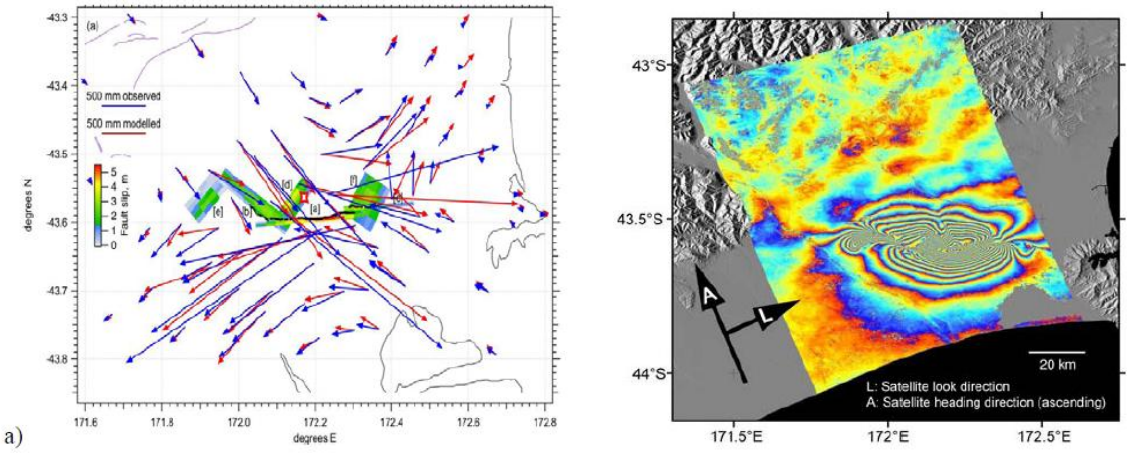

(a) **(b)**

Figure 2.2. ***a) GPS co-seismic measured (blue) and modelled (red) horizontal displacements; b) InSAR image recorded by the Advanced Land Observing Satellite [Holden, et al., 2011]***

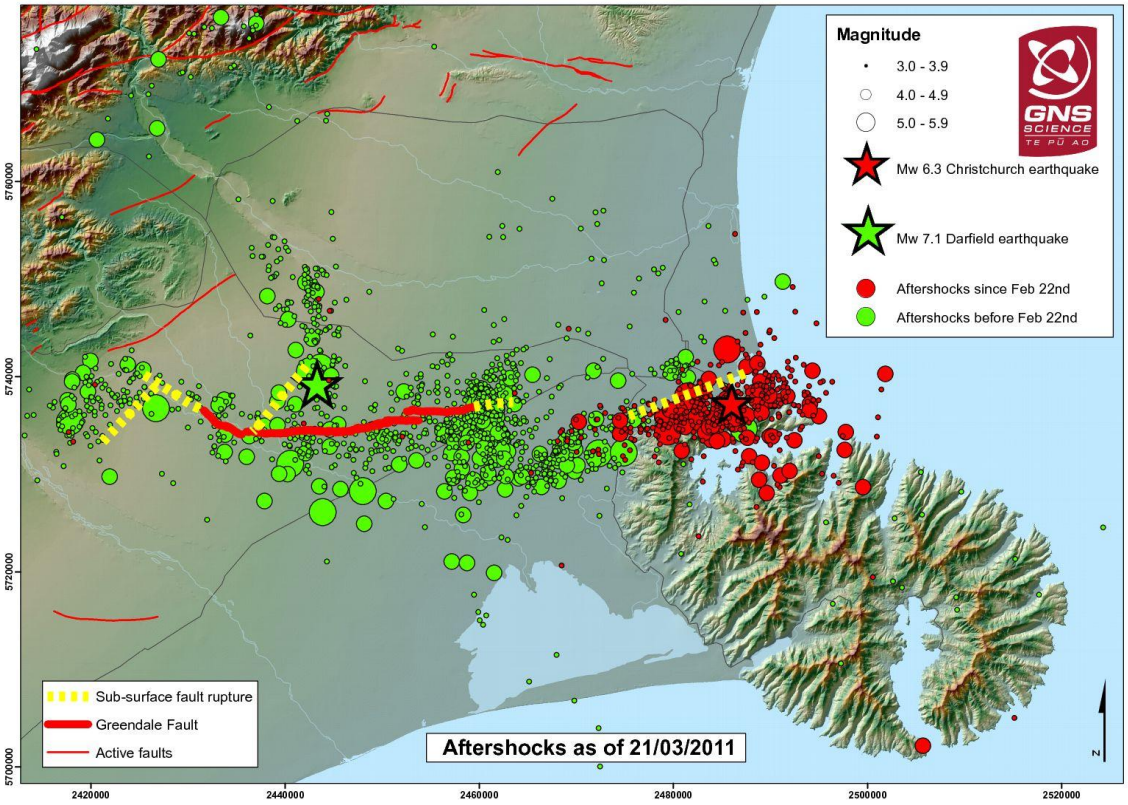

Figure 2.3. ***Location of the Greendale Fault Rupture, with measured displacement magnitude and direction shown. Also shown is the epicentre of both the 2010 and 2011 earthquakes.***

The overall lack of structural damage to the short to mid-span bridges is mainly due to their high overstrength and stiffness. The approximate period range of Canterbury bridges can be roughly estimated to be less than 0.8s, as indicated by rectangles in Figure 2.4a and Figure 2.4b. Acceleration response spectra of typical sites of both Darfield and Christchurch events compare the New Zealand Design Spectra [21] for site soil class D, 500 year return period. The average horizontal acceleration response spectra of five strong motion stations (CCCC, HPSC, HVSC, PRPC, SHLC), close to bridges damaged during the Canterbury earthquakes are considered for the comparison.

Within the period range of 0-0.8 seconds, it is immediately evident that during the Darfield event (Figure 2.4a) the spectral accelerations were less than or equal to the design spectral accelerations. Recorded values of peak horizontal ground accelerations were 0.2-0.3g in the Christchurch CBD, and up to 0.6g in the Port Hills area due to site amplification effects.

During 22nd February Christchurch earthquake, horizontal accelerations of 1.5g and vertical accelerations of 1.6g were recorded near the epicenter at the Heathcote Valley Primary School (HVPS), (Figure 2.4b). In the area of Southeast Christchurch, PGA values were much higher than the design level in the period range of New Zealand road and highway bridges. More importantly, due to the shallowness of the fault and the vicinity of the bridges to the epicenter, exceptional values of vertical acceleration were also registered, especially compared to those from other events

shown in Table 2.1. This certainly contributed to unexpected phenomena identified in pier damage of some bridges.

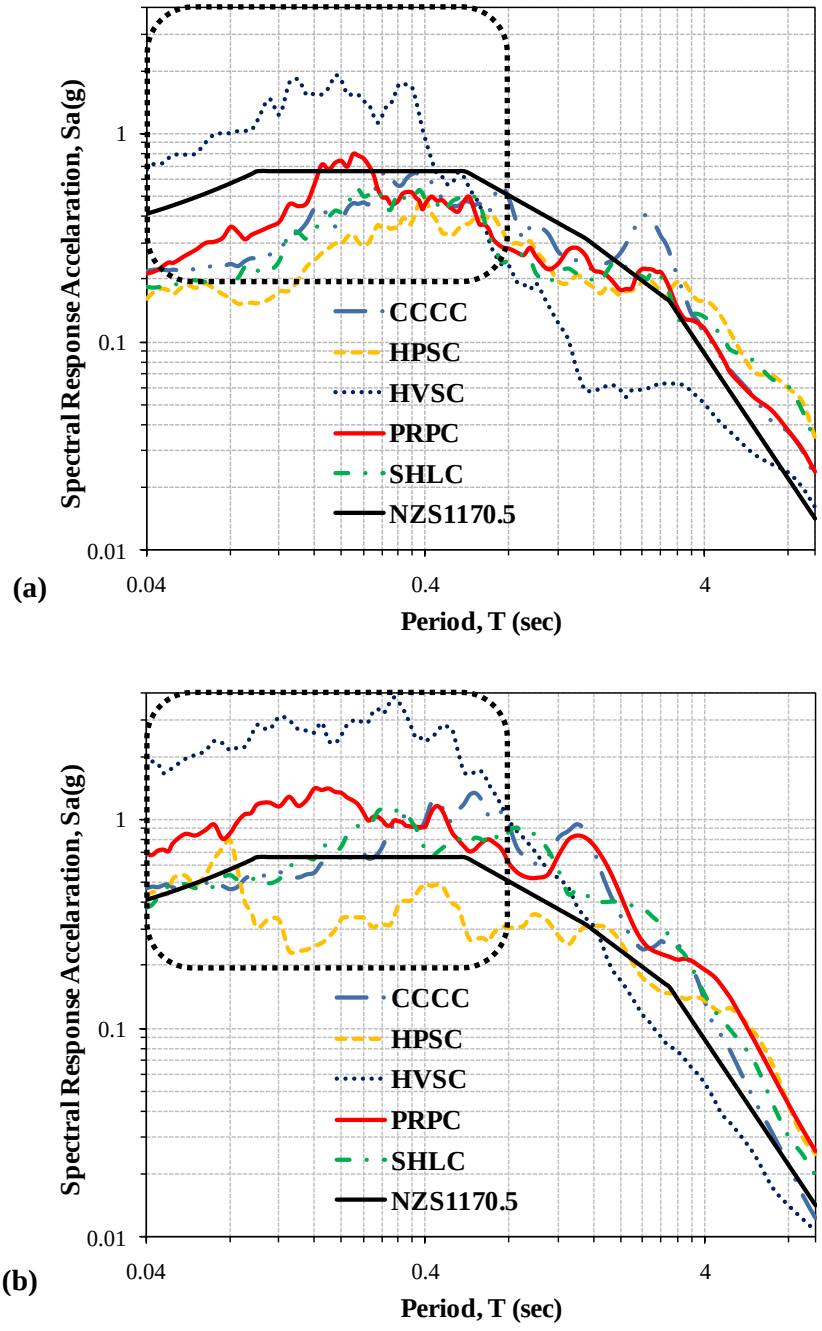

Figure 2.4. ***Response spectra of the geometric mean of the horizontal accelerations at strong motion station recordings in central and eastern Christchurch compared to NZS1170.5 design response spectrum for Christchurch, site subsoil class D for 500 year return period: a) Darfield earthquake; b) Christchurch earthquake. Four letter symbols represent different strong motion stations (see* Figure 2.1 *for locations).***

2.3 Damage due to liquefaction

During the Darfield earthquake, extensive liquefaction and lateral spreading occurred in Kaiapoi, Brooklands and eastern Christchurch suburbs, with the majority of damaged bridges that were closed or had limited damage inside these areas. This strong geographical link indicated that liquefaction induced lateral spreading would be the primary mechanism for bridge damage. The effects of the Christchurch earthquake were much more localized, however the significant ground motions in the city resulted in large areas of severe liquefaction damage. Bridges along both the Avon and Heathcote rivers suffered from varying levels of damage due to lateral spreading, with ground conditions and distance from the epicenter influencing this response. Figure 2.5 shows a comparison between the prediction liquefaction potential and the regions of liquefaction identified during a reconnaissance of the Canterbury area after February 22, 2011 event. In the last figure bridges that were severely damaged are also indicated.

(a)

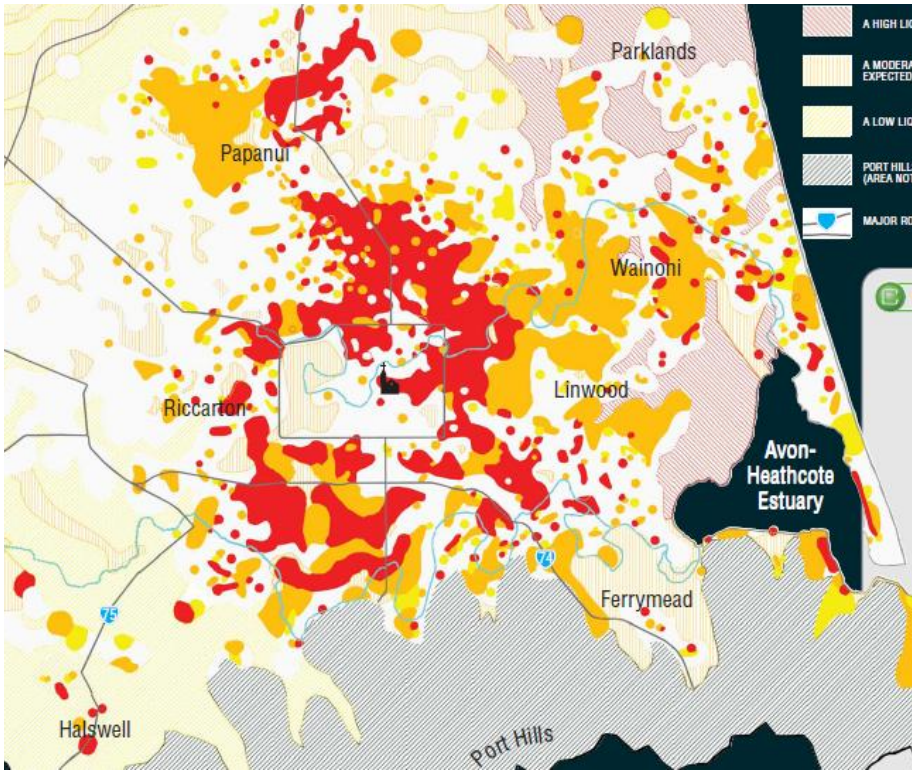

(b)

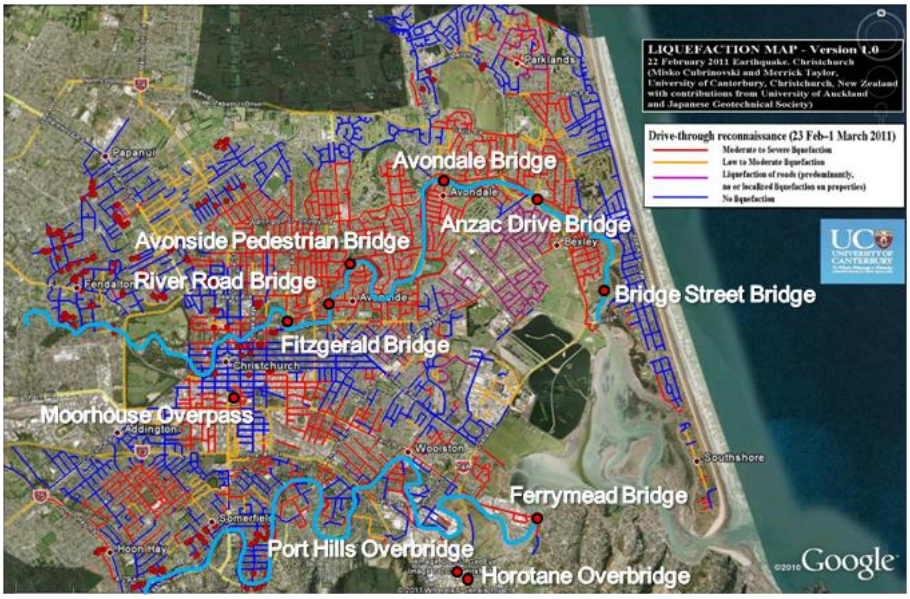

Figure 2.5. ***Comparison of predicted and observed liquefaction potential for Christchurch: a) prediction of liquefaction potential for a low ground water level where red and orange are the areas with high and medium susceptibility to liquefaction [Environment Canterbury, 2000c.]; b) Liquefaction potential hazard map of Canterbury region as of 10/12/2004 (ECAN)***

The type of bridge damage along the Avon was fairly consistent, with settlement and lateral spreading of approaches, back rotation and cracking of the abutments and some pier damage. In most cases the bridge decks restrained the movement of the top of the abutment, limiting longitudinal movements but inducing internal actions in the structure. All moderate to severely damaged bridges had pile foundations, with lateral spreading forces placing large demands on the abutment piles, and likely resulting in plastic hinging below grade. The approach fill of several bridges subsided by up to 1.0 meter due to the cumulative effect of these earthquakes, resulting in temporary closure. In most cases, settlement and spreading of the approaches impacted their serviceability. The Christchurch CBD bridges crossing the Avon River performed well, with the most common damage minor lateral spreading, compression or slight slumping of approach material, and minor cracking in abutments. Compared to the Avon River, bridges crossing the Heathcote River suffered much less damage, with less extensive liquefaction. Apart from the Ferrymead Bridge (-43° 33' 30.24", 172° 42' 31.12") at the mouth of the Heathcote, all bridges were either undamaged or suffered only minor damage. Typical damage was minor approach settlement, with little impact on the bridge abutments and superstructure.

2.4 Road Bridges

Most of the bridges severely damaged by the earthquakes were located in the areas highly prone to liquefaction. However, bridges suffered only a moderate amount of damage compared to residential houses and commercial buildings. This is due to two main reasons: firstly most bridges in the Canterbury area have small to moderate spans, exhibiting a sturdy seismic response; secondly they were designed to resist forces substantially larger than the demands imparted in these recent events.

Nevertheless, because some bridges critical to the city infrastructure network sustained substantial damage, and extensive traffic disruption was evident immediately following the events. Figure 2.6 shows the critical road bridges after the Christchurch earthquake, while Table 2.2 lists the bridges subdivided by construction type, indicating that since the 1960s the precast typology has become predominant. Among this bridges, Moorhouse Ave Overbridge will be considered in Chapter 6: numerical analyses will be carried out to assess the performance of the structure during both the two earthquakes.

Figure 2.6. ***Overall views of some of the damaged bridges after February 22, 2011. Clockwise from top left: Gayhurst Rd. Bridge; Fitzgerald Ave. Bridge; Ferrymead Bridge; Avondale Bridge; Moorhouse Ave Bridge; Bridge Street Bridge***

Table 2.2. ***Some of Canterbury bridges subdivided by construction type and era***

Integral Bridges		**Precast Bridges**	
Bridge	**Era**	**Bridge**	**Era**
Pages Road Bridge	1931	Fitzgerald Avenue Twin Bridges	1964
Gayhurst Road Bridge	1954	Ferrymead Bridge (Ferry Road)	1965
Avondale Road Bridge	1962	Bridge Street Bridge	1980
Moorhouse Avenue Bridge	1964	Anzac Drive Bridge	2000

2.4.1 Abutments and Foundations

Abutments presented two different damage types, residual displacements/rotations of substructure and damage to the structure (cracks, concrete crushing and spalling), both caused by lateral spreading of the approaches and river-banks. One commonly observed effect of lateral spreading on bridges was the tendency for the abutments to rotate backwards toward the riverbanks or converge inwards, meaning that the bridge superstructure acted as a rigid strut while the foundations

underwent forced rotations or movements in the direction of lateral ground flow (Figure 2.7a). This effect was most prevalent on bridges with deep abutments or closely spaced abutment piles. These types of abutments are in contrast to the current design philosophy [21] for lateral spreading banks that uses a shallow beam type abutment, and a small number of deep piles. These are designed to allow the laterally spreading slope to spill past the abutment.

During the Darfield earthquake the western abutment of Bridge Street Bridge (-43° 31' 30.84", 172° 43' 26.76") rotated by approximately 5° due to lateral spreading, and light cracking was observed on the tension face of the abutment piles after that event. This pile damage was exacerbated during the Christchurch earthquake, with further abutment rotation to more than 12° at the west end of the span (Figure 2.7b), and plastic hinging was clearly visible on the abutment piles of the western abutment (Figure 2.8a). Great uncertainties remain with regards to potential plastic hinging below the ground surface. Hinging is likely to have occurred in many of the bridges with visible abutment damage as this has been witnessed in bridges with similar soil conditions in recent earthquakes [22]. The June 13, 2011 aftershocks have also brought the exposed pile height beneath the abutment to 1.3 meters.

Other bridges that suffered foundation damage due to abutment rotation are shown in Figure Figure 2.7c-d. In particular, piles of Avondale Road Bridge (-43° 30' 2.22", 172° 41' 16.21") and Gayhurst Road Bridge (-43° 31' 17.90", 172° 40' 21.99") were inspected during the securing works following February 22, 2011 (Figure 2.8b-c). Plastic hinging, spalling of concrete and yielding of reinforcing steel were evident, especially for Bridge Street Bridge (-43° 31' 30.84", 172° 43' 26.76") and Fitzgerald Ave Bridge (-43° 31' 34.67", 172° 39' 2.02"), (Figure 2.8a-d).

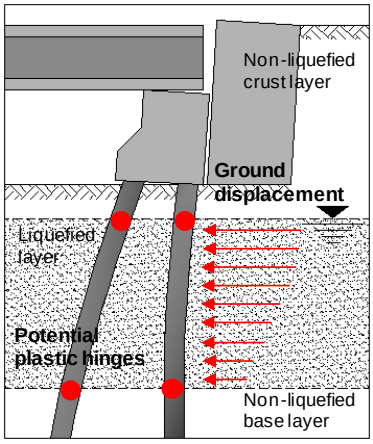

(a)

(b)

(c) **(d)**

Figure 2.7. ***Damage at the abutments: a) Sketch of the forces acting on abutments and foundations in undeformed condition; b) Back rotated abutments of Fitzgerald Bridge [Courtesy of OPUS]; c) Back rotated abutments of Bridge Street Bridge [Photo by M. Bruneau]; d) Damaged abutments of Avondale Road Bridge [Courtesy of OPUS]***

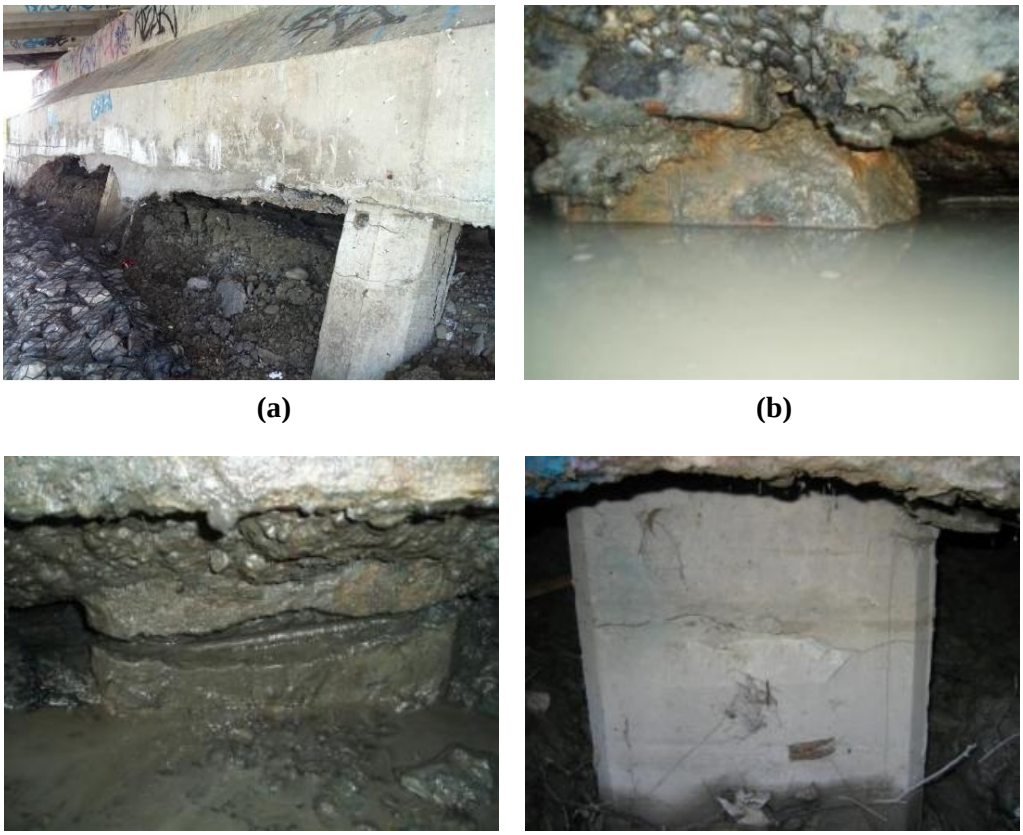

(a) **(b)**

(c) **(d)**

Figure 2.8. Damage to pile foundations: a) Plastic hinging in abutment piles of Bridge Street Bridge [Photo by L. Wotherspoon]; b) Exposed piles during the securing works on Avondale Road Bridge [Courtesy of OPUS]; c) Exposed piles during the securing works on Gayhurst Road Bridge [Courtesy of OPUS]; d) Flexural cracks on Fitzgerald Ave Bridge piles [Courtesy of OPUS]

2.4.2 Superstructure

Overall, road bridges exhibited little damage to their superstructure, even if most of the City Council bridges constructed in the 1950s-60s were designed with rudimentary seismic codes. Deck damage was limited in these bridges due to their overall robustness.

Figure 2.9 show clear examples of this minor damage, which is mainly caused by deck-abutment pounding and/or permanent displacements.

(a) **(b)**

Figure 2.9. ***Damage to Bridge St. Bridge deck: (a) abutment gap closure [Courtesy of OPUS] and (b) pounding of the deck on the abutment after Christchurch event [Photo by A. Kivell]***

2.4.3 Piers

Pier damage was caused either by ground shaking with a combination of vertical and horizontal components, or by lateral spreading. Bridge piers performed well in most cases, without experiencing extensive plastic hinging due to ground shaking. Flexural cracks are an expected consequence of the design structural failure mechanism of the bridge, and the limited damage did not compromise the structural integrity of the bridge. However unrepaired cracks may become a potential threat to the design life of the bridges close to marine environments, providing an accelerated pathway for chloride ingress and compromising the overall durability of the structure [23, 24].

Some bridges experienced pier cracking as a result of extensive lateral spreading. For example, Gayhurst Road Bridge (-43° 31' 17.90", 172° 40' 21.99") exhibited only one horizontal crack along one face of a pier, approximately one meter from the deck soffit (Figure 2.10a). Lateral spreading placed a lateral force on the pier base and caused a large moment at the stiff pier-deck interface, thus cracking the pier. The liquefied soil layer would have also reduced the lateral stiffness of the pier foundation system, allowing rotation of the bottom of the pier towards the centre of the river. Ferrymead Bridge (-43° 33' 30.24", 172° 42' 31.12") was undergoing a major upgrade (deck widening) when the earthquake occurred. Lateral spreading caused significant damage to the replacement structure and some temporary construction platforms. The existing structure also sustained damage due to lateral spreading, with permanent rotation and cracking of a number of the piers situated in the estuary (Figure 2.10b).

(a) **(b)**

Figure 2.10. ***a) Damaged pier in Gayhurst Road Bridge [Photo by L. Hogan]; b) Cracked and rotated piers of Ferrymead Rd. Bridge [Photo from CCC]***

Only Moorhouse Overpass Bridge (-43° 32' 23.82", 172° 38' 11.98") suffered significant pier damage during the Christchurch earthquake due to transverse ground shaking. The columns had widely spaced transverse reinforcement, making the structure susceptible to a brittle failure mechanism (Figure 2.11a). Observations after the Christchurch event indicated that the damaged columns had started to buckle (Figure 2.11b) putting the central span at risk of collapse. In this instance, the damage was induced by extensive ground shaking; large horizontal accelerations and a vertical velocity pulse may have combined to cause a flexural-bucking failure mechanism in the columns. Numerical analyses on this bridge will be performed in Chapter 6 to assess the behavior of the structure and to estimate the effects of retrofit solutions.

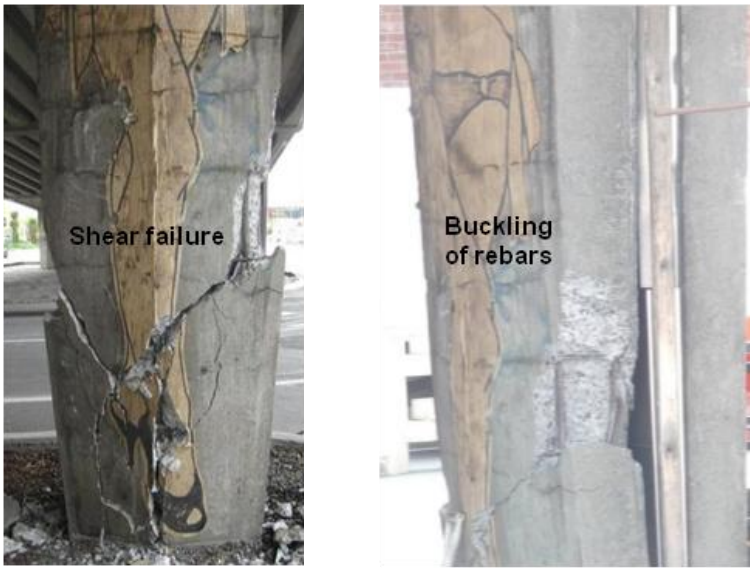

(a) **(b)**

Figure 2.11. ***Damage to Moorhouse Ave Bridge: a) Expansion joint at one of the piers [Courtesy of OPUS]; b) Shear failure mechanism of the pier [Photo by A. Palermo]***

2.4.4 Approaches

In general, approach damage was caused by liquefaction induced lateral spreading, with movement of the river banks towards the river. Differential movements led to the formation of large vertical offsets between the bridge deck and the approach. A typical example is Davis Road Bridge (-43° 40' 13.97", 172° 30' 52.00"), with a difference in elevation of 500 mm after the Darfield event between the unmoved bridge deck and the approach (Figure 2.12a). In some instances, while the bridges remained essentially intact, the approaches were severely damaged, making access to the bridge difficult or impossible. In terms of Gayhurst Road Bridge, cracks in the approaches parallel to the axis of the bridge provided evidence of the resistance against lateral spreading induced by the monolithic span (Figure 2.12 b). Particularly interesting is the influence of the bridges river banks. While the lateral spreading crack pattern was usually parallel to the river, the presence of the bridge restrained the lateral spreading movement inducing a sort of "strut effect", resulting in extensive cracking perpendicular to the river as shown in Figure 2.12 c-d.

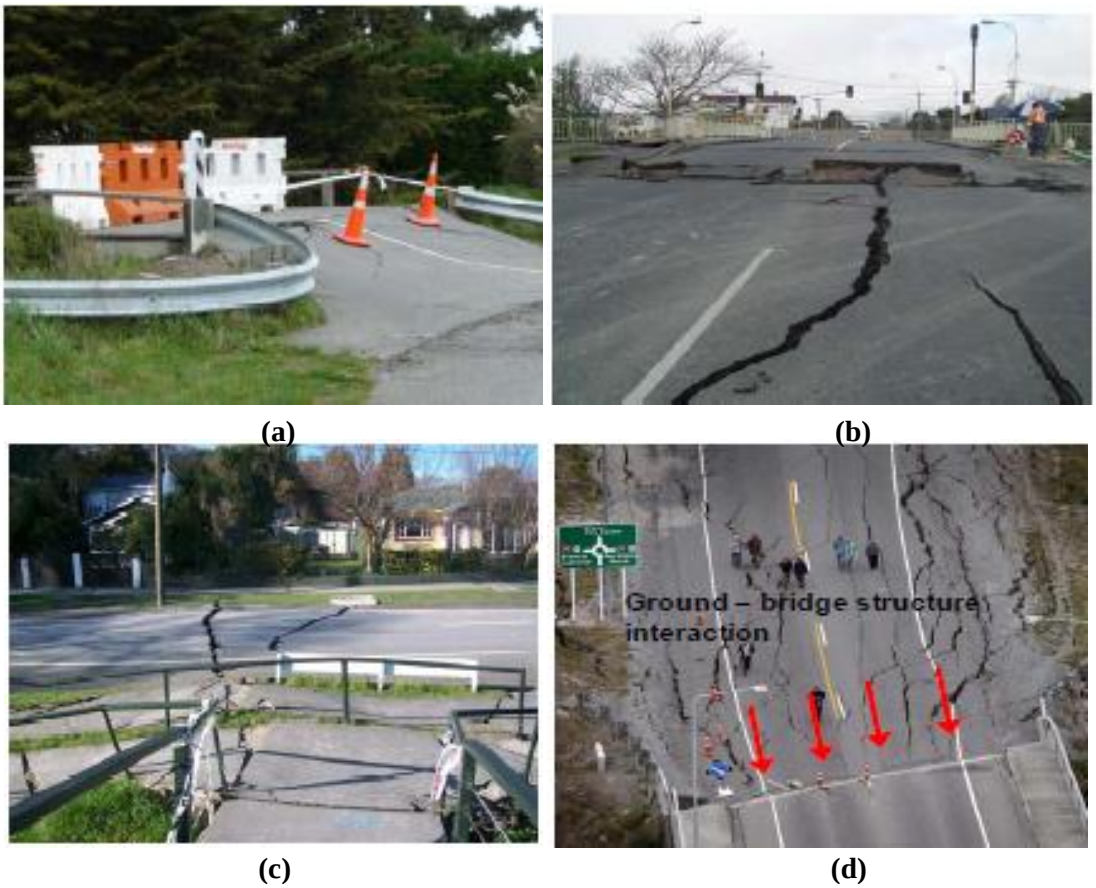

Figure 2.12. ***Relative vertical movement between approach and deck at: a) Davis Road Bridge, Lincoln [Photo by L. Wotherspoon]; b) Gayhurst Road Bridge [Photo by L. Hogan]; c) Bridge Street Bridge [Photo by L. Wotherspoon] d) Snell Bridge [Photo by M. Le Heux]***

2.5 Highway Bridges

Few highway bridges were severely damaged during both Darfield and Christchurch events. One of the reasons for this success is a recent seismic retrofit program to reduce the seismic risk of the National Highway bridges. Several bridges in the Canterbury region have undergone some form of seismic retrofitting during the past ten years in particular, after an overall seismic screening of the National Highway network [25].

One of the most widespread retrofit programs was undertaken by Transfund New Zealand (now incorporated into NZTA) [26], which saw the installation of tie-rods and steel brackets acting as the transverse shear key between pier-to-deck and deck-to-abutments, respectively. Similar devices were installed on bridges on most of the regions highways.

The post-earthquake investigations have not been in depth enough to ascertain the level of demand that these devices experienced during the seismic shaking. However, no retrofitted bridges were severely structurally damaged during Darfield earthquake. Lateral spreading had been identified as an issue on some key life-line bridges, and in some instances the bridges remained essentially intact, while the approach spans partially or totally failed, making access to the bridge either more difficult or impossible. For example, the twin continuous bridges at Chaney's overpass on State Highway 1 north of Christchurch (Figure 2.13a) were found to be structurally sound, and were tied to their abutment walls to prevent unseating. However due to liquefaction of the soils surrounding the bridge (Figure 2.14a), the approach to the southbound lanes of State Highway 1 settled by approximately 5-10 cm. After a brief closure for inspection, this busy route was reopened with signage reducing the speed to 30 km/h (down from 100km/h) for the safety of motorists.

Similar to road bridges, the Christchurch event caused more damage to the Highway bridges. Port Hills Overbridge and the Horotane Overbridge (-43° 34' 21.3276", 172° 41' 41.0856"), (Figure 2.13b-c) both of which are within 200 meters of each other and close to the epicenter suffered structural damage. The two bridges had been recently retrofitted under the previously mentioned retrofit program. Both retrofits were designed to link spans together and to the abutments in order to create an "integral cast-in-place bridge" concept. This method appears to have worked well, and despite both bridges sustaining damage, they were able to service traffic soon after the earthquake. The six-span Port Hills Overbridge suffered pier damage due to transverse ground shaking, and the bolts that tied the spans to the abutments also elongated. The Horotane Overbridge suffered abutment damage due to slope failure of the embankments. The ties between spans and at the abutments also elongated and pulled out as they had in the Port Hills Overbridge. Additionally, 60% of the bolts that attached the soffit of the precast concrete beams to the abutment seat extension had sheared off. If these spans had not been tied together and the seats not extended it is quite likely the spans would have collapsed. Numerical analyses on this latter two bridges will be carried out to assess the performance of the structures with records of Darfield and Christchurch earthquakes (see Chapters 4 and 5).

Similar to other road bridges, Anzac Drive Bridge (-43° 30' 3.34", 172° 42' 4.03"), (Figure 2.13d), part of Highway SH74 suffered extensive permanent abutment rotations up to 6-8 degrees during February 22, 2011 event, which then increased up to 10 degrees after June 13 aftershock (Figure 2.14b). This amount of rotation and the lateral spreading loads placed large demands on the abutment steel piles, and likely resulted in plastic hinging below grade. Piles after the June 13 aftershock were exposed over a length of 1300 mm in the south abutment.

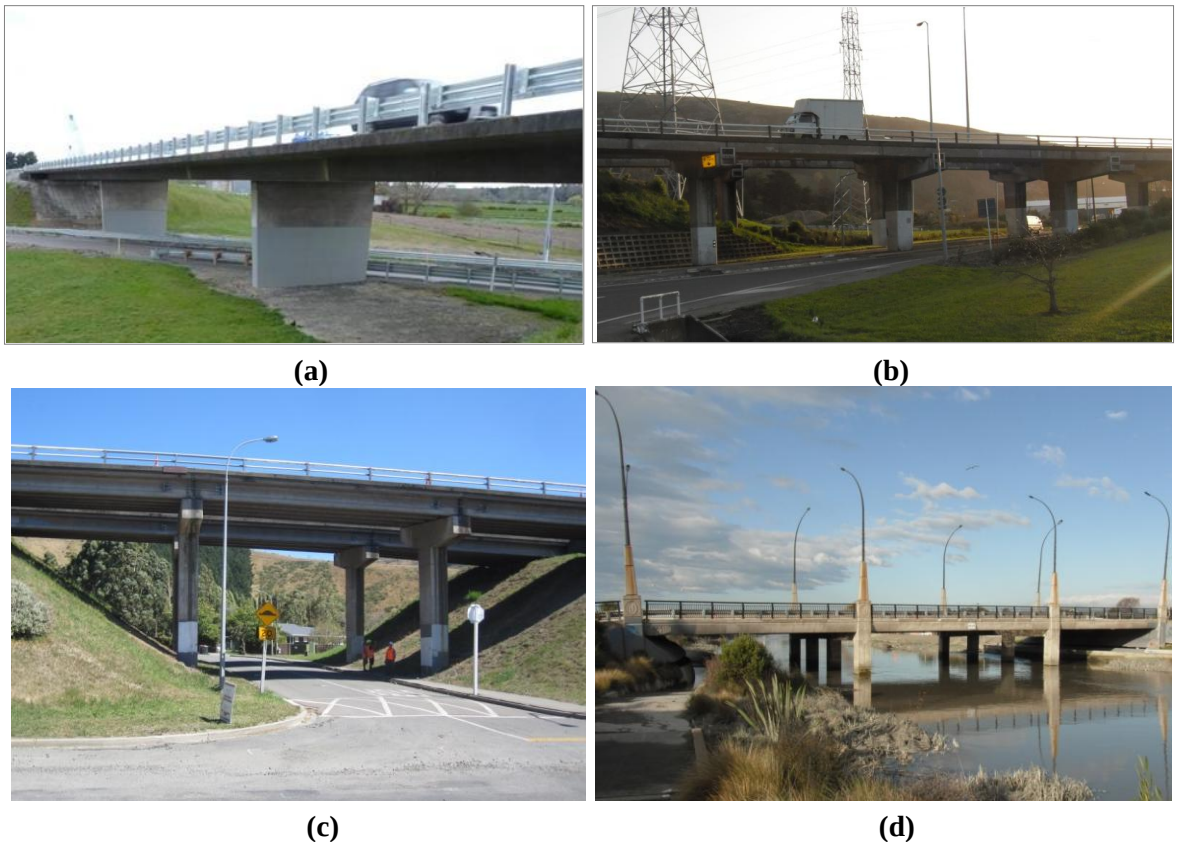

(a) **(b)**

(c) **(d)**

Figure 2.13. ***Overall view of some damaged highway bridges after February 22, 2011. a) Channeys Pass Road Bridge [Photo by M. Anagnostopoulou]; b) Port Hills Overbridge [Courtesy of OPUS]; c) Horotane Overbridge [Courtesy of OPUS]; d) Anzac Drive Bridge [Photo by E. Camnasio]***

(a) **(b)** **(c)**

Figure 2.14. ***a) Liquefaction around the piers of Channeys Pass Road Bridge [Photo by M. Anagnostopoulou]; b) Backwards rotation of the abutments of Anzac Drive Bridge [Photo by A. Palermo]; c) Plastic hinging at the pier caps of Anzac Drive Bridge [Photo by E. Camnasio].***

2.6 Pedestrian Bridges

Pedestrian bridges experienced similar damage to road bridges during both earthquakes. However, due to their relatively small deck stiffness, compressive forces as a result of lateral spreading, i.e. "strut effect" and settlement of the river banks buckled most of the bridges during the Darfield earthquake, with further damage following the Christchurch earthquake. Figure 2.17, Figure 2.15 and Figure 2.17 show some of the most damaged pedestrian bridges after the latter event.

After September 4, 2010, Dallington and Porritt Park Pedestrian Bridges had visible damage to their abutments. At the Dallington Pedestrian Bridge (-43° 31' 4.39", 172° 40' 37.30"), briefly named Snell bridge (Figure 2.15a), a post-tensioned double flanged concrete arch deck, a horizontal crack split the entire abutment at each end of the bridge (Figure 2.15b). During the Darfield earthquake, a three pinned arch formed in response to lateral spreading. In the 2011 event, the superstructure continued to deform at mid-span where the previous plastic hinge formed (Figure 2.15, detail 2), spalling concrete cover under negative bending and deforming the superstructure in torsion about the longitudinal axis of the bridge. In concrete bridges with flat decks, such as pre-cast panels or cast-in-situ slabs, a compressive load passing through the deck is unlikely to cause a hinge to form as it did in this case. This is because there is no lever-arm between the point of application of the compressive force at the river banks, and at the point of resistance at the centre of the bridge, therefore there is no moment demand. The Dallington Pedestrian Bridge had a lever arm due to the arch form, so there is a moment demand, and a weak point at the centre where the section is skinniest, thus leading to the plastic hinge formation that was observed. The same bridge also exhibited severe damage to the pile caps of the abutment on the side of the river that was subjected to extensive lateral spreading (Figure 2.15, detail 1). The crack was widened to enable inspection of the underlying reinforcement, so it was not as large as the figure illustrates. Fortunately, the bridge has been retrofitted more than ten years ago, since it acts also as a "utility" bridge, carrying two 65kW power cables. Additional details on this bridge can be found in [27].

The other case, Porritt Park Pedestrian Bridge (-43° 30' 52.25", 172° 40' 58.71") (Figure 2.16a), experienced large rotation and translation of the south abutment. This abutment sits on six small piles approximately 200 mm in diameter (Figure 2.16b). It is likely that the piles do not extend very deep and as such, they provided minimal lateral stiffness to the system, only serving to increase the surface area the soil wedge interacted with, exacerbating the problem. This rotation resulted in extensive cracking at the abutment face, as well as hinging at the deck-abutment connection. Rotation imposed on the bridge by the abutment also led to a plastic hinge forming in the double tee beam at 1.5 beam diameters from the abutment (Figure 2.16c). This distance is a likely point at which joint reinforcement was curtailed. After the June 13 2011 aftershocks the deck lost bearing support resulting in collapse. After the Christchurch event, significant damage developed in the Fifield Terrace Footbridge (-43° 33' 18.83", 172° 39' 33.89") superstructure, which rotated about the vertical plane (Figure 2.17a). The point of weakness in the deck was where the steel studs linking the pier to the superstructure were situated, which would have likely been compounded by rotation of the piers. The deformation was so large that the rectangular hollow steel section at the extremity of the deck ruptured through its weld (Figure 2.17b). A significant rotation of steel piers was also visible after this event (Figure 2.17c).

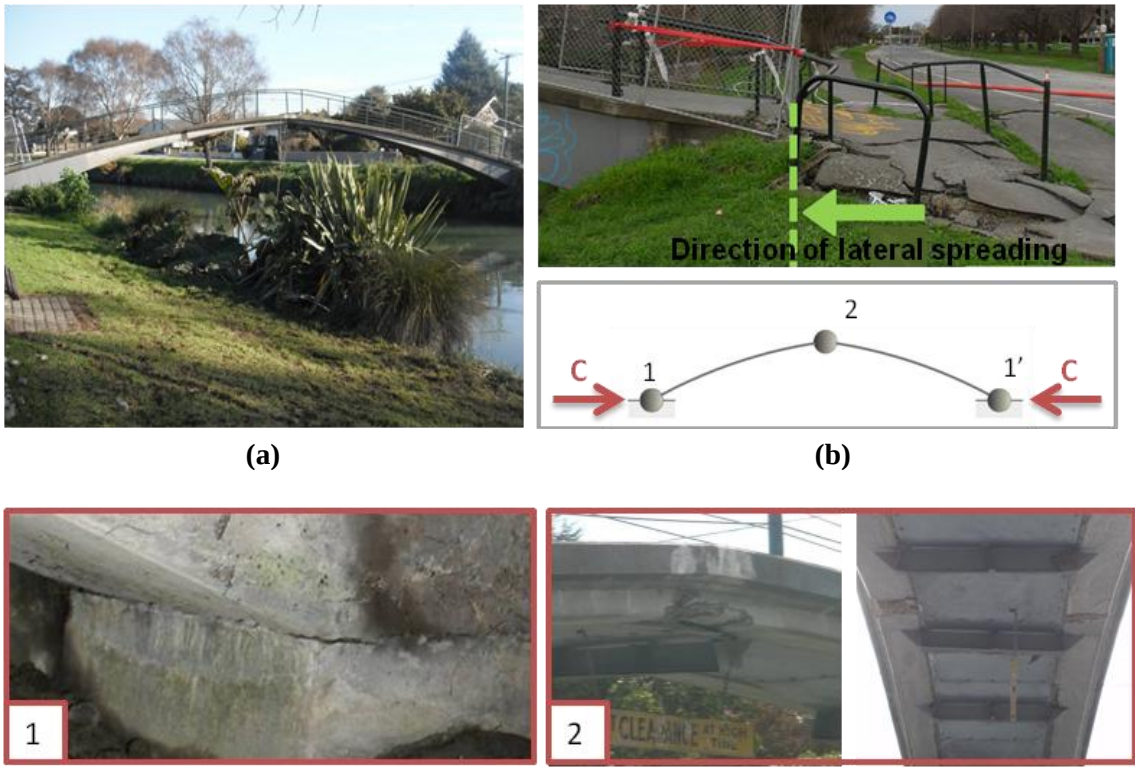

(a) **(b)**

Figure 2.15. ***a) Overall view of the Snell Place Footbridge with indication of the three-hinge arch mechanism [Photo by A. Palermo]; b) Plastic hinge formation at the mid span [Photo by M. Le Heux]; c) Close up view of the plastic hinge at mid span from the side [Photo by A. Kivell] and from the bottom [Photo by M. Le Heux]; b) Damage to abutment: close up of the crack [Photo by M. Le Heux]***

(a) **(b)** **(c)**

Figure 2.16. ***Porritt Park Pedestrian Bridge: a) End view [Photo courtesy of OPUS International Ltd]; b) Backward rotation of abutment and exposure of piles [Photo courtesy of OPUS International Ltd]; c) Repairing damage to approach and river bank lateral spreading [Photo by L. Hogan]***

(a) **(b)** **(c)**

Figure 2.17. ***Overall view of some damaged pedestrian bridges after February 22, 2011. a) Dallington Bridge (Snell Place); b) Porritt Park Bridge; c) Fifield Terrace Bridge.***

2.7 Lifelines Damage

Ground shaking and liquefaction/lateral spreading were devastating not only on bridge structures but also on pipeline systems crossing these bridges. Many utilities are located along the longitudinal bridge axis under the deck or within the bridge deck. Lifeline networks were severely damaged along the Avon River due to extensive liquefaction and lateral spreading. Quite surprisingly, areas where bridges or stiff infrastructure interacted with river banks had damaged pipes as well. This confirms that pipe connections were not appropriately designed to accommodate deck-to-pipe, or abutment-to-pipe relative displacements.

A typical example is Dallington Pedestrian Bridge, which acting as a strut between the laterally spreading river banks resisted the lateral movement of the ground behind the abutments, creating extensive cracks parallel to the bridge and perpendicular to the alignment of the road and buried pipes (Figure 2.18f). This bridge has two 66kW power cables placed under the bridge deck, providing electricity to twenty thousand inhabitants, and without the retrofit performed by Orion (New Zealand power Supplier Company) ten years ago, would have collapsed. As such, even a modest pedestrian bridge is shown to have strategic importance. Some moderate to extensive damage was observed in many road bridges where pipes were distorted and/or leaking in the proximity of the connections from deck-to-abutment, and abutment-to-approaches. As shown in Figure 2.18, the main issues arises with stiff pipes, such as sewage and water pipes, as they are fully fixed to the deck and usually run through the abutments. On the other hand, the flexibility of power and/or telephone cables were able to accommodate larger displacement demands.

(a) **(b)**

(c) **(d)**

(e) **(f)**

Figure 2.18. ***a) Damage to pipelines at Kainga Road Bridge after September 4, 2010 [Photo by A. Palermo]; b) Gayhurst Road Bridge: damage to lifelines [Photo by A. Palermo]; c) Repairing works at at Bridge Street Bridge [Photo by A. Palermo]; d) Close-up view of damaged pipes along the deck of Ferrymead Bridge [Courtesy of OPUS] e) Damaged pipelines at Bridge Street Bridge after June 13, 2011 [Photo by E. Camnasio]; f) Dallington Pedestrian Footbridge: damage to electrical services to the Dallington area [Photo by M. Le Heux]***

3 DATABASE OF CHRISTCHURCH BRIDGES

3.1 Introduction to the Database

3.1.1 Need of the Database

The conclusions of the preliminary report were based on the observations of a small subset of bridges of the Canterbury region that OPUS in cooperation with the University of Canterbury witnessed. Since the group concentrated on the bridges that were known to be damaged, the findings presented in the visual observation chapter above had a bias towards higher levels of damage than what actually occurred. To avoid this bias and to provide a better overview of the damage to bridges after the two last earthquake, the Darfield and the Lyttleton ones, a database has been compiled. The goal of the database is to offer an unbiased method of assessing the performance and cause of damage to bridges in Canterbury. This has been done, considering, besides the bridges already assessed in the previous chapter, also all the ones that exist within the earthquakes affected zone. With regard to the Darfield Earthquake, 800+ bridges were inspected and information of damage put into the database. The latter was then filled in again after the Lyttleton Earthquake but this time information were limited to bridges in Christchurch and the updating concerned just 220+ bridges. This will enable the assessment of the overall performance of bridges; the determination of what actually led to the most severe damage occurring; and an assessment of the performance of different types of structural materials, construction period, length, bridge use, etc.

3.1.2 Boundaries of the Database

In general the database cover all the bridges in the region bordered in the North by the Ashley River, in the South by the Rakaia River, and in the West by the Castle Hill Area, as shown in Figure 3.1a. This area was chosen as in it the strong shaking was experienced (MMI $\geq$ VI) and it encompassed the most of the damaged bridges after the first strong earthquake of the 22th of September 2010. The last important seismic event, the Lyttelton Earthquake, struck mainly the Christchurch area, so that only 220+ bridges were inspected and updated in the Database. The boundaries are so narrowed and reach out the edge of the city (Figure 3.1b).

Only bridges owned by the various governmental authorities were considered in the database and so no private bridges were considered.

For reasons of expediency bridges shorter than three meters were not included, as the potential information lost by not considering these bridges was not worth the resource in implementing them into the database.

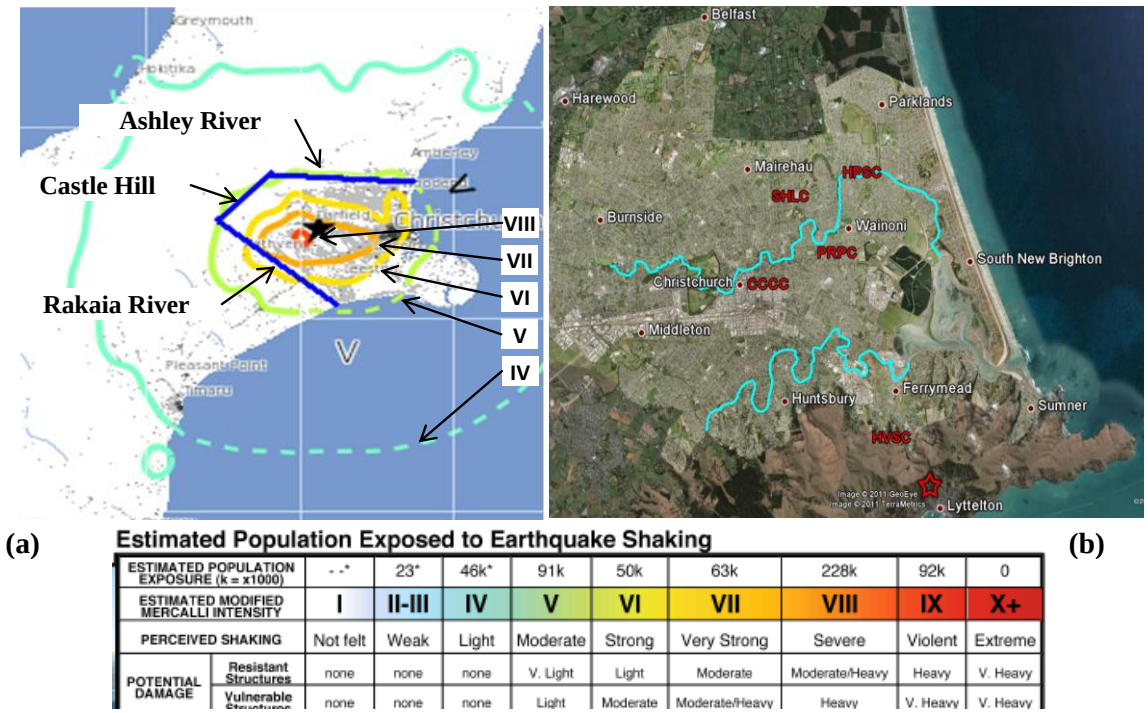

Estimated Population Exposed to Earthquake Shaking

ESTIMATED POPULATION EXPOSURE (k = x1000)		- -*	23*	46k*	91k	50k	63k	228k	92k	0
ESTIMATED MODIFIED MERCALLI INTENSITY		I	II-III	IV	V	VI	VII	VIII	IX	X+
PERCEIVED SHAKING		Not felt	Weak	Light	Moderate	Strong	Very Strong	Severe	Violent	Extreme
POTENTIAL DAMAGE	Resistant Structures	none	none	none	V. Light	Light	Moderate	Moderate/Heavy	Heavy	V. Heavy
	Vulnerable Structures	none	none	none	Light	Moderate	Moderate/Heavy	Heavy	V. Heavy	V. Heavy

Figure 3.1. ***(a) Boundaries of the database with the plot of intensity of shaking from USGS; (b) The Christchurch region in which are included damaged bridges considered after the Lyttelton Earthquake***

3.1.3 Bridges Information in the Database

Besides the gathering and the classification of the damage, discussed in more detail in the next section, the database provide for each bridge also a series of general information. They were collected from the five authorities who own and manage the considered region's bridges: New Zealand Transport Agency (NZTA), ONTRACK (a.k.a. KiwiRail), the Christchurch City Council, OPUS, the Waimakariri District Council, and the Selwyn District Council. The additional information are here listed:

- **Identity:** each bridge has a "Governing Authority Bridge Number". This means that each authority has their own identification system for naming the bridges. Although it resulted in a mixture of different naming systems, it was decided to keep their names and naming systems.

- **Location:** for the majority of the bridges the location is given by the street, the suburb and the river crossing. Updating the database after the last seismic event, the exact bridge location using a unified coordinate system, such as longitude and latitude, was implemented.

- **Description:** characteristics of bridges were implemented using the descriptive data provided by the authorities. These include: length, number and sometimes spacing of spans, pier type, deck type, age, material of construction, bridge use. Several authorities even had an ordered photographic record for the bridges.

3.1.4 Damage Quantifying Procedure

In order to process the analyses of data, it was necessary to find a criterion to move from the qualitative assessment of the damage to the quantitative one. To make the assessment easier and at the same time more precise, bridge damage was split into the following nine different categories:

1. Deck and superstructure damage;
2. Bearing damage between deck and abutment or piers;
3. Pier damage;
4. Abutment damage;
5. Bridge pavement damage;
6. Approach pavement damage;
7. Approach settlement;
8. Damage to services crossing the bridge;
9. Damage to the surrounds in the interaction zone with the bridge (such as lateral spreading of river banks, guardrail damage, and bulging of soils due to interaction with bridge).

The damage in each category was given in a numerical value based on its severity. A total of four damage states were defined for bridge components, from 0 (none) to 3 (extensive or complete damage). To associate the level of damage observed to each value of the scale, the criterion provided by *HAZUS* was used. HAZUS is one of the most well known software platform that integrates the components of seismic risk and interactive environment to provide decision-makers with tools to assess the impact. The description of each severity index is shown in Table 3.1, below:

Table 3.1. ***Classification of severity of damage used in the database***

Level of Damage	Description
ds1 NONE	No observed damages
ds2 SLIGHT/ MINOR DAMAGE	Minor damage which is not a safety concern, and only required to be repaired for visual reasons, as minor cracking and spalling to the abutment, cracks in shear keys at abutments, minor spalling and cracks at hinges, minor spalling at the column (damage requires no more than cosmetic repair) or minor cracking to the deck
ds3 MODERATE DAMAGE	Moderate damage which is not extensive enough to cause closure of bridge, but does require repair (not necessarily immediately) for functional and safety reasons. It is defined for example by any column experiencing moderate (shear cracks) cracking and spalling (column structurally still sound), moderate movement of the abutment (<2"), extensive cracking and spalling of shear keys, any

	connection having cracked shear keys or bent bolts, keeper bar failure without unseating, rocker bearing failure or moderate settlement of the approach.
ds4 EXTENSIVE OR COMPLETE DAMAGE	Severe damage which resulted in temporary closure or collapse of bridge. That state is so defined by any column degrading without collapse – shear failure - (column structurally unsafe), significant residual movement at connections, or major settlement approach, vertical offset of the abutment, differential settlement at connections, shear key failure at abutments. At the worst by any column collapsing and connection losing all bearing support, which may lead to imminent deck collapse, tilting of substructure due to foundation failure.

3.1.5 Capabilities of the Database

The database is able to provide both macro and micro data. On the microscopic level, for every bridge a report can be produced as the one given in Figure 3.2. The report details all the information held in data form in the database. In addition to the details stored within the database, there is a complimentary digital folder containing additional photos and information on a proportion of the bridges. Links to each bridges appropriate folder location are given in the database.

On the macroscopic level, basic statistical tools are available within the database for analysing the bridge stock and its response to the earthquake. In addition the data is able to be exported to tabular form to allow for more advanced analysis and filtering. The remainder of this chapter will focus on analysis at the macroscopic level.

The database capability is not limited to the 2010 Darfield and 2011 Christhchurch Earthquakes damages; it is built to be readily extended to include any future event. Similarly it can be expanded geographically and descriptively if the resources and motivation subsist.

For further information on the database, or if access to it is desired, contact the manager of the database, Dr. A. Palermo of the University of Canterbury, at alessandro.palermo@canterbury.ac.nz.

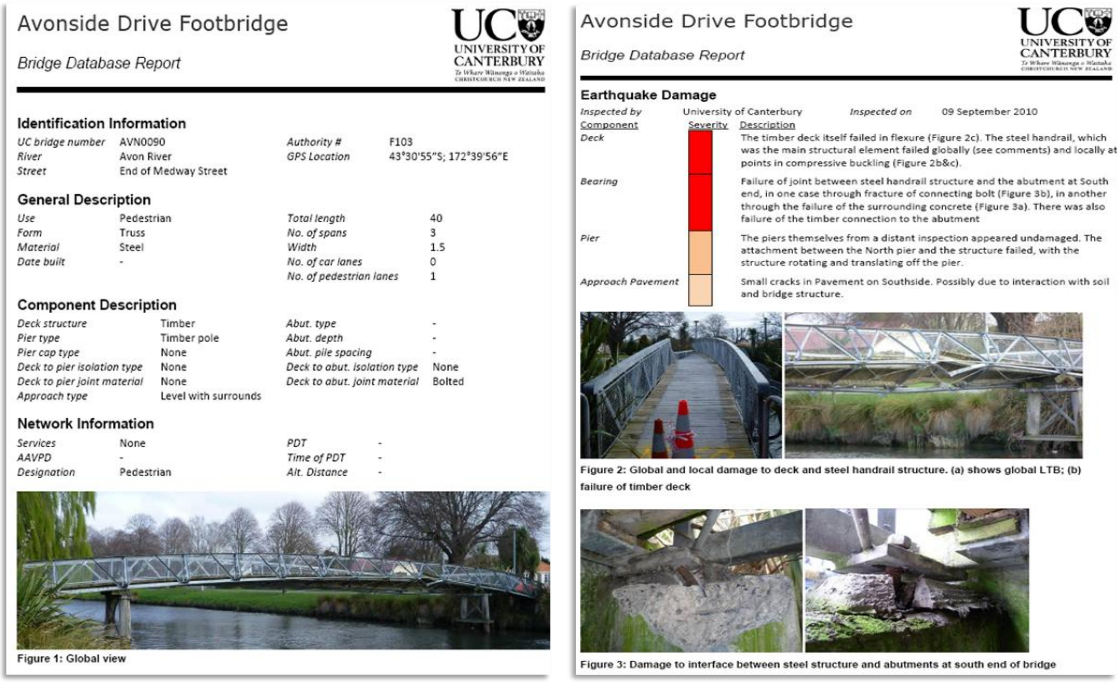

Avonside Drive Footbridge

Bridge Database Report

UC UNIVERSITY OF CANTERBURY

Identification Information

UC bridge number	AVN0090	*Authority #*	F103
River	Avon River	*GPS Location*	43°30'55"S; 172°39'56"E
Street	End of Medway Street		

General Description

Use	Pedestrian	*Total length*	40
Form	Truss	*No. of spans*	3
Material	Steel	*Width*	1.5
Date built	-	*No. of car lanes*	0
		No. of pedestrian lanes	1

Component Description

Deck structure	Timber	*Abut. type*	-
Pier type	Timber pole	*Abut. depth*	-
Pier cap type	None	*Abut. pile spacing*	-
Deck to pier isolation type	None	*Deck to abut. isolation type*	None
Deck to pier joint material	None	*Deck to abut. joint material*	Bolted
Approach type	Level with surrounds		

Network Information

Services	None	*PDT*	-
AAVPD	-	*Time of PDT*	-
Designation	Pedestrian	*Alt. Distance*	-

Figure 1: Global view

Avonside Drive Footbridge

Bridge Database Report

UC UNIVERSITY OF CANTERBURY

Earthquake Damage

Inspected by University of Canterbury *Inspected on* 09 September 2010

Component	Severity	Description
Deck		The timber deck itself failed in flexure (Figure 2c). The steel handrail, which was the main structural element failed globally (see comments) and locally at points in compressive buckling (Figure 2b&c).
Bearing		Failure of joint between steel handrail structure and the abutment at South end, in one case through fracture of connecting bolt (Figure 3b), in another through the failure of the surrounding concrete (Figure 3a). There was also failure of the timber connection to the abutment
Pier		The piers themselves from a distant inspection appeared undamaged. The attachment between the North pier and the structure failed, with the structure rotating and translating off the pier.
Approach Pavement		Small cracks in Pavement on Southside. Possibly due to interaction with soil and bridge structure.

Figure 2: Global and local damage to deck and steel handrail structure. (a) shows global LTB; (b) failure of timber deck

Figure 3: Damage to interface between steel structure and abutments at south end of bridge

Figure 3.2. ***Example of a bridge report produced by the Database.***

3.2 Bridges in Christchurch

In total there were 223 Bridges in the studied region described in section 3.1.2. All those bridges fall into two different categories of use, car and pedestrian, in the proportions shown in Figure 3.3.

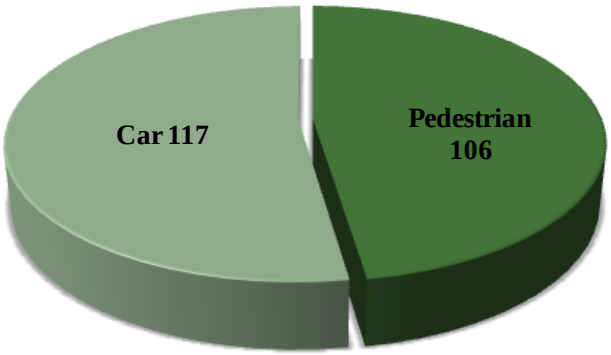

Figure 3.3. ***Bridges in the Database updated after Lyttelton Earthquake.***

There was interest as to the lengths of the bridge stock of the city. A histogram of bridge length is presented in Figure 3.4. As would be expected, the frequency decreases exponentially with length. This is shown in how the median bridge length in the city is 10 m. The 86% of the bridge stock has a length lower than 30 m, much less than the maximum length of bridge of 205 m.

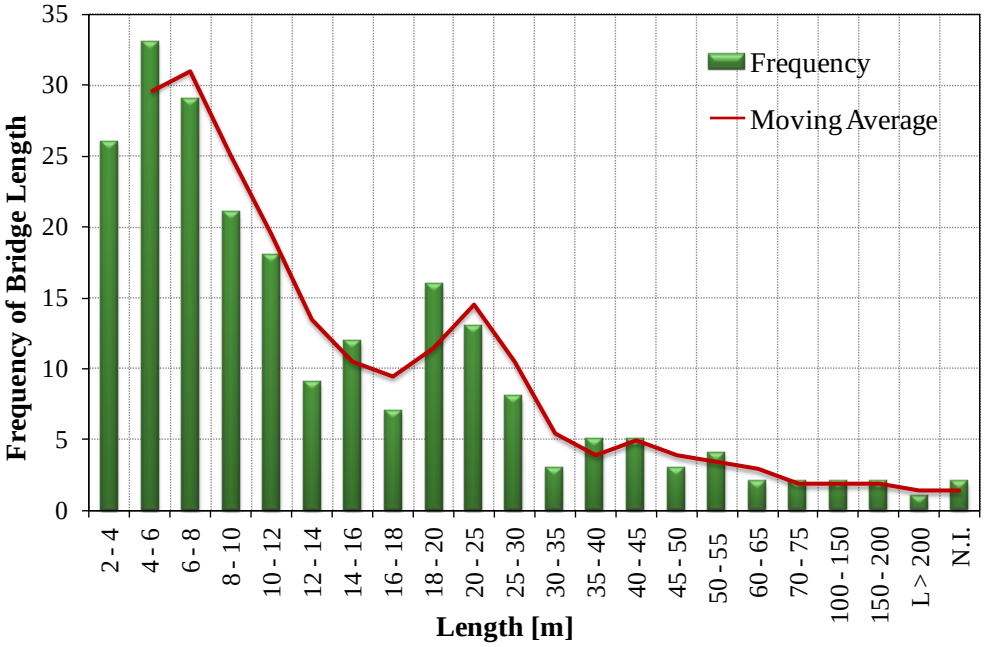

Figure 3.4. ***Histogram of bridge length in Christchurch region***

Also of interest to this study was the age of the bridges of the region. This is helpful, as it gives an indication as to what seismic design philosophy the bridges were designed for. A histogram of the decades in which the bridges were constructed is presented in Figure 3.5. The immediate conclusion is that there was minimal bridge building pre World War 2, and then a large amount of bridge building which lasted for five decades. The median of bridge age is 1965. The 85% of bridges are built after 1930 and only the 37% after 1980.

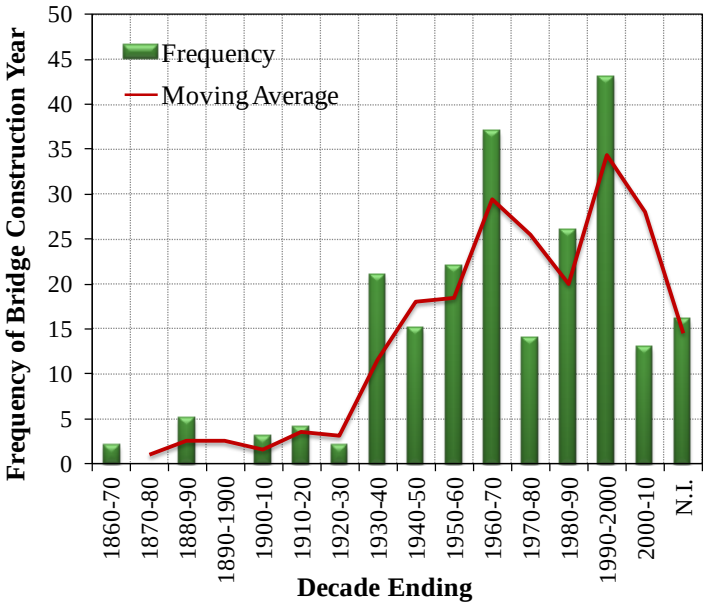

Figure 3.5. ***Histogram of bridge construction date in Christchurch region***

As already presented, the database gathers together damage as well as the bridges typological characteristics, the most significant for our purpose are the structural material type and the structural form. The percentage of the total bridge stock of certain structural material type is given in Figure 3.6: over half the bridges in the surveyed region are concrete, timber and steel surprisingly have relatively equal proportions, while masonry and mixed bridges take up a very small percentage.

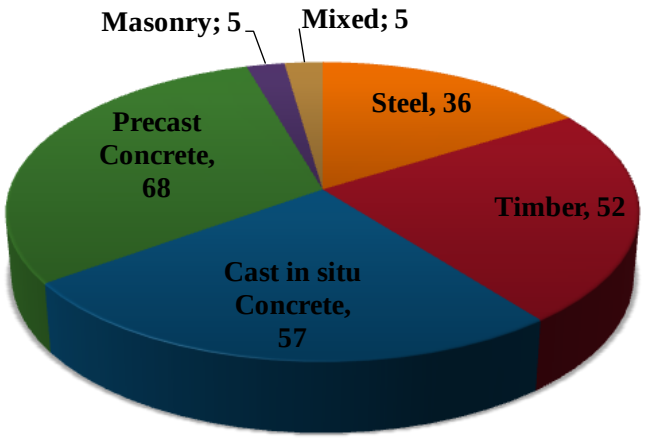

Figure 3.6. ***Christchurch Bridge stock classified by structural material type***

To provide a more precise picture of the typological scenario, the structural materials are connected to each category of use, as shown in Figure 3.7.

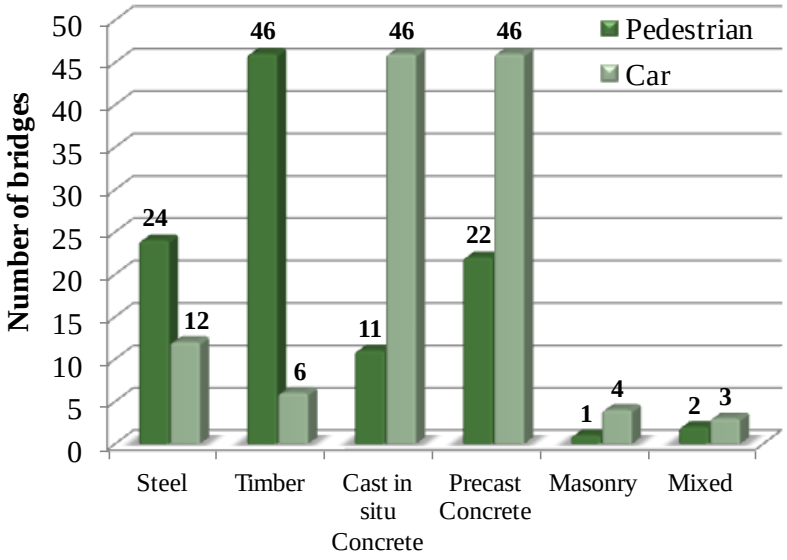

Figure 3.7. ***Proportions of the bridge category of use for each structural material type***

As expected most of the timber and steel bridges are pedestrian. To be more precise, the percentage of pedestrian bridges for the two material categories was the 88% for the timber and the 67% for the steel. The concrete was instead mostly used in the construction of car bridges, with a percentage of

81% of cast in situ concrete bridges and of 68% of precast concrete ones. Also masonry and mixed bridges, thought in a very smaller percentage compared to the other categories, were mainly designed just for the transit of the cars.

In regard to the bridge structural form, the database envisage the classification shown in the pie chart in Figure 3.8: according to it, the most common structural form is timber beams, followed by cast-in-situ slabs and precast slabs. It is plain that the concrete, cast-in-situ or precast, is dominant even in the deck structure, a minor percentage is taken up by steel beams.

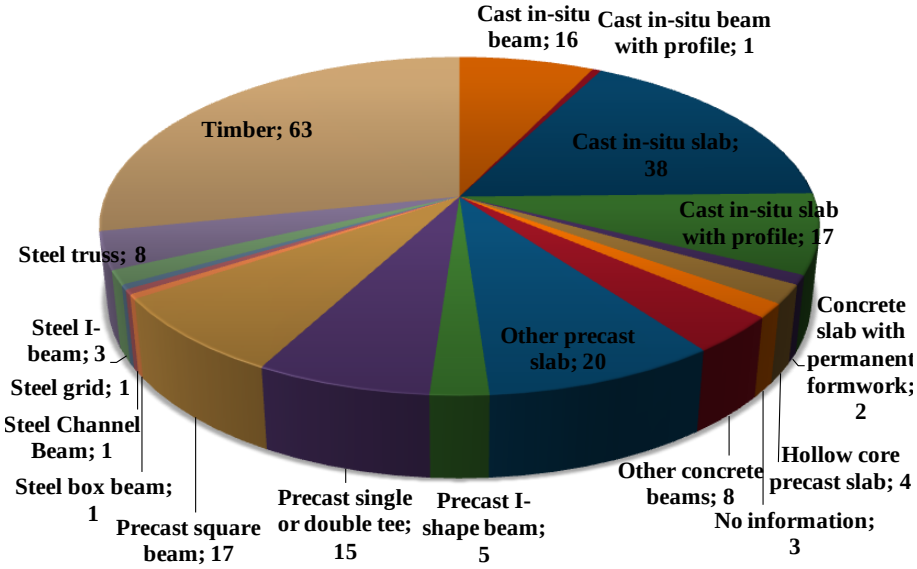

Figure 3.8. ***Christchurch Bridge stock proportioned by structural form according to the database classification***

3.3 Overall Damage to Christchurch Bridges

A first global assessment on the extent of the damage caused by the Christchurch Earthquake of February 22nd is shown in Figure 3.9b. To better evaluate the importance of the last event, a pie chart with the extent of the damage due to the Darfield Earthquake is also exhibited. As already outlined in section 3.1.4, the damage was graded into nine different categories with the damage in each category being given a severity rating from 0 (no damage) to 3 (complete/extensive damage).
To summarize the total bridge damage in the interests region a representative damage for the whole bridge is desired. The criterion to obtain an index for the level of the total damage, was to sum the severity ratings of the different damage categories. Therefore, for example, a bridge with a damage severity of 2 for the deck, and 3 for the bearings would be given a total bridge damage severity rating of 5. To place the bridge in one of four classes of damage described in Table 3.1, a summed damage of 1 to 2 was classified as minor bridge damage, medium damage was set as 3 to 9, and severe total bridge damage was set as greater than or equal to 10. Two of the damage categories, although helpful to have in separate categories, in effect represent the same damage. That is the category of approach pavement damage and the category of damage to the surrounds. The former is actually a subset of the latter. In order not to overestimate the damage of a particular bridge, in the

summation of the total damage only the maximum of these two categories was used to respect their dependence on each other.

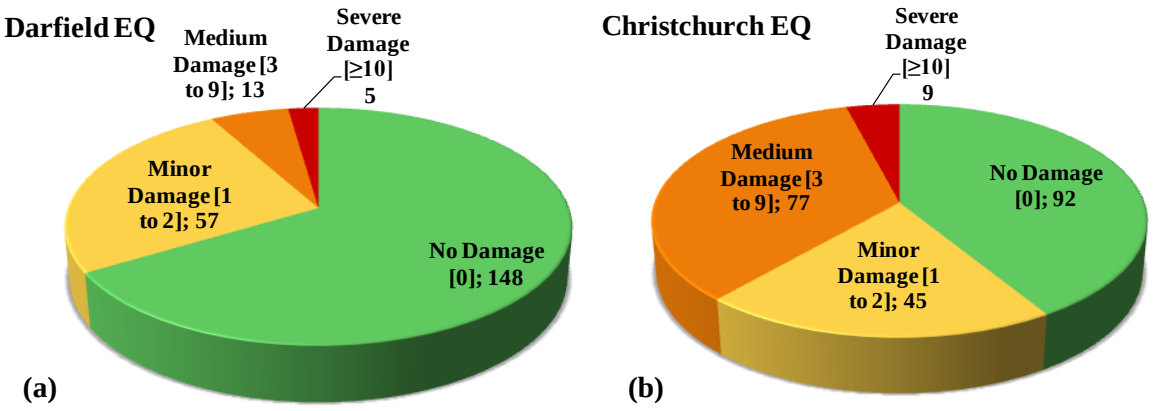

Figure 3.9. ***Christchurch Bridges stock grouped on the basis of the severity of damage after (a) Darfield and (b) Christchurch Earthquakes.***

The general performance of the bridges during both the earthquakes was good. However it is clear that the first earthquake caused less damage than the following one, with the 92% of bridges without or with minor damage, a percentage much greater if compared to the 61% of the last event. Moreover the number of bridges with severe damage observed increased twice, remaining in a small percentage (4%) though.

Broadly speaking for the majority of bridges in the database both were 1/500 year design level events. Considering that the NEHRP Recommended Seismic Provisions (National Earthquake Hazards Reduction Program) recommend that in a maximum credibility event (1/2500 year event), the probability of collapse should be less than 10% for an ordinary structure, the amount of severe structural damage to bridges for these 1/500 year events is appropriate.

The provisions also recommend that for a structure of a higher importance level the probability of collapse in the maximum credible event should be less than 3%. The Transit New Zealand Bridge Manual [29] defines this higher performance level of bridges as those that are either critical for emergency response, or are on routes of strategic importance. Among the bridges with severe damage observed after the 22th February earthquake, only three of them belong to this category: ANZAC Bridge, South Brighton Bridge and Moorhouse Avenue Overbridge. The latter will be considered for numerical analyses in the Chapter 6.

3.4 Damage as Function of the Structural Form

In order to assess the connection between the damage and the material type or the structural form, the bridges of the database are classed in the different categories already defined and for each of them the percentage of damaged bridges is determined. A more precise assessment is given, joining the results of the last earthquake with them of the previous one.

As shown in Figure 3.10, the percentages of the damage according to the material typology have a similar trend for both the events, in minor proportion as for the Darfield earthquake though, with the exception for the masonry bridges, in equal numbers.

Looking at the performance during the Christchurch earthquake, it is immediately evident that timber bridges performed better than the others. This is likely due to the lightness of the material which entail a minor activation of seismic masses compared to the heavier masses of steel and concrete equivalent bridges. In confirmation of this, masonry, precast concrete and steel bridges did not performed well, with a very high percentages of damaged bridges, between 67% ÷ 80% .

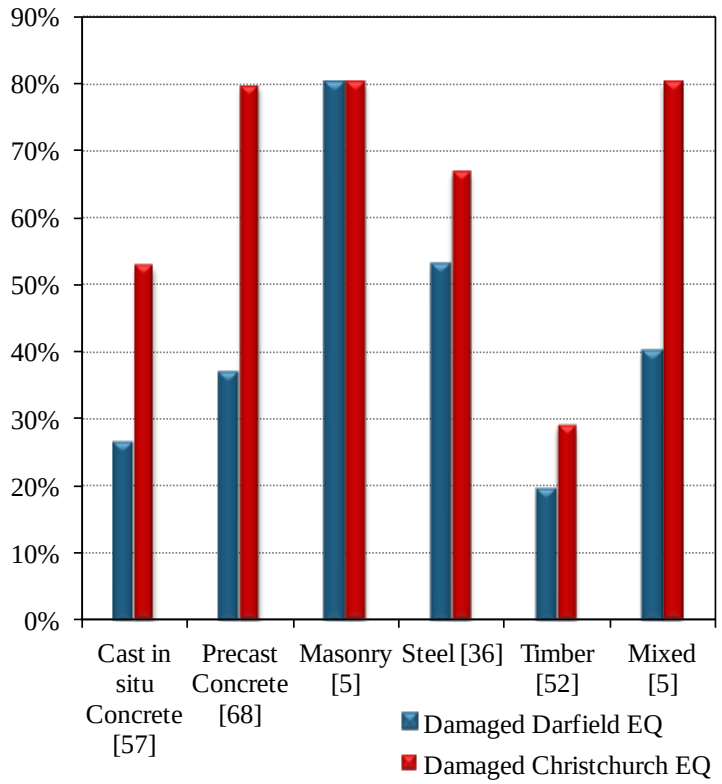

Figure 3.10. ***Percentage of damaged bridges according to the material type after the Christchurch and Darfield Earthquakes.***

The amount of the damaged bridges after the Lyttelton Earthquake is possibly influenced by the effects of the previous event. To assess if this was the case the percentages of the bridges already moderately or severely damaged are presented in Figure 3.11, together with the percentages estimated after February 22nd. The graphic shows that the consequences of the first event were all minor compared to the last one, a part from the masonry typology, with the 50% of bridges already damaged. So broadly speaking we could say that, focussing on the material typologies, the performance of bridges in the Lyttelton earthquake didn't suffer the influence of the previous one, since the damage was very small.

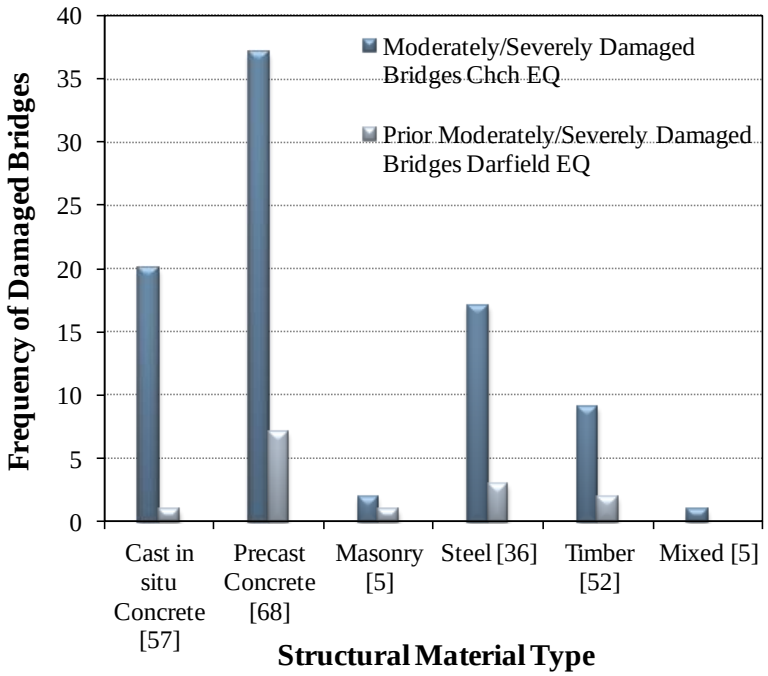

Figure 3.11. ***Comparison between the moderately and severely damaged bridges for each material type category after Christchurch and Darfield Earthquakes***

If we consider the structural form classification, results of the Christchurch earthquake show that there are categories with all bridges damaged, such as the concrete slab with permanent formwork, the hollow core precast slab, the precast I-shape beam, the steel channel beam and the steel I-beam. In general the trend confirms the observation already made previously (Figure 3.12), that is that bridges with concrete and steel as materials, did not perform well. However there were some categories of bridges with the steel deck, such as the steel box beam and the steel grid, which didn't suffered any damage. The structural form class with the lowest number of damaged bridges is the timber, with a percentage of 32%.

Comparing this results with the Darfield ones, there is a minor number of damaged bridges in each category a part from the steel I-beam, where the two percentages are equal. Bridges belonging to some categories such as the cast in situ beam with profile, the concrete slab with permanent formwork and the steel channel beam, didn't show any damage after the Darfield earthquake, while they were all damaged after the last event. It is true to say that this is linked to the low number of bridges in these categories.

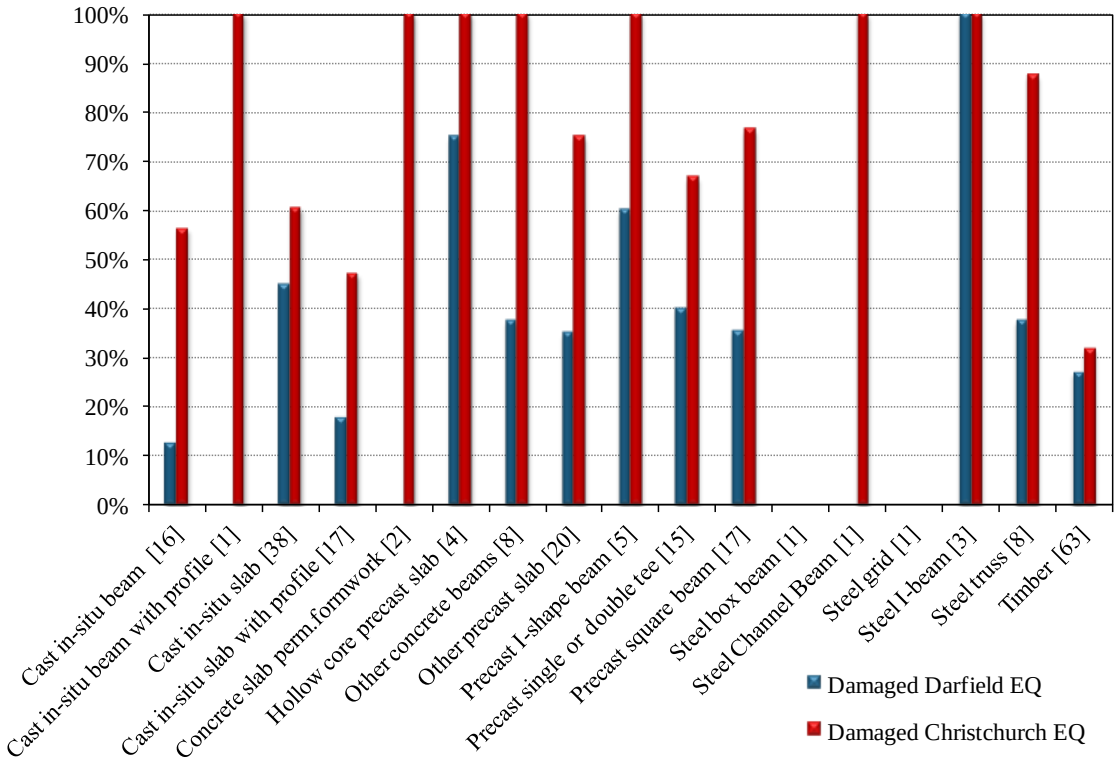

Figure 3.12. ***Percentage of damaged bridges according to the structural form after the Christchurch and Darfield Earthquakes.***

As already done for each material typology, the influence of the previous earthquake is assessed also in this case. The Figure 3.13 shows that the structural form categories which suffered the biggest influence of the first earthquake are the "other concrete beam" and the "precast I-shape beam" ones with the 60% of bridges already moderately or severely damaged. A part from this two cases, in general the percentages of bridges damaged after the Darfield Earthquake are small, so that most of the damage observed after the February 22nd result just from the ground motion of the last event.

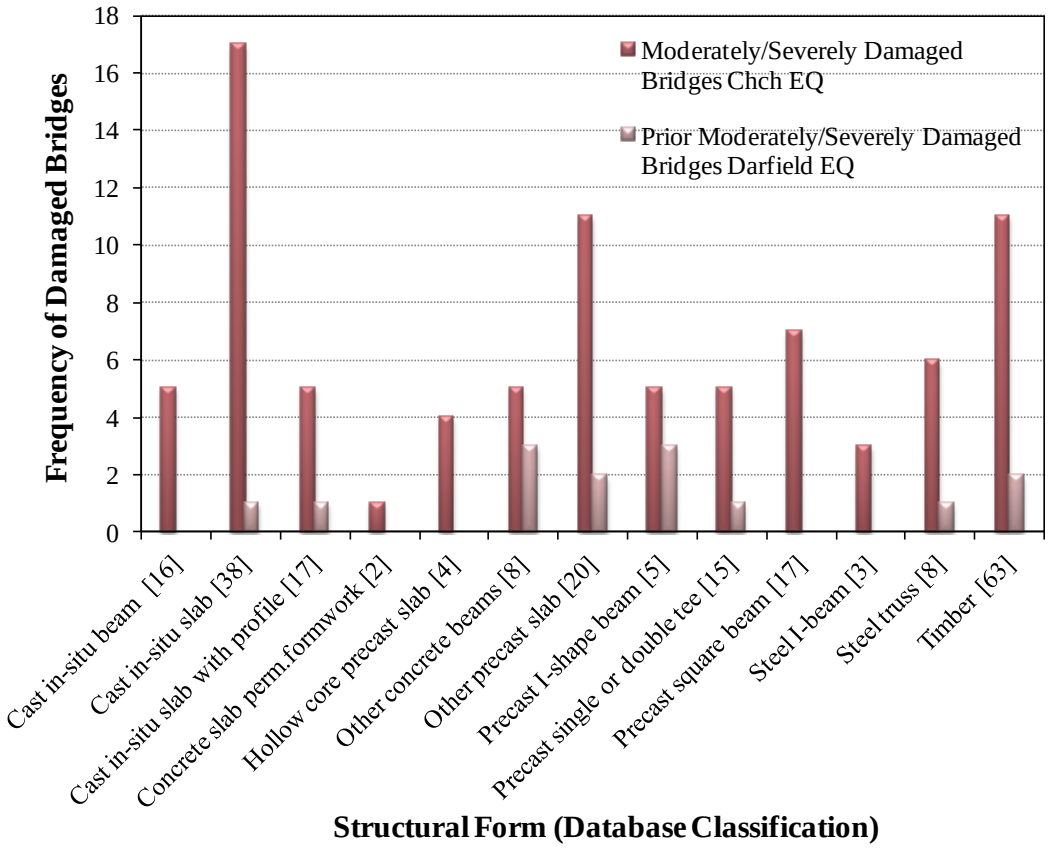

Figure 3.13. ***Comparison between the moderately and severely damaged bridges for each structural form category after Christchurch and Darfield Earthquakes***

3.5 Damage as Function of Age of Bridge

The aim of this section is to point out if there is any connection between the number of damaged bridges and the year of construction. This is interesting since the from the possible correlation, some remarks can arise about the design philosophies and techniques of construction of the given time. To do this in the classification already done on the basis of the age of building, damaged bridges are sorted and compared against the entire bridge stock (inclusive of the damaged bridges). Because much less bridges were damaged than that built for each decade, it would be difficult to compare the trends due to the magnitude difference in scale. To overcome this each of the series were normalised by the total count of bridges in that series (i.e. to make the sum of each series equal to 1). This is done for damaged bridges observed after both the earthquakes. The three series are shown in Figure 3.14.

The graphic shows that in general the three series have a similar trend with a lot of up and down peaks. The stretch from the 1980's of the total bridges series it's slightly different from the other ones. In fact the two series of damaged bridges have a low average up to the 1950's, that considerably increase till the 1970's and then from the 1980's onwards both averages are about 2/3 of the pre 1970's value, while the value of the total bridge series rise of the 30%.

Because the series have more or less the same trend, it shows that there is little correlation between the age of the bridge being built, and the damage observed in the earthquakes. In particular it was

expected that, because of the progressive improvement in engineering since 1870's, the older bridges would have been more damaged than the newer bridges. This actually did not happen with a surprising increase of damaged bridges built between 1950 and 1970. The decade of bridges constructed between 1980 and 2010 abide by the expectations with a lower level of damage.

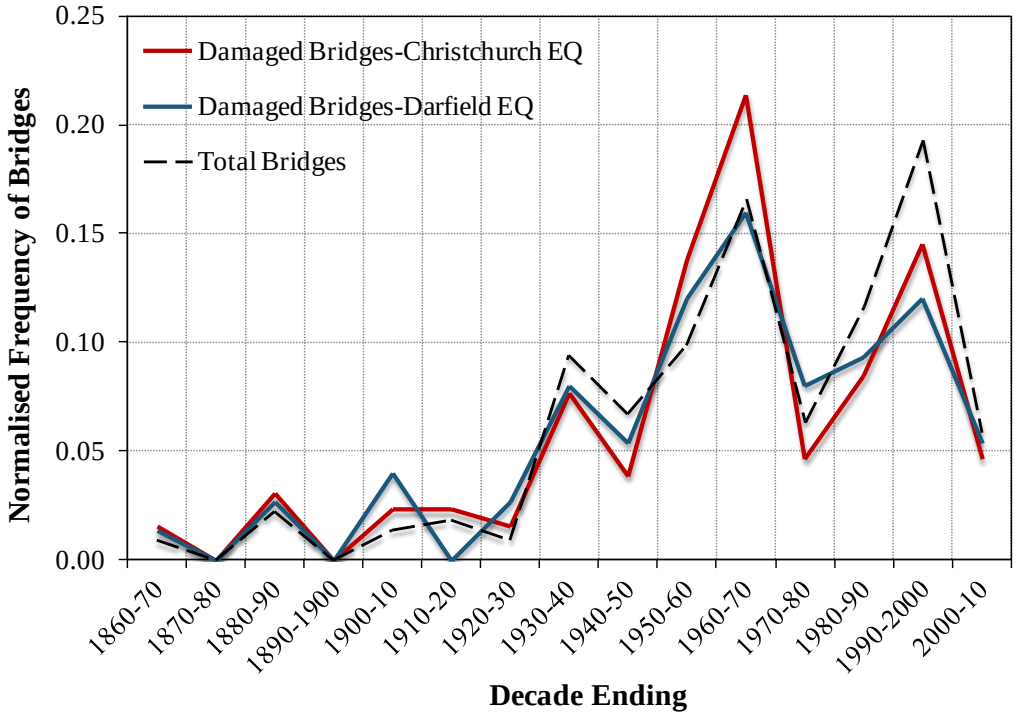

Figure 3.14. ***Normalised year of construction of bridge: for the entire bridge stock and for the bridges that suffered damage in Christchurch and Darfield earthquakes***

3.6 Lateral Spreading, Liquefaction and Slope Failure Action on Christchurch Bridges

The damages that occur during an earthquake can be divided in two categories: damages due to ground shaking and damages due to phenomena of the soil such as lateral spreading, liquefaction an slope failure. Broadly speaking structural elements of a bridge can be separated in the ones mostly damaged by the ground motion and the ones more subjected to soil phenomena. The sketch of Figure 3.15 shows the two groups highlighted in different colours.

In order to investigate if the effects of the Christchurch earthquake on the soil influenced the performance of the bridges, and which parts of the structure were hit by those phenomena, the bridges that exhibited damage were split into two broad categories:

- Bridges at which there was some evidence of lateral spreading, liquefaction or slope failure impacting the bridge;

- Bridges with no such evidence.

Figure 3.16 shows the percentage of the moderately/severely damaged bridge stock of bridges in which occurred soil phenomena, and bridges which suffered only the ground shaking. At a fist estimate, we could say that the ground motion was the main cause of the damage during the Christchurch earthquake, impairing by itself the performance of more than 60% of bridges.

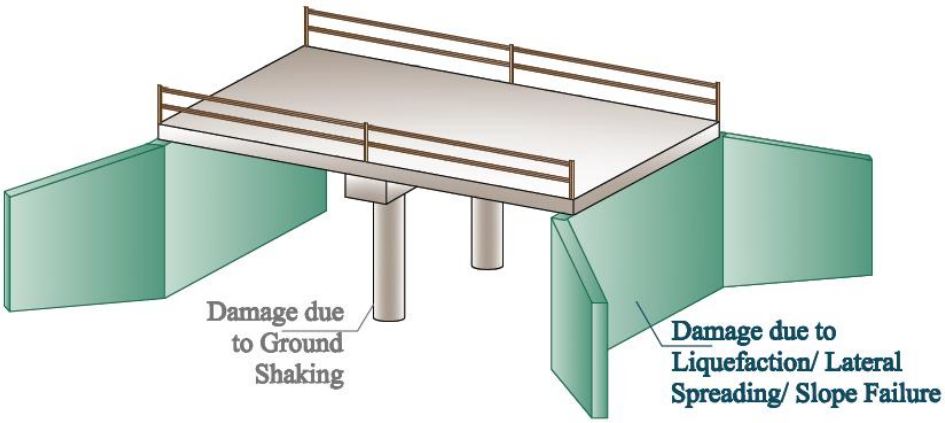

Figure 3.15. ***Sketch of the bridge with part highlighted depending on the cause of the damage***

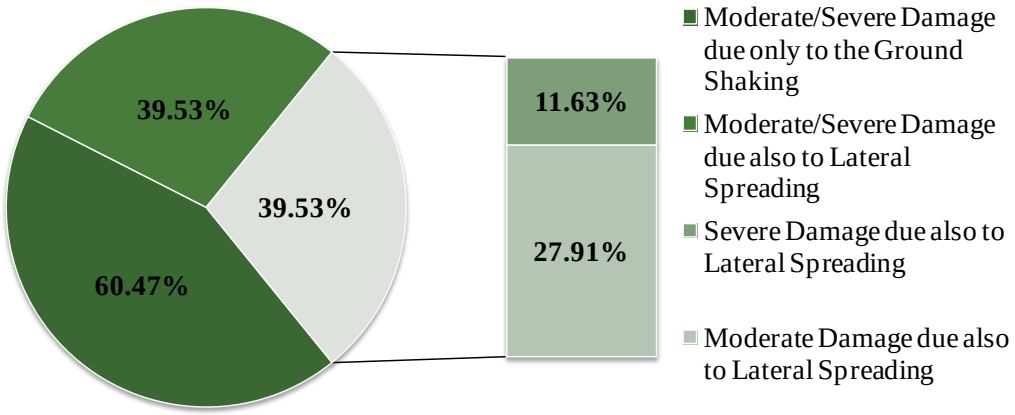

Figure 3.16. ***Pie chart showing the proportions of bridges moderately/ severely damaged with and without lateral spreading, liquefaction or slope failure observed.***

To deepen the assessment, the soil influence is estimate for each category of the bridge. Figure 3.17 presents the number of bridges with the type of damage, with or without lateral spreading, at the given bridge site. The first immediate observation is that the most common bridge damage was at the approach pavement and at the surroundings, with respectively 76 and 77 observed cases of damage out of 350. To be noticed also that the latter category is the one with the highest percentage, 60%, of bridges where lateral spreading was observed and recorded.

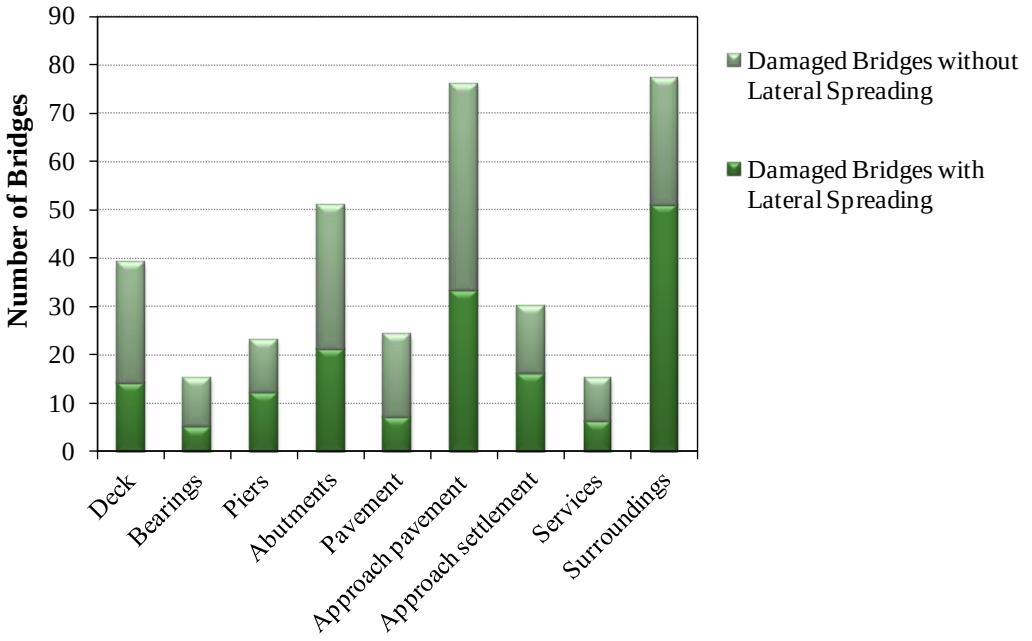

Figure 3.17. ***Number of bridges exhibiting a given category of damage. With bridges divided into those affected and not affected by lateral spreading.***

Figure 3.17 is not a good representation of the distribution of damage between the damage categories, since using number of bridges as the ordinate does not give respect to the three levels of damage severity. For example a bridge with just hairline cracks on the deck, would receive the same weighting in Figure 3.17 of one bridge in the deck damage category as a bridge on which the entire deck collapsed. To give weight to the different levels of severity, the raw values of severity index of damage are then summed for each damage category to give the summed severity index. This means that one severely damaged component of the bridge has a weighting equivalent to three bridges showing minor damage. Although not a perfect method of weighting damage, it does lead to a truer representation of performance than what was obtained by simply using number of bridges. The results of this weighting system are presented in Figure 3.18.

We can see from this figure that the proportions have not changed and the most impacted components of bridges by this earthquake were indeed the surroundings, which over the entire region took 21% of the summed severity index. The next highest was damage to the approach pavement (20%), and then damage to the abutments (15%). Lateral spreading was associated with 46% of the summed severity total.

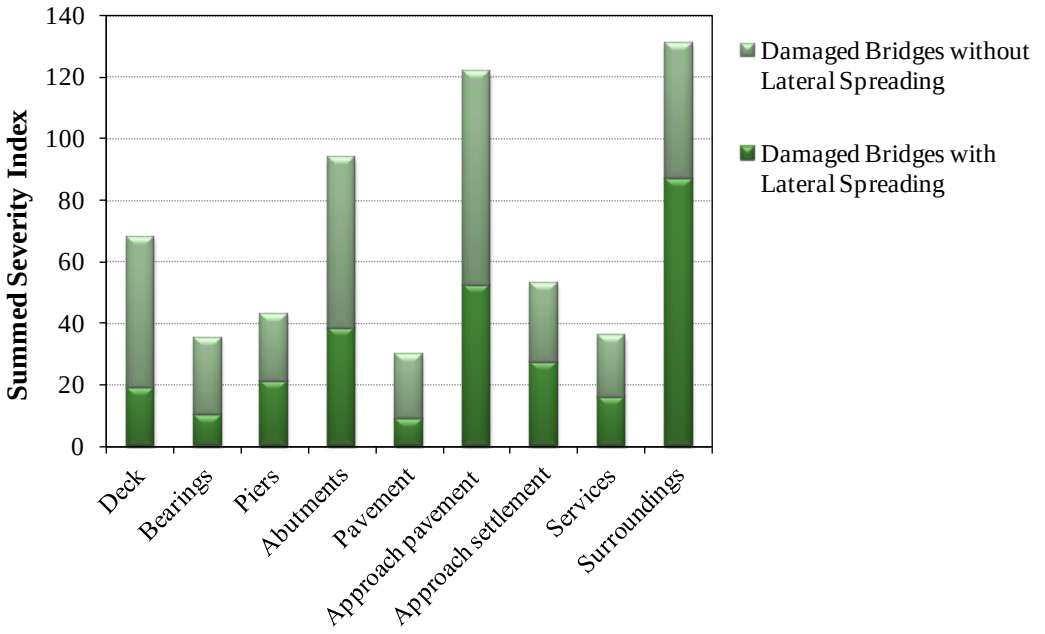

Figure 3.18. ***Summation of the damage severity index for the different categories of damage. With bridges divided into those affected and not affected by lateral spreading.***

In section 3.3 it was shown that 45 of the 131 damaged bridges had a total summed severity that indicated minor damage (i.e. summed severity of 1 or 2). In general this level of damage was inconsequential to both the bridges performance, and to the interest of this investigation. Therefore it was decided to filter the dataset which damage severity was investigated on in order to concentrate on the more consequential damage. This is done in the two following figures. Figure 3.19 is based on a dataset of just the moderately damaged and severely damaged bridges and Figure 3.20 is then based on a dataset of just the severely damaged bridges.

For the database set in Figure 3.19 which contains the moderately and severely damaged bridges, the list of which component damage severity received from greatest to smallest remains almost unchanged from the complete dataset given in Figure 3.18. A slightly lower proportion of the bridges shows evidence of lateral spreading. That means that the cause of the damage changed a little bit.

For the dataset of moderately and severely damaged bridges 43% of damage is associated with bridges where lateral spreading occurred, a percentage similar to that one of the previous case.

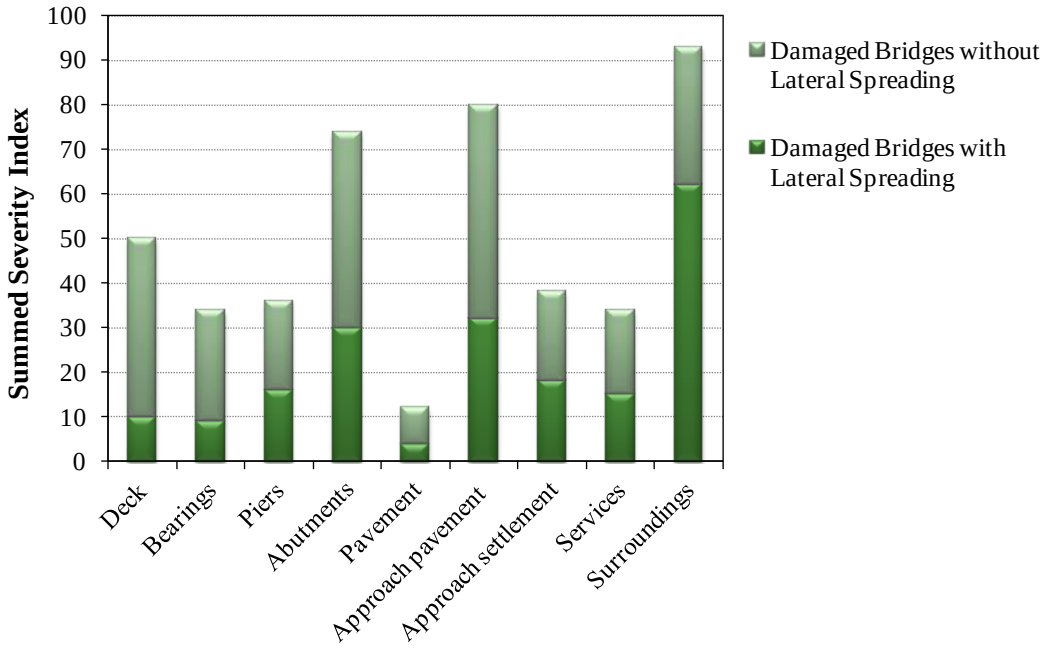

Figure 3.19. ***Summation of the damage severity index for the different categories of damage for bridges considered moderately or severely damaged only. With bridges divided into those affected and not affected by lateral spreading.***

Figure 3.20 gives the summed severity index for bridges which are considered severely damaged (total bridge severity ≥ 10). This figure is quite different from the figures that included the bridges with minor and moderate damage.

The immediate observations are that the damage to the deck are not caused by soli phenomena as well as there is a very small percentage of damage with lateral spreading in the summed severity index of bearings. Moreover the bridge pavement have not suffered any severe damage as result of the last seismic event. The order of what damage components had the highest severity index didn't changed. The graphic confirms that the earthquake of February 22nd have mostly damaged the surroundings of bridges, subjected more than the other categories to the effects of lateral spreading, liquefaction and slope failure (~77% of the total summed severity index). The large proportion of damage to the approach pavement also in the severely damaged bridge category is understandable considering the observation of the visual inspections that the majority of closures of bridges were due to damage to the approach of the bridge.

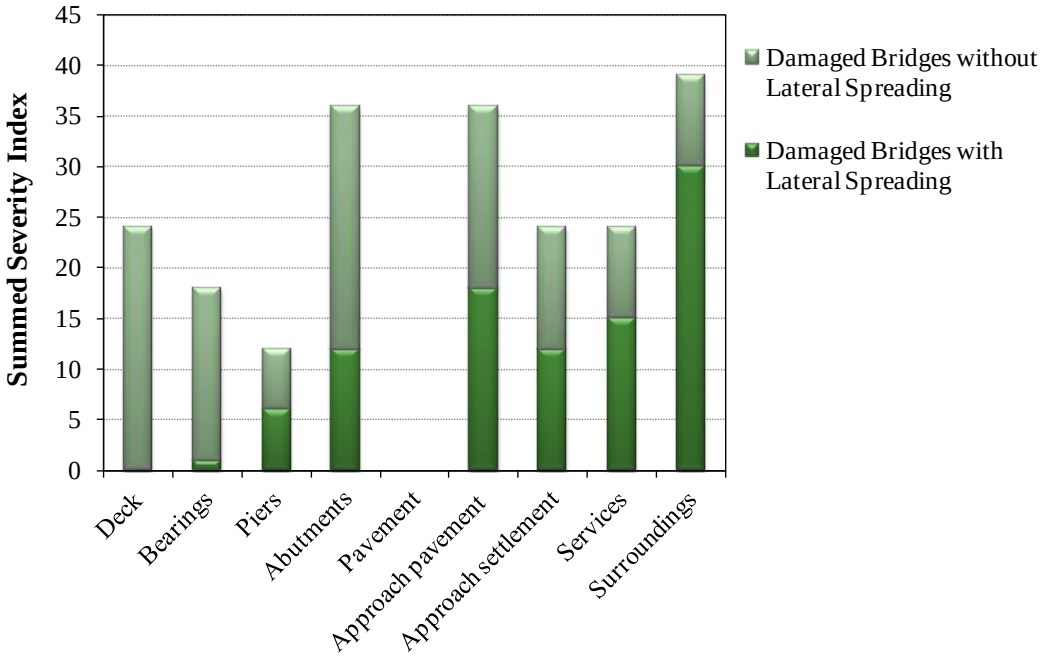

Figure 3.20. ***Summation of the damage severity index for the different categories of damage for bridges with considered severely damaged only. With bridges divided into those affected and not affected by lateral spreading.***

Two chief observation can be done at the end of this section. The first one is that there are parts of bridges which sensibly suffered the influence of soil phenomena and for which the evidence of lateral spreading, liquefaction and slope failure, increases as the minor and moderate damage is not taken into account. Piers, abutments, approach pavement and settlement, services and surroundings belong to this category. On the other hand there are categories, such as the deck and the bearings, for which that evidence significantly decreases up to reset to zero.

During the Christchurch earthquake the lateral spreading was not the main cause of damage while during the previous earthquake in September 22nd 2010, there were no bridges severely damaged due to the shaking. The effect of the shaking phase of the Darfield earthquake only caused minor to moderate damage and was generally within what would be considered the serviceability limit of the bridge. As it will be shown in the modal assessment of the case studies (Chapter 4, 5 and 6), accelerations during Christchurch earthquake were so high instead, that the presence of severely damaged bridges just because of the ground motion is justified.

So if we made the crude assumption that the bridges without soil phenomena observed were damaged only by the seismic shaking, and vice versa, we could draw a link between design emphasis and damage. That is bridges in Christchurch were designed well to resist the level of seismic shaking of Darfield earthquake, while there has been less emphasis of the design of bridges against soil phenomena, like lateral spreading, liquefaction or slope failure, as resulted from the inspections from the field after both the earthquakes.

3.7 Conclusions of the Database Observations

The database of the University of Canterbury was updated inserting damage of 223 bridges in Christchurch after the earthquake of February 22nd, 2011. The database was compiled to offer an unbiased statistical tool for assessing the bridges of the city as it contained information to identify, locate and describe each bridge and the severity and type of damage that occurred at the bridge site.
The majority of the bridges in the city have a length smaller than 30 m, with only the 14% with a length over the 7% over 50 m. The largest bridge construction period was the five decades inclusive and following WW2, thus predating the majority of current understanding of liquefaction and lateral spreading. .The material construction of over half the bridges is the concrete.
The performance to the earthquake was acceptable according to typical seismic codes, although worse than the previous one in September. In fact the 38.6% of bridges suffered medium to severe damage, a much greater percentage if compared to the 8% of the first seismic event. However only 4% of the entire stock was considered severely damaged, with three bridges in this category considered of a high importance. The damage that hampered the performance of these bridges was because of both the ground shaking and the soil phenomena such as lateral spreading, liquefaction and slope failure.
The three main structural material types of steel, cast-in-situ concrete, and precast concrete, all performed to a similar standard. As expected masonry bridges did not perform well, with 80% of them experiencing some type of damage. Surprisingly, timber bridges performed better than both steel and concrete.
There was no correlation between the year of construction of the bridge, and the damage observed at the bridge. This is concerning, as it would be hoped that as time progressed, and building codes and engineering knowledge advanced, that bridge performance would improve.
Severely damage occurred because of the ground shaking and soil phenomena, unlike during the Darfield earthquake, where the latter was the chief cause of the severe damage. Therefore the remaining chapters of this study will concentrate on cases study with different causes of damage: ground motion and slope failure.

3.8 Further Objective of the Research

The post earthquake collection of comprehensive damage observation data has been recently increased and improved. Following the Christchurch earthquake series of 2010 and 2011 empirical damage data of the impacted built-environment have been recorded and processed by different research groups. The observed data covered all the components of civil infrastructure system, including the building stock [30-32], bridges [33] and lifelines utilities [34]. Specific investigation on individual building failures [35] and geotechnical aspects were deeply investigated [36]. Researchers in different field investigated damage data individually. To enhance the information exchange and a more comprehensive damage analysis across sub-disciplines, also accounting for interdependencies, a database of all the impacted structures and infrastructures has been proposed. In particular as for bridges, by converting the available damage information into GIS (Geographic Information System) format, the database was used in combination with the software MAEviz. This is an open-source software which integrates spatial information, seismic data, and visual information into an environment for performing seismic loss assessment and analysis. It can be used to generate damage estimates from scientific and engineering principles, test multiple mitigation strategies, and support modelling efforts to estimate higher level impacts of earthquake hazards,

such as impacts on transportation networks, social, or economic systems. It can be classified as one of the Earthquake Loss Estimation (ELE) tools, supporting and informing the emergency response and recovery planning.

In this way is possible to make comparison the field observation on Christchurch bridges, collected in the database, and the post-dicted results of impact assessment obtained using the hazard map generated by MAEviz. The software platform uses a different structural form classification. That one considered by the database was helpful to group bridges in the nine most common classes used in MAEviz:

Table 3.2. Structural Form classes used in MAEviz and the relative percentage in the Christchurch bridge stock

Bridge Name	Abbreviation	Number	Percentage
Multispan continuous concrete girder	MSC concrete	5	2.2%
Multispan continuous slab	MSC slab	8	3.6%
Multispan continuous steel girder	MSC steel	4	1.8%
Multispan simply supported concrete girder	MSSS concrete	19	8.5%
Multispan simply supported concrete box girder	MSSS conc box	0	0.0%
Multispan simply supported slab	MSSS slab	7	3.1%
Multispan simply supported steel girder	MSSS steel	0	0.0%
Single span simply concrete girder	SS concrete	105	47.1%
Single span simply steel girder	SS steel	9	4.0%
Other		63	28.3%
No information		3	1.3%

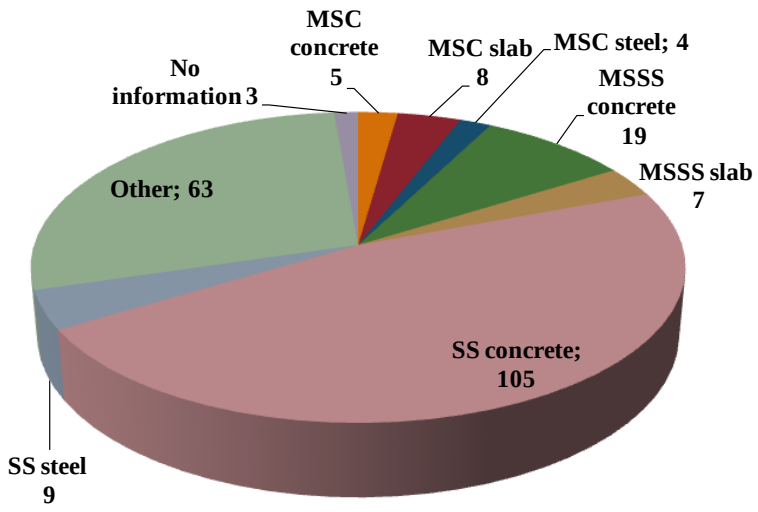

Figure 3.21. ***Christchurch Bridge stock proportioned by structural form according to the MAEviz classification***

The MAEviz tool has been run to calculate the structural damage at each bridge point (Figure 3.22b) with the generated hazard map. Hazard map is one is one of the indispensable components of earthquake loss assessment. To represent the ground motion generated by 22nd February 2011 Christchurch earthquake, and avoiding to add the uncertainties correlated to the use of attenuation laws, a Peak Ground Acceleration, PGA, map in standard gravity (g) for the CBD area was generated based on dense instrument record [37] via interpolation/ extrapolation technique (Figure 3.22).

(a)

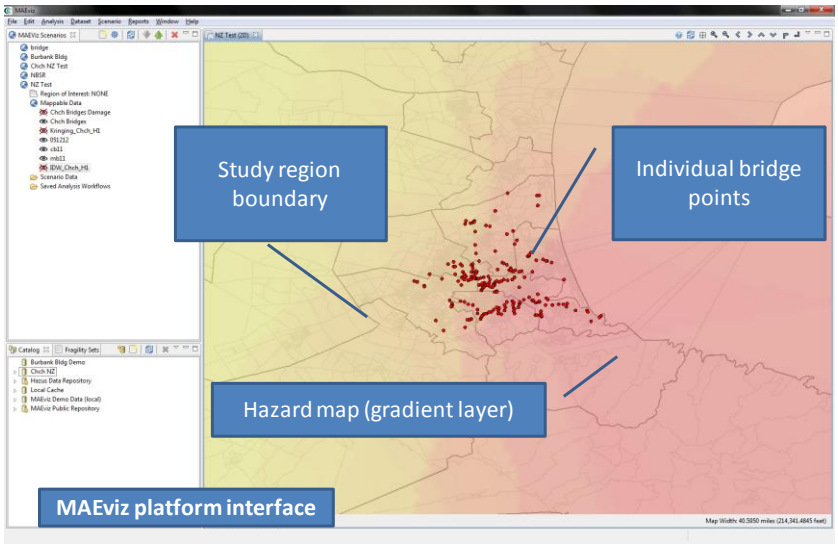

(b)

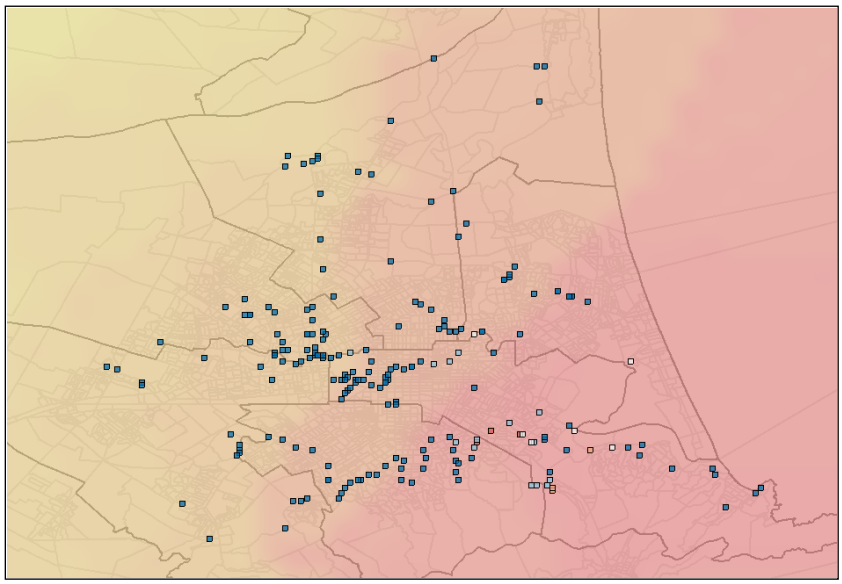

Figure 3.22. ***(a) MAEviz analysis platform, including boundary, bridge points and hazard map; (b) CBD bridge damage data (different colours depending on different damage level).***

Similar to other loss assessment tools, the structural damage is presented in term of probability of exceeding a given limit state. The resulted damage is still described in terms of tagging system (i.e., green, yellow or red) so that a bridge is yellow-tagged when its probability of exceeding life safety limit state is grater than 50% and its probability of exceeding collapse prevention limit state is lower than 50%.

Figure 3.23 shows the pie chart obtained from analysis run with MAEviz. Comparing these results with the percentage of different level of damage as observed from the field after Christchurch Earthquake (Figure 3.9a), the gap is glaring. The percentage of bridges slightly damaged prominently increase, passing from 61% to 86%, and, as a consequence, the amount of bridges belonging to the other categories, decrease. However it's interesting to note that the percentage of severely damaged bridges is almost the same, being down by only 1%.

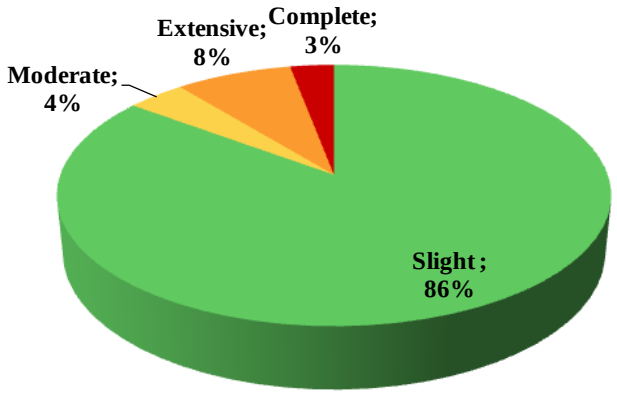

Figure 3.23. ***Pie chart showing Christchurch Bridges stock grouped on the basis of the severity of damage as resulted from MAEviz analysis.***

Many reason may explain the differences:

1. The default fragility model is specified for Central US, which may not be appropriate to represent New Zealand bridges, due to the difference from construction materials and techniques, bridge characteristics, and code consideration.

2. The subjective nature in the database filling procedures may sometimes mislead the structural damage. For example, a yellow bridge may be recognized as red or green, depending on the examiners as well as the level of examination.

3. The correlation between damage-limit states and tagging colours might need to be adjusted.

In spite of some fault in results, the preliminary study on Christchurch bridges demonstrated the possibly of application of already existing ELE components and procedures, implemented within open-source platforms, to New Zealand reality.
However challenges remain and further research is required to improve the reliability and robustness of the outcome, in particular when to be used for actual prediction of future scenario. The major challenge is providing hazard and fragility model specific for New Zealand which are currently under development. In particular of interest is the development of fragility curves able to relate the severity level of liquefaction with the probability of reach the damage. To do this a relationship between the PGA and the severity level of liquefaction has to be found.
Finally the inclusion of social and economic effects due to structural damage into MAEviz is another important challenge.

4 PORT HILLS OVERPASS

4.1 Description of the Structure

Port Hills Overpass is located about 7 km south-east of central Christchurch and about 2.2 km North-West of the Christchurch Portal entrance to the Lyttelton Road tunnel. The No 1 Overpass Bridge (-43.5711, 172.6934), constructed in 1963, carries the south bound lane of SH 74 and an on-ramp lane across Port Hills Road. The No 2 Bridge, constructed at the same time, carries the single north bound lane of SH 74 across Port Hills Road. Both bridges are of similar construction with six simply supported spans of prestressed concrete log type beams supporting a reinforced concrete topping. Piers height ranges between 7-8.5m and are slightly tapered downward. The pier caps and abutments are both orthogonal with respect to the bridge axis. The bridge abutments and the reinforced concrete single stem rectangular piers are founded on spread footings. The spans vary in length between 9.4 to 12.6 m. The bridge n°1 is the largest, with two car lanes and a total width of approximately 9m and an overall length of 72.4 m. The n°1 is also the bridge which has suffered major damage during the Lyttelton Earthquake and for this reason the numerical analyses will be carried out only on it.

Figure 4.1. ***Overall view of Port Hills Road.***

The Overpass bridges have been recently, in 2009, retrofitted by fixing fabricated steel shear keys to the underside of the beams at both the abutments and piers to resist longitudinal earthquake loads. Linkage rods were fitted between brackets located on either side of the piers by drilling through the tops of the piers to form a tight linkage between adjacent spans. The down-stand of the brackets prevents relative movement between the spans and the piers. Linkage at the abutments was provided by rods extending between the brackets and the soil face of the abutment seating beams.

New shear keys fixed to the faces of the abutments and piers provide resistance to transverse loads and prevent sliding of the superstructure on the inclined pier caps in an earthquake event (Figure 4.2a). The spans were originally held down to the abutments and piers with 12 mm diameter dowels anchored into the infill concrete between the log beams. They were also linked by longitudinal 12 mm diameter bars anchored into the infill concrete. The new shear keys and linkage bolts provide a large increase to the resistance of the original linkage system which was considered inadequate for current design loads.
Circular steel shrouds were added at one pier column on each bridge where they passed through a significant depth of soil on the abutment slopes (Figure 4.2b). The pier annulus was constructed to prevent soil restraint to the pier which may have cause undesired plastic hinging due to ground motion in the transverse direction. The soil restraint shortens the effective length of the column, in what is known as a 'captive-column' effect.

(a) **(b)**

Figure 4.2. ***Retrofit solutions fitted to the bridge (a) Shear keys and pier linkages; (b) Circular steel shroud***

4.2 Earthquake Performance

The Overpass was located about 42 km east and 1.3 km north of the epicenters of the Darfield and Christchurch earthquakes respectively. Although records from the closest SMA (HVSC at 1.6 km from the bridges) are likely to have been significantly influenced by topographic effects, the bridge is really close to the epicenter of the second earthquake and this had clearly influence on its performance.
During the Darfield earthquake, Port Hills Overbridge performed well. The installation of tie-rods and devices such as the transverse shear key allowed the bridge to sustain seismic forces without structural damage. Nevertheless, the post-earthquake investigations have not been in depth enough to ascertain if these devices were activated during the seismic shaking.
After the Lyttelton earthquake the qualitative damage of structural/non structural elements observed are listed in Table 4.1. It has to be noticed that the retrofitted links between the spans and the bolts connecting the span to the abutment had elongated, but the bridge was still able to service traffic with the damage it sustained.

Table 4.1. ***Summary of the level of damage observed on the bridge after the Lyttelton earthquake***

Deck	Null	**North Approach**	Null
Services	Null	**South Approach**	Null
Piers	Moderate	**Substructure**	Moderate
North Abutment	Moderate	**Surrounds**	Null
South Abutment	Moderate	**-**	-

4.2.1 Superstructure and services

Superstructure of Port Hills bridge didn't suffer damage after the Lyttelton earthquake. No cracks developed meaning that the deck behaved elastically during the seismic excitation (Figure 4.3a). Figure 4.3b-c show the good performance of the recent retrofitting: links between the spans rotated and elongated but they were able to keep the spans connected. The nominal 10 mm gaps between the new shear keys and the abutment face at the south-east abutment of the No 1 Bridge closed up with no clearance on two of the four keys.

(a) **(b)** **(c)**

Figure 4.3. ***(a) Overall view of bridge superstructure; (b) Rotation of the bolts; (c) Elongation of the links between the spans***

4.2.2 Piers

In the Christchurch earthquake the bridge sustained damage to the central pier with the formation of a plastic hinge at its base and two of the corner reinforcing bars buckling over a length of 150 mm cracking and spalling of the concrete occurred around the base of the pier, exposing the reinforcing steel (Figure 4.4). Flexural cracking developed also in the lower halves of the other pier stems except those adjacent to the abutments, and some settlement of the approach pavement. Soil gapping at ground level occurred at the faces of most of the pier stems with separation cracks up to 15 mm wide.This damage was induced by ground shaking which activated the transverse response of the bridge and apparently came with the second aftershock soon after the main quake.

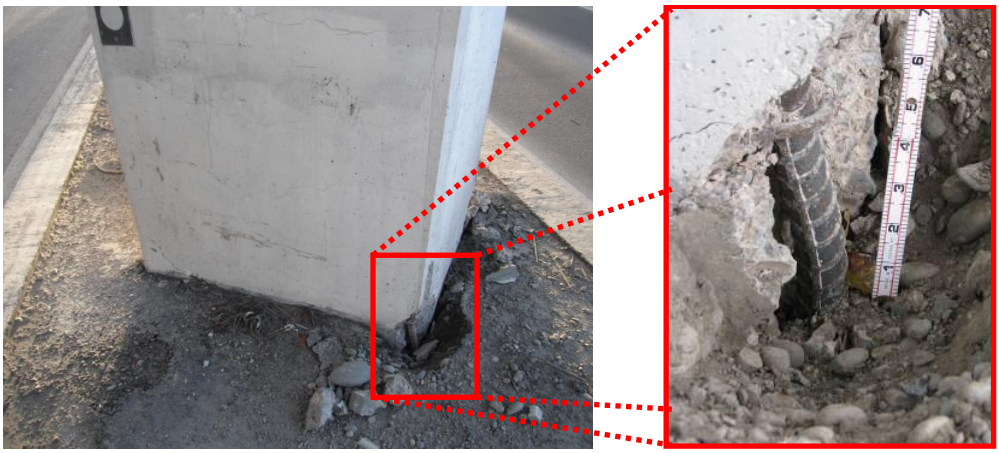

Figure 4.4. ***Damaged pier of Port Hills overbridge: detail of buckled reinforcing steel at the base of the pier***

4.2.3 Abutments

In the vicinity of the abutments, there was evidence of partial embankment slope failure. Some ground fell down on the road but the retrofit intervention regarding the regularization of piers height along the bridge avoided to concentrate the seismic transversal forces into the external piers, which were previously much shorter and then stiffer.

4.2.4 Foundations

No evident damage was suffered by the foundations. Further investigation would be needed to find out the conditions of foundations below ground level.

4.2.5 Approach and Surroundings

Wide cracks running parallel to the roadway at the top of the approach embankment developed in the soil on the east side at the south-east end of the bridges. There was also minor settlement and displacement of the approach pavement and back-fill at the abutments.

4.3 Numerical Analyses

4.3.1 Introduction

In order to assess the response of the bridge when subjected to seismic events, analyses were undertaken using the software Ruaumoko 3D [40]. Static push-over and push pull analyses, both with a displacement controlled procedure, are used to determine the displacement capacity, which is compared then with the demand obtained from the registered spectra. That comparison provides a first assessment on the need of retrofitting the existing structure. Then time-history analyses are performed using the accelerograms recorded during the Darfield and Christchurch earthquakes: the analysed bridge is located in a way that different peak ground acceleration can be considered as acting on the structures, according to the nearest ground motion record station, thus resulting in damage of varying severity. Lastly the structure was subjected to ground motions recorded during 10 famous earthquakes: having to be representative of the seismicity of the area within which the work is inserted, the accelerograms were scaled to be compatible with the design spectrum imposed

by the New Zealand code. Analyses were performed on models at increasing levels of complexity and considering first the design properties and secondly the properties actually registered by measurements with the hammer.

4.3.2 Assumptions of work

4.3.2.1 Piers

The development of realistic frame models requires a detailed characterization of individual bents, since generally the stiffness for the frame models is contributed directly by the bents.
The drawings show that the piers are slightly tapered, with the minimum section at the base, where they stand on shallow foundations. In the calculation of the properties of the columns it was taken account of that characteristic considering two types of section: the base and the top. To find the moment-curvature relationship for the sections, to be used in the Ruaumoko3D input file, the software Cumbia was used. The analyses were carried out for each pier, since they are different from each other by the size of the base section and the high. The columns were considered as "single bending columns" with a height equal to the length of the central portion of the pier: this assumption has no influence on the sectional properties, but only on the length of the plastic hinge which is expected to arise at the base of the elements. Since the bridge columns are expected to form flexural plastic hinges under the seismic action, and since subsequent to the plastic hinge formation most of the bridge displacement can be attributed to inelastic rotation in these plastic column hinges, to simulate the piers the beam elements have an effective stiffness that takes cracking into account. For the piers the Giberson model has been assumed: the model consists of a linear elastic element with rotational springs at the ends whose behavior is described by a moment-rotation relationship obtained by the integration of curvatures for a fixed length of plastic hinge.

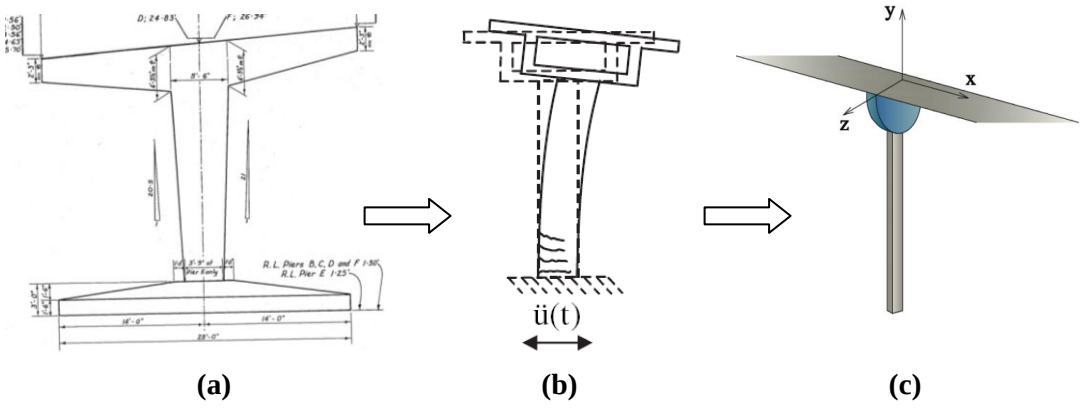

Figure 4.5. ***(a) Pier of the bridge from the drawings; (b) Sketch of the behavior of the pier; (c) Pier as considered in the model***

4.3.2.2 Superstructure

Satisfactory response of the bridge relies on the capacity of the column to displace inelastically through several cycles of response without significant degradation of the strength or stiffness. The superstructure, due to its in-plane rigidity, is assumed to move as a rigid body under seismic loads, and the entire modelling is reduced to the stiffness modelling of the bents with geometric constrains

simulating the superstructure. In order to simulate the deck are therefore used beam elements with a stiffness corresponding to the uncracked value.

4.3.2.3 Foundations

The type of foundation of the bridge is spread footings and, at the base, the piers were assumed to be fixed. This was a realistic assumption as there was no evidence of the spread footings having rocked in the earthquake. If this had happened, there would likely have been obvious damage to the surrounding pavement above the footings.

4.3.3 Section properties

4.3.3.1 Material properties

As already mentioned, the analyses were conducted by considering first the design material characteristics, then the actual ones, measured by hammer tests.
For the first model, the characteristic strength values were approximated from those ones given in the drawings and summarized in Table 4.2:

Table 4.2. ***Design properties***

CONCRETE

Concrete compressive strength of the piers f_c'	21 MPa (f_c' = 3000 psi specified strength in drawings)
Concrete compressive strength of the deck f_c'	34 MPa (f_c' = 5000 psi specified strength in drawings)
Density of concrete ρ	2400 kg/m$^{3.}$
Elastic Modulus for the piers (using the formula from NZS 3101 section 5.2.3)	$Ec = \left(3320\sqrt{fc'} + 6900\right)\left(\frac{\rho}{2300}\right)^{1.5}$ = 23572 N/mm^2
Elastic Modulus for the deck (using the formula from NZS 3101 section 5.2.3)	$Ec = \left(3320\sqrt{fc'} + 6900\right)\left(\frac{\rho}{2300}\right)^{1.5}$ = 27990 N/mm^2
Shear Modulus G for the piers	10081.70 N/mm^2
Shear Modulus G for the deck	11662.40 N/mm^2

STEEL

Steel yield strength f_y	300 MPa*

* the value of the yield strength shown in the drawings(140 MPa (f_s = 20000 psi)) is much lower than that one suggested by the Bridge Manual for bridges built in 60's of 250 MPa (6.3.2-b). That value was raise to 300 MPa since it was the value measured for most of the bridges built in the same period in Christchurch.

In the second model, the concrete properties measured in site are:

Table 4.3.*Actual properties*

CONCRETE

Concrete compressive strength f_c'	38 MPa
Density of concrete ρ	2400 kg/m$^{3.}$
Elastic Modulus (using the formula from NZS 3101 section 5.2.3)	$Ec = \left(3320\sqrt{fc'} + 6900\right)\left(\frac{\rho}{2300}\right)^{1.5}$ = 29170 N/mm^2
Shear Modulus G	12543.10 N/mm^2

STEEL

Steel yield strength f_y	300 MPa

4.3.3.2 Calculation of the moment-curvature relationship

As mentioned in the introduction, in order to find the section properties and in particular the moment-curvature relationship for the piers to be used in the Ruaumoko3D input file, the section analysis program Cumbia [41] was used. Cumbia is a set of Matlab codes to perform monotonic moment curvature analysis and force-displacement of reinforced concrete members of rectangular or circular section. The constitutive model for the confined elements is that proposed by Mander, Priestley and Park (1988). The code allows the analysis of members subjected to axial load and single or double bending. In the calculation of the properties, the piers have been considered as single bending members as suggested by Priestley, Seible and Calvi [7] for bridges with single-column bents. For the plastic hinge length, a reasonable estimate when the plastic hinge forms against a supporting member, such as the spread footing of Port Hills, is given by:

$$L_p = 0.08L + 0.022f_{ye}d_{bl} \geq 0.044f_{ye}d_{bl}$$

Where L is the distance from the critical section of the plastic hinge to the point of the contraflexure, d_{bl} is the diameter of the longitudinal reinforcement and f_{ye}=1.1f_y= 330 MPa.
The properties of each column have been calculated considering the sections at the base and at the top, shown in the Figure 4.6.

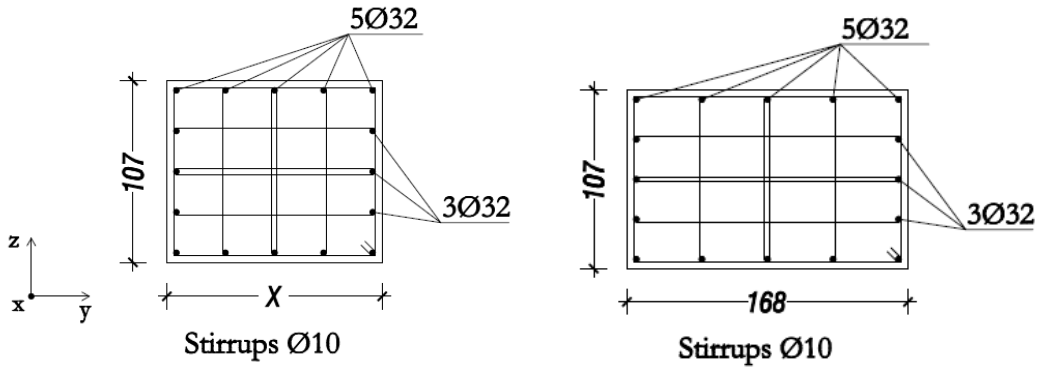

Figure 4.6. ***(a) Section of the base of the column; (b) Section of the top of the column***

Table 4.4. ***Sizes of the base's side of the piers.***

	X [m]
Pier B	1.264
Pier C	1.235
Pier D	1.207
Pier E	1.168
Pier F	1.143

The results obtained are summarized in APPENDIX B.

4.3.4 Assessment of the performance of the bridge

4.3.4.1 Description of the model

The model to better represent the mono-pier bridges is the single column-bents model, in which the piers are constrained at the base and free to move at the top. In the case study under consideration, this condition has been reproduced assuming the base of the piers fully fixed and allowing at the top the rotation around the x-x axis. This model simulate at best the behaviour of the bridge when it is subjected to a seismic action. Other restraint conditions were taken into account without finding any confirmation in the real performance of the bridge after the earthquakes.
The columns has been represented by a stepped discretization to approximate the actual geometric domain. Moreover, since the superstructure is supported on bearings, to account the increasing displacement in the bearings, a two mass model was considered, a mass for the superstructure and the other one, lumped, for the cap beam, as shown in Figure 4.7:

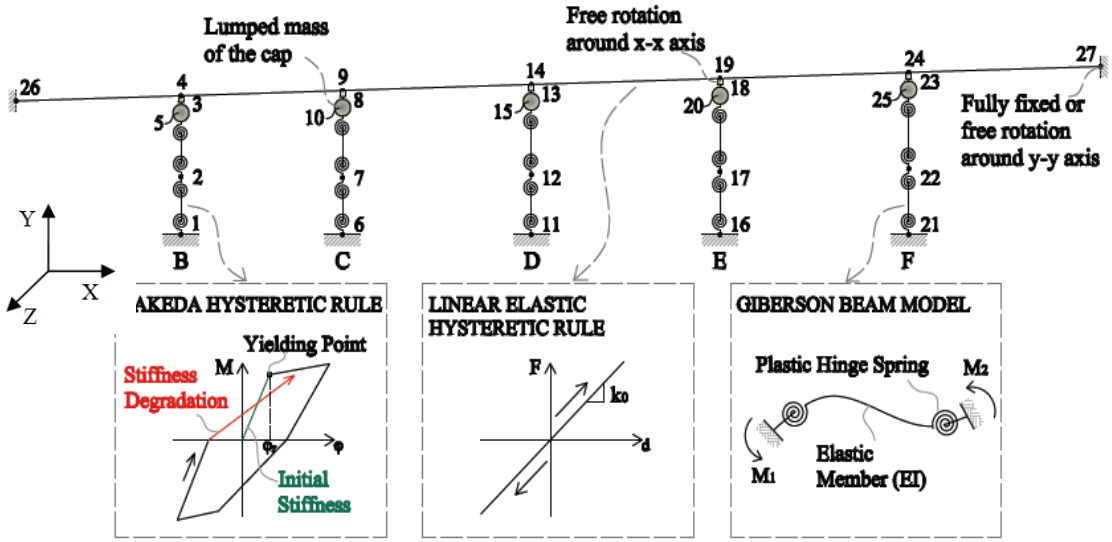

Figure 4.7. ***Model of the bridge***

Since, as shown in the drawings, each span is connected to the contiguous one by linkage rods (Figure 4.8a), the deck has been assumed continuous. Looking to the connection between the deck

and the abutment (Figure 4.9a), the analyses have been carried out changing in the model the restraint conditions next to the abutments. Two configurations have been taken into consideration:

1. Fully fixed deck
2. Free rotation of the deck around y-y axis

The second assumption is quite reasonable since there was cracking observed between the deck and the approach.

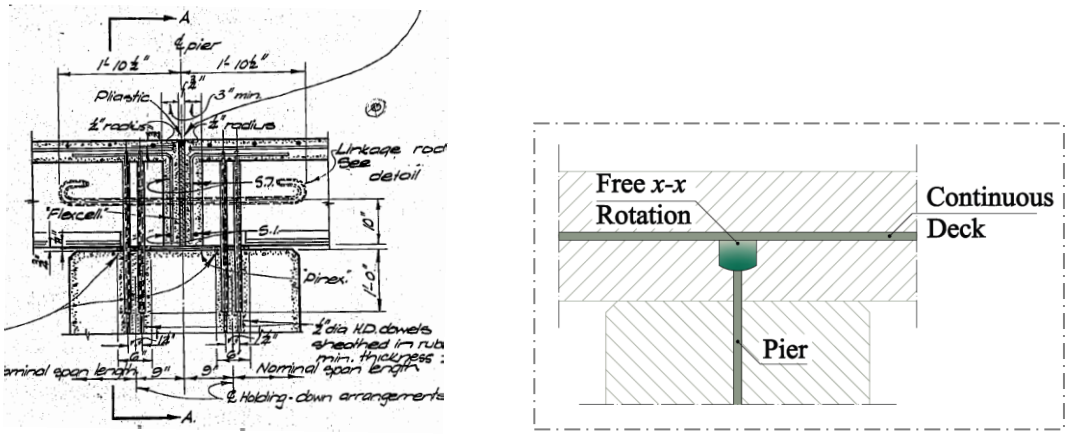

(a) **(b)**

Figure 4.8. ***Detail of the connection between the deck and the pier (a) in the drawings and (b) in the model.***

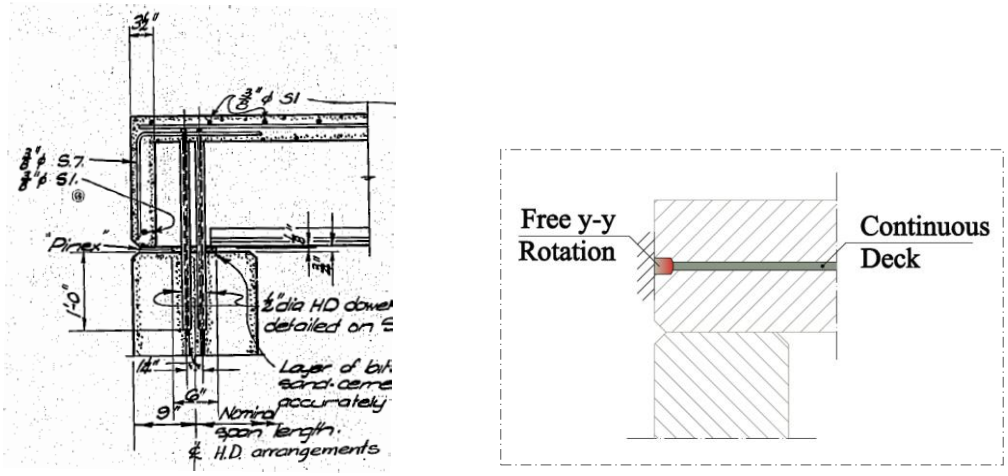

(a) **(b)**

Figure 4.9. ***Detail of the connection between the deck and the abutment (a) in the drawings and (b) in the model.***

The analyses carried out are:

1. Static Push Over Analysis (Load controlled method);
2. Push Pull Analysis;
3. Time History Analysis:
   i) Christchurch Earthquake

a) Christchurch Cashmere High School (CMHS) records
b) Catholic Cathedral College (CCCC) records
c) Heathcote Valley Primary School (HVSC) records

ii) Darfield Earthquake
a) Catholic Cathedral College (CCCC) records
b) Heathcote Valley Primary School (HVSC) records

iii) 10 Earthquake with the scaling of the spectra according to NZ code

All these analyses are performed with the software Ruaumoko3D [40]: in the tridimensional models characteristic of the bridge as mass, stiffness and damping can be appropriately located and concentrated at specified point of the model.

4.3.4.2 Modal Assessment

In order to determine what level of the current code level of seismic shaking the bridge was subjected to, a spectral analysis was performed. The response spectra were formed based on the motions of both Darfield and Christchurch earthquakes recorded at the nearest seismic stations. The NZS1170.5 [21] response spectra was determined for the bridge site for a 1/500 year earthquake. The modes of the bridge were then compared against the response spectra, and the code spectra to see what percentage of the code acceleration was activated for the range of the modes. Even if using the current code standard to assess a bridge built in the 1970's was not the most correct to undertake this analysis, since it is only for comparative purposes, it will be sufficient.
The natural period of the structure fall in the range 0.17-0.27 s, depending on the material properties and on the costraint conditions. The first three modal frequencies, considering design properties and fully fixed abutments are shown in Table 4.5. The structure is very stiff with the largest natural period being less than 0.3 s, as the most of the bridges of 1960-70's in Christchurch area. The sudden sharp rise, seen in Table 4.5, as periods tend towards zero is unusual. It is believed to be caused due to inaccuracies introduced into the numerical analysis when the period approaches the size of the time step. Carr [42] suggests that accuracy cannot be guaranteed below a period of $T < 10\Delta t$, as shown by the broken grey line on the Figure 4.11 for the time step of the acceleration record of $\Delta t = 0.05s$.

Table 4.5. ***Frequencies and fundamental periods of the structure with the corresponding percentage of damping.***

MODE	Frequency	Period	% Damping	Transverse mass (%)	Longitudinal mass (%)
1	5.625	0.178	5.00	61	19
2	13.44	0.074	5.00	61	19
3	22.44	0.045	6.78	73	57

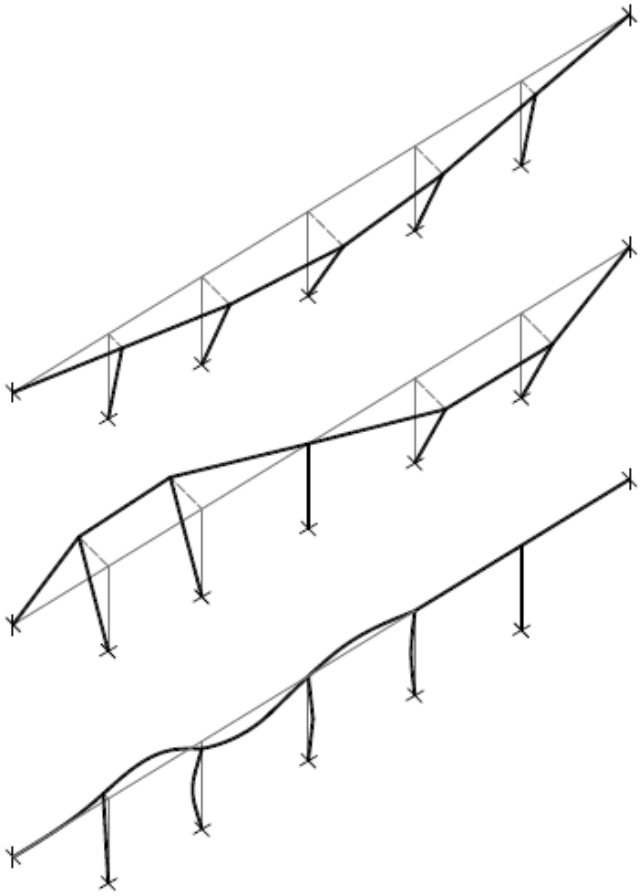

Figure 4.10. ***Mode shapes 1, 2 and 3***

A site response spectra was made for the two orthogonal horizontal acceleration records measured at the closest SMA Heathcote Valley Primary School (HVSC), and from the next closest stations , that are Christchurch Cashmere High School (CMHS) and Christchurch Cashmere High School (CMHS) and Catholic Cathedral College (CCCC). The results are shown in Figure 4.11.

The code curve for 5% damping was plotted on the same figure. The hazard factor was set at Z = 0.22, which is the standard for Christchurch. The risk factor was R = 1.0, as the eastern suburbs of Christchurch were estimated to have been subjected to a 1/500 year event for the shorter period structures [19]. The near-fault factor was set at 1.0 to account for the lack of nearby faults. The soil was determined to be a NZS1170.5 Class C soil. This was determined based on the CPT tests which were converted into a SPT blow count using the Kulhawy & Mayne [43] emperical correlation between the ratio between normalized cone tip resistance and uncorrected SPT blow counts, and fine content (FC).

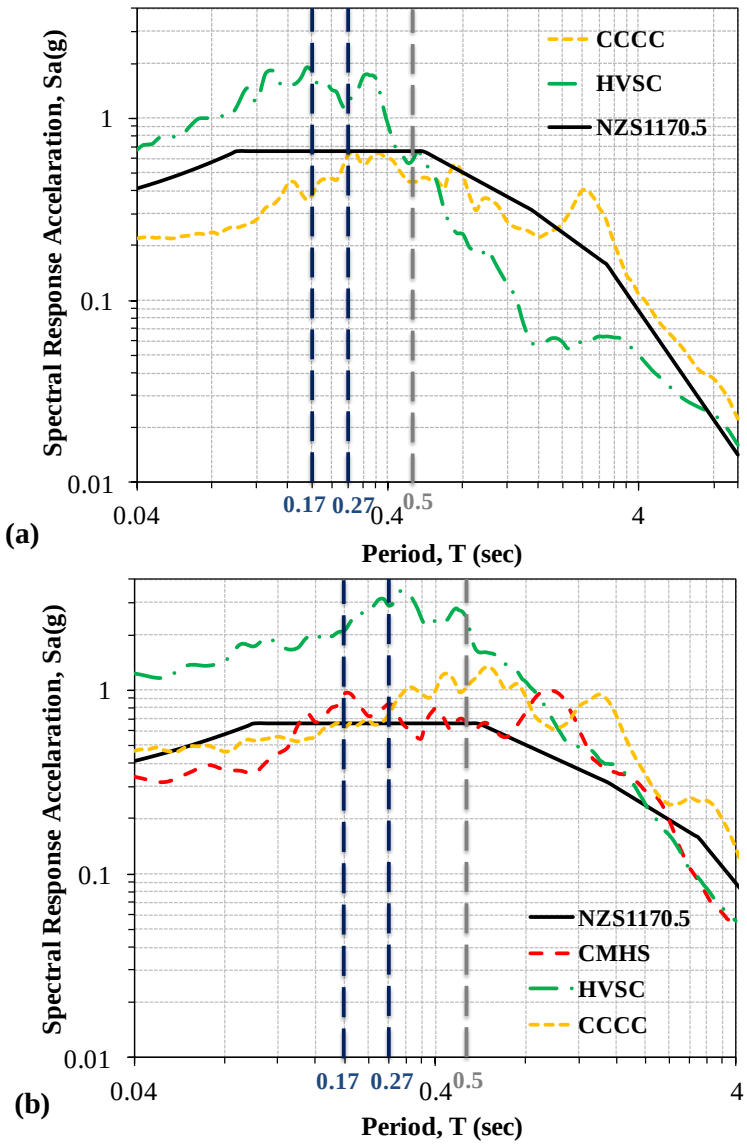

Figure 4.11. ***Site Response for Port Hills Overbridge for the fundamental periods of the structure, depending on the model and on the material properties, with (a) Darfield earthquake records and (b) Lyttelton earthquake records.***

First of all the figures show that there is a difference in frequency content between the two earthquakes. Considering the records from Catholic Cathedral College (CCCC), the 2010 earthquake demand in the range of natural periods of the structure, is below the NZS1170 design spectral acceleration, whereas in the 2011 event the demand acceleration is match quite well the trend of the design spectrum. The site response from HVSC, though nearby the bridge under consideration, for both earthquakes is much greater than the design one, due to topographic effects: the seismic waves are amplified because the recording station is located on a promontory, with the same geotechnical characteristics of the site of interest.

Comparing the code demand response to the site demand response for the given period of the bridge, for the first mode of the bridge, for 5% damping, the spectral acceleration in the 2010 earthquake of the site has an average value of 0.45 g, less than the NZS 1/500 year design spectrum value of 0.66 g. This observation implies a good dynamic response of the bridge to the earthquake, moreover confirmed by the absence of significant damage after the event. This conclusion is dampened a little since the bridge was built in the 1970's to different seismic standards.
If the 2010 earthquake demand at natural periods below 1.5 s was almost below the NZS1170 design spectral acceleration, in the 2011 event, the demand acceleration was well above the design acceleration for most of the natural period range given. For the range above 1.5 s both earthquakes were above the NZS1170 design spectral acceleration. For the range of the natural periods of the structure, the CCCC records match quite well the design spectrum, while the CHMS ones are slightly higher than spectral design accelerations with a maximum of 0.95 at 0.2 s. It can be concluded then that the structure after the Christchurch earthquake have also been damaged by forces due to the dynamic excitation of the mass of the bridge.

4.3.4.3 Nonlinear Static Push Over Analysis

This is one of the most powerful equivalent seismic load analysis tools to determine the sequence of inelastic actions, the formation of local mechanism, and the formation of a global collapse mode. In the analysis all forces are scaled until the first collapse of the columns occurs. Since change of member stiffness due to the cracking and formation of flexural hinge can constitute events, to simplify matters, the reduced stiffness is used for the piers as mentioned in the introduction.

4.3.4.3.1 MOMENT - CURVATURE RELATIONSHIP

The Table 4.6 reports the results obtained from the analysis in terms of moment-curvature relationship. The comparison with the table it's possible to notice the good correspondence with the values obtained with Cumbia [41]. This first analysis allows a prediction of failure modes of the structure: the results show that the first column to plasticize first and to collapse then, is the middle one, the pier D. The comparison with the actual behaviour of the structure gives a first indication of the good approximation of the model, at least in global terms. In fact, from the inspections, at the base of the central pier there was the formation of a plastic hinge and two of the corner reinforcing bars buckling over a length of 150 mm. At the top the lack of any crack means that the pier in this part behaved elastically, justifying the choice to put a hinge at the connection with the deck.

Table 4.6. Moment – curvature graphics of each pier

	DATA	TOP	BASE
PIER B	▪ Element: Giberson ▪ Hysteretic rule: Takeda ▪ $E_{c,design}$ 23572 MPa ▪ $E_{c,real}$ 29170 MPa ▪ Bilinear Factor - 0.002	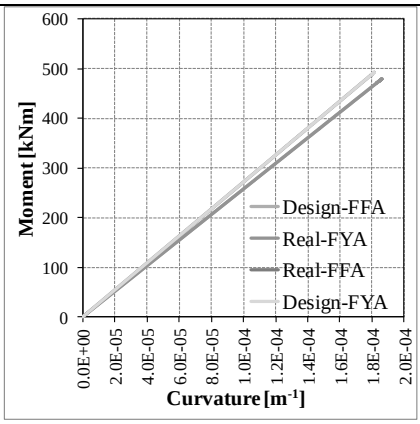	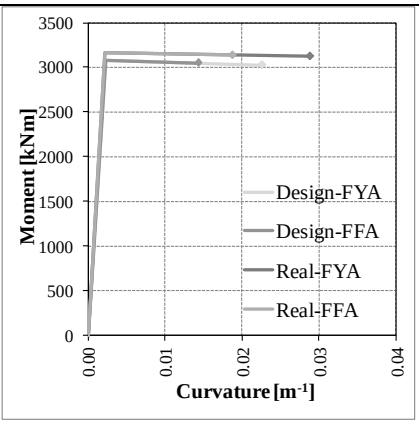
PIER C	▪ Element: Giberson ▪ Hysteretic rule: Takeda ▪ $E_{c,design}$ 23572 MPa ▪ $E_{c,real}$ 29170 MPa ▪ Bilinear Factor - 0.002	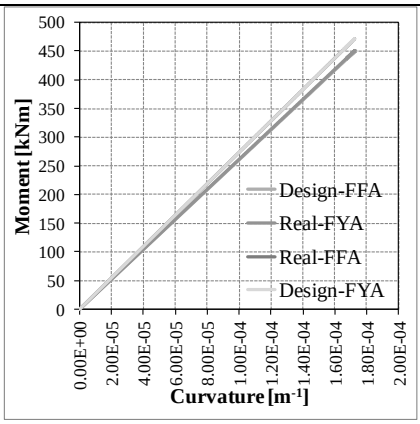	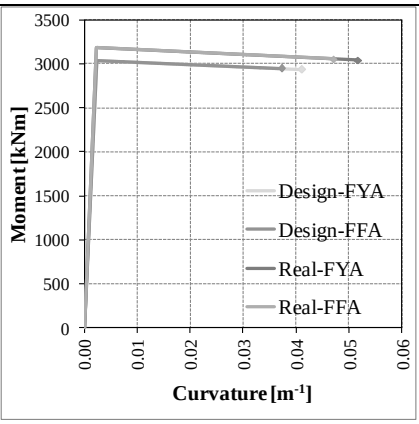
PIER D	▪ Element: Giberson ▪ Hysteretic rule: Takeda ▪ $E_{c,design}$ 23572 MPa ▪ $E_{c,real}$ 29170 MPa ▪ Bilinear Factor - 0.003	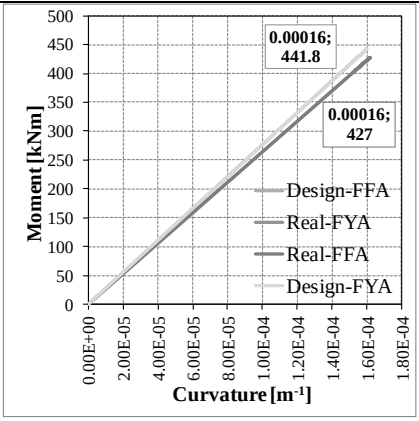	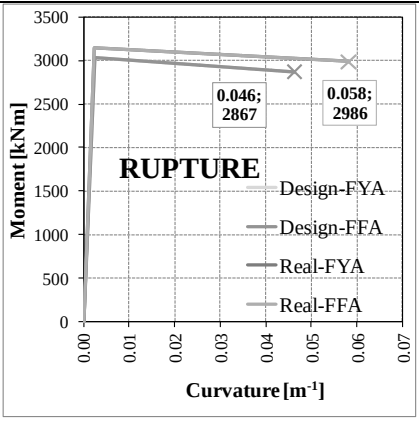

PIER E	▪ Element: Giberson ▪ Hysteretic rule: Takeda ▪ $E_{c,design}$ 23572 MPa ▪ $E_{c,real}$ 29170 MPa ▪ Bilinear Factor - 0.003	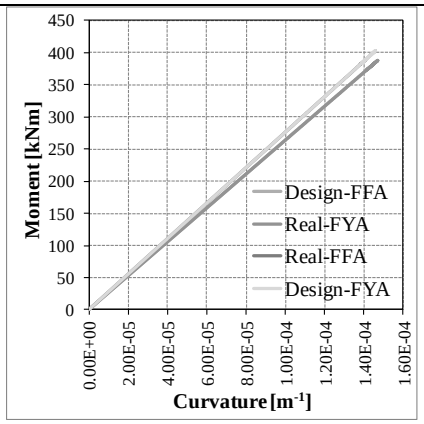	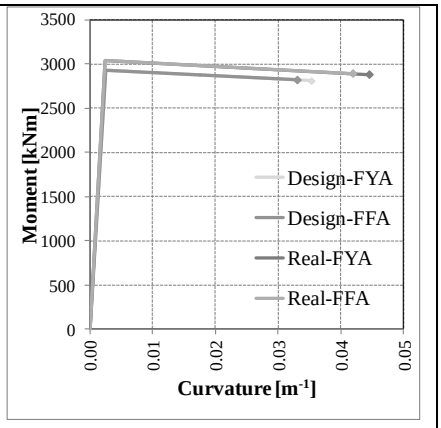
PIER F	▪ Element: Giberson ▪ Hysteretic rule: Takeda ▪ $E_{c,design}$ 23572 MPa ▪ $E_{c,real}$ 29170 MPa ▪ Bilinear Factor - 0.001	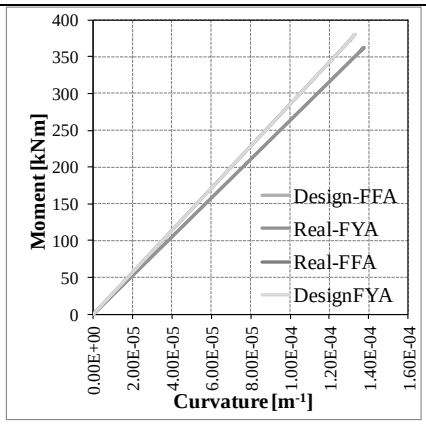	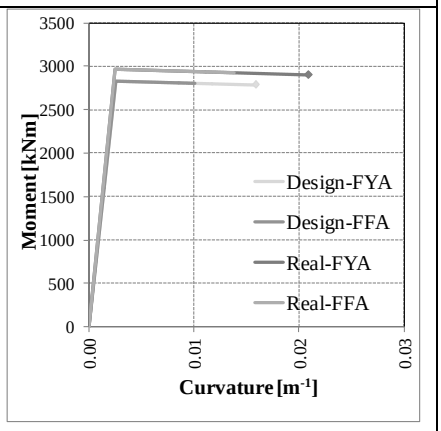

4.3.4.3.1.1 TIME-DISPLACEMENT RELATIONSHIP

The comparison between the two models in terms of displacement is shown in the graph of Figure 4.12.

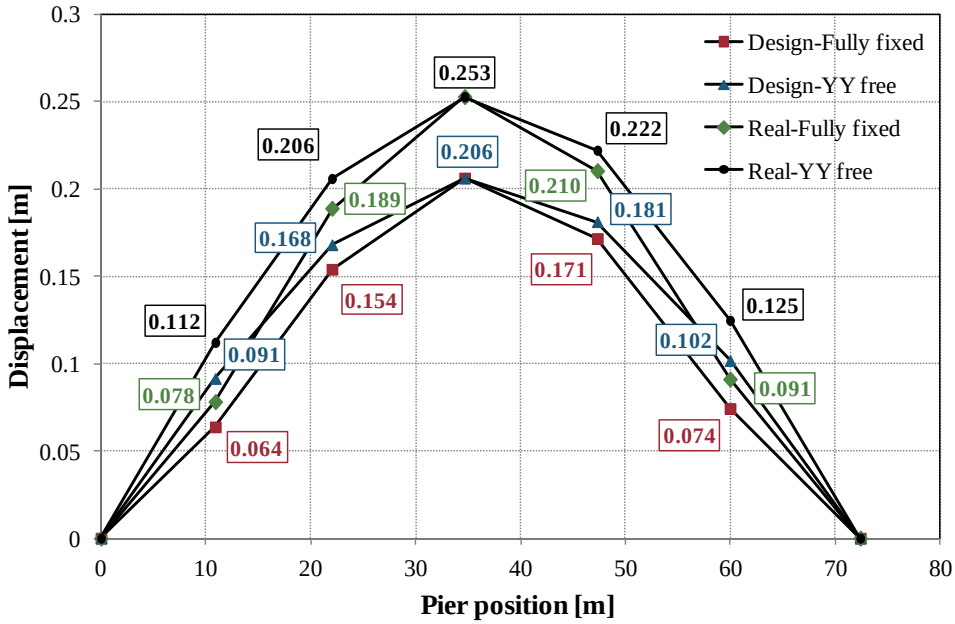

Figure 4.12. ***Displacement profile of each model***

The graphic shows that the peak displacement reached by the pier D is the same, in both prototype, for the fully fixed and for the free rotation around y-y axis case. Moreover, it's interesting to notice that, changing over from design to actual properties, the maximum displacement increase in just 5 cm.

4.3.4.3.1.2 PUSH OVER CURVES

The push over curves of the two different restraint conditions considered are shown below (Figure 4.13). From them it's possible to find the displacement ductility factor considering just the force acting at the base of the pier D.

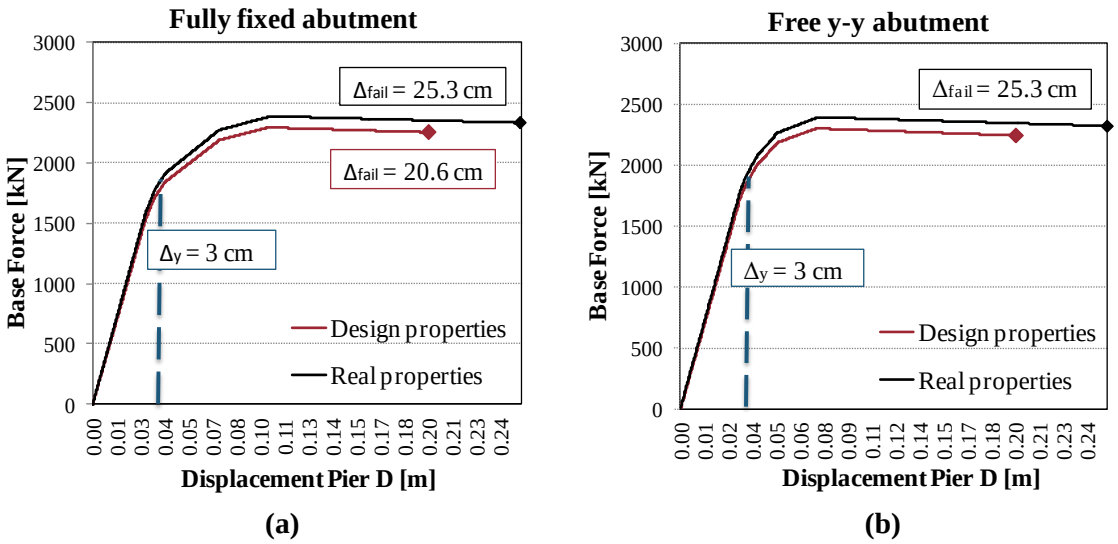

Figure 4.13. ***Pushover curves of the central pier for different material properties and for the two configuration of the model: (a) with fully fixed abutment and (b) with the deck free to rotate around the y-y axis.***

$$\mu_{design} = \frac{\Delta_{\varepsilon c=0.064}}{\Delta_y} = \frac{0.14}{0.03} = 4.75$$

$$\mu_{real} = \frac{\Delta_{\varepsilon c=0.064}}{\Delta_y} = \frac{0.21}{0.03} = 7.43$$

The P-Delta effects weren't considered since the natural period of the structure don't exceed 0.45 s, so that the most restrictive criteria suggested by the Bridge Manual, Section 5 (§5.2.8) [29] is satisfied.

4.3.4.4 Push pull analysis

In order to anticipate the performance of the structure, the assessment was complemented with a push pull analysis to evaluate the dissipative behavior of the bridge. The structure is subjected to increasing levels of force until the collapse. The Figure 4.14 shows the result of the analysis: the total envelope of the curve match the static pushover curve and the underlying area correspond to the dissipate energy of the system.

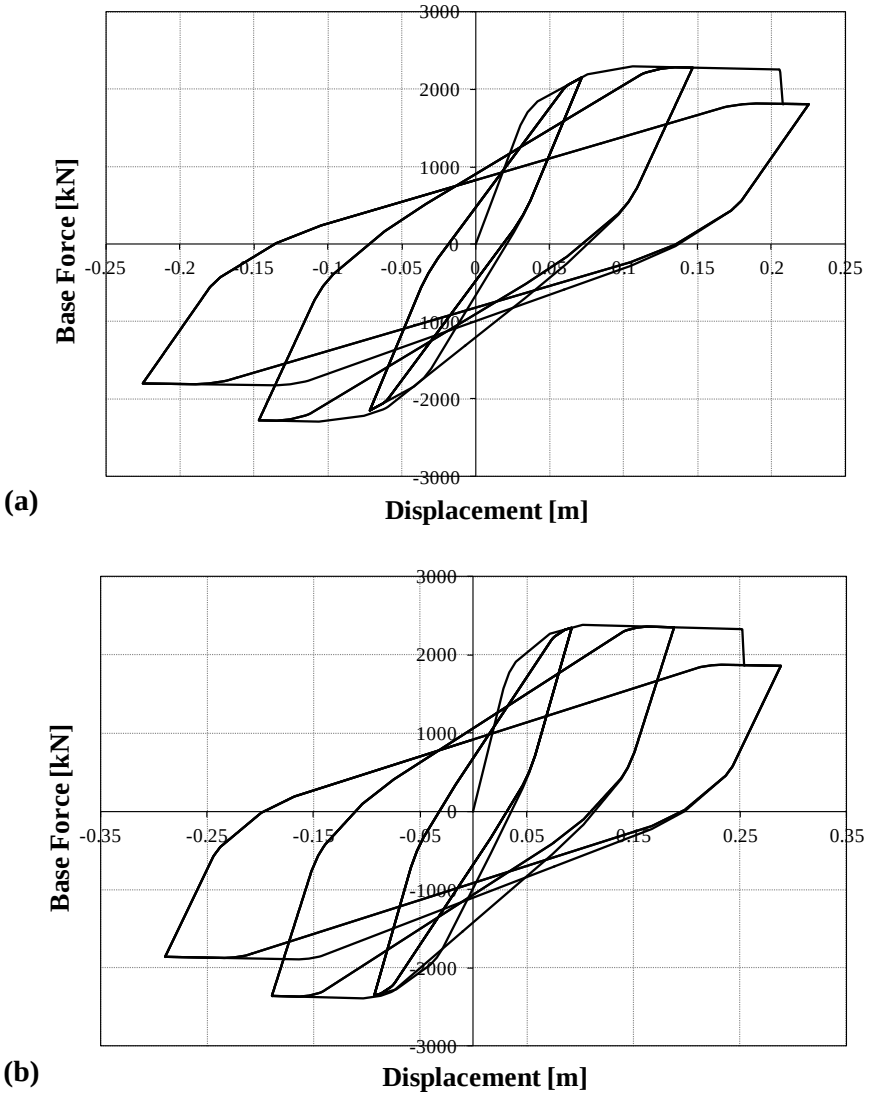

Figure 4.14. ***Push pull curves of the central pier for (a) design and (b) actual properties***

4.3.4.5 Nonlinear Time History Analysis

The M_w 7.1 Darfield earthquake, on September 4, 2010 , occurred with an epicenter near the town of Darfield, 30-40 km west of the Christchurch Central Business District (CBD). Large vertical accelerations were registered in the region of fault rupture, typical of the near-source strong motion recordings. The M_w 6.1 February 22, 2011 Christchurch earthquake, considered part of the aftershock sequence of the 2010 Darfield event, had an epicenter less than 10km from the Christchurch CBD between Lyttelton and the south eastern edge of the city (Figure 4.15). The close proximity and shallow depth of this event caused higher intensity shaking in Christchurch relative to the Darfield event. Despite the short duration (15-20 seconds) the February 22, 2011 event recorded one of the highest maximum Peak Ground Acceleration (PGA_{max}=2.1g, close to epicenter) in the world experienced close to an important city. In the CBD, ground motions were characterized by large vertical accelerations as well, resulting from a reverse-thrust faulting mechanism. Further

aftershocks occurred during the following months, one of the strongest was the M_w 6.0 on June 13, 2011, with an epicenter again on the south eastern edge of the city (Table 4.7).

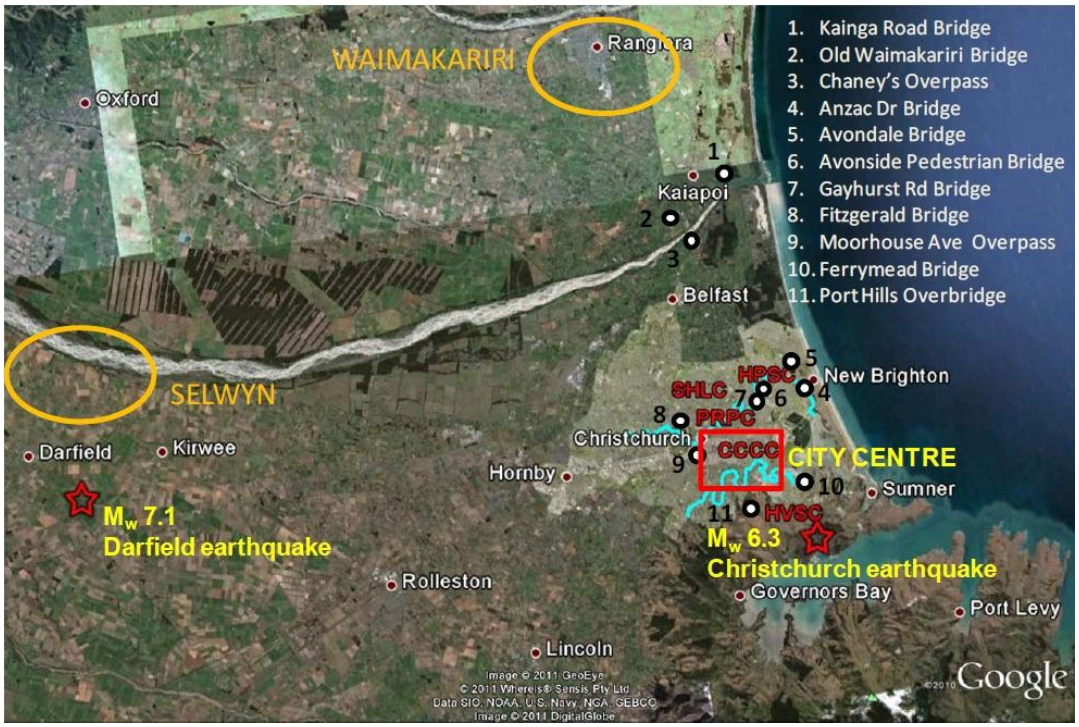

Figure 4.15. ***Aerial view of Christchurch and surrounding region, indicating the locations of a selection of damaged bridges, strong motion stations, Central Business District (CBD, red square) and the epicentres of the major earthquakes (Google Inc., 2011)***

Table 4.7. ***Comparison of peak ground accelerations in the vicinity of Christchurch for the Darfield, Lyttelton and Sumner earthquakes (geometric mean of horizontal PGAs)***

Event	M_w	PGA	
		Maximum Horizontal	Maximum Vertical
Darfield, September 4, 2010	7.1	0.71g	0.95g
Lyttelton, February 22, 2011	6.2	1.31g	1.63g
Sumner, June 13, 2011	6.0	1.35g	1.05g

4.3.4.5.1.1 LYTTELTON EARTHQUAKE , FEBRUARY 22, 2011

A non-linear time history analysis was performed using existing earthquake records. Data records obtained from Strong Motion Accelerographs were used. Records from the closest SMA (Heathcote Valley Primary School, HVSC) to the Port Hills Road Overpass were deemed by Wood et al (2011) to be too large to accurately represent the ground motion at the bridge site due to topographic effects, so records from the next closest stations, Christchurch Cashmere High School (CMHS) and Catholic Cathedral College (CCCC), were used also (see Appendix C). The soil conditions at the Cashmere site were assumed to be similar to those at the bridge site, but the sites were much further away from the bridge and epicenter, so the PGA recorded at these stations is expected to be smaller than that felt at the bridge site. Analysis was conducted with all records, used separately; the response of the bridge in reality is likely to have been between the responses predicted by each record.

Since in this earthquake the vertical component was important compared to the horizontal ones, time history analyses are performed considering only the two orthogonal horizontal components first, and introducing then the contribution of the vertical acceleration. This procedure allow to catch the influence of the vertical components on the response of the bridge.

In order to better identify the differences between the different boundary conditions, we choose to address separately the two cases with the design and with the real properties. The actual displacement of the structure at the level of the deck, are so compared with the cracking and the yielding displacement. The first one can be obtained knowing the cracking moment, given by the following condition:

$$f_{ct} = \frac{N_{Ed}}{bh} + \frac{M_{cr}}{bh^2} \cdot 6$$

Assuming the concrete tensile strength equal to zero:

$$M_{cr} = \frac{N_{Ed}}{bh} \cdot \frac{bh^2}{6}$$

The cracking curvature is given by the formula:

$$\emptyset_{cr} = \frac{M_{cr}}{EI_{gr}}$$

Where I_{gr} is the inertial moment of the concrete section. Therefore the cracking displacement is calculated as:

$$\Delta_{cr} = \frac{\emptyset_{cr} \cdot L^2}{3}$$

Where L is the length of the pier.

The same formula is used to calculate the yielding displacement:

$$\Delta_{y} = \frac{\emptyset_{y} \cdot L^2}{3}$$

Where φ_y is the yielding curvature as resulted from analyses with Cumbia and L is the length of the pier.

a) *Analyses with only horizontal components of the motion.*

First of all the components of the motions need to be thrown on the axis of the bridge. The drawings show the orientation of the bridge and with simple trigonometric calculations it's possible to find the component of the earthquake acting on the structure, for each ground motion record (Figure 4.16, Figure 4.17 and Figure 4.18).

1. Christchurch Cashmere High School, CMHS

$$X_{COMP} = N10E \cdot \cos 29.5° + S80E \cdot \cos 60.5°$$

$$Y_{COMP} = 0$$

$$Z_{COMP} = N10E \cdot \text{sen}\, 29.5° - S80E \cdot \text{sen}\, 60.5°$$

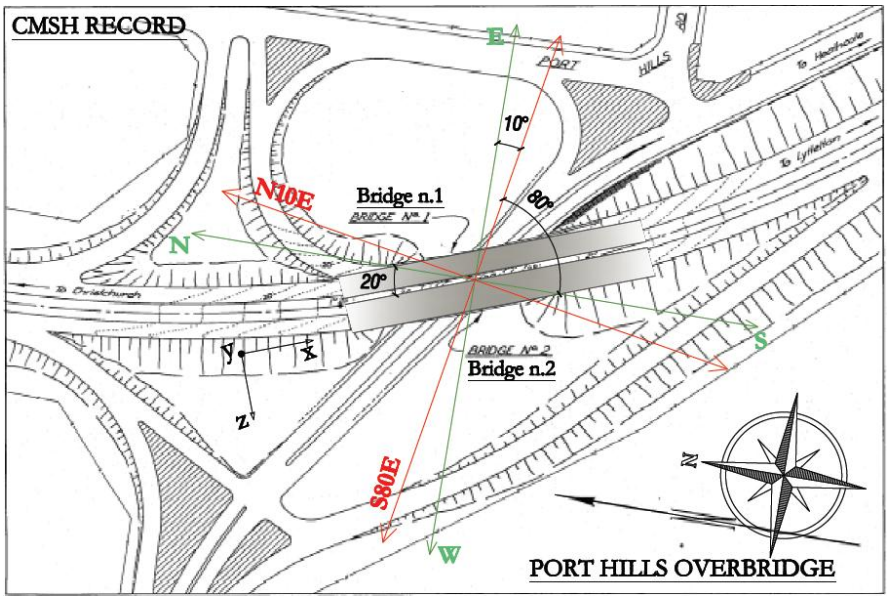

Figure 4.16. ***Components of the motion recorded at Christchurch Cashmere High School station***

3. Catholic Cathedral College ,CCCC

$$X_{COMP} = N26W \cdot \cos 6.5° + N26W \cdot \cos 83.5°$$

$$Y_{COMP} = 0$$

$$Z_{COMP} = N26W \cdot \text{sen}\, 6.5° + N26W \cdot \text{sen}\, 83.5°$$

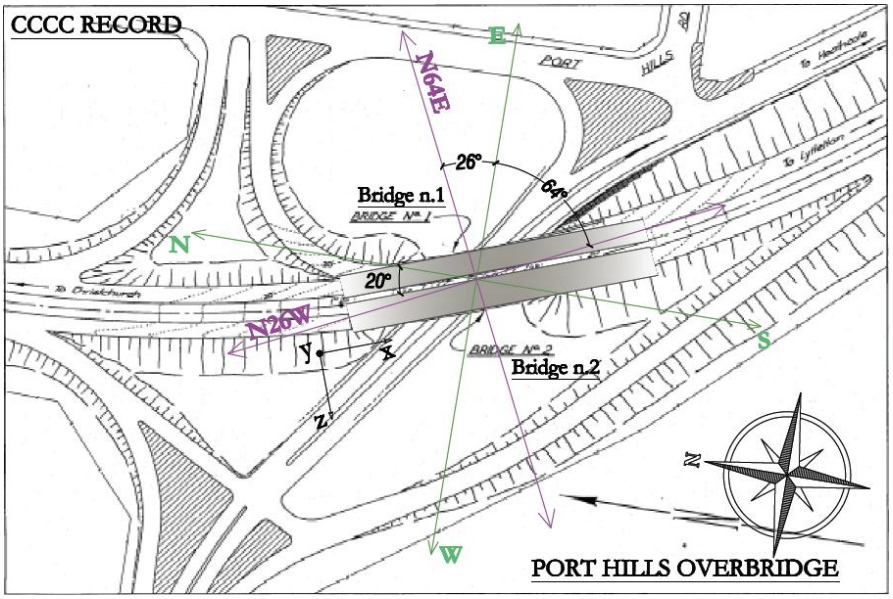

Figure 4.17. ***Components of the motion recorded at Catholic Cathedral College station***

4. *Heathcote Valley Primary School, HVSC*

$$X_{COMP} = S26W \cdot \cos 45.5° + S64E \cdot \cos 44.5°$$

$$Y_{COMP} = 0$$

$$Z_{COMP} = S26W \cdot \text{sen}\, 45.5° - S64E \cdot \text{sen}\, 44.5°$$

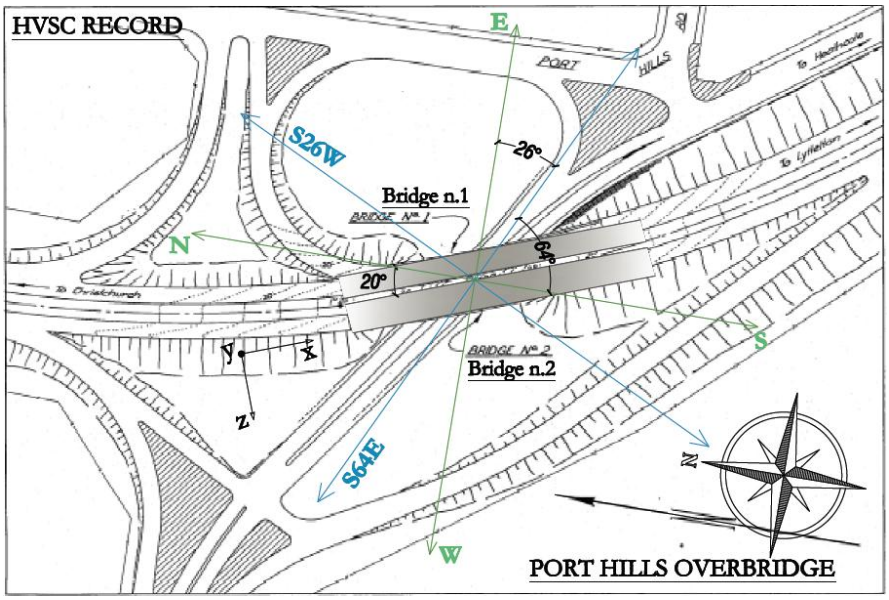

Figure 4.18. ***Components of the motion recorded at Heathcote Valley Primary School station***

The results of the time history analyses, considering the design properties, are shown below.

1. Christchurch Cashmere High School, CMHS

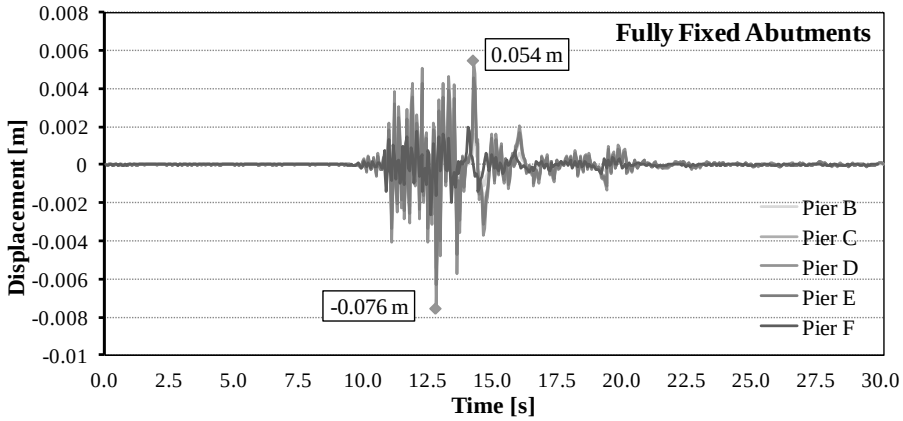

Figure 4.19. ***Displacement time history of the top of the piers in the fully fixed abutments model, with records from CMHS***

Table 4.8. ***Summary of the displacement of the top of the piers in the fully fixed abutments model, with records from CMHS***

	X	Δ_{max}	Δ_{min}	ϕ_y	H	Δ_y		
Piers	**m**	**m**	**m**	**m^{-1}**	**m^2**	**m**		
B	10.90	0.0016	-0.0021	0.0023	5.85	0.0258	elastic	elastic
C	22.02	0.0040	-0.0054	0.0023	6.13	0.0291	elastic	elastic
D	34.67	0.0054	-0.0076	0.0024	6.45	0.0336	elastic	elastic
E	47.32	0.0046	-0.0063	0.0025	6.77	0.0382	elastic	elastic
F	59.97	0.0020	-0.0026	0.0026	7.09	0.0429	elastic	elastic

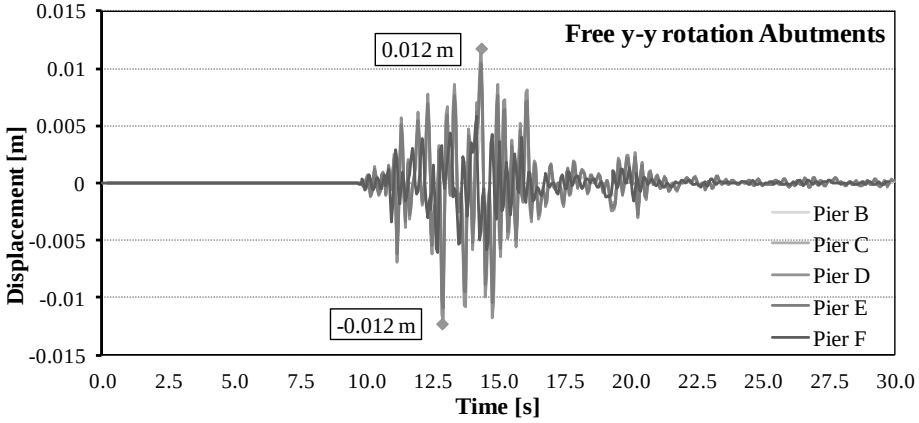

Figure 4.20. ***Displacement time history of the top of the piers in the free YY abutments model, with records from CMHS***

Table 4.9. ***Summary of the displacement of the columns in the free YY abutments model, with records from CMHS***

	X	Δ_{max}	Δ_{min}	ϕ_y	H	Δ_y		
Piers	**m**	**m**	**m**	**m^{-1}**	**m^2**	**m**		
B	10.90	0.0050	-0.0052	0.0023	5.85	0.0258	elastic	elastic
C	22.02	0.0094	-0.0098	0.0023	6.13	0.0291	elastic	elastic
D	34.67	0.0117	-0.0123	0.0024	6.45	0.0336	elastic	elastic
E	47.32	0.0104	-0.0109	0.0025	6.77	0.0382	elastic	elastic
F	59.97	0.0059	-0.0061	0.0026	7.09	0.0429	elastic	elastic

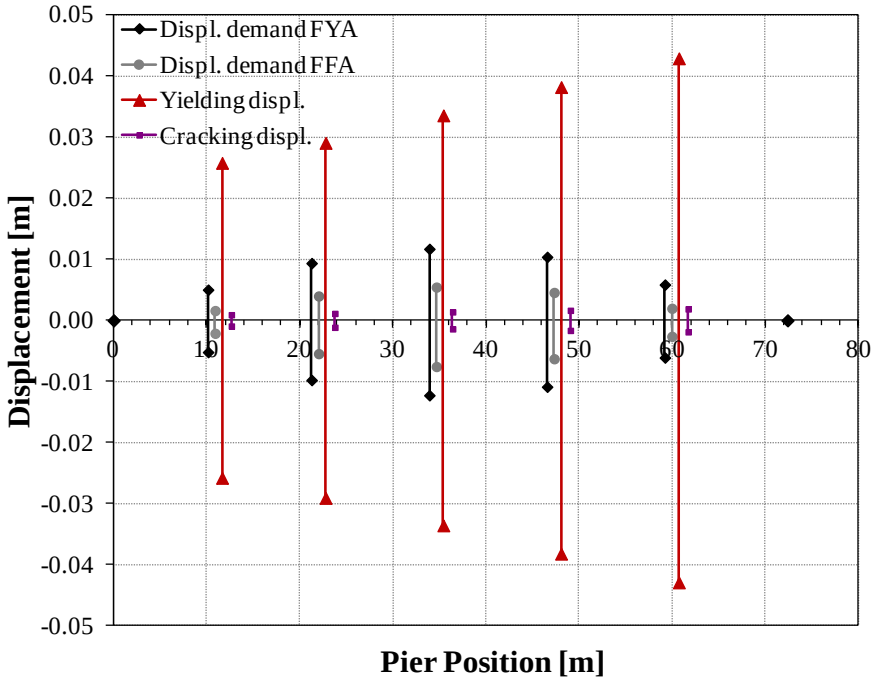

Figure 4.21. ***Comparison between the displacements of the structure of the two configurations (FFA and FYA) and the yielding ones, with records from CMHS***

2. Catholic Cathedral College ,CCCC

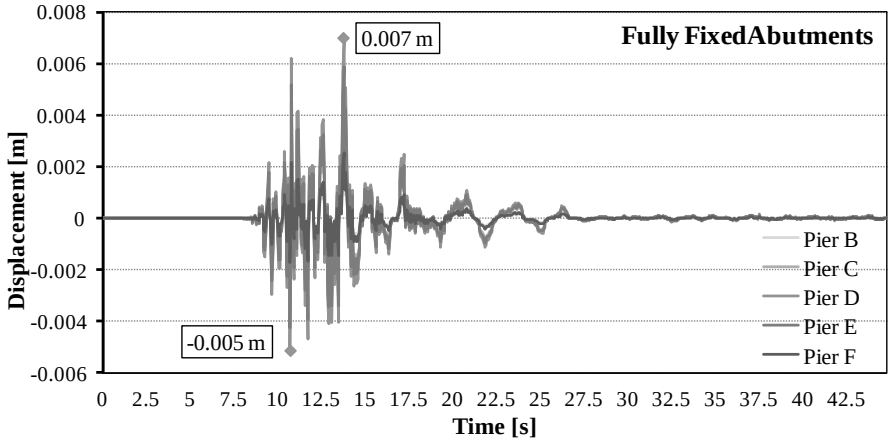

Figure 4.22. ***Displacement time history of the top of the piers in the fully fixed abutments model, with records from CCCC***

Table 4.10. ***Summary of the displacement of the top of the piers in the fully fixed abutments model, with records from CCCC***

	X	Δ_{max}	Δ_{min}	ϕ_y	H	Δ_y		
Piers	**m**	**m**	**m**	**m^{-1}**	**m^2**	**m**		
B	10.90	0.0021	-0.0014	0.0023	5.85	0.0258	elastic	elastic
C	22.02	0.0051	-0.0037	0.0023	6.13	0.0291	elastic	elastic
D	34.67	0.0070	-0.0051	0.0024	6.45	0.0336	elastic	elastic
E	47.32	0.0059	-0.0042	0.0025	6.77	0.0382	elastic	elastic
F	59.97	0.0025	-0.0017	0.0026	7.09	0.0429	elastic	elastic

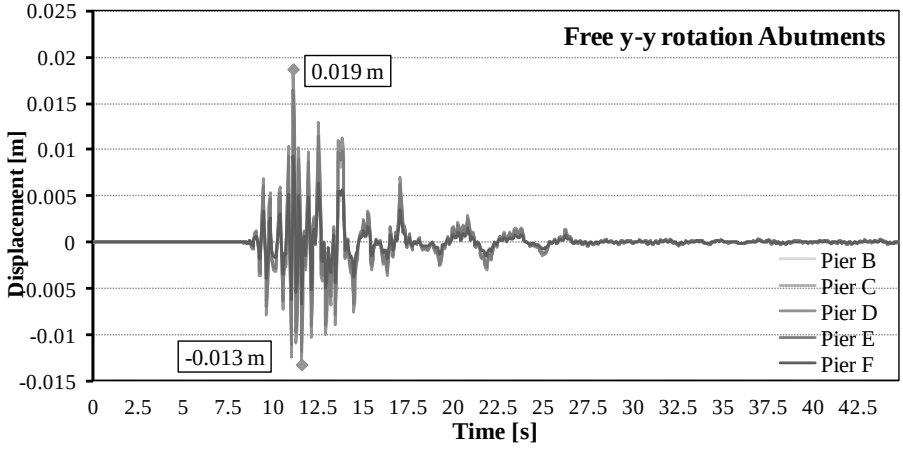

Figure 4.23. ***Displacement time history of the top of the piers in the free YY abutments model, with records from CCCC***

Table 4.11. ***Summary of the displacement of the columns in the free YY abutments model, with records from CCCC***

	X	Δ_{max}	Δ_{min}	ϕ_y	H	Δ_y		
Piers	**m**	**m**	**m**	**m^{-1}**	**m^2**	**m**		
B	10.90	0.0079	-0.0056	0.0023	5.85	0.0258	elastic	elastic
C	22.02	0.0149	-0.0106	0.0023	6.13	0.0291	elastic	elastic
D	34.67	0.0186	-0.0133	0.0024	6.45	0.0336	elastic	elastic
E	47.32	0.0165	-0.0118	0.0025	6.77	0.0382	elastic	elastic
F	59.97	0.0093	-0.0066	0.0026	7.09	0.0429	elastic	elastic

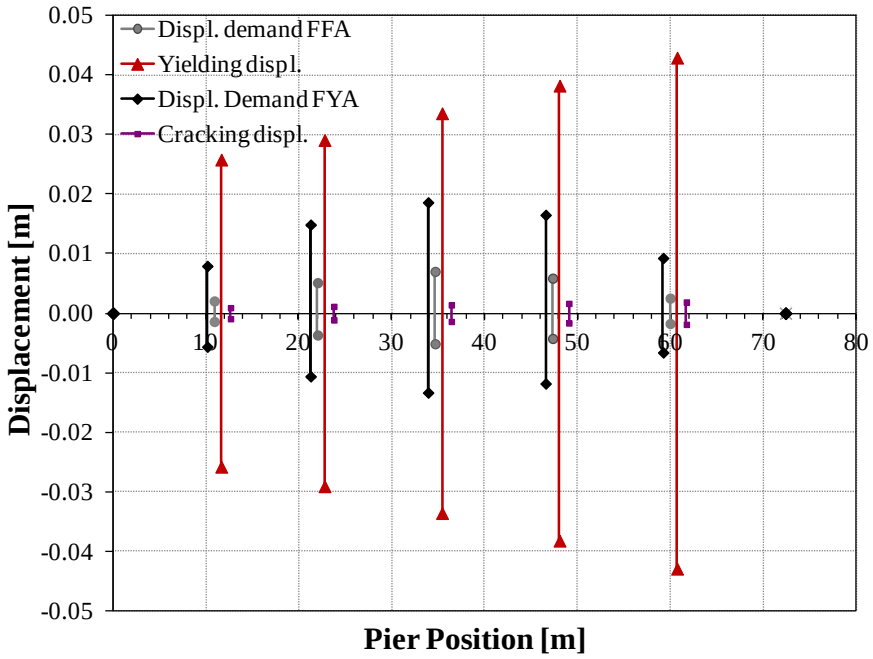

Figure 4.24. ***Comparison between the displacements of the structure of the two configurations (FFA and FYA) and the yielding ones, with records from CCCC.***

Heathcote Valley Primary School, HVSC

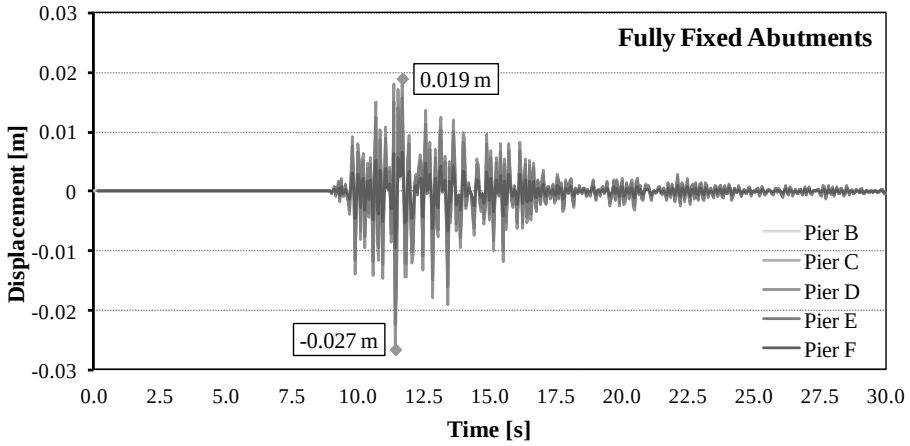

Figure 4.25. ***Displacement time history of the top of the piers in the fully fixed abutments model, with records from HVSC***

Table 4.12. ***Summary of the displacement of the top of the piers in the fully fixed abutments model, with records from HVSC***

	X	Δ_{max}	Δ_{min}	ϕ_y	H	Δ_y		
Piers	**m**	**m**	**m**	**m^{-1}**	**m^2**	**m**		
B	10.90	0.0054	-0.0077	0.0023	5.85	0.0258	elastic	elastic
C	22.02	0.0138	-0.0195	0.0023	6.13	0.0291	elastic	elastic
D	34.67	0.0189	-0.0266	0.0024	6.45	0.0336	elastic	elastic
E	47.32	0.0158	-0.0223	0.0025	6.77	0.0382	elastic	elastic
F	59.97	0.0067	-0.0096	0.0026	7.09	0.0429	elastic	elastic

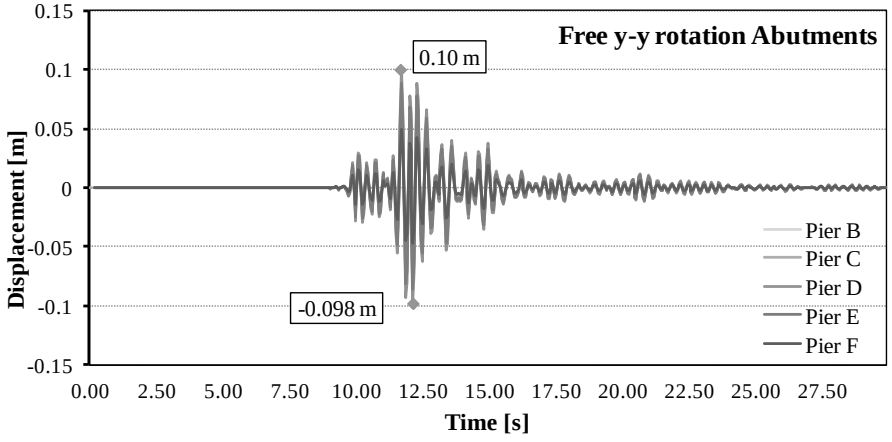

Figure 4.26. ***Displacement time history of the top of the piers in the free YY abutments model, with records from HVSC***

Table 4.13. ***Summary of the displacement of the columns in the free YY abutments model, with records from HVSC***

	X	Δ_{max}	Δ_{min}	ϕ_y	H	Δ_y		
Piers	**m**	**m**	**m**	**m^{-1}**	**m^2**	**m**		
B	10.90	0.0430	-0.0417	0.0023	5.85	0.0258	yielded	yielded
C	22.02	0.0806	-0.0785	0.0023	6.13	0.0291	yielded	yielded
D	34.67	0.1003	-0.0979	0.0024	6.45	0.0336	yielded	yielded
E	47.32	0.0882	-0.0860	0.0025	6.77	0.0382	yielded	yielded
F	59.97	0.0490	-0.0477	0.0026	7.09	0.0429	yielded	yielded

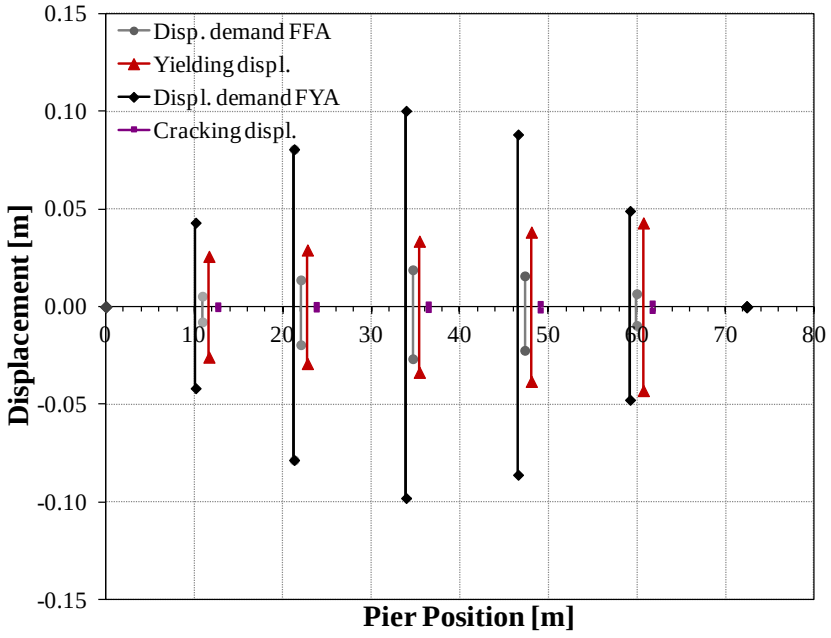

Figure 4.27. ***Comparison between the displacements of the structure of the two configurations (FFA and FYA) and the yielding ones, with records from HVSC.***

Some observation can be made at this point of the analysis. First of all in all the cases displacements exceed the cracking point. This is consistent with field observations but at the same time do not allow to identify the model and the records which better simulate the real performance of the structure during the Christchurch Earthquake. Graphics show that the bridge remains in the elastic range in both the configurations when subjected to records from CMHS and CCCC. The only one case in which the yield displacement is exceeded is when the deck is free to rotate around the vertical axis and ground motion records from HVSC act on the structure. Signals of the formation of plastic hinges after the earthquake were observed. Results seem to suggest that the connection next to the abutment is not totally fixed and that the ground motion suffered from the structure was stronger than the ones recorded at CMHS and CCCC stations. It's nevertheless true that this results are obtained without considering the vertical component of the earthquake, that can influence the performance of the bridge as its contribution was very important, with values of acceleration never recorded before. Results obtained with the actual properties are not reported since the differences are in the order of the 5%.

b) Analyses including the vertical component of the motion.

The vertical acceleration of the ground motion is now taken into account to simulate the real performance of the structure since its contribution in the Lyttelton earthquake was very important, with values up to 2.2g in HVSC station. To catch the response of the piers, the BEAM –COLUMN model is used for the piers. By knowing the yielding moments in the two orthogonal directions (y and z) and the axial yield forces (compression and tension), it's possible to identify for each pier the interaction diagram of the concrete section (Figure 4.28). Each stress state (that is each tern N, M_y and M_z) thus identifies a point in the 3D space. The section has an elastic behavior if the point is inside the domain. Therefore for all the values of the axial force acting on the piers during the earthquake, different interaction domains M_y-M_z are obtained sectioning the 3D surface with the plane N=cost.

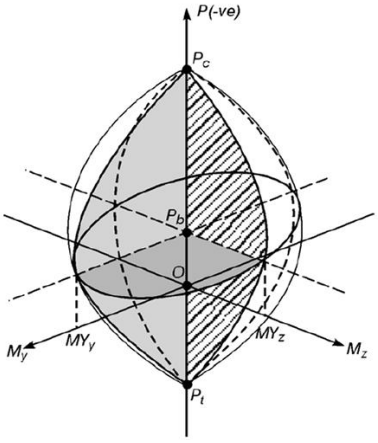

Figure 4.28. ***Interaction diagram of a reinforced concrete section [Ruaumoko3D Manual]***

The yielding interaction surface built by Ruaumoko3D [40] is given by the following equation [44]:

$$\left\{\frac{P - PB}{Py - PB}\right\}^{\beta} + \left\{\frac{Mz}{MBz}\right\}^{\alpha} + \left\{\frac{My}{MBy}\right\}^{\alpha} = 1.0$$

Where:

- PB is the axial compression force at the balance point;
- PC is the axial compression yield force;
- PT is the axial tension yield force;
- MBz is the yielding moment at P=PB about the z-z axis;
- MBy is the yielding moment at P=PB about the y-y axis;
- Py is PC when the axial force P is more compressive than PB and equal PT when P is greater than PB;
- α and β are the interaction factors for the flexural and axial terms $1.0 \leq \alpha$ and $\beta \leq 2.0$.

All the data request are below summarized in Table 4.14 for each column.

Table 4.14. ***Summary of the data used in the construction of the interaction diagram***

Pier	Section	PC	PB	MBz	MBy	PT
B	Base	-40829.3	-1633.05	3164.69	2678.72	3812.3
	Top	-57521.5	-1475.25	4206.07	2637.71	3812.3
C	Base	-40003.7	-1739.7	3179.03	2687.93	3812.3
	Top	-57521.5	-1573.19	4298	2693.67	3812.3
D	Base	-39192	-1834.91	3139.78	2759.29	3812.3
	Top	-57521.5	-1658.36	4265.11	2732.12	3812.3

E	Base	-38093.8	-1846.72	3040.30	2761.55	3812.3
	Top	-57521.5	-1658.36	4265.11	2732.12	3812.3
F	Base	-37380.5	-1841	2965.54	2753.08	3812.3
	Top	-57521.5	-1645.58	4246.51	2728.37	3812.3

When the vertical component of the motion is considered, the cyclic forces acting on the piers cause a variation of the stiffness directly proportional to the variation of the axial load. To take into account this important effect, a new hysteresis rule is used, the Revised Takeda [45] shown in Figure 4.29. The behavior of the sections is assumed to be symmetric so that the factors α and β result equal. The moment curvature relationships, already calculated with Cumbia, show that the shape of the graphics can be approximated by a bi-linear curve. This means that using the Revised Takeda rule, the first stretch of the curve has a very high gradient.

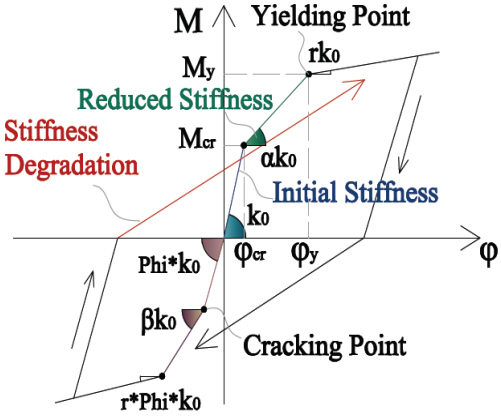

Figure 4.29. ***Revised Takeda***

The results of the time history analyses, considering the real properties, are shown below.

1. Christchurch Cashmere High School, CMHS

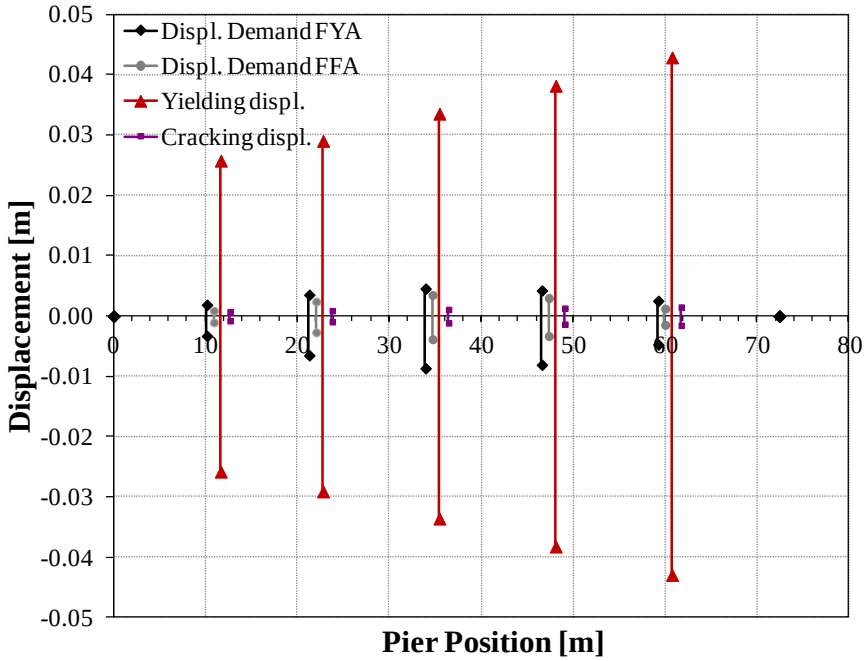

Figure 4.30. ***Comparison between the displacements of the structure of the two configurations (FFA and FYA) and the yielding ones, with records from CMHS.***

2. Catholic Cathedral College ,CCCC

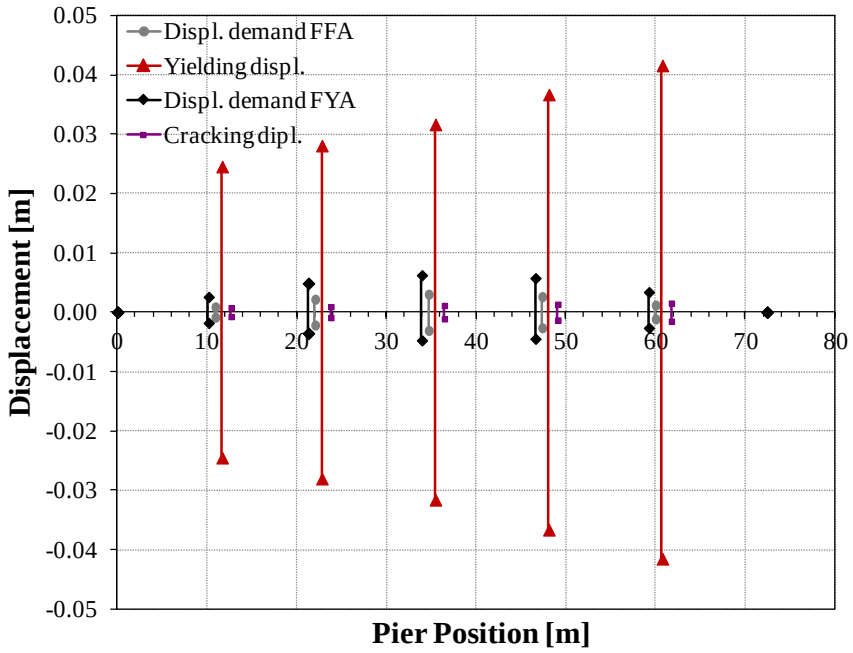

Figure 4.31. ***Comparison between the displacements of the structure of the two configurations (FFA and FYA) and the yielding ones, with records from CCCC.***

3. Heathcote Valley Primary School, HVSC

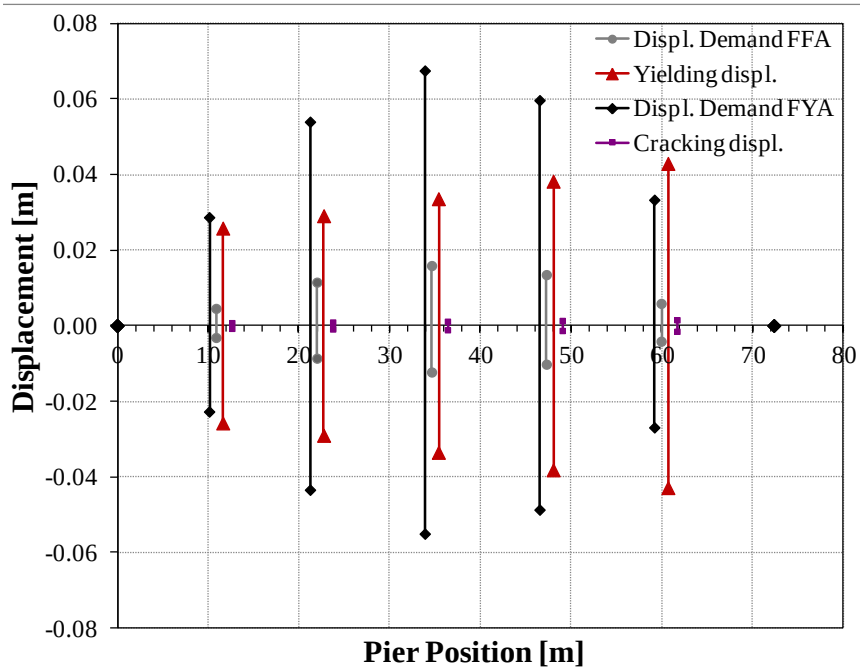

Figure 4.32. ***Comparison between the displacements of the structure of the two configurations (FFA and FYA) and the yielding ones, with records from HVSC.***

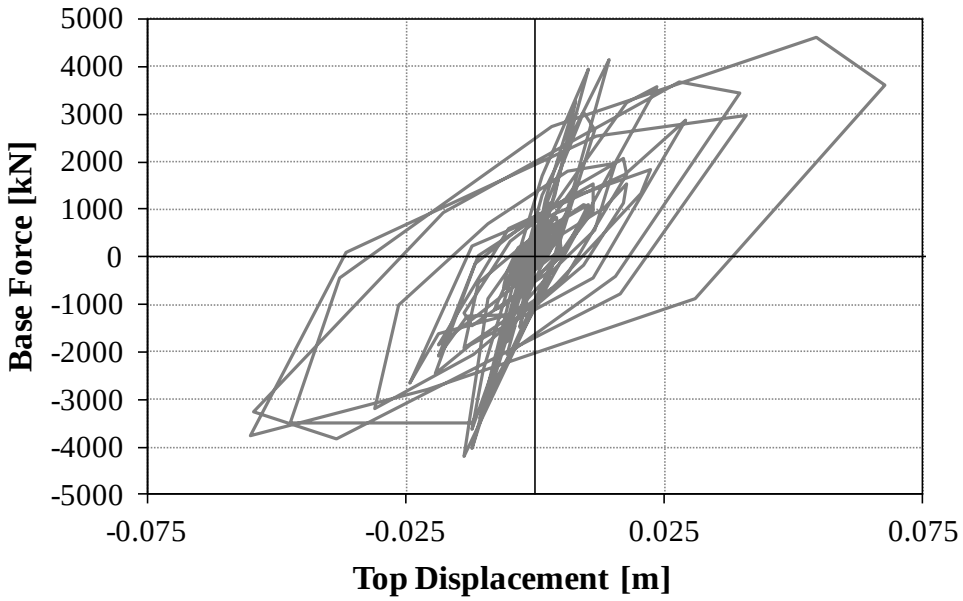

Figure 4.33. ***Base shear vs top displacement of the central pier (Pier D) when subjected to HVSC records.***

Results show that the bridge performed well remaining in the elastic range when subjected to CCCC and CMHS records (with vertical acceleration of 0.8g). Nevertheless, the observed damage showed the inelastic behavior of the central piers, even if the overall performance was better than expected from the high spectral acceleration values. This inconsistency can be due to the distance of the stations from the bridge and the epicenter; even if the soil conditions were assumed to be similar, the PGA recorded at this station is expected to be smaller than that felt at the bridge site. A good correspondence between the numerical analyses and the reality is found subjecting the structure to the HVSC records. However, the "real" axial load variation in the bridge was probably smaller since accelerations of HVSC incorporate seismic amplification effects. Figure 4.32 shows that the displacement demand for the model with fully fixed abutment (FFA) is lower than the displacement at the yield of the base section of the piers. On the contrary, the model with the superstructure pinned around the y-y axis (FYA) develops plastic hinges at the bottom, with top displacements greater than the yielding ones. The real response of the bridge is hence likely to have been more similar to the response evaluated by the second "limit case" model. In fact, since the bridge is prefabricated with post-installed mechanical connections, the fully fixed model overestimates the stiffness of the retrofit linkages.

Results of the analyses with the vertical component show that the displacements of top of the piers are lower than the ones obtained ignoring this contribution. This is reasonable considering that the axial force during the earthquake is compressive and tensile, and the tension force decrease the horizontal displacement of the pier. The output of the second analyses is also more similar to the real behavior of the bridge, with the piers next to the abutment still in the elastic range and the central ones yielded.

The high values of the vertical accelerations recorded are translate in a significant variation of the axial force acting on the columns, which caused ductility reduction of the piers. To evaluate the variation of the axial force, the time history of the vertical loading is plotted, and then, with Cumbia, moment-curvature relationships are obtained, for the maximum and the minimum values of the axial force. The ductility reduction is estimated considering two of the records used, CMHS

and HVSC, and the of the model with the deck free to rotate around the y-y axis. Figure 4.34 and Figure 4.35 show the results obtained for the central pier, pier D, the most damaged.

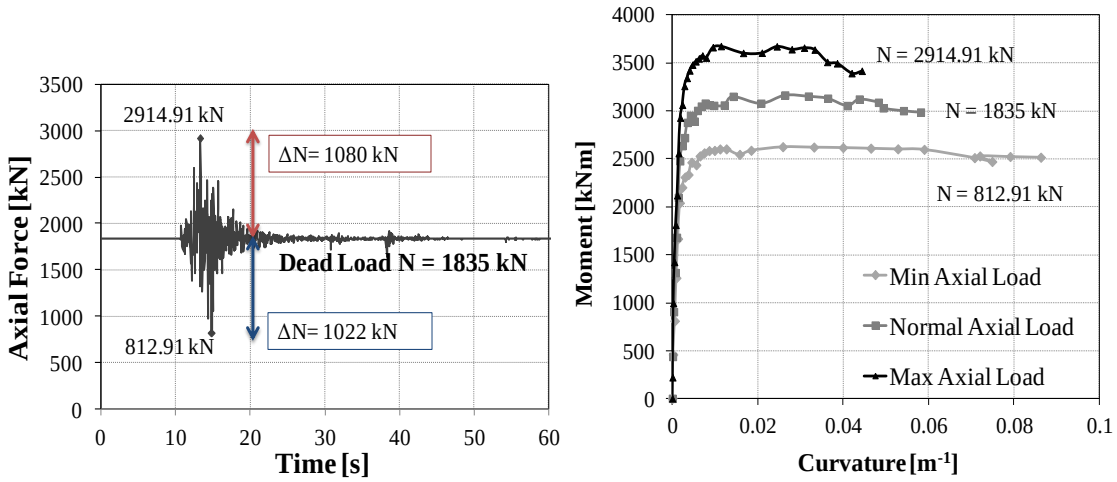

Figure 4.34. ***(a) Time history of the axial force loading the central pier (Pier D) when subjected to CMHS records. (b) Evolution of the moment-curvature with varying axial force.***

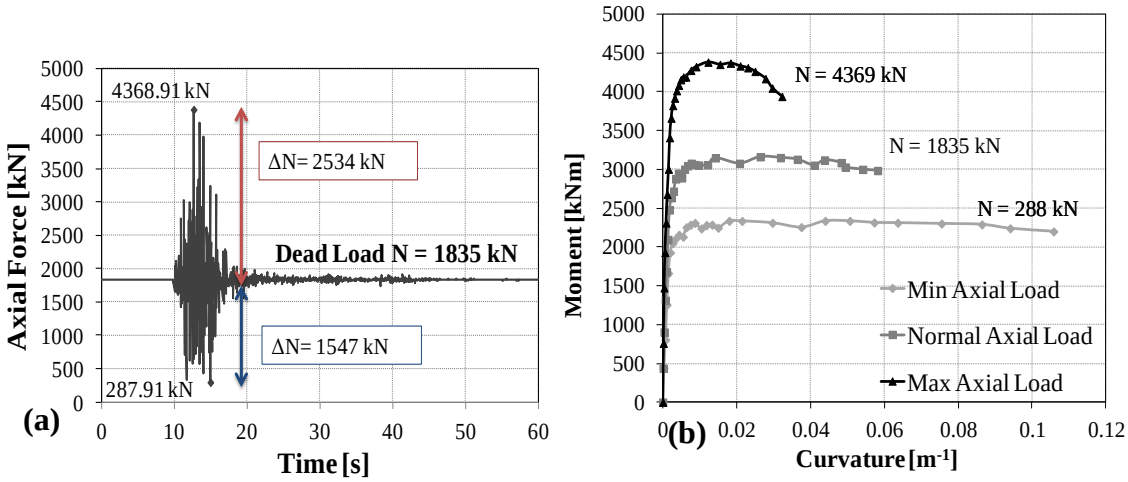

Figure 4.35. ***(a) Time history of the axial force loading the central pier (Pier D) when subjected to HVSC records. (b) Evolution of the moment-curvature with varying axial force.***

The vertical accelerations recorded at the CMHS station induce a moderate variation of the axial force on the pier D. The moment curvature relationship change as shown in Figure 4.34b: the yielding moment in the column increases by 15% compared to the static case when subjected to the maximum axial load, otherwise decrease by 19%. On the other hand on the curvature ductility there's the opposite effect: in the first case (maximum axial load) there is a decrease of 25%, in the second case (minimum axial load) there's an increase of the 56%.

When subjected to HVSC records instead, the moment capacity and curvature ductility in the pier D is drastically changed. When the axial load variation caused by the earthquake sums to the static load there is an increment of 38.60 % in the moment capacity but a reduction of 49.24% curvature

ductility respect to the situation with no axial variation effect. Vice versa for lower total axial load (N-ΔN) the moment capacity reduces of 28.09% while the ductility increases of 93.69%.
The variation of the axial force exert influence also on the shape of the pushover curve, as shown in Figure 4.37. Considering the maximum axial force acting on the pier D when subjected to HVSC records, the ultimate displacement is 0.19 m, 25 % less than the one found in "normal condition". On the other hand the reduction of the axial load during the earthquake as result of the action of tension forces, increase the ultimate displacement of the 34%, reaching 0.34 m. In the same graphic HVSC response spectrum and NZS1170.5 design spectrum are shown for a comparison between the capacity of the structure and the demand to estimate the peak deformation of inelastic SDOF system: the intersection of the two diagrams correspond to the demand point. From the graphic it's possible to notice that the displacement demand of the SDOF system do not fit the one found with time history analyses. The difference is considerable: the maximum displacement obtained with this method is 0.20 m, while nonlinear time history analysis on the MDOF system shows a peak displacement of ~0.07 m (Figure 4.32). The reason of this discrepancy in results can be found in the conversion of the spectrum from the acceleration versus natural period format to the shear force versus displacement format. In fact the force has been found multiplying the accelerations by the equivalent mass of the bridge given by the formula [46]:

$$m_e = \left(\sum_{i=1}^{n} m_i \cdot \Delta_i\right) \cdot PF$$

Where:

- m_i is the lumped mass at the top of each pier, that is the sum of the weight of half column and the weight of the deck in the influence area.
- Δ_i is the top displacement of each pier as resulted from the static pushover analysis
- PF is the participation factor found according to the equation below:

$$PF = \frac{\sum_{i=1}^{n} m_i \cdot \Delta_i}{\sum_{i=1}^{n} m_i \cdot {\Delta_i}^2}$$

To consider the mass of the SDOF system, the actual equivalent mass of the bridge, an assumption has to be made: because of displacement shape is aimed to closely match the fundamental mode shape, the fundamental mode of free vibration does not have to change during the response of the structure and the effective mass of the fundamental mode has to be greater than 80% of the total mass [47]. The fundamental mode of free vibration is dominant in bridge structures where columns do not hinder movement of the deck in the transverse direction. This is most common in regular bridges and/or irregular bridges where the short stiff columns have suffered significant damage and hinging has occurred [48]. The assumption mentioned cannot be imposed on the bridge under consideration since, because of its irregularity, the first free mode of vibration is not the fundamental one.

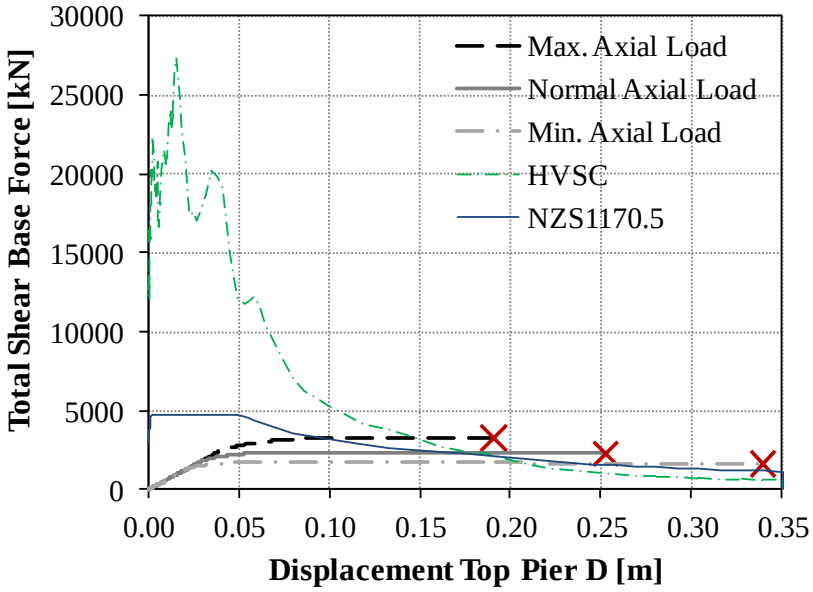

Figure 4.36. ***Evolution of the moment-curvature with varying axial force. HVSC response spectrum and code spectrum are included for a comparison between the demand and the capacity of the bridge.***

4.3.4.5.1.2 DARFIELD EARTHQUAKE , SEPTEMBER 4, 2010

In order to have an overall view of the performances of the bridge, as well as to understand the importance of the last event, a nonlinear time history analysis is performed with the accelerograms of the Darfield Earthquake. The record used are from Catholic Cathedral College ,CCCC, and Heathcote Valley Primary School, HVSC. The results of the analyses are shown below (Figure 4.37 and Figure 4.38).

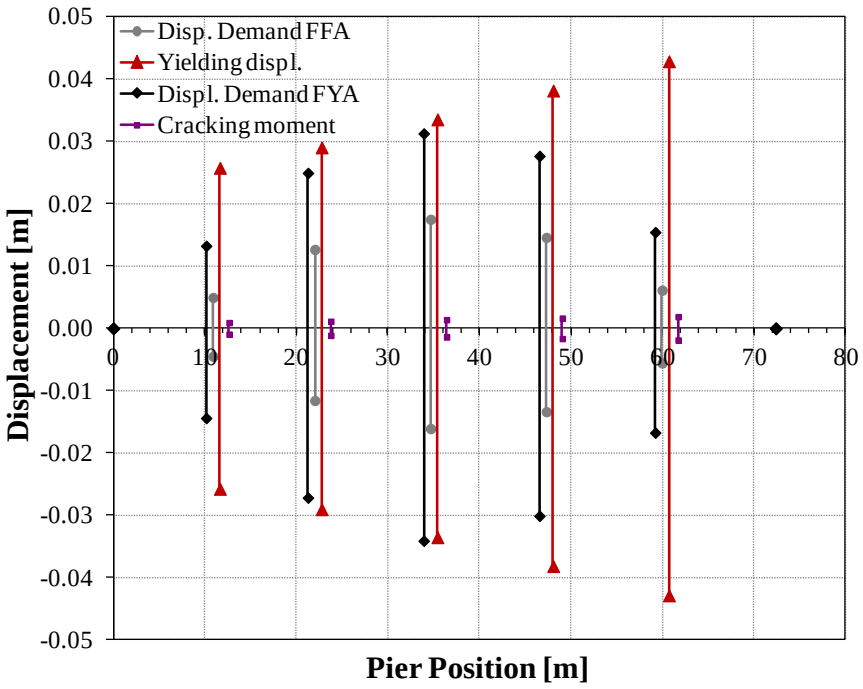

Figure 4.37. ***Comparison between the displacements of the structure of the two configurations (FFA and FYA) and the yielding ones, with records from CCCC.***

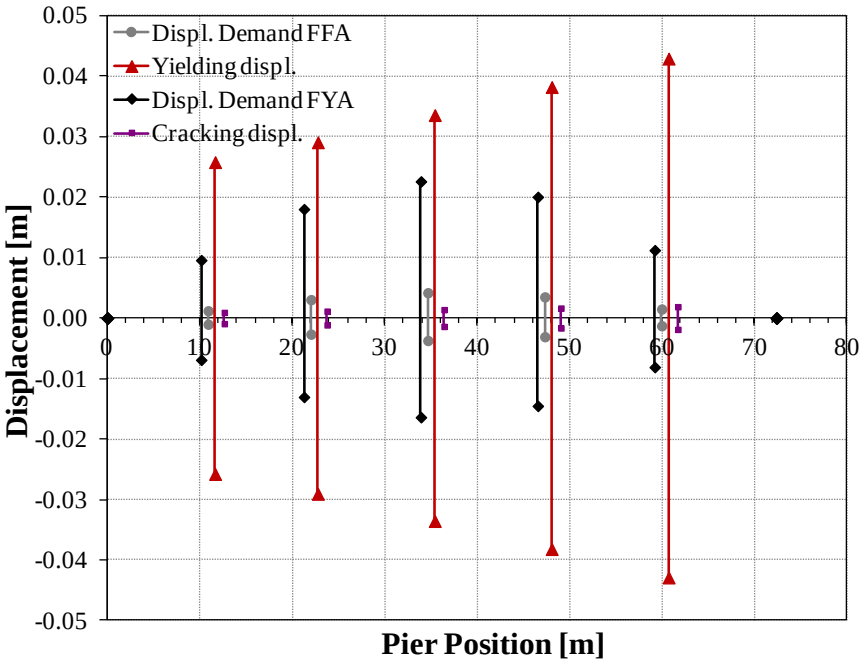

Figure 4.38. ***Comparison between the displacements of the structure of the two configurations (FFA and FYA) and the yielding ones, with records from HVSC.***

The numerical results show that the bridge performed well during the Darfield event, with displacements lower than the one et the yield even when subjected to the ground motion from

HVSC. This confirm that even if the Lyttelton Earthquake was lower in terms of magnitude than the Darfield one, the damage was greater because the PGA recorded was more important.

4.3.4.5.1.3 SCALING OF 10 EARTHQUAKES ACCORDING TO THE NEW ZEALAND CODE

Time history analyses can be carried out using as input both natural and artificial or simulated accelerograms. However, the natural ones seem to be the most direct representation of ground motion, bringing itself features such as amplitude, frequency content, energy, duration and phase of real events. After the simulation with accelerograms of earthquakes within the study area, analyses with 10 records of earthquakes occurred in different part in the world are developed. It is found that the use of earthquakes even with the level of seismicity similar, but recorded off from the territory of interest, may give results not representative of real local conditions, related to the physical characteristics of the territory subjected ground motion. Therefore, when natural accelerograms are used, the search of the "best" seismic input requires the alteration of real accelerograms through scaling techniques [49]. An ensemble of 10 Californian earthquake records (Table 4.15), scaled to match the design response spectrum defined by the European Code EC8 [50], for a soil class C, was adopted (the PGA of the average spectrum is 0.4g).

Table 4.15. ***Characteristics of ground motion records used for time history analysis.***

	Earthquake Event	Year	M_w	Station	Soil Type (NEHRP)	Scaling Factor	Scaled PGA (g)
EQ1	Cape Mendocino	1992	7.1	Rio Dell Overpass-FF	C	1.2	0.462
EQ2	Landers	1992	7.3	Desert Hot Springs	C	2.7	0.416
EQ3	Landers	1992	7.3	Yermo Fire Station	D	2.2	0.334
EQ4	Loma Prieta	1989	6.9	Hollister Diff. Array	D	1.3	0.363
EQ5	Loma Prieta	1989	6.9	Gilroy Array #7	D	2.0	0.452
EQ6	Northridge	1994	6.7	Canoga Park-Topanga	D	1.2	0.427
EQ7	Northridge	1994	6.7	Glendale – Las Palmas	D	1.1	0.393
EQ8	Northridge	1994	6.7	LA – N Faring Rd	D	2.2	0.601
EQ9	Northridge	1994	6.7	Sunland – Mt Gleason	C	1.7	0.461
EQ10	Superstition	1987	6.7	Plaster City	D	2.2	0.409

It was necessary to scale all them referring to the design spectrum of the NZ Code. The parameters used for the construction of the NZ design spectrum were the following [21]:

$$C(T) = C_h(T)\, Z\, R\, N(T, D)$$

- Annual probability of exceedance = 1/1000 (ULS)
- Site subsoil class = C
- Hazard factor Z (Christchurch) = 0.22
- Return period factor R = 1.3
- Near fault factor N = 1.0

The method currently used is to scale the peak acceleration recorded to make it match the Peak Ground Acceleration. The only PGA however cannot be considered a parameter sufficiently representative of the real offensive potential of an earthquake. Another method of scaling is to scale so that it coincides with the design spectrum for a range of fixed periods, that is the natural period of the structure. For the bridge under consideration the natural period for the structure in question, the natural period varies in different cases considered and lies in the range of 17 ÷ 0.27 seconds. Since on average the adopted accelerograms contain energy over the entire range of the periods of interest, the records are scaled so that their average fit the spectral acceleration demand curve from NZS 1170.5 [21] (Figure 4.39).

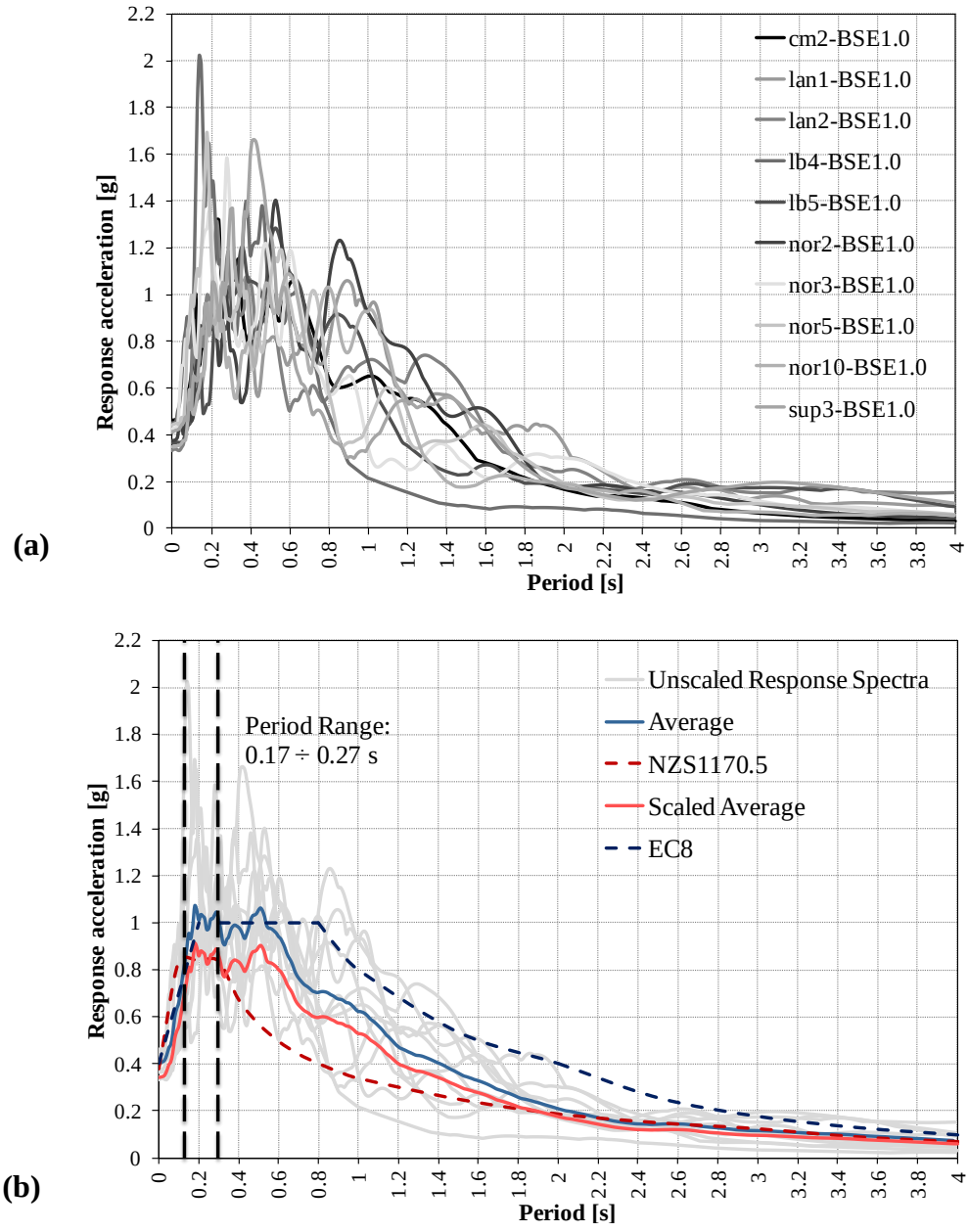

Figure 4.39. ***(a) Californian earthquake response spectra (b) Earthquake scaling to the NZS 1170.5 [2004]***

The results of the analyses are shown below (Figure 4.40 and Figure 4.41).

Design properties

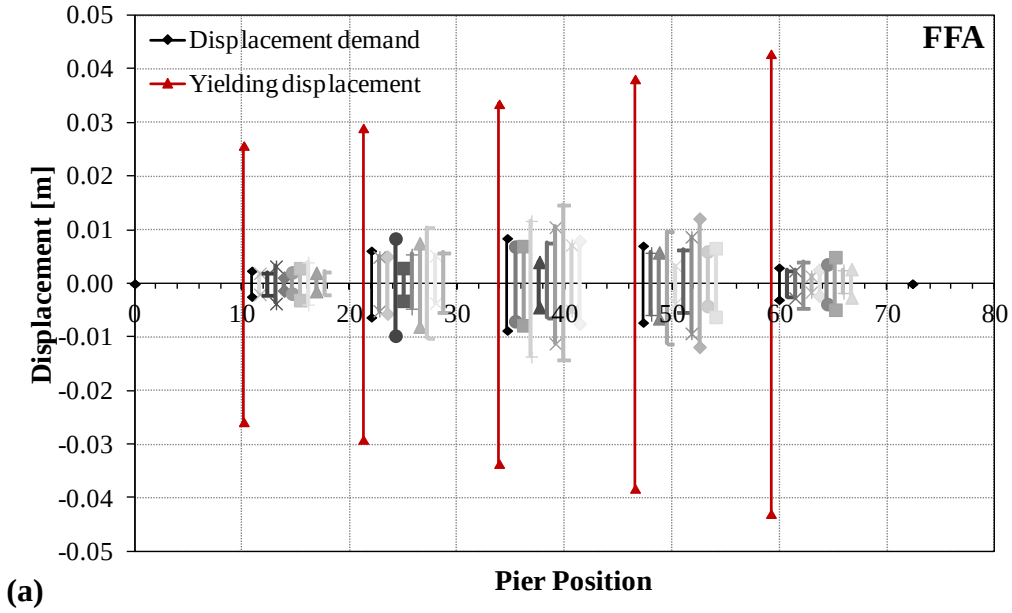

(a)

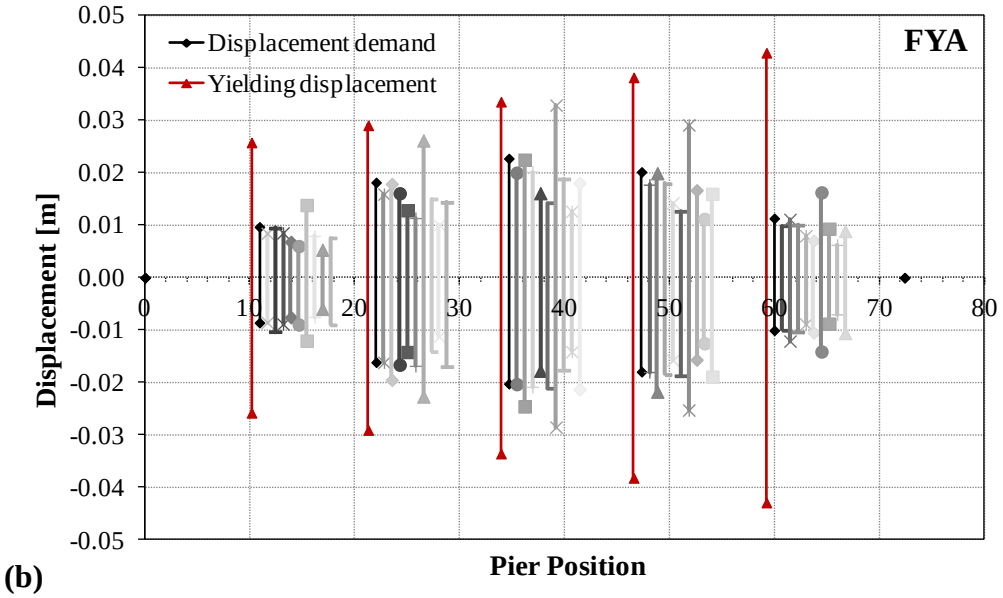

(b)

Figure 4.40. ***Comparison between the displacements demand and the displacement at the yield using the design properties for the (a) Fully Fixed Abutments and (b) Free YY Abutments configurations.***

Real Properties

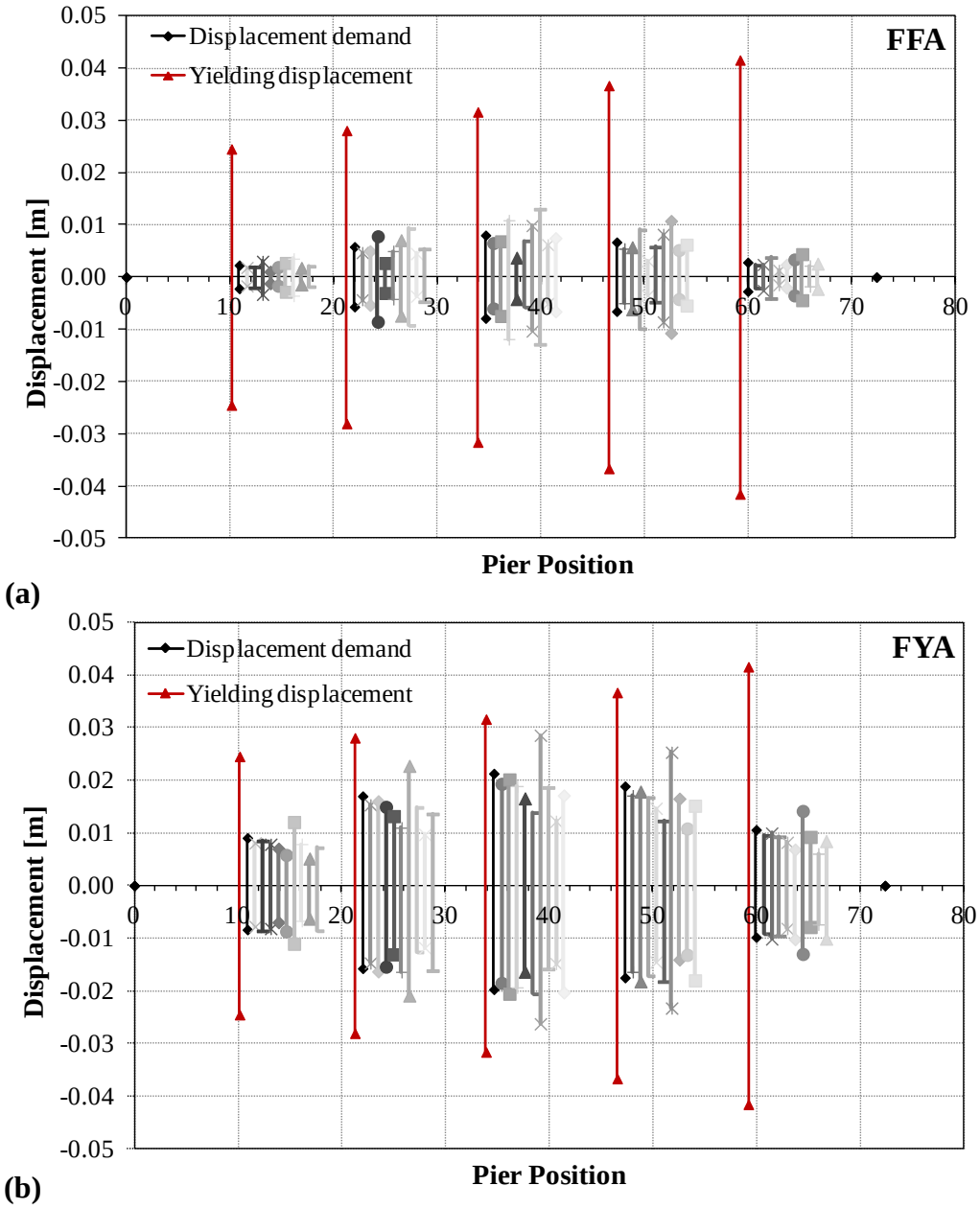

Figure 4.41. ***Comparison between the displacements demand and the displacement at the yield using the actual properties for the (a) Fully Fixed Abutments and (b) Free YY Abutments configurations.***

Through this analysis "in step", assuming as input accelerograms representative of the local seismic characteristics, it's possible to assess the nonlinear dynamic behavior of the structure.
Results show that in both the configuration of the model, even changing the concrete properties, the displacement at the deck level do not exceed the yielding ones and so the piers behave elastically. This is obtained using an ensemble of earthquakes able to guarantee a safety level greater or at least equal to that one provided for the New Zealand code. It's interesting to notice that the New Zealand

safety level is less strict than the European one, and so supposing to place the bridge in an European area, the performance might very well change, getting up to the plastic range.

4.4 Conclusion

The Port hills Overpass performed generally well during the February 2011 earthquake, even if the damage indicated some inelastic behaviour of the central piers. The distribution of load through deck diaphragm action might also in part explain the good performance of the structure.

The retrofitted shear keys at the abutments probably prevented significant damage as the loading on the original dowels in the Christchurch earthquake would have been significantly greater than their strength capacity.

Push over, modal and time history analyses were run on the bridge. Two configurations of the model were considered with a fully fixed restrain or a hinge allowing rotations around the vertical axis next to the abutments, to pick out the actual response of the bridge during the last seismic event. The natural period of the structure has found to be between 0.17 s and 0.27 s. Modal analyses showed that this corresponded to the design spectral accelerations a part from the case of HVSC records. To assess the real performance of the bridge ground motion records from CMHS, CCCC, and HVSC were used in a non-linear time-history analysis of the structure in both conditions and considering first only horizontal components, and then including the vertical one. Although the assumptions made for the models, the real performance of the bridge seemed to be similar to numerical results obtained with HVSC records, with the central piers yielded at the base. Moreover the actual performance was a middle way of that ones of the two "limit cases" considered. The high vertical accelerations drastically varied the moment-curvature capacity of the piers and this caused inspected displacement demands. The results of these analyses will be used by Christchurch City Council and New Zealand Transportation Agency as complementary assessment tool for further retrofit actions on these bridges.

5 HOROTANE VALLEY OVERPASS

5.1 Description of the Structure

The Horotane Valley Overpass (-43.5725, 172.6947), constructed in 1963, consists of twin bridges each carrying two lanes of SH 74 across Horotane Valley Road. The Overpass is located about 2 km West of the Christchurch portal to the Lyttelton Road tunnel. Both bridges are similar except that the No 2 Bridge carrying the west bound lanes widens towards its west end to provide additional width for an off-ramp. Each bridge has three simply supported spans with prestressed concrete beams supporting a reinforced concrete deck. . There are 5 principal beams for Bridge n°1 and 6 for Bridge n°2 seating upon neoprene pads on pier caps. Transversal cast-in-situ beams stiffen the deck. The spans are 13.9 m and 12.5 m for the end and central spans respectively. The bridge abutments and the single stem rectangular piers are founded on spread footings. The spans are well linked to the abutments and piers by both holding down dowels and linkage rods.

Figure 5.1. ***Overall view of Horotane Valley Overpass.***

The Overpass bridges have recently been strengthened by fitting fabricated steel shear keys at the abutments, primarily to resist transverse loads. Each of the nine brackets at each abutment (single abutment structure for both bridges) is fitted with a 30 mm diameter bolt into the bottom of the beams. This provides additional longitudinal restraint in addition to that provided by the original linkage. Additional linkage rods were added between the outer beams at each pier. These were designed to improve the deck diaphragm action under transverse loading and avoid unseating.

5.2 Earthquake Performance

The Overpass was located about 1.3 km from the epicenter of the Christchurch earthquake. As already told for Port Hills Overpass records from the closest SMA (HVSC at 1.6 km from the bridges) are likely to have been significantly influenced by topographic effects.
Since this overpass was recently retrofitted, it didn't suffer of any structural damage after the Darfield earthquake. Retrofits were designed to link spans together and to the abutments in order to create an "integral cast-in-place bridge" concept (Figure 5.2). The performance of Horotane Overbridge, like other bridges in the region witnessed the effectiveness of the retrofit programs undertaken by Transfund New Zealand in the past. In fact, the bridge was able to service traffic soon after the earthquake.

Figure 5.2. ***Steel linkages between spans after the retrofit program.***

After the Lyttelton earthquake, the damage suffered by the bridge was limited too, as explained in the following. Table 5.1 lists the damage of structural/non structural elements qualitatively.

Table 5.1. ***Summary of the level of damage observed on the bridge after the Lyttelton earthquake.***

Deck	Null	**SouthEast Approach**	Null
Beams	Null	**NorthWest Approach**	Null
Piers	Minor	**Services**	Null
SouthEast Abutment	Minor	**Substructure**	Null
NorthWest Abutment	Minor	**Surrounds**	Null

5.2.1 Superstructure and services

The deck and beam elements of the bridge exhibited little damage following the Lyttleton earthquake. No cracking to bridge pavement was observed throughout the length of the deck (Figure 5.3a-b). No flexural cracking of the beams was observed neither (Figure 5.3c). The ties between spans and at the abutments also elongated and pulled out. Additionally, 60% of the bolts that attached the soffit of the precast concrete beams to the abutment seat extension had sheared off. While initially alarming, this failure of the retrofit bolts highlights the necessity of bridge retrofits. If these spans had not been tied together and the seats not extended it is quite likely the spans would have collapsed.

(a) **(a)** **(a)**

Figure 5.3. ***(a-b) General view of the superstructure and (c) deck soffit of the bridge***

5.2.2 Piers

Following the Christchurch earthquake, fine horizontal cracking was observed on the lower half of all four piers (Figure 5.4). Crack widths were up to 0.2 mm and the cracks were located between about 500 to 2600 mm above ground level. The cracks were more pronounced on the column faces nearest to the roadway under the bridge. Measured distances between the bases of the piers indicated that these spacings had shortened by 200 mm on the No 1 Bridge and 260 mm on the No 2 Bridge.

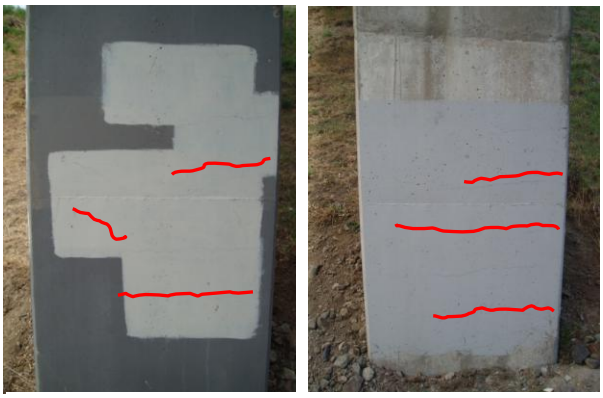

Figure 5.4. ***Flexural cracked piers***

5.2.3 Abutments

The Horotane Overbridge suffered abutment damage and a small slope failure of the embankments (Figure 5.5a). The East end of the No 2 Bridge displaced horizontally about 100 mm in a southwards direction. This resulted in severe vertical cracking at the junction between the abutment seating and the abutment wall between the two bridges. There was minor spalling at the ends of beams where they were seated on the abutments (Figure 5.5b).

The North-West abutments had settled by about 60 mm: a transverse crack was developed at the top of the North-West slope near the concrete abutment, however this was not continuous across the slope.

The South-East concrete abutment structure back rotated by 3.4°.

All four abutments appeared to have moved forward by up to 20 mm. Cracking and movement of abutments developed outwards perpendicular to the bridge axis. A significant transverse crack 10cm wide and 60cm deep opened up at the top of the South-East slope that was continuous across the width of the bridge (Figure 5.5d). A transverse scarp also developed near the toe of the 13m long slope, extending across the width of the bridge between the bridge columns. The movement of the abutments caused even the shearing of two of the bolts on the new linkage brackets (loaded in shear) at the west abutment of the No 1 Bridge. Bolts on the new linkage brackets also sheared on both abutments of the No 2 Bridge (Figure 5.5c).

(a) **(b)** **(c)** **(d)**

Figure 5.5. ***Damage at the abutments: a) Slope failure; b) Flexural cracking (c) Sheared bolt at the abutment retrofit; (d) Transversal crack at the top of the South-East slope***

5.2.4 Foundations

Although the bases of the piers were not visible there was no evidence of soil gapping or concrete cracking at ground level so no evident damage was suffered by the foundations. Further investigation would be needed to find out the conditions of foundations below ground level.

5.2.5 Approach and Surroundings

There was significant differential settlement between the approach pavements and the abutments of both bridges as evidenced by repairs to the asphaltic concrete pavement near the abutments. The approach roadway kerbs were damaged in several locations by compression against the abutments resulting from forward movement of the backfill. Buckling of the guardrails and shearing of their connection bolts occurred at several of the joints between the approach guardrails and the bridge end posts.

(a) **(b)**

Figure 5.6. ***a) Cracks on the top of the embankment; b) Cracks in the pavement under the bridge***

5.3 Numerical Analyses

5.3.1 Introduction

The type of analysis conducted and the working assumptions are the same as described for the previous case study (see paragraphs 4.3.1).

5.3.2 Section properties

5.3.2.1 Material properties

For the first model (using the design properties), the characteristic strength values were approximated from those ones given in the drawings (Table 5.2):

Table 5.2. ***Design properties***

CONCRETE

Concrete compressive strength of the piers f_c'	21 MPa (f_c' = 3000 psi specified strength in drawings)
Concrete compressive strength of the deck f_c'	38 MPa (f_c' = 5500 psi specified strength in drawings)
Density of concrete ρ	2400 kg/m$^{3.}$
Elastic Modulus for the piers (using the formula from NZS 3101 section 5.2.3)	$Ec = \left(3320\sqrt{fc'} + 6900\right)\left(\frac{\rho}{2300}\right)^{1.5}$ = 23572 N/mm^2
Elastic Modulus for the deck (using the formula from NZS 3101 section 5.2.3)	$Ec = \left(3320\sqrt{fc'} + 6900\right)\left(\frac{\rho}{2300}\right)^{1.5}$ = 29142 N/mm^2
Shear Modulus G for the piers	10081.70 N/mm^2
Shear Modulus G for the deck	12142.52 N/mm^2

STEEL

Steel yield strength f_y	300 MPa*

* the value of the yield strength shown in the drawings(140 MPa (f_s = 20000 psi)) is much lower than that one suggested by the Bridge Manual for bridges built in 60's of 250 MPa (6.3.2-b). That value was raise to 300 MPa since it was the value measured for most of the bridges built in the same period in Christchurch.

In the second model, the concrete properties measured in site are:

Table 5.3. ***Actual properties***

CONCRETE

Concrete compressive strength of the piers f_c'	21 MPa (f_c' = 3000 psi specified strength in drawings)
Density of concrete ρ	2400 kg/m$^{3.}$
Elastic Modulus for the piers (using the formula from NZS 3101 section 5.2.3)	$Ec = \left(3320\sqrt{fc'} + 6900\right)\left(\frac{\rho}{2300}\right)^{1.5}$ = 32126.9 N/mm^2
Shear Modulus G	13814.57 N/mm^2

STEEL

Steel yield strength f_y	300 MPa

5.3.2.2 Calculation of Moment Curvature relationship

The drawings show that there are three different sections in the piers. As already done in the previous analyses, also in this case study only the top and base section are taken into consideration.

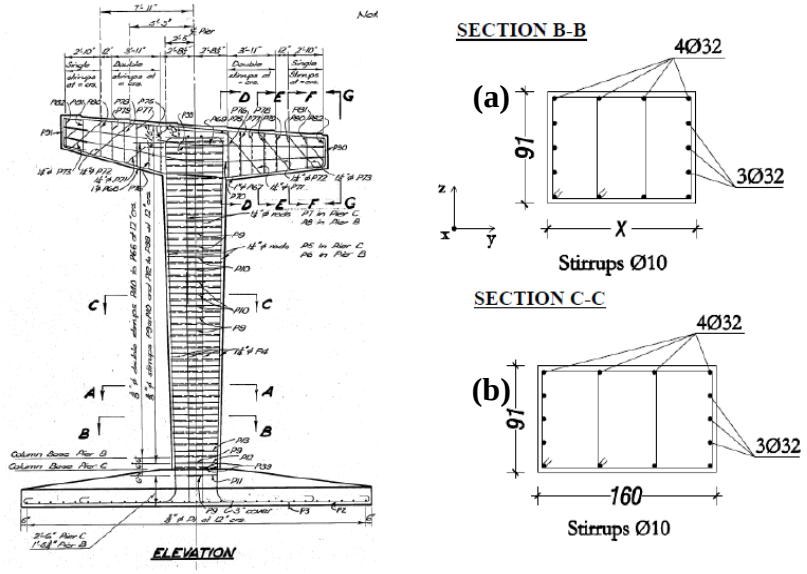

Table 5.4. ***Sizes of the base's side of the piers***

Pier	X [m]
B	1.257
C	1.245

Figure 5.7. ***Detail of the column from the drawings: (a) Section of the base of the column; (b) Section of the top of the column***

The table summarizing the results obtained with Cumbia [41], is shown in APPENDIX B

5.3.3 Assessment of the performance of the bridge

5.3.3.1 Description of the model

The model of the bridge on which the analyses will be conducted, is shown below (Figure 5.8). On that model all the considerations already laid out for Port Hills Overpass are still valid (see paragraph 4.3.4.1).

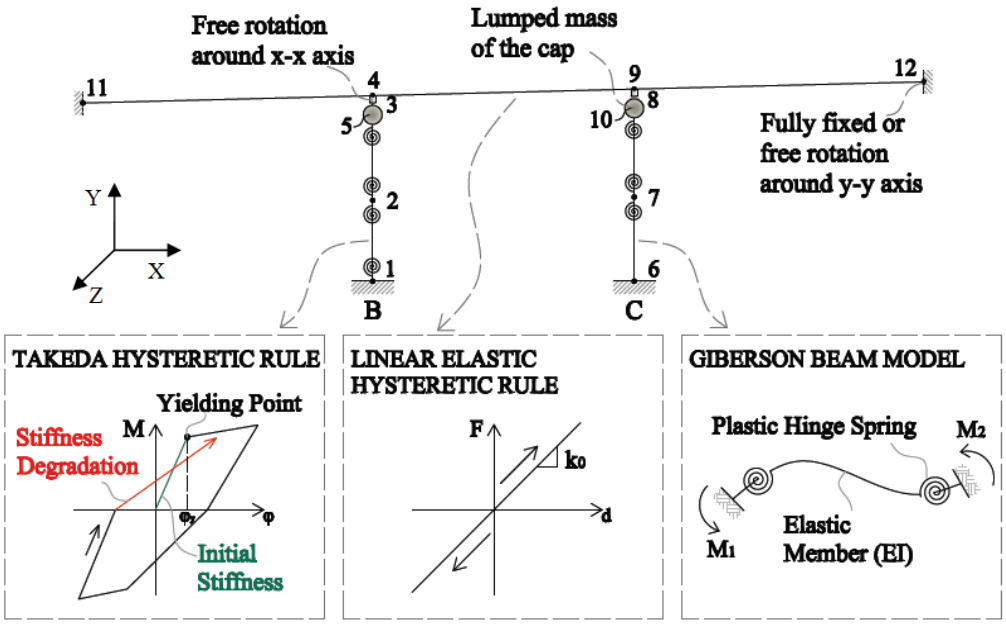

Figure 5.8. ***Model of the bridge***

The details of the connections between the deck and the abutments and the piers, are shown in Figure 5.9a-b. The presence of linkage bolt in the two principal direction, x and y, constrict any relative movement between the spans, so that the hypothesis to consider the deck as a single element continuous, is quite reasonable. As done in the previous analyses, two different restraint conditions have been considered next to the abutments: the fully fixed case and the one with the free rotation around the y-y axis. Even if the connection of the deck to the abutment is made up of two bolts which block the rotations, the second case is taken into consideration because, as already told in the overview of the damage, the movement of the abutment caused severe shear cracking in the backwall and shearing of the bolts of the new linkage brackets. Because of the horizontal displacement of the abutments, also severe vertical cracking at the junction between the abutment seating and the abutment wall between the two bridges appeared (Figure 5.10). The actual response of the bridge is expected to be a middle way between the two limit cases considered.

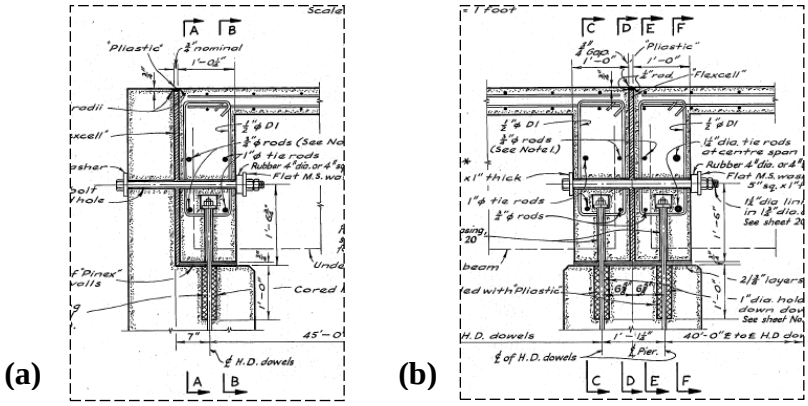

Figure 5.9. ***Detail from the drawings of the connection (a) between the deck and the abutment and (b) between the deck and the pier***

Figure 5.10. ***Transverse crack at the northwest abutment***

5.3.3.2 Modal Assessment

As already done in the previous case study, a spectral analysis was performed, in order to determine what level of the current code level of seismic shaking the bridges were subjected to. The response spectra were formed based on the motions of both Darfield and Christchurch earthquakes recorded at the nearest seismic stations, the same ones already used for Port Hills Overbridge. In order to assess what percentage of the code acceleration was activated, a comparison between the response and the code spectra, for the range of the modes of the structure, was carried out.

The structure is really stiff, so much so the natural period of the structure fall in the range 0.085-0.092 s, depending on the material properties and on the contraint conditions. The first three modal frequencies, considering design properties and fully fixed abutments are shown in Table 5.5.

Table 5.5. ***Frequencies and fundamental periods of the structure with the corresponding percentage of damping***

MODE	Frequency	Period	% Damping	Transverse mass (%)	Longitudinal mass (%)
1	11.73	0.09	5.00	28	68
2	21.45	0.05	5.00	28	68
3	22.57	0.04	5.81	52	77

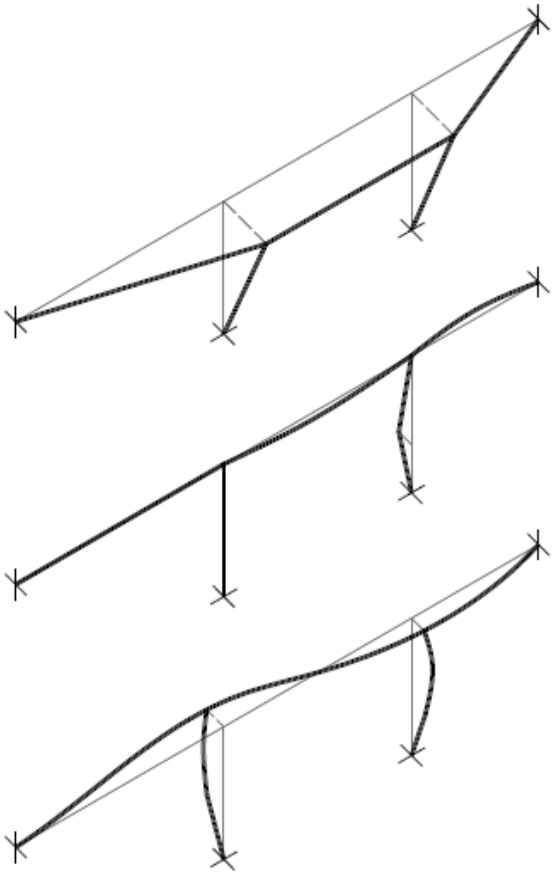

Figure 5.11. ***Mode shapes 1, 2 and 3***

A site response spectra was made for the two orthogonal horizontal acceleration records measured at the same closest stations of Port Hills Overpass. Figure shows the comparison between the site and the design spectra.

(a)

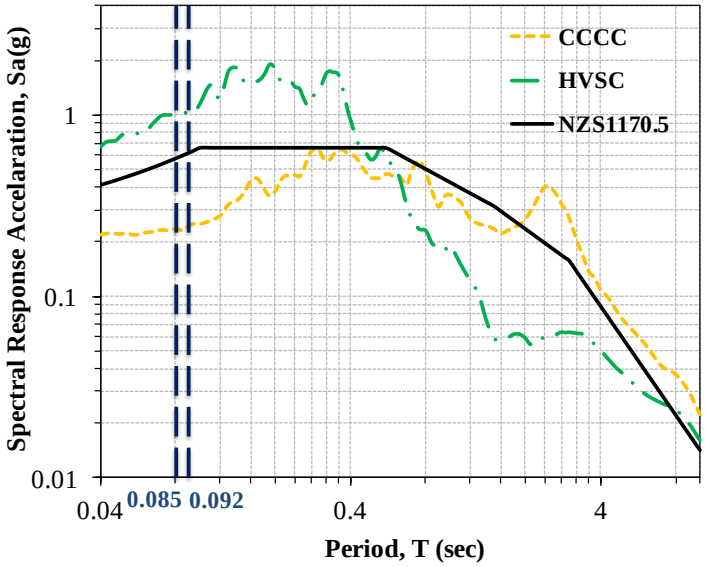

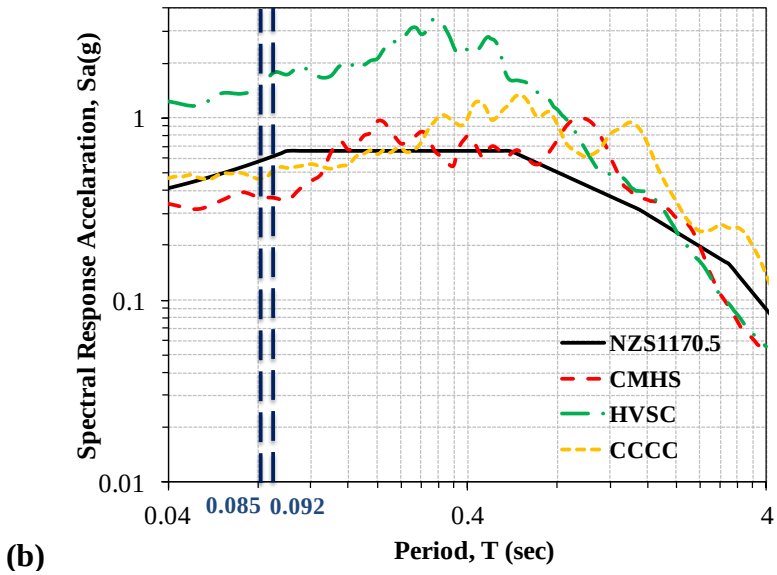

Figure 5.12. ***Site Response for Horotane Valley Overpass for the fundamental periods of the structure, depending on the model and on the material properties, with (a) Darfield earthquake records and (b) Lyttelton earthquake records.***

As already stated earlier, the spectra show the difference in frequency content between the two earthquakes. This time both Darfield and Christchurch earthquake demands are below the NZS1170 design spectral acceleration in the range of natural periods of the structure, though the first is lower than the second one. This consideration is clearly valid for all records, except those coming from the station HVSC, higher than the others because of the topografics effects, as already explained for the previous case study. Comparing the code demand response to the site demand response for the given period of the bridge, for the first mode of the bridge and for 5% damping, the spectral accelerations of the site have an average value of 0.24g and 0.50g, respectively for the 2010 and 2011 earthquake, less than the NZS 1/500 year design spectrum value of 0.61 g. So for this bridge it is very improbable that the damage observed was due to the dynamic response of the structures to the earthquake. In fact as confirmed by the observation in situ, the damage to the bridge was due only to the slop failure of the ground next to the abutments after the Christchurch earthquake. No damage was pointed out instead as result of the Darfield earthquake.

5.3.3.3 Nonlinear Static Pushover Analysis

5.3.3.3.1 MOMENT - CURVATURE RELATIONSHIP

The results in terms of moment-curvature relationship shown in the Table 5.6 are consistent with the values obtained with Cumbia [41]. Numerical analysis shows that the pier B reach first the failure point. Nevertheless the behaviour of the structure is symmetrical with the transversal axis of the bridge so that the two piers perform similarly. It's possible to notice also that even in this case, the difference between the results with design and actual properties is minor.

Table 5.6. ***Moment curvature relationship for different material properties and configurations of the model***

	Pier B	**Pier C**
DATA	Element - Giberson Hysteretic rule: Takeda $E_{c,\ design}$ = 23572 MPa $E_{c,\ real}$ = 32126.9 MPa Bilinear Factor = - 0.001	Element - Giberson Hysteretic rule: Takeda $E_{c,\ design}$ = 23572 MPa $E_{c,\ real}$ = 32126.9 MPa Bilinear Factor = - 0.001
TOP	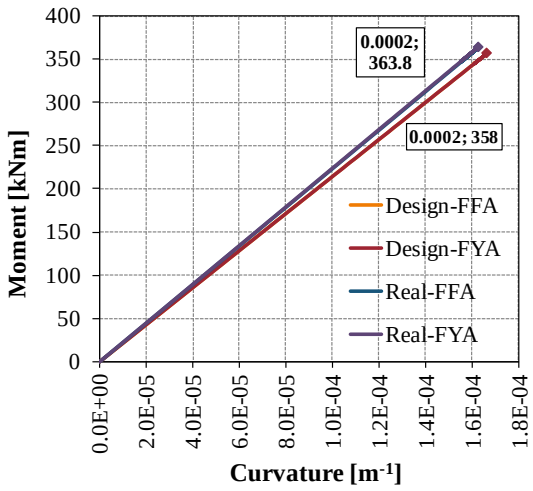	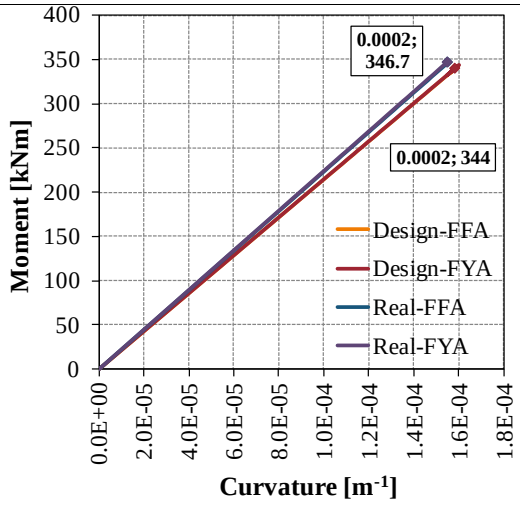
BASE	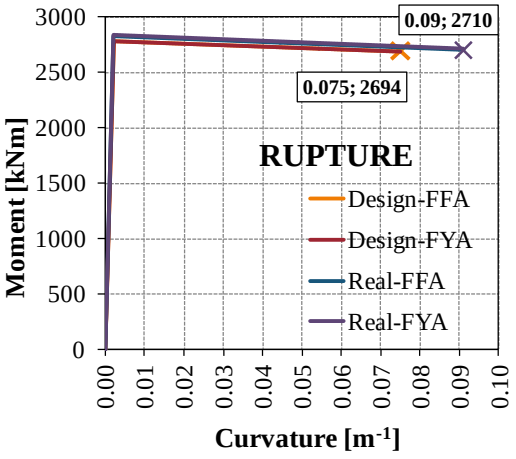	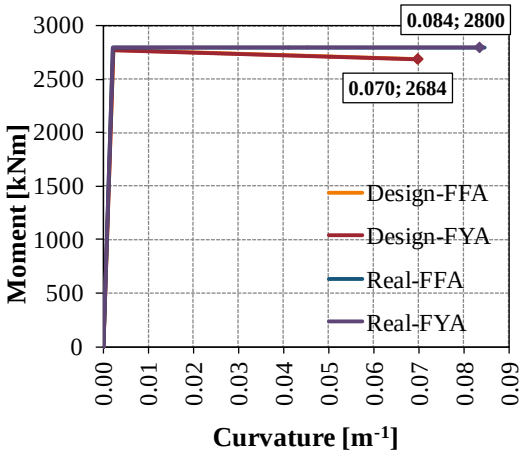

5.3.3.3.2 TIME – DISPLACEMENT RELATIONSHIP

The comparison between the two models in terms of displacement is shown in Figure 5.13:

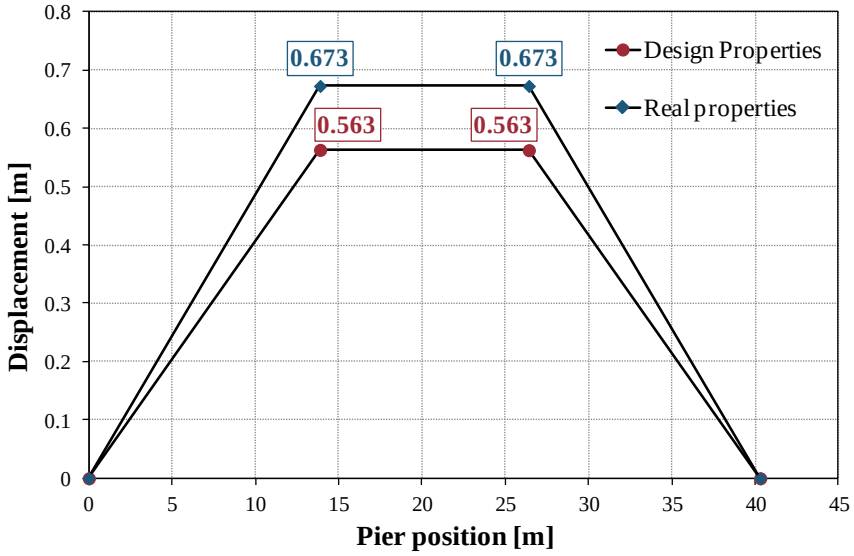

Figure 5.13.*Displacement profile of each model*

The graphic confirms that the two piers perform equally, reaching the same maximum displacement. Compared to the values obtained for Port Hills Overpass, the displacement at the deck level is much greater due to the high of the bridge, bigger than the previous one. Moreover the displacement is the same for both the configurations of the model, with the constrain at the abutments fully fixed or with the rotation around the y axis allowed. Changing the material properties, the difference in terms of displacement is more considerable than the previous case study, with a value around 10 cm.

5.3.3.3.3 PUSH OVER CURVES

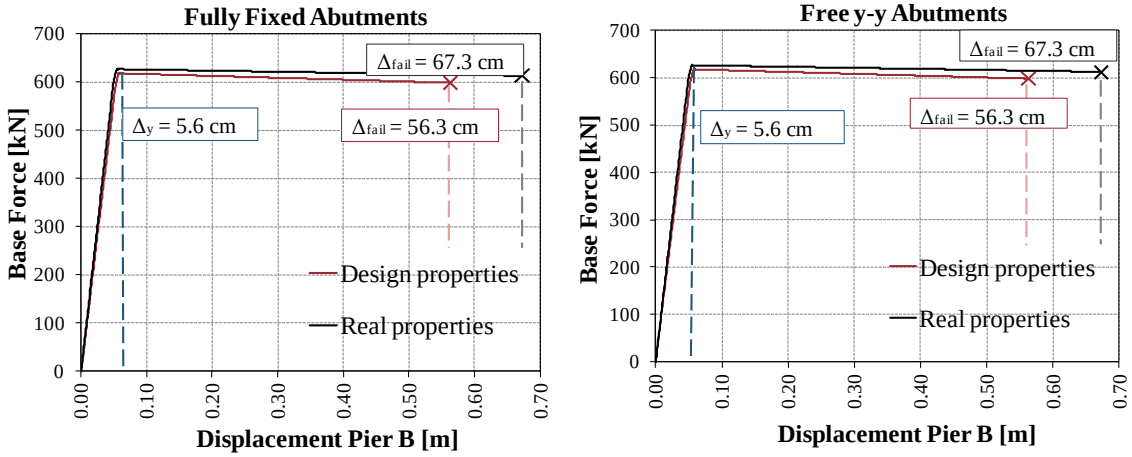

Figure 5.14 shows the push over curves of the two different models considered. The high inclination of the elastic part of the curve indicates that the structure is very stiff. Considering also

the length of the plastic stretch, also an high displacement ductility factor is expected as confirmed by the calculation carried out.

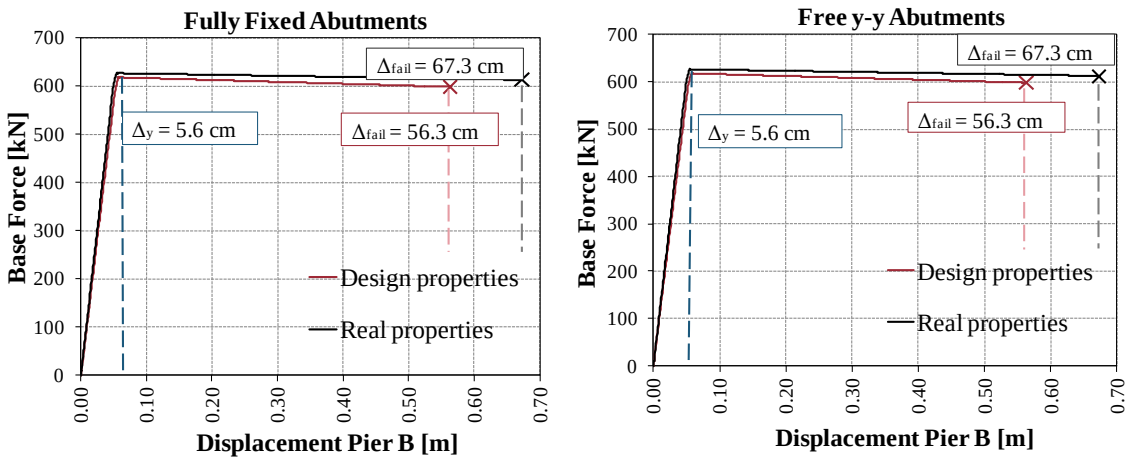

Figure 5.14. ***Pushover curves of pier B for different material properties and for the two configuration of the model: (a) with fully fixed abutment and (b) with the deck free to rotate around the y-y axis.***

$$\mu_{design} = \frac{\Delta_{failure}}{\Delta_y} = \frac{0.563}{0.056} = 10.0$$

$$\mu_{real} = \frac{\Delta_{failure}}{\Delta_y} = \frac{0.673}{0.056} = 12.02$$

5.3.3.4 Push Pull Analysis

In order to evaluate the dissipative behavior of the bridge, the structure is subjected to increasing levels of force until the collapse. The Figure 5.15 shows the hyseretic cycles ensued from the analysis. Consideration already done for Port Hills Overbridge are still valid.

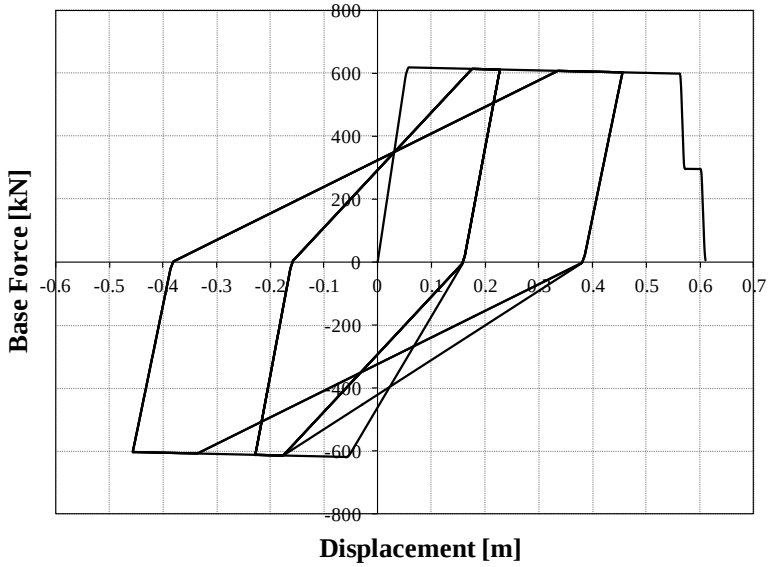

(a)

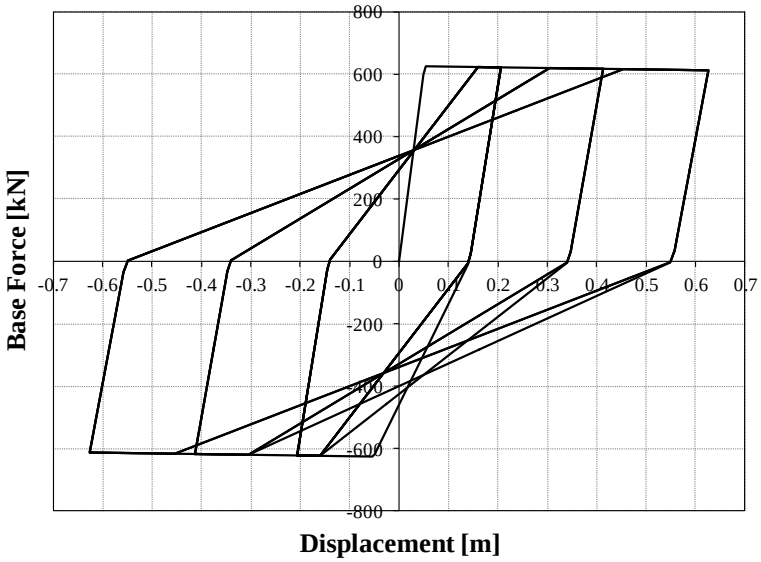

(b)

Figure 5.15. ***Push pull curves of the central pier for (a) design and (b) actual properties***

5.3.3.5 Nonlinear Time History Analysis

5.3.3.5.1 LYTTELTON EARTHQUAKE , FEBRUARY 22, 2011

Since the bridge is close to Port Hills Overpass, the preliminary remarks already made for the previous case study can apply to Horotane Valley Overpass. Time history analysis were carried out first with just the two horizontal components and then including the vertical one.

In contrast to the results obtained for Port Hills Overpass, in this case, when time history analysis are run with record from CHMS and CCCC stations, the displacements at the deck level are minor. In fact, in the most unfavorable case (with design properties and free rotation of the deck next to the abutments) the top of the piers reach a maximum displacement of 1 mm for both CMHS and CCCC records. The same result is achieved including the vertical component of the motion. This is ascribable to the short natural period of the structure which implies a high stiffness. For this reason, only the results of the analysis with HVSC record are shown. As already explained, the HVSC station is the closest to the bridge, the accelerations recorded are amplified due to topographic effects though. Since the displacements are the same in both cases with and without the vertical component, only one graphic is shown.Before running the numerical analysis, the components of the motion need to thrown on the axes of the bridge, as shown in Figure 5.16.

3. Heathcote Valley Primary School, HVSC

$$X_{COMP} = S26W \cdot \cos 73.17° + S64E \cdot \cos 16.83°$$

$$Y_{COMP} = 0$$

$$Z_{COMP} = S26W \cdot \operatorname{sen} 73.17° - S64E \cdot \operatorname{sen} 16.83°$$

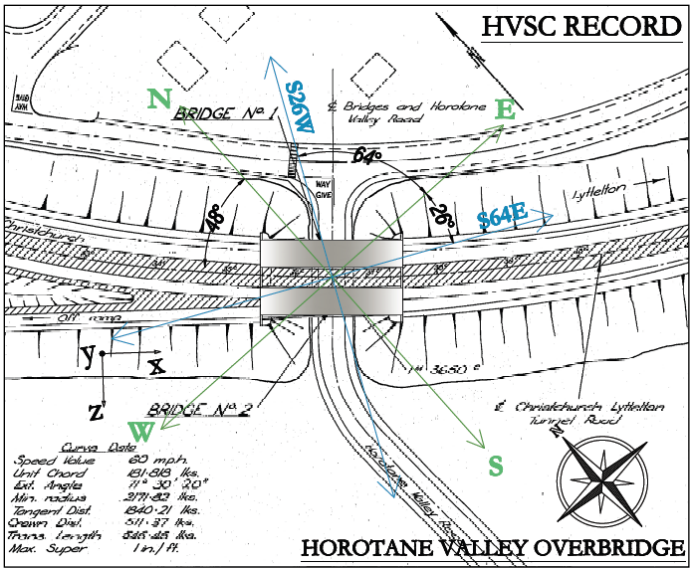

Figure 5.16. ***Components of the motion recorded at Heathcote Valley Primary School station***

The results of the time history analyses, considering the design properties, are shown below.

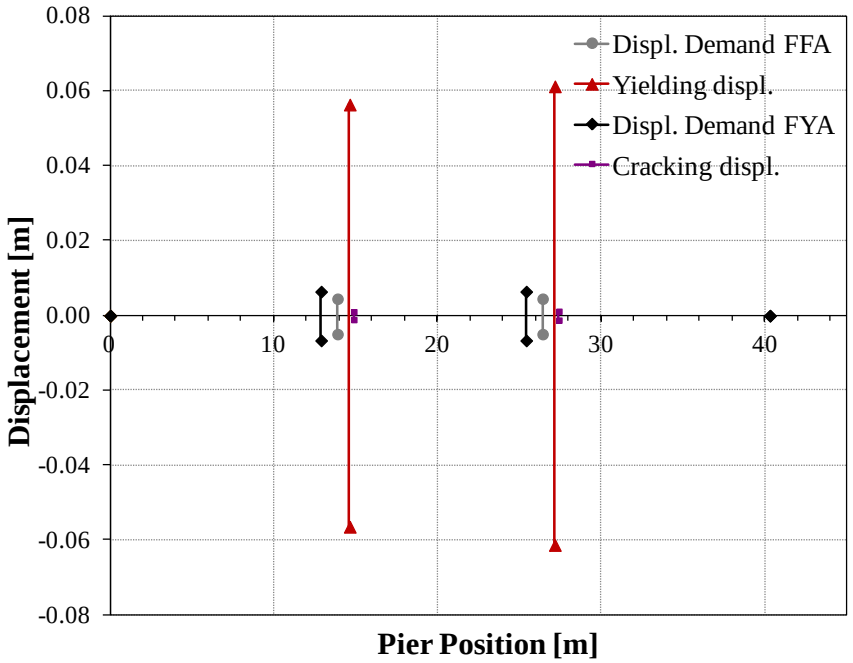

Figure 5.17. ***Comparison between the displacements of the structure of the two configurations (FFA and FYA) and the yielding ones, with records from HVSC.***

When actual material properties are considered, the displacements decrease reaching at the peak 4 mm in the first model (Fully Fixed Abutments, FFA) and 5 mm in the second one (free rotation of the deck around the vertical axis, FYA).

The numerical results, even if not consistent with the expectation from the modal analysis, confirm what actually happened. In fact after the Lyttelton earthquake, the damage found were minimal, only fine horizontal cracking in the piers was observed.

5.3.3.5.2 DARFIELD EARTHQUAKE , SEPTEMBER 4, 2010

When analyses with records of the Darfield Earthquake are performed, results show displacements at the top of the piers are really small. Allowing the rotation next to the abutments, the peak displacement is 2.2 mm with design material properties and 1.8 mm with the actual ones.

5.3.3.5.3 SCALING OF 10 EARTHQUAKES ACCORDING TO THE NEW ZEALAND CODE

For the explanation of this kind of analyses we refer to the preamble made for Port Hills Overpass (4.3.4.5.1.3).

As already told, the method currently use to scale accelerograms is to make match the PGA of the average of the earthquakes with the PGA of the NZ design spectrum [49]. Even if this technique is not very accurate, in this case it can be applicable. In fact the natural period of the bridge fall in the range 0.085-0.092 s and this means that the structure during an earthquake is subjecter to the same accelerations at the ground level. Since the 10 earthquakes were already ascaled according to the Eurocode 8 design spectrum, with a PGA of 0.4g, the scaling factor to reduce the PGA to 0.38g (according to NZS 1170.5 code [21]) is 0.95, as shown in Figure 5.18.

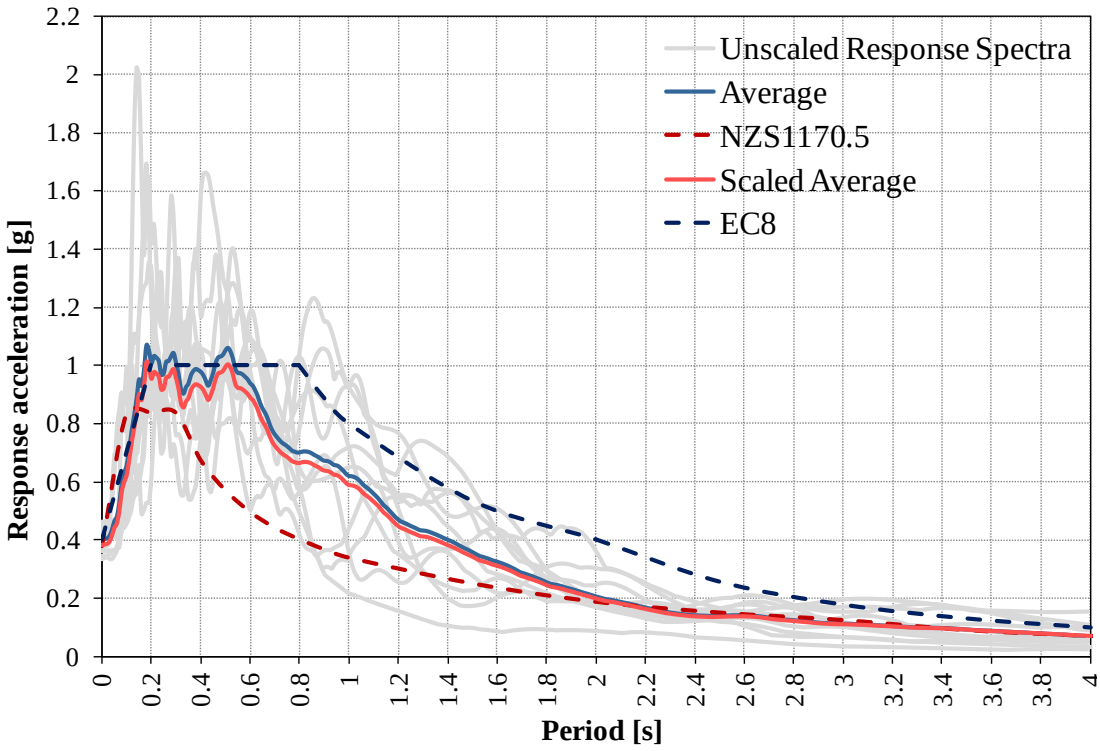

Figure 5.18. ***Earthquake scaling to the NZS 1170.5 [2004]***

The results confirm the tendency of the bridge to sustain very small relative displacements. By way of example, Figure 5.19 shows the maximum displacements achievable by the structure, that is when the second configuration of the model and design properties are used.

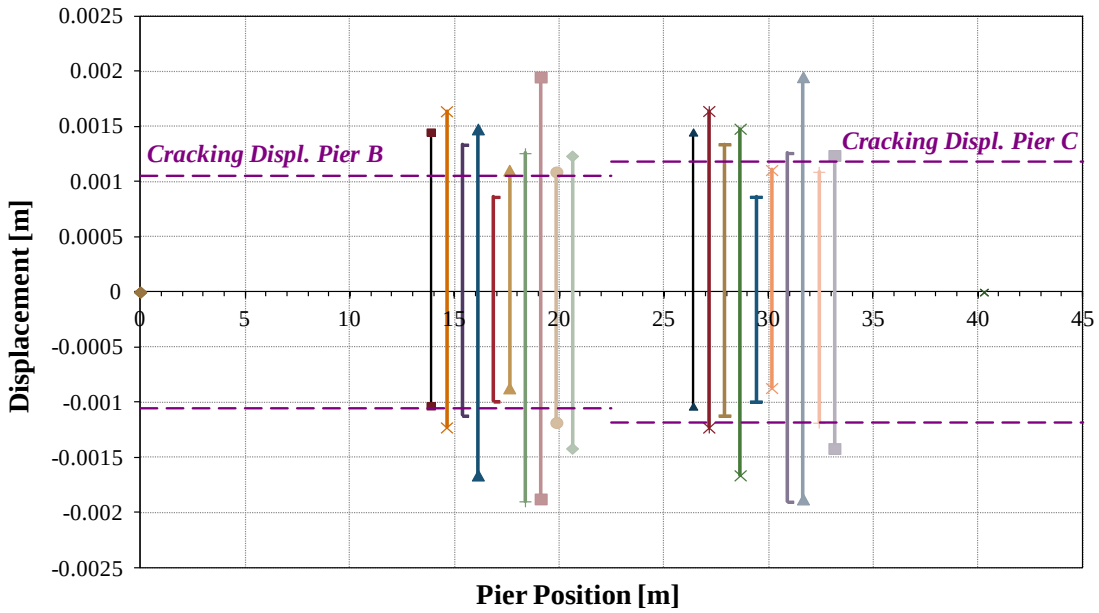

Figure 5.19. ***Displacements demand at the top of the pier for the FYA model and using design properties.***

5.3.3.6 Slope failure

As already presented in the overview of the damages, although the bridge in general performed well during the Lyttelton earthquake, surface sliding of soil was evident under the west abutments and wide cracks and separation gaps between the soil and abutments were evident at the east abutments indicating significant down-slope movements. A significant differential settlement between the approach pavements and the abutments of both bridges was evidenced by repairs to the asphaltic concrete pavement near the abutments. Buckling of the guardrails and shearing of their connection bolts occurred at several of the joints between the approach guardrails and the bridge end posts, due to the movement of the slope.

The purpose now is to take into consideration that phenomenon even if earthquake resistant assessment for slope stability is often based on experience and sound judgment rather than on detailed numerical simulation. The complexities and uncertainties about loading conditions and soil response associated with earthquake problems often limit the usefulness of sophisticated analyses for practical assessment of the bridge performance [51].

An estimate of the horizontal abutments movement to be expected may be obtained using the simplified method of Newmark [52]. The advantage of this method is that it provides an index of permanent deformations. To note well that is used the term “index” to indicate that the estimate of deformation has a number of simplifying assumption which limit the precision of the result. We make two main assumptions: that the unstable soil mass is a rigid block on an inclined plane and that the abutment slides but doesn’t tilt. Sliding of the abutment relative to the soil is initiated when the soil acceleration reaches the limiting value k_y (yield coefficient): every time the ground acceleration exceeds the yield coefficient value, some permanent displacement will be accumulated. The total permanent displacement is therefore not a function of the nature of the soil, but depend on the time history characteristics. The procedure for the Newmark time history analysis consists so of two steps [53]:

1) Identify the yield acceleration of the slope, that is the horizontal pseudo-static coefficient required to bring the factor of safety to unity.
2) Double integrate all relative accelerations.

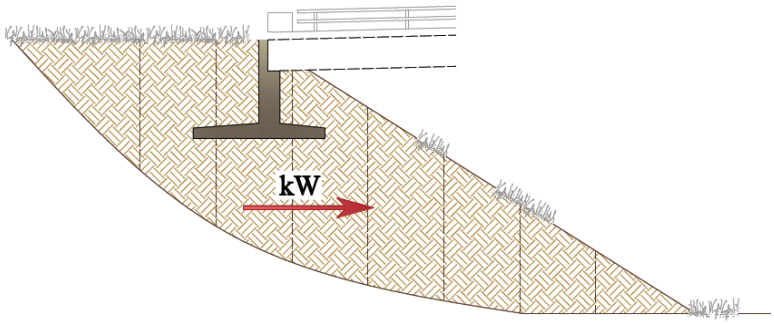

Figure 5.20. ***Failure mechanism of the portion of soil at bridge abutments***

A detailed seismic assessment of the bridge completed in 2004 predicted slope failures at ground accelerations greater than 0.12g [33]. The shallow slope failures observed following the Christchurch earthquake were therefore expected although the slopes performed better than predicted.

In order to assess at best the real performance of the bridge, the slope failure is thus simulated adding to the transitory displacement at the abutment, the permanent displacement. Since in the z direction the ground is confined, only the permanent displacement in the x direction is considered. To do this, each component of the records has to be thrown on the axes of the bridge and only the ones parallel to the longitudinal axis are taken into account. The permanent displacement will be calculated for two of the records used till now in the analyses, CMHS and HVSC. This allows to pick out how the different energy contents of the two records, influences the response at the abutments.

Figure 5.21 and Figure 5.22 show the accelerations and velocity traces for soil (continuous line) and structure (dashed line) for the two components of CMHS record, thrown to the longitudinal axis of the bridge, with a limiting structure acceleration of 0.12g

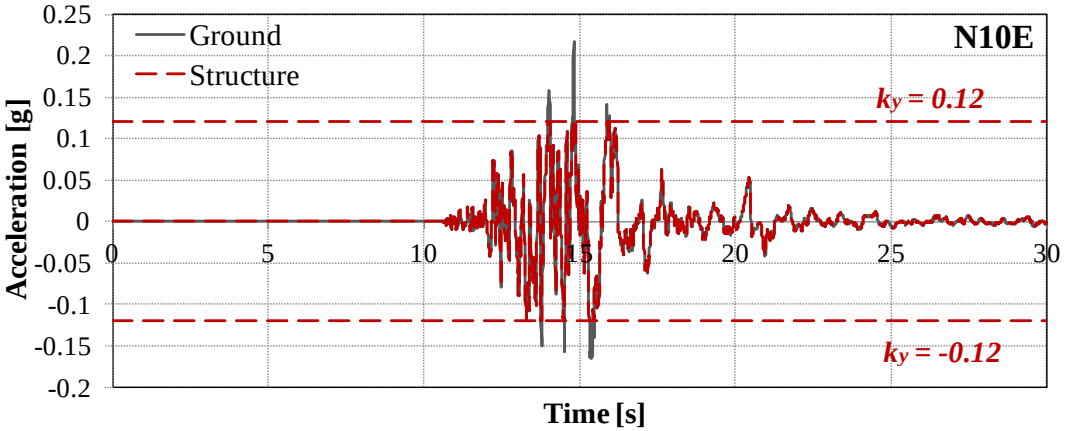

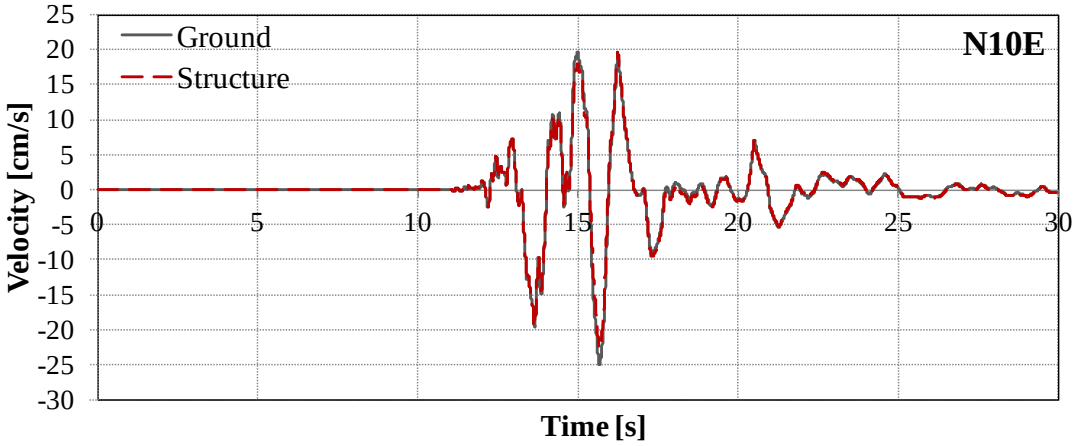

Figure 5.21. ***Acceleration and Velocity Time Histories for ground and structure, CMHS-N10E component***

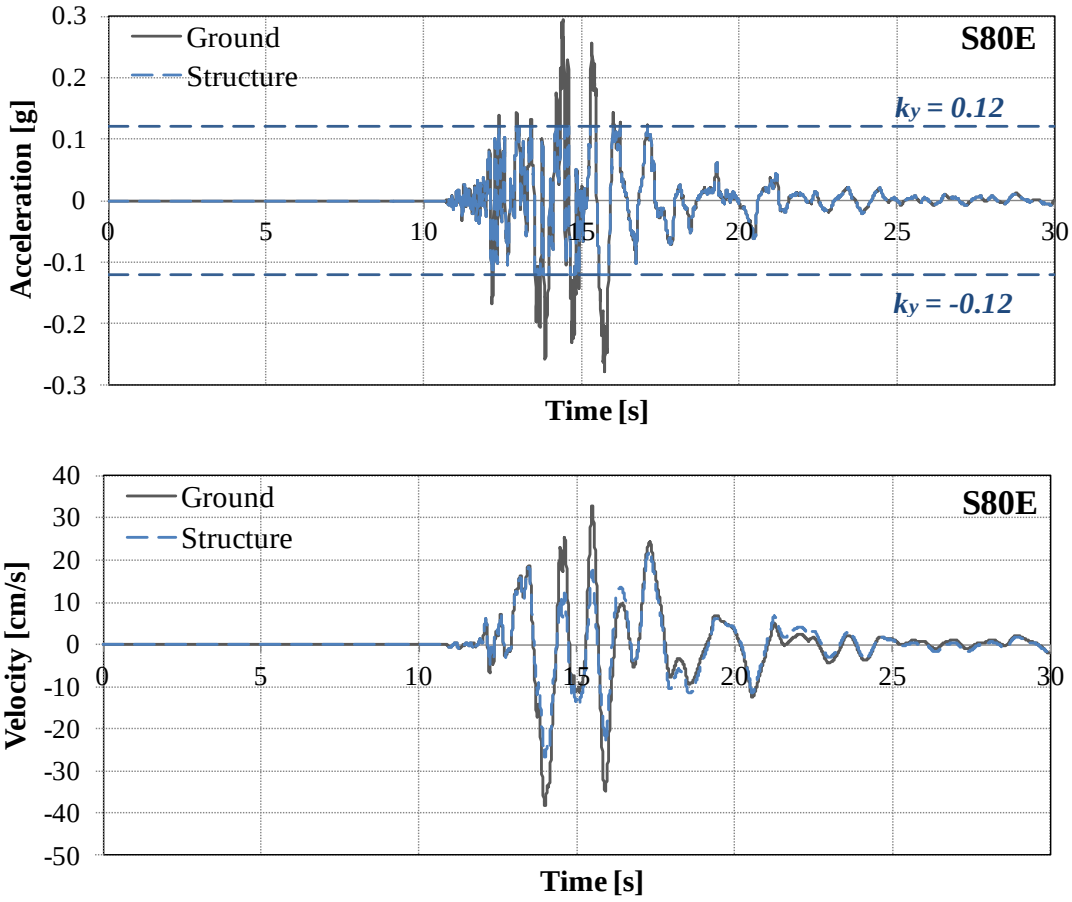

Figure 5.22. ***Acceleration and Velocity Time Histories for ground and structure, CMHS-S80E component***

The corresponding relative structure displacements are shown in Figure 5.23. The displacements in the same direction are added together to find the total displacement of each abutment. Results show that the abutments slide equally.

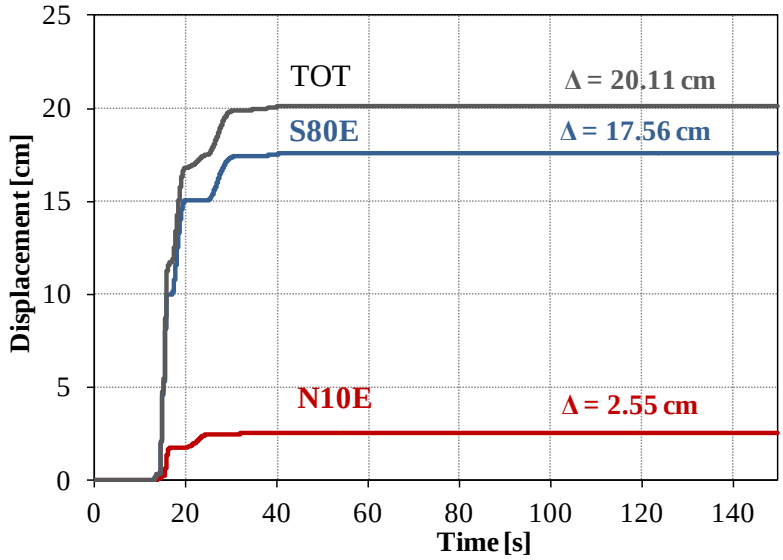

Figure 5.23. ***Displacement Time History of (a) Abutment A and (b) Abutment D relative to soil, CMHS***

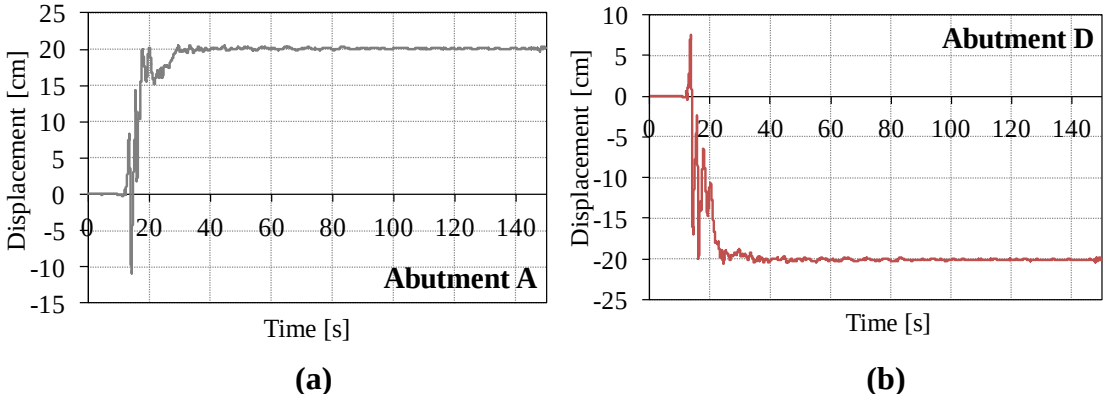

Figure 5.24. ***Total displacement time history for (a) Abutment A and (b) Abutment D with records from CMHS.***

Considering the HVSC records the time histories already plotted for CMHS are shown below.

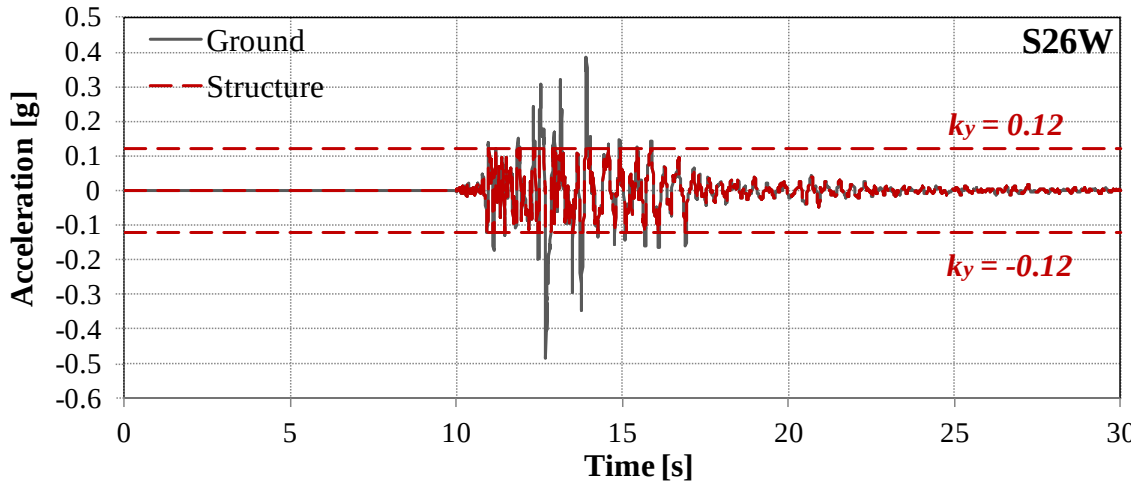

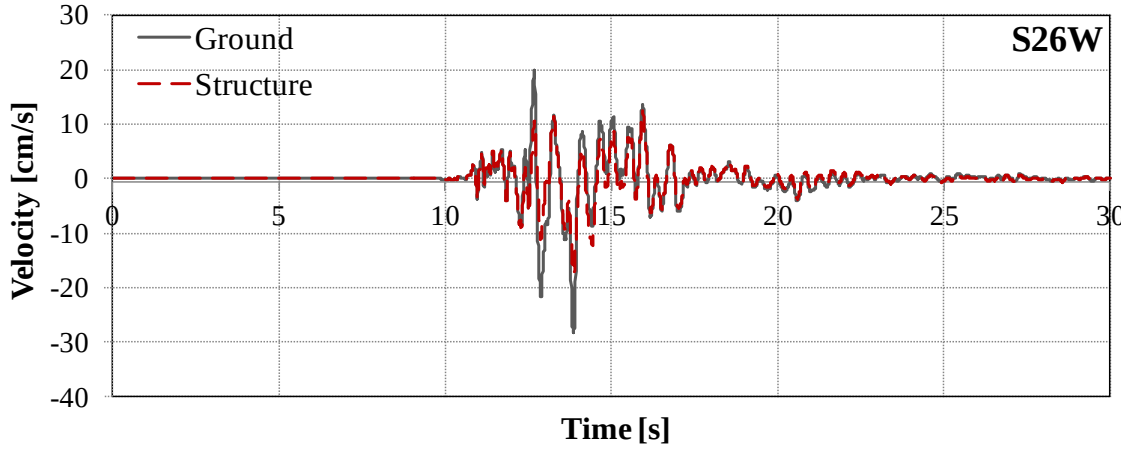

Figure 5.25. ***Acceleration and Velocity Time Histories for ground and structure, HVSC-S26W component***

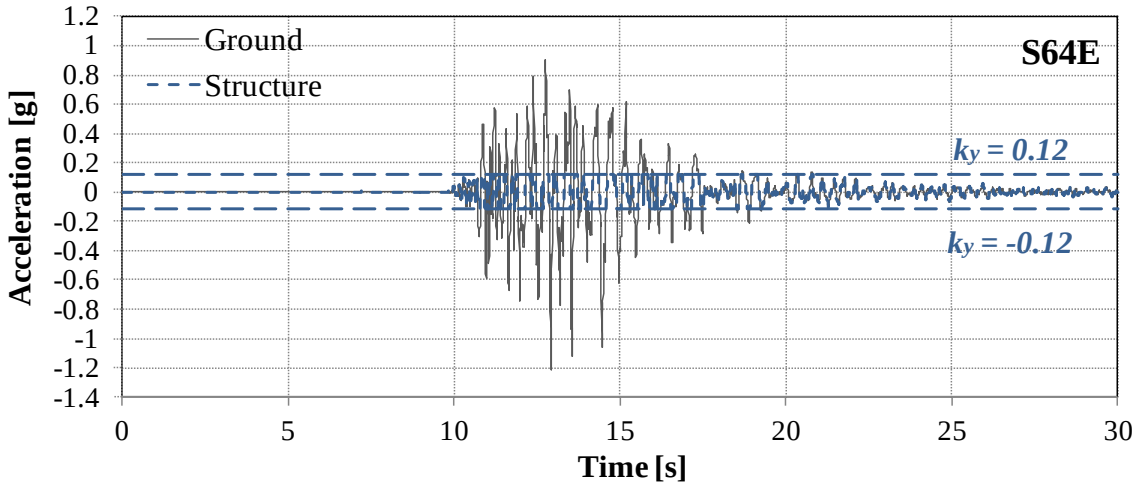

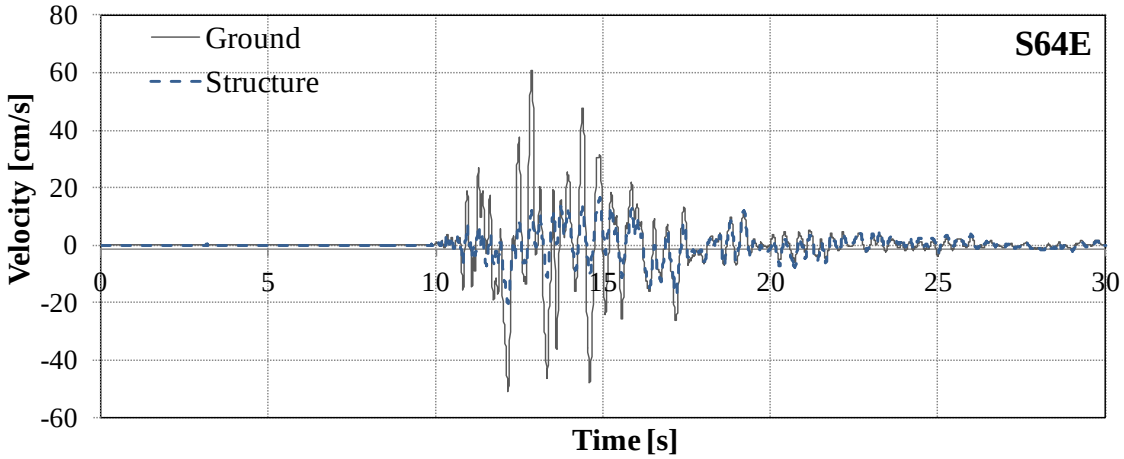

Figure 5.26. ***Acceleration and Velocity Time Histories for ground and structure, HVSC-S64E component***

The corresponding relative structure displacements are shown in Figure 5.27.

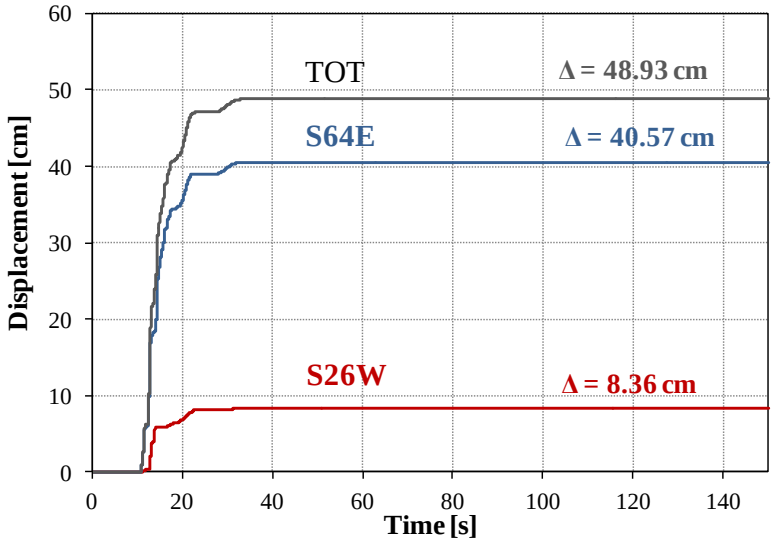

Figure 5.27. ***Displacement Time History of abutments relative to soil, HVSC***

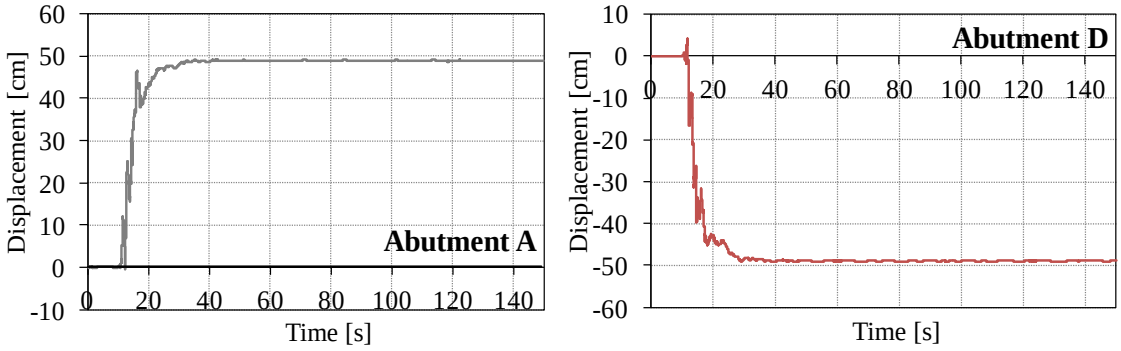

Figure 5.28. ***Total displacement time history for (a) Abutment A and (b) Abutment D with records from HVSC.***

The permanent displacement accumulated is much greater than the previous one, and this is understandable. In fact an earthquake of equal magnitude but with a more peaky character would be expected to lead to displacements considerably in excess of those predicted for CMHS records [51]. As already told in the overview of damages, the movement of the abutments caused shearing of two of the bolts on the new linkage brackets (loaded in shear) at the west abutment of the No 1 Bridge. This happened as, taking into account the flexibility of the beam rubber bearings on both the abutments and the piers, and the linkage bolts at the abutments, it was estimated that the abutments were very much stiffer than the piers in the longitudinal direction and would initially have resisted most of the longitudinal earthquake loads. These are due to the combination of the ground motion and the permanent displacement resulting from the slope failure. To estimate the quantity of the loads taken by the vertical bolts, the connection between the deck and the abutments will be represented by two multi-spring elements: one for the existing holding down dowel connecting the diaphragm to the abutment, and the other one for the strengthening rods put into the bottom of the

beams. The horizontal linkages activate only when subjected to tensile forces and so their function is to avoid the separation between the deck and the abutments. Since the slope failure push the abutments close together, putting the horizontal rods in compression, they are not taken into account.

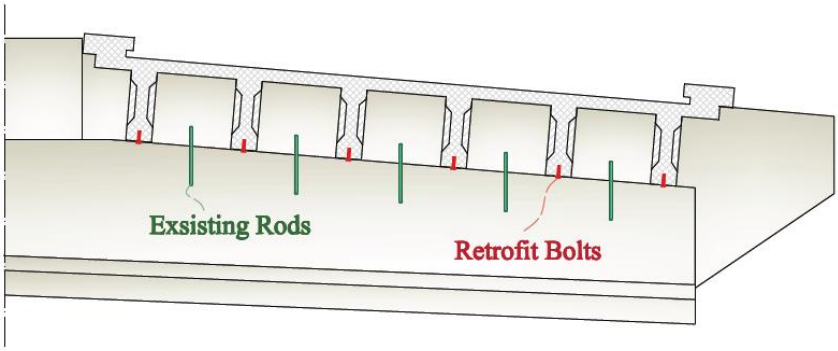

Figure 5.29. ***Frontal view of the West abutment of No 1 Bridge.***

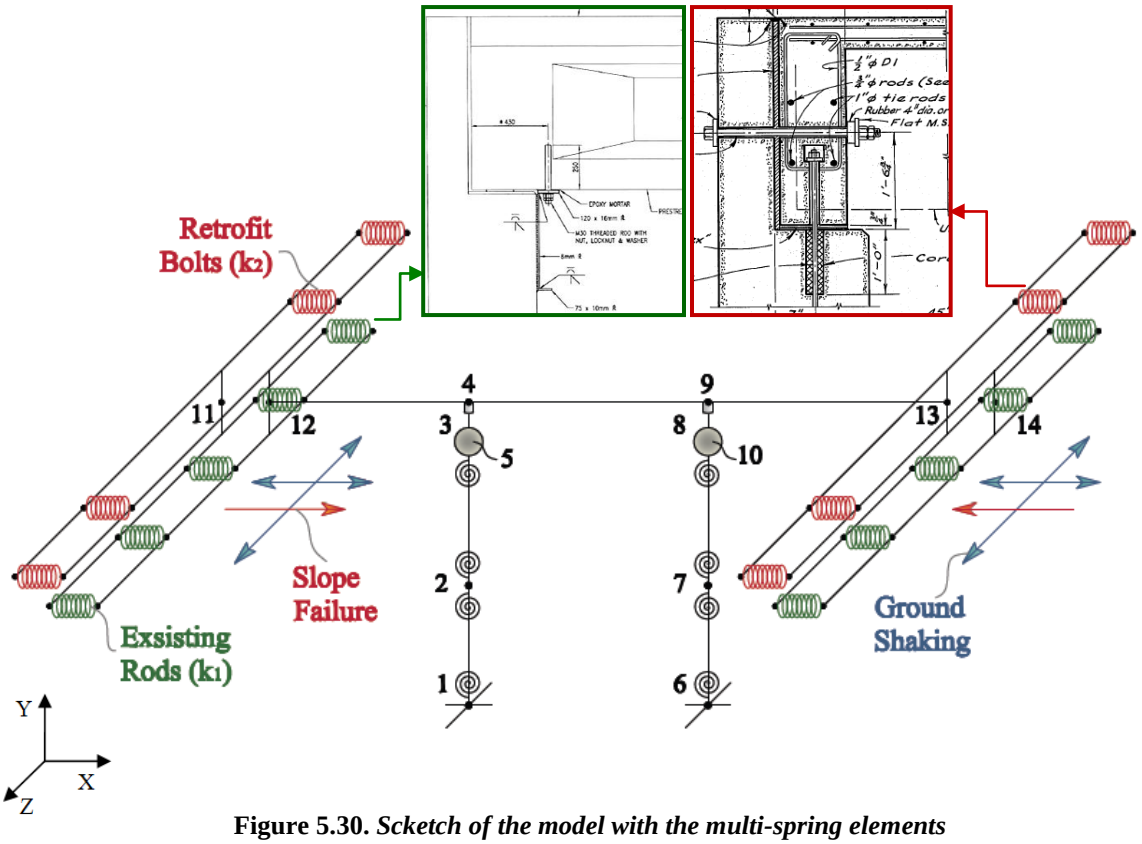

Figure 5.30. ***Scketch of the model with the multi-spring elements***

The model show that the two rows of bolts work in parallel and in turn each of them behave as a group of springs in parallel in both the two directions. The total stiffness of each multi-spring element is therefore the sum of the individual stiffness. Since the vertical linkages were designed to sustain shear forces, we consider the translational stiffness of the rod, liken to a double bending

beam. It is hence a case of estimate the length of the two beams, one for the existing rods and one for the strengthening bolts.
The drawings show that the extisting holding down dowels have a total vertical length of 4' (~1.2 m) with a stretch 1' long (~ 30 cm), between the abutment and the diaphragm, in a hole filled with a plastic material "Pliastic". Considering that in this stretch the rod is free to deform, the length of the beam for the existing linkages is assumed to be 30 cm.
The determination of the actual length of the beam for the retrofit bolts is less immediate. As shown in Figure 5.31, they are fully fixed in the concrete all the length of the bolt. For numerical analyses it will considered a length of calculation of 3 cm.

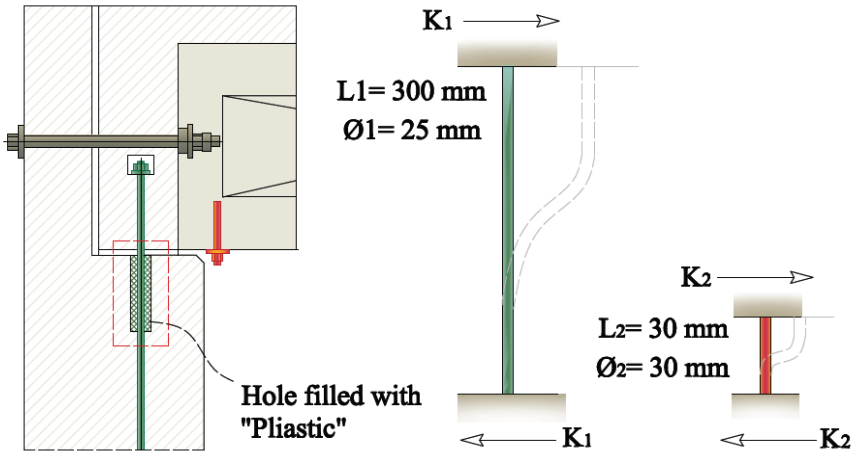

Figure 5.31. ***Schematization of the bolts for numerical analyses***

The grade of the bolts and the rods is 8.8. The properties are shown in Table 5.7.

Table 5.7.*Properties of bolts grade 8.8.*

Ultimate strength f_{su}	800 N/mm^2
Yielding strength f_y	640 N/mm^2
Tensile strength $f_{d,N}$	560 N/mm^2
Shear strength $f_{d,V}$	396 N/mm^2

Results of the analysis are shown in Figure 5.32: adopting an elasto-plastic rule to represent the behaviour of the bolts, it's possible to pick out the brittle failure of retrofit bolts, as expected from a shear failure, at ~1120 kN. It has been chosen to represent in the graphic all the hysteretic cycles (dotted line), even if the rule does not represent the real behaviour of the element, only to better identify the time of the rupture during all the seism simulation. This can be seen more clearly in Figure 5.33 where in the shear force time history is indicated the instant when the shear failure occurs (~11 s). In Figure 5.32 is shown also the behaviour of the existing bolts, that, because of the lower stiffness, absorb a shear force much smaller than the retrofit, remaining in the elastic range.

Although retrofit work did not perform well, if the deck had not been tied together with the abutments, all the forces would have weighted on the existing bolts causing the pounding between the two elements. Figure 5.34 shows the structure with the maximum internal forces of each element.

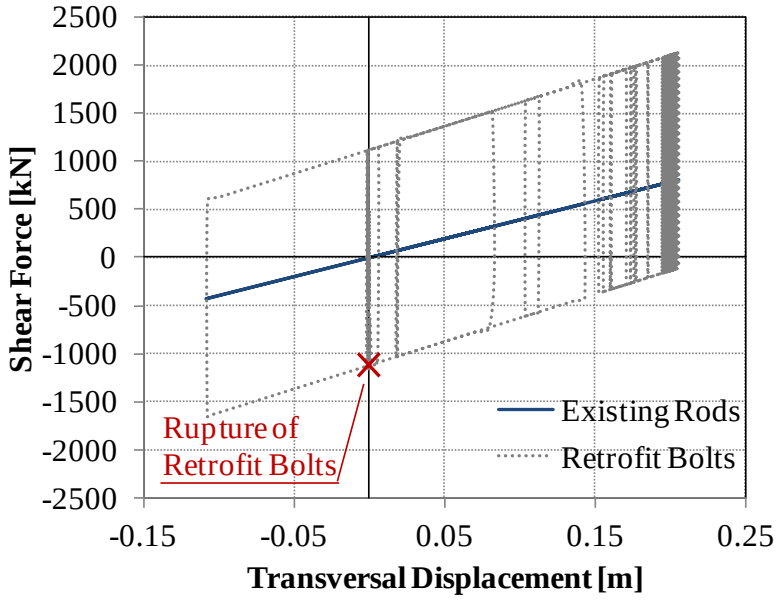

Figure 5.32. ***Shear vs transversal displacement of retrofit bolts and existing rods, with the indication of the shear failure of the retrofit bolts.***

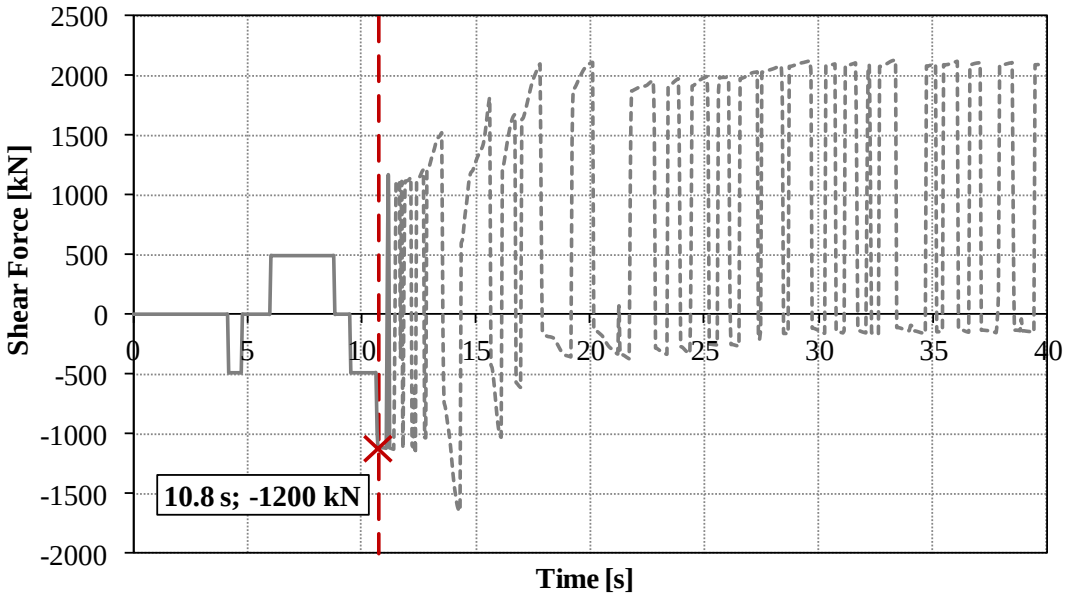

Figure 5.33. ***Time History of the Shear Force acting on retrofit bolts, with the indication of the breaking point.***

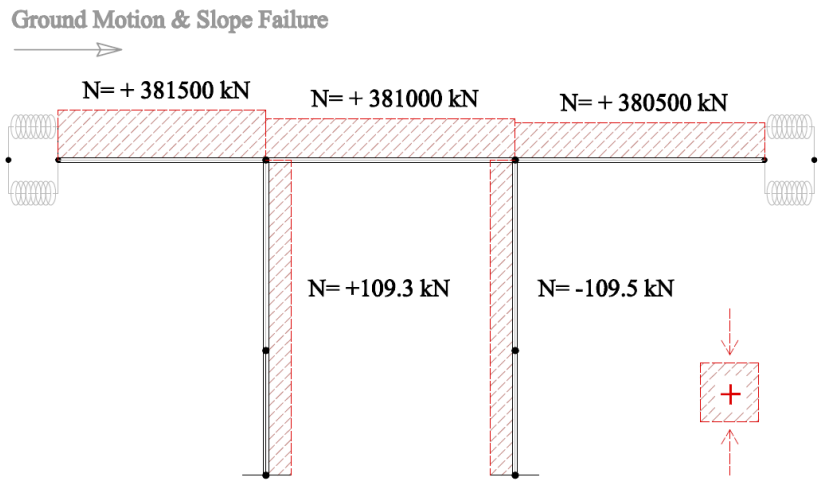

Figure 5.34. ***Maximum axial forces***

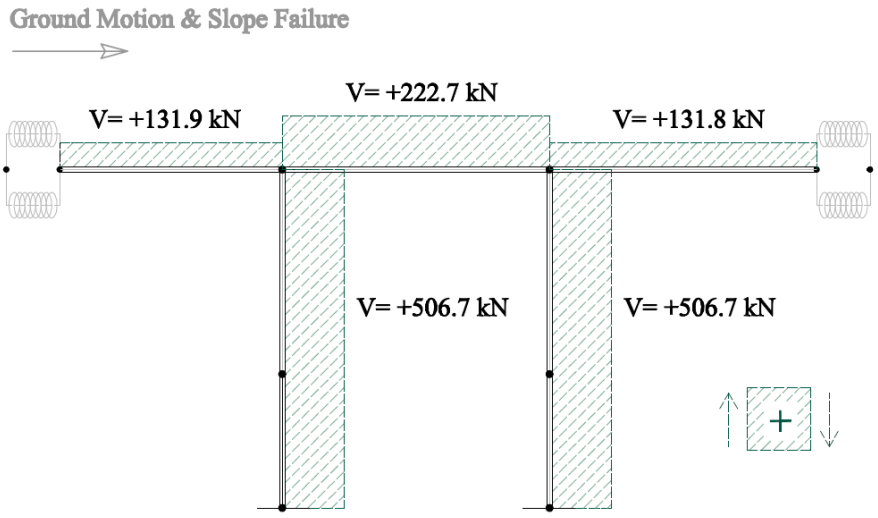

Figure 5.35. ***Maximum shear forces***

5.4 Conclusion

The performance of Horotane Valley Overpass was in general satisfactory in the Christchurch earthquake. Damage due to the ground shaking was unimportant with only fine horizontal cracking observed on the lower half of all four piers. The slope failure was the chief cause of damage to the bridge. All four abutments moved forward causing severe shear cracking in the backwall and shearing of two of the bolts on the new linkage brackets (loaded in shear) at the west abutment of the No 1 Bridge. Bolts on the new linkage brackets also sheared on both abutments of the No 2 Bridge. The movement of the abutments along the longitudinal axis of the bridge was likely the cause of pronounced cracks on the column faces nearest to the roadway under the bridge.

Also on this bridge push over, modal and time history analyses were run, considering the two configuration already used for Port hills Overpass' analyses: with fully fixed restrain or with a

hinge allowing rotations around the vertical axis next to the abutments. Results confirmed what actually happened to the structure considering only the action of the ground motion. Very small relative displacements were recorded due to the high stiffness of the structure. In fact the natural period of the bridge was found to be in the range of 0.085÷0.092, by which the acceleration recorded at CMHS and CCCC station were smaller than spectra accelerations.

Another configuration of the model was taken into account to pick up better the bridge performance during the slope failure. Next to the abutments, two multi-spring elements were used to represent the existing and retrofit bolts. Results of numerical analysis showed that strengthening bolts underwent the shear failure while the existing ones remained in the elastic range, as supposed to have been in the reality. Although the shear failure of the bolts was the proof that the strengthening work didn't perform well, however it was used for absorbing a percentage of the force, "helping" the existent rods in remaining in the elastic range. The retrofitted bolts at the abutments probably may have prevented thus damage as the loading on the original dowels would have been greater.

The results of these analyses will be used by Christchurch City Council and New Zealand Transportation Agency as complementary assessment tool for further retrofit actions on these bridges.

6 MOORHOUSE AVENUE OVERBRIDGE

6.1 Description of the Structure

The Moorhouse Avenue Over-bridge (-43.5399, 172.6367) is an eleven span reinforced concrete structure providing grade separation between Moorhouse Ave and Colombo St. Moorhouse Ave itself is one of the four avenues that encase the central business district (CBD) of Christchurch City, allowing traffic to flow around the CBD. The over bridge is shown in Figure 6.1 and is approximately 270 m long and 17 m wide.

Figure 6.1. ***View from South-West of Moorhouse Overbridge [A. Palermo].***

The structure was constructed in 1964 in three separate sections, linked with expansion joints located at Piers 4 and 7, as shown in Figure 6.2b. The westernmost section is joined to the centre section using tie-bolts across the expansion joint. There is no structural connection between sections at the Pier 7 expansion joint. The aim of the tie-bolts at the Pier 4 expansion joint is believed to be to reduce pounding between the centre section and outer sections under longitudinal deformation of the bridge. In 1995-1996 the original slide-plate joints at the expansion joints were replaced with elastometric plug joints. After 18 months problems occurred with the eastern expansion joint as the western abutment joint was not moving freely due to the steel tie bolts, causing all expansion to occur at the eastern expansion joint. Contech© provided new Proceq Tensa-Grip GS 80 joints,

fabricated from steel extrusions and an expansion seal manufactured from weather resistant elastomer (BBR Contech, 2003) solving the problem.

The superstructure of the overbridge comprises of longitudinally orientated precast T-sections prestressed in the longitudinal and transverse through the flange of the 'T-beams' allowing for transfer of loads between beams. On the edge of the structure the concrete curb was connected above by a cold joint to the flange. The arrangement of piers and superstructure is illustrated in Figure 6.2a.

The deck is connected to the piers with post-tensioned concrete beam pier caps. The post-tensioned tendon profile is curved so to best counter tensile stresses. In the longitudinal direction the piers all have a pinned connection to the pier cap, while in the transverse direction they all have a moment connection, allowing for resistance of lateral loads in the longitudinal direction in the middle section.

Each pier consists of two hexagonal reinforced concrete columns, tapered to the base at 1 in 27. Appendix A shows a typical section through a pier. In the longitudinal direction all piers use a concrete pinned connection to the pier cap, and all but piers 5 and 6 have a pinned connection to the pile cap. Piers 5 and 6 provide a moment connection to the pile cap in both the longitudinal and transverse direction whereas all other piers only provide a moment connection in the transverse direction at both the top and bottom of each pier. Because of this, longitudinal lateral loads are borne by the abutments in the two end sections of the bridge. Whereas in the centre section of the bridge piers 5 and 6 act as cantilevers to resist the lateral loads. In the pinned region of the piers the high strength steel was bent though no confinement was provided at the pin location. Longitudinally it was found that the section at the hinge was over reinforced suggesting that the concrete at that region is likely to be severely damaged when rotation in applied to the joint.

Piers 4 and 7 are split in the transverse direction along the expansion joints as shown in Figure 6.2b. This was done by constructing two 'half piers' which allowed greater flexibility at the top of the pier. The increased slenderness and can be seen as a key factor in the buckling of the western piers of pier 7.

The abutments are reinforced concrete retaining wall structures filled with soil. These provide lateral load resistance in the longitudinal direction in the eastern and western sections. The tie-bolt across the Pier 4 expansion joint means the eastern abutment also provides additional lateral load resistance in the transverse direction to the centre section.

The foundations of the bridge are comprised of octagonal reinforced concrete piles with pile caps. The non-structural components of the bridge include hand rails and light posts.

Modern design philosophies (Capacity design) were not in use which has resulted in regions where the seismic performance of the structure is deficient through the presence of brittle failure mechanisms. The structure has four vehicle lanes; two in the eastern direction and two in the western direction with no pedestrian facilities on the bridge itself. The only services on the bridge are those which provide lighting and driver information, though below the structure exist several sewer, water, power and telecommunication facilities. An overall plan view, longitudinal elevation and a typical transverse section are shown in Appendix A.

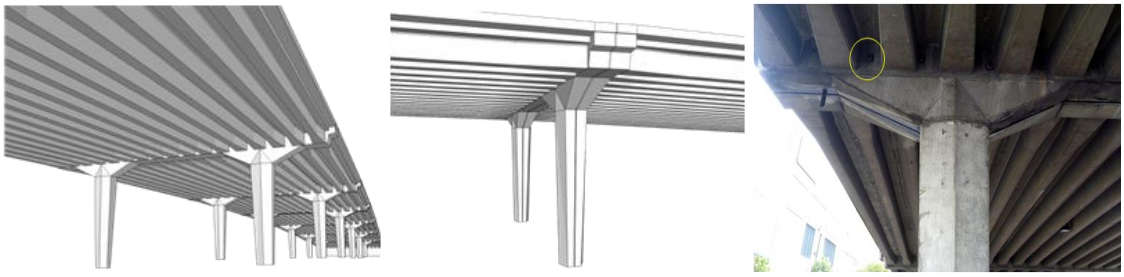

(a) **(b)** **(c)**

Figure 6.2. ***a) Illustration of pier and superstructure arrangement. b) Illustration showing typical expansion joint. c) Pier 4 expansion joint with tie bolts shown.***

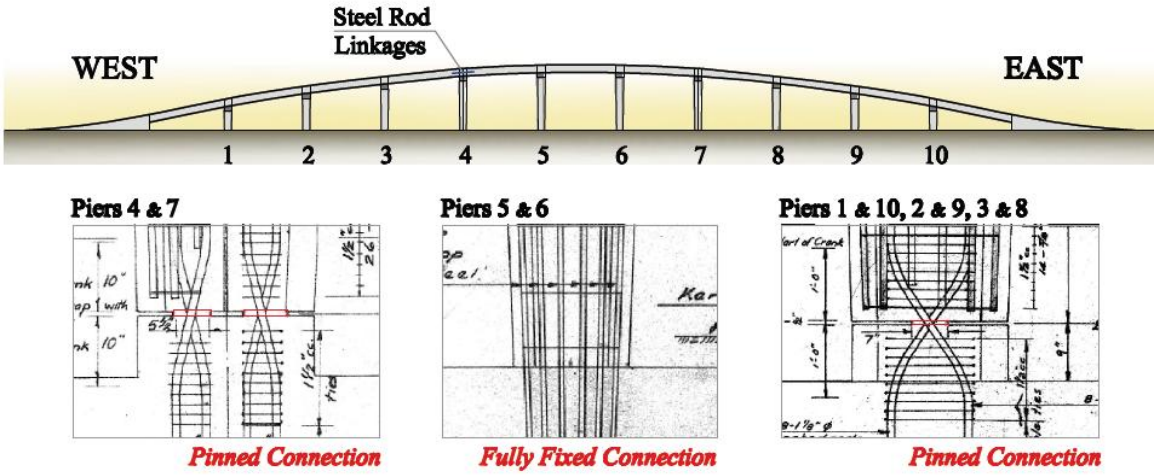

Figure 6.3. ***Sketch of the bridge with the details of the connections between the piers and the footings***

6.2 Earthquake Performance

The overall performance of the structure was unsatisfactory with significant shear cracking and buckling of the split piers below the eastern expansion joint (Pier 7). The mechanism of damage is shown in Figure 6.4b-c. This damage affected the vertical load carrying capacity of the structure along with the lateral capacity. As a result of this damage, the bridge was closed following the February earthquake for over 5 weeks (reopened: 31st March, 2011) while strengthening works were undertaken. This caused vehicle traffic to be restricted to a single lane in both directions either side of the over bridge. A summary of the extent of damage is given in Table 6.1.

Table 6.1. ***Summary of the level of damage observed on the bridge after the Lyttelton earthquake***

Deck	Moderate	**North Approach**	Null
Services	Null	**South Approach**	Null
Piers	Severe	**Substructure**	Moderate
North Abutment	Moderate	**Surrounds**	Null
South Abutment	Moderate	**Foundations**	Unknown

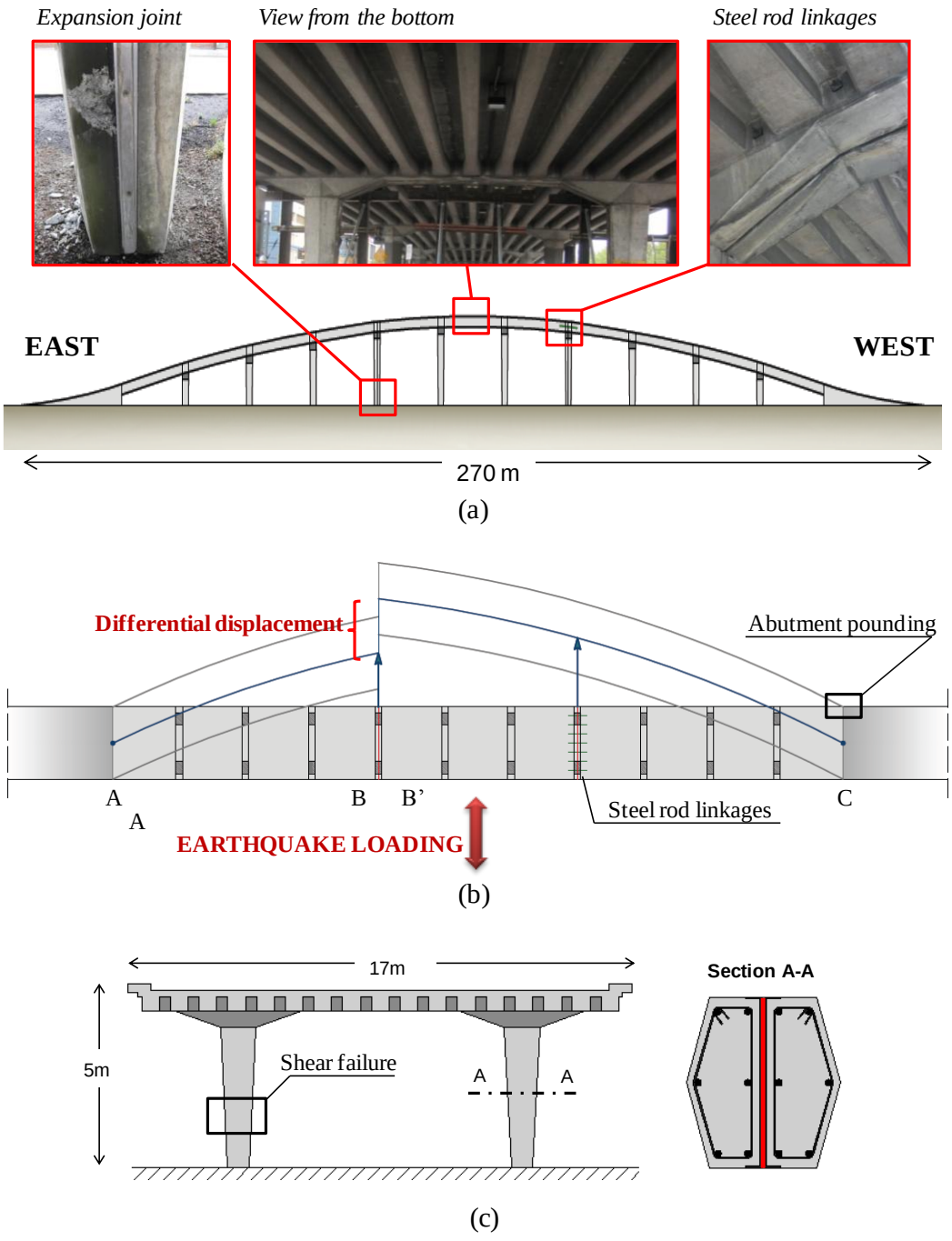

Figure 6.4 ***a) Sketch of the bridge elevation with location of the expansion joints and steel rod linkages b) Sketch of the bridge plan view and qualitative displacement profile under transversal loading; c) Sketch of the typical transverse pier elevation and transversal section of piers with expansion joints;***

6.2.1 Superstructure and Services

A drop in deck height of approximately 10 mm occurred at the central section of the bridge on the south side of the eastern expansion joint, shown in Figure 6.5b. This has occurred because the shear failure in the pier below accompanied by secondary buckling of the column. Spalling due to

pounding resulted in exposure of reinforcing steel at this location. In the longitudinal direction, only piers five and six provide lateral resistance to the structure, with the remaining forces being taken through the abutments at either end. The structure has been designed such that the 'fixed' piers, five and six, provide longitudinal lateral resistance for the central section while the abutments provide resistance for each of the end sections. Variations in behavior of these sections created differences is the seismic response of the structure, this has been attributed as the cause of the pounding damage.

Ground shaking in the February earthquake was primarily in the east-west direction (corresponds to the longitudinal direction of this bridge). It is reasonable to assume that the inclusion tie bolts in the western expansion joint constrained the motion of the central section, reducing pounding damaged.

(a) **(b)** **(c)**

Figure 6.5. ***(a) 10 mm drop in deck height of centre section of bridge at east expansion joint due to failure of pier beneath. (b) Opening of the expansion joint of the deck (c) Crack of the deck in corresponce to the expansion joint***

The services in the immediate vicinity of the Moorhouse Overbridge include high-pressure (HP) gas lines, low-pressure (LP) gas lines, water pipes, sewer pipes, electricity and a brick storm-water channel. The bridge structure itself carries none of these services except electricity to power the lights on the underside of the deck. The services are all beneath the pavement on Moorhouse Ave and Colombo St. The damage to these services was not clear from the damage assessment. They are assumed to be operational as the pavements surrounding the bridge were subject to little damage, indicating minimal deformation of the surrounding soil.

Considering the deck connection to the substructure, a small amount of spalling on the north face at the top of the south column of pier 6 (Figure 6.6a) was noted, indicating that a rotation of the pin connection has occurred, as shown in Figure 5. Also minor vertical cracking occurred in a number of pier caps due to transverse movement of the piers. Minor vertical cracking occurred at the location of the pinned connection in Piers 2 and 3 and formed on the shear plane due to the pinned detail at this location and to the transverse movement of the piers (Figure 6.6b-c).

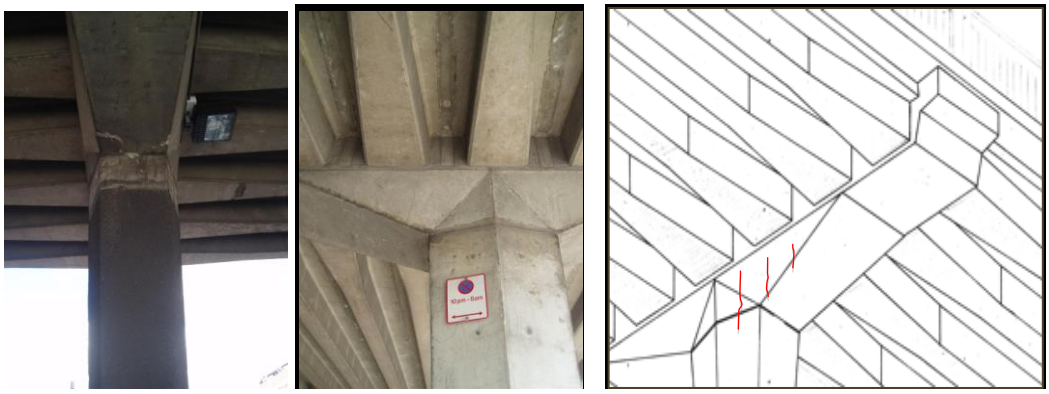

(a) **(b)** **(c)**

Figure 6.6. ***(a) Spalling on the northern face on the capping beam above south column of pier 6. (b) Vertical cracking in pier cap due to transverse movement. (c) Sketch of location of fine vertical cracking***

6.2.2 Piers

Pier 1

Hairline vertical cracks were noted on the western faces of both columns but they are most likely historical. On the northern faces of both of the columns there were also hairline horizontal cracks. Flexural cracks indicated movement in the transverse/vertical direction.

Pier 2

The south column exhibited fine vertical cracks at the top of the southern face. This is due to the configuration of the moment connection at the top of the column, shown in Figure 6.7. In fact is possible to notice that the width of the compression concrete at the joint (7''= ~180 mm) roughly corresponds to the distance between the vertical cracks. These cracks are on a shear plane from the compressive forces at the connection caused from transverse movement. Fine horizontal cracking at approximately 700 mm from the top of the north column on the southeast faces was also noted.

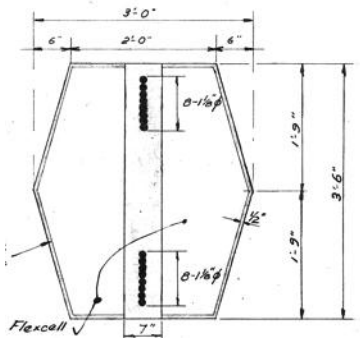

Figure 6.7. ***Detail of the transverse moment connection***

Pier 3

Figure 6.8. ***Pier 3, south column, fine vertical cracks at the top and horizontal flexural cracks.***

The south column exhibited fine vertical cracks at the top of the southern most face similar to that on pier 2. On the same column fine horizontal flexural cracks were noted on the south face approximately 1.3 m from the top. It's worthwhile that the hight tensile steel bars used for the pinned connections have a development length that ends at approximately 1.1 m from the top of the column. For this reason it is belived that these bars were providing some flexural tensile capacity during the transverse/vertical ground motions. The south column is shown in Figure 6.8. The north column had fine horizontal cracks on the

southeast faces approximately ⅔ of the way up the column. This can be explained by similar reasoning to above.

Pier 4

Fine diagonal shear cracks in the same direction towards the base on west and east faces, were found on both the north and south columns.

Pier 5 & 6

Inspection of these piers were difficult due to the cladding.

Pier 7

Severe shear cracking has occurred in both north and south columns signifying that large transverse movement has taken place. This was due to the insertion of steel rod linkages in the deck at the expansion joint at only one side of the bridge, which induced irregularity in the structures transverse response. In fact, with the west and central part of the bridge linked, the lateral load from seismic mass in the west section were transferred to the central section and the bridge pier at the eastern expansion joint suffered extensive displacement demand. The slenderness of the pier affected the vertical load carrying capacity of the structure along with its lateral capacity. Both columns also have notable secondary buckling on the west side of the split joint that looks to have occurred after the initial shear failure and put the central span at risk of collapse. The observations made, indicate that damage was induced by extensive ground shaking: large transverse horizontal accelerations may have caused a flexural-bucking failure mechanism in the columns. Moreover other specific damage were found on each column. On the north one diagonal cracks are present toward the top on the western faces. Horizontal flexure cracks are present near the centre on both the western and eastern faces due to vertical ground movement (Figure 6.9). The south column suffered instead greater extent of secondary buckling. On the eastern face relatively small diagonal shear cracks are also present at approximately ⅓ height and smaller horizontal flexure cracks at half height. Spalling and exposed reinforcing was noted at roughly ⅔ height on the south face (Figure 6.10).

(a) **(b)** **(c)**

Figure 6.9. ***North column (a) West face (b) Detail of shear fail at the base of the west face (c) Exposure of the steel bars at the North face***

(a) **(b)** **(c)**

Figure 6.10. ***South column (a) West face (b) South face (c) North face***

Pier 8 & 9
Minor damage to both columns, minor flexural cracking and some shrikage cracks.

Pier 10
Minor flexural cracking.

6.2.3 Abutments

Substantial spalling and buckling of reinforcing steel has occurred on the southern kerb at the western deck/abutment connection due to a large transverse deflection of the bridge in the southern direction: in fact the ground shaking in the longitudinal direction has caused the deck to pull away from the abutment, causing the vertical tension cracks whilst also elongating the reinforcing steel. When put back into compression, the concrete kerb has spalled and the reinforcing bars have buckled, as shown in Figure 6.11b. It's important also to notice that in this area vertical cracks reduce in size toward the base of the abutment (Figure 6.11a). The damage to the western abutment was more severe than that to the eastern abutment: this happened as the western abutment had to resist lateral loads generated by the mass of both the western and centre sections of the bridge.

(a) **(b)** **(c)**

Figure 6.11. ***Damage at southwest deck/abutment connection a) Tension cracks due to separation of deck/abutment during ground shaking (b) Buckling of reinforcement in reinforced concrete kerb (c) Minor cracking in northeast beam/abutment connection***

6.2.4 Foundations

The bridge is founded on 16" octagonal reinforced concrete piles. Damage to the foundations is not known as these could not be directly inspected during the assessment.

6.2.5 Approach and Surroundings

The surrounding land did not suffer any major damage. The pavement was subject to minimal damage but was in an operational condition at the time of inspection though had become uneven due to liquefaction. Liquefaction did not cause any major damage the structure though it impact on the behaviour underlying soil in the shaking is likely to have altered the ground motion that the bridge experienced. There has not been any lateral spreading with no nearby watercourses.

(a) **(b)**

Figure 6.12. ***View of the bridge (a) from the west side and (b) from the east side.***

6.3 Retrofit

Initially temporary strengthening works were erected around the failed pier. These consisted of two built up square block concrete columns with timber blocking between to prop the bridge while further work was undertaken. A multi span structural steel frame was designed and constructed soon after the event spanning between the two failed columns at pier 7 approximately 500 mm to the west, shown in Figure 6.13. This lead to the bearing of the tapered deck beams on the steel portal to be on a smaller cross-section and was meant only as a temporary solution to stop complete collapse of the damaged section. This solution did not provide any additional lateral stability and so the over bridge was not reopened to vehicle traffic on 31st March 2011 when the final temporary solution was implemented.

Figure 6.13. ***Temporary strengthening at failed pier at date of inspection (22/03/11).***

Piers 4 & 7 were identified as positions of weakness, especially in the transversal direction. To improve the transversal capacity of the damaged structure Opus International Consultants Limited© elected to construct dual cross-bracing units at each of the piers (Figure 6.14a). These were straddled the piers and used doubled up 310UC137 steel sections to act as a diagonal bracing system. Full drawing of the repair can be found in the document 'R702 Moorhouse Avenue Overbridge, Earthquake Strengthening and Seismic Strengthening Report' by Opus International Consultants Limited© (Figure 6.14c) .

(a) **(b)**

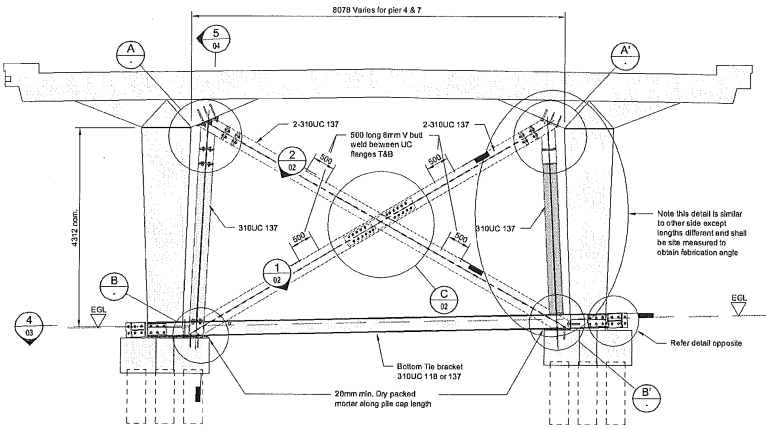

(c)

Figure 6.14. ***(a) Transverse bracing system implemented at Pier 4 & 7 (b) Detail of the connection between the steel beams (c) Detail of the retrofit work from the drawings (Opus International Consultants Limited].***

6.4 Numerical Analyses

6.4.1 Introduction

A numerical analysis of the Moorhouse Avenue Overbridge is undertaken using Ruaumoko3D [40]. Within this package it is possible to undertake modal analysis, pushover analyses along with non-linear time history analysis using lumped plasticity models. Analyses were run in the 3D version of the program to provide validation of results.

Four models, described in section 6.4.4.1, will be analysed. A modal assessment is first carried out to see what's the level of the demand in the NZ code scale. Then in order to assess the capacity of the structure a static push over analysis is performed. Finally the models will be subjected to ground motions recorded during the Darfield and Christchurch earthquakes.

6.4.2 Section properties

Section properties are summarized in APPENDIX B.

6.4.3 Calculation of the Moment Curvature Relationship

Response-2000 was used to determine the section properties of the piers, the yield surface of the piers at the top and base and the shear capacity of the piers.

Response-2000 is a tool for reinforced concrete section analysis using the Modified Compression Field Theory. The assumptions used in Response-2000 are that plane sections remain plane, there is no significant transverse clamping (or confinement) stress acting throughout the depth of the member and the Modified Compression Field Theory (MCFT) can be used for biaxial stress-strain behaviour throughout the depth of the member [54].

Transverse confinement of the longitudinal steel in reinforced concrete members is not accounted for in Response-2000. Increasing the level of confinement in a member causes an increase in member strength, meaning Response-2000 may underestimate the strength of some members. A

low level of confinement is present in the piers of the Moorhouse Avenue Overbridge so it was assumed that the section properties determined through the use of Response-2000 would be an acceptable approximation of the properties of the piers. Results of the moment curvature relationship at the base of the piers are shown below. As already presented in the description of the structure, all the piers a part from the 5 and 6 ones, have a pinned connection at the base (see APPENDIX A), so that the reduced section in considered for the calculation.

Pier 1 and 10

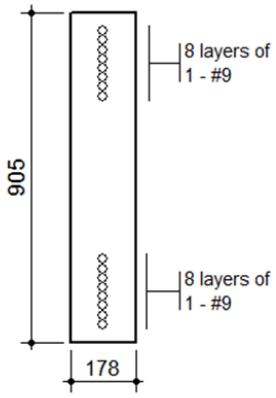

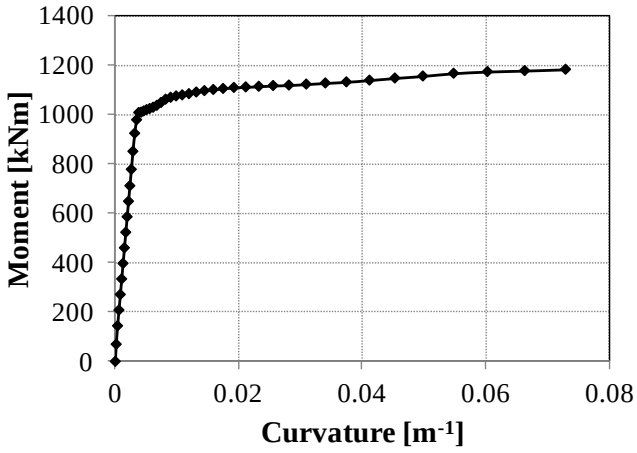

Pier 2 and 9

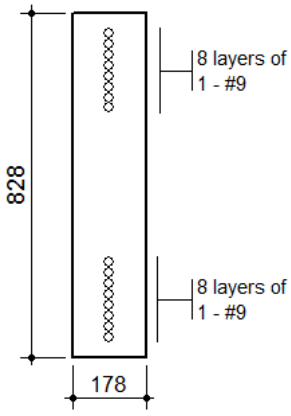

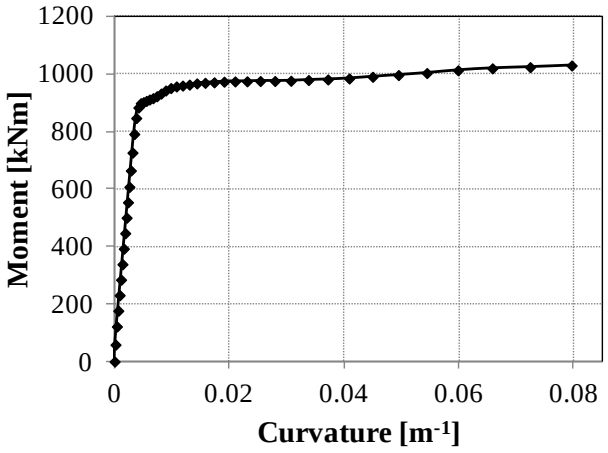

Pier 3 and 8

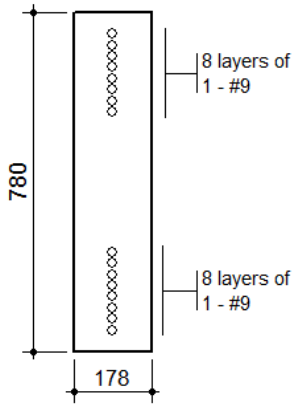

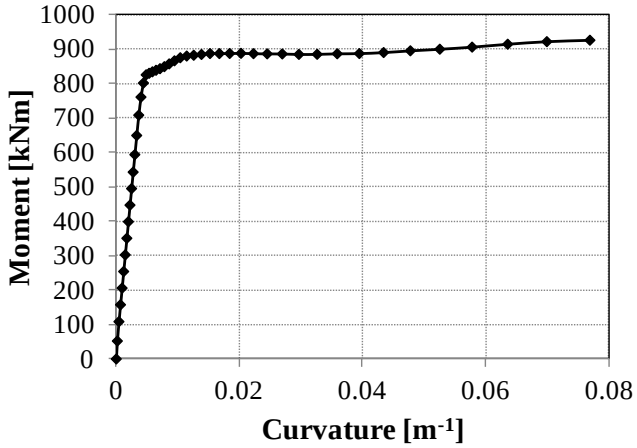

Pier 4 and 7

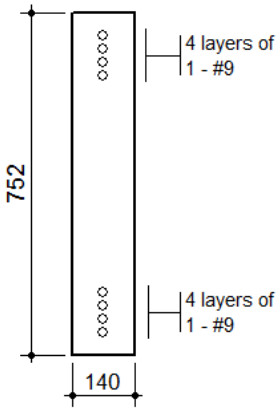

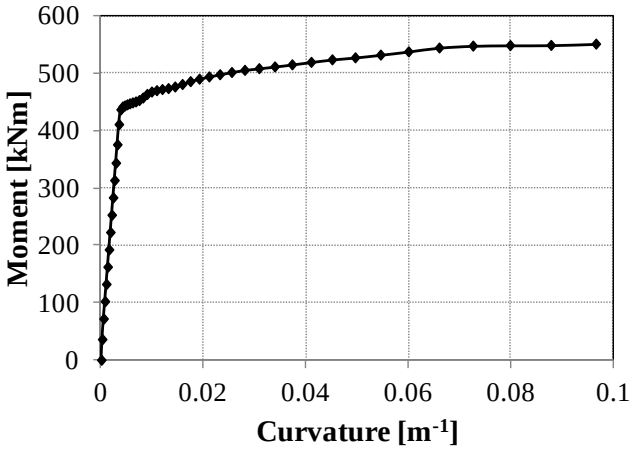

Pier 5 and 6

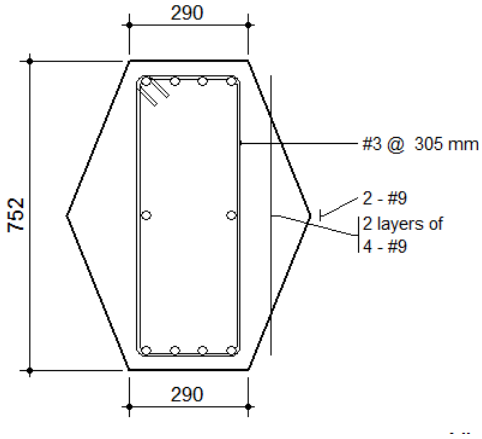

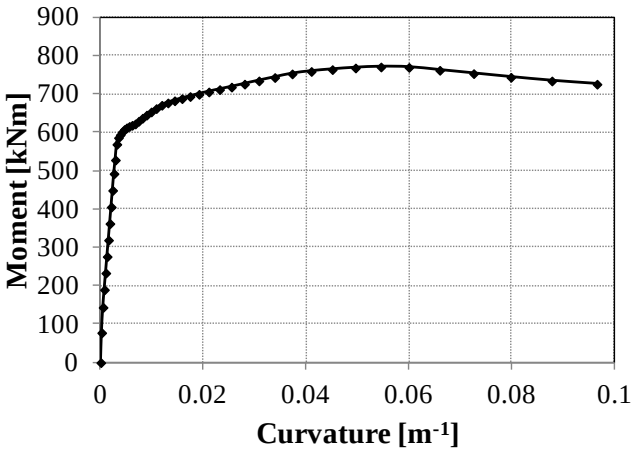

6.4.4 Assessment of the performance of the Bridge

6.4.4.1 Description of the Model

The 3D Model adopted for the structure is shown below in Figure 6.15.

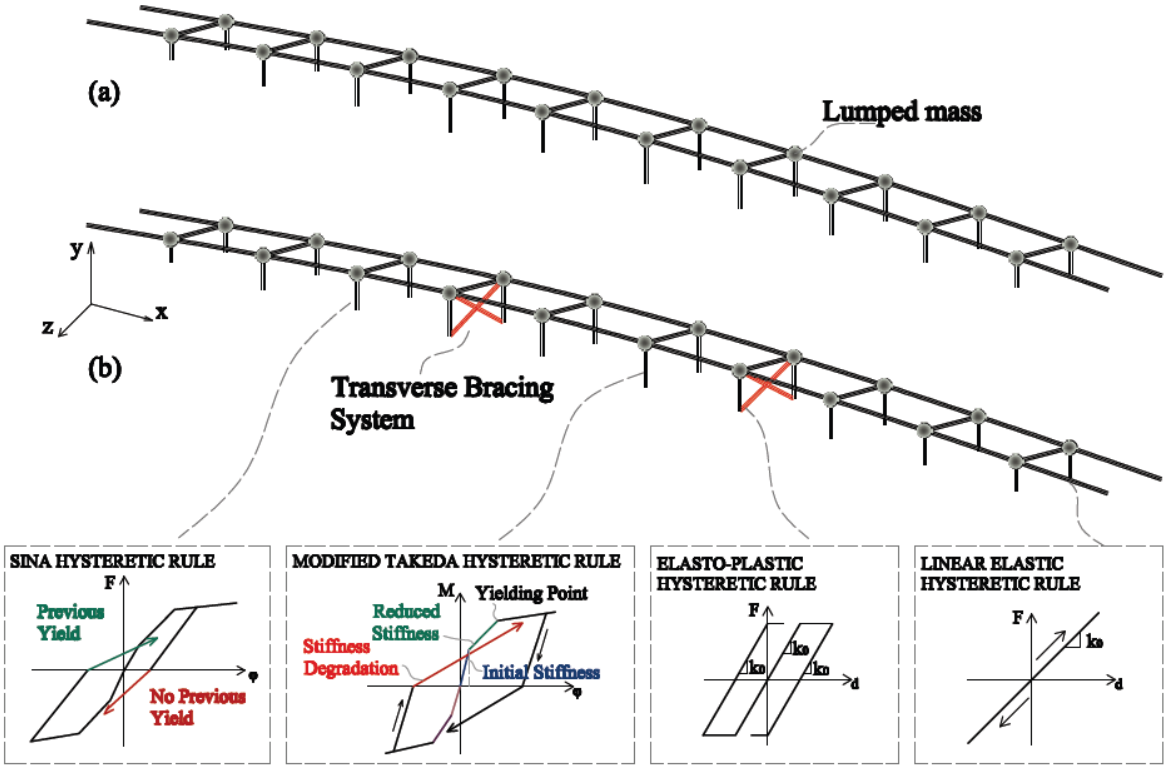

Figure 6.15. ***Visual representation of the structural model in Ruaumoko: (a) undamaged and damaged, (b) repaired with cross-bracing.***

Ruaumoko [40] allows for the inclusion of a number of features to provide an accurate representation and analysis of the structure.

The deck, pier caps and ties across the expansion joints were modelled as beam members with no axial force interaction. It was assumed that these members remained elastic throughout both seismic events as there were no signs of damage to these components and these components were assumed to be very stiff relative to the piers.

A modified Takeda hysteretic loop [45] was used in regions where inelastic flexural behaviour was anticipated in reinforced concrete members. Inelastic axial behaviour of the steel transverse bracing system implemented in repairing the structure was modelled using a simple Bilinear hysteretic model. Pounding elements were utilised in the gap region at pier 7 along with strength degradation allowance associated with inelastic behaviour. Strength and stiffness was also manually altered between models to capture damage that occurred prior to the model being run. As it was observed that the structure displayed heavy shear damage to in the split piers along with shear cracking a number of others, inelastic shear behaviour was also included in all piers using a SINA hysteretic model [45]. This allows for shear degradation of the piers due to shear deformation as well as plastic rotations at the ends of the members.

A lumped mass approximation was used with the mass lumped at the top of each pier. Tributary areas of each pier were used in determining the amount of mass that was to be lumped at the top of each pier. Using a density of 2400 kg/m^3 it was found that Piers 5 and 6 had a tributary weight of 1100 KN. Each split pier had a tributary weight of 550 KN and all other piers had a tributary weight of 1050 KN. The lumped weight included the weight of the deck within the tributary area, the weight of the pier cap and the weight of the pier above pier mid-height. The mass of vehicles on the bridge at the time of seismic loading was assumed to be negligible.

Performance of the bridge was assessed in five conditions.

In the first one, known as 'Undamaged', it was assumed to have full section properties (uncracked) with no strength reduction. The second assessed the structures damaged performance; members such as piers had their stiffness reduced. The level of reduction was depended on the pier location. Pinned and fixed piers had their stiffness reduced by 1/3, the 'split' piers had their stiffness reduced to $0.4EI_{initial}$. In addition to this the two heavily damaged piers that made up the frame at pier 7 were assigned a 50% reduction in strength along with stiffness reduction. The level of stiffness reduction of 1/3 was taken as an approximate average reduction over the elastic section to account for cracked and uncracked regions. $0.4EI_{initial}$ is taken from NZS1170.5 [21] as the cracked section modulus. For the repaired condition, 310UC137 members were included attached as cross-bracing along with vertically reinforcing the pier. Members were attached to the adjacent halves of the split piers and then linked in the central node

Two retrofitted model were also taken into account. The first one is a Fibre Reinforced Polymer (FRP) based retrofit. FRP is a composite material generally consisting of carbon, aramid, or glass fibres in a polymeric matrix (e.g. epoxy resin). Among many options, this reinforcement may be in the form of preformed laminates or flexible sheets. The laminates are stiff plates or shells that come pre-cured and are installed by bonding the plate to the concrete surface with epoxy. The sheets are either dry or pre-impregnated with resin (pre-preg) and cure after installation onto the concrete surface. This installation technique is known as wet lay-up. The uses of external FRP reinforcement may be generally classified as flexural strengthening, improving the confinement and ductility of compression members, and shear strengthening. One limit to increasing the moment capacity is that eventually the shear capacity of the member is exceeded. In these situations, it has been shown that externally bonded FRP sheets may be used to increase the shear capacity as well [55].

The FRP retrofit model assumes that FRP wrap is applied to the western half of Pier 7 to prevent shear failure. It was assumed that the damage to Pier 7 due to shear failure was repaired prior to application of FRP wrap and the section properties of all piers were returned to their as-built value. The effect of FRP wrapping was approximated in the model by disabling any inelastic shear behaviour of Pier 7. Shear failure was not prevented in the other piers. It was assumed that the application of FRP wrap would increase the stiffness of Pier 7 by 10%. The increase in stiffness is an approximation and further investigation would be required to accurately determine the effect of FRP wrap on the stiffness of the pier. It was assumed that the application of FRP wrap had no effect on the moment or ductility capacity of the pier. The second retrofitted model was the Tie-Bolt Retrofit model. In this model, tie-bolts were added to the Pier 7 expansion joint connecting the centre and eastern sections of the bridge, making the Pier 7 expansion joint similar to the Pier 4 expansion joint. It was assumed that the damage to Pier 7 was repaired and the section properties of all other members were returned to their as-built values.

The second retrofitted model was the Tie-Bolt Retrofit model. In this model, tie-bolts were added to the Pier 7 expansion joint connecting the centre and eastern sections of the bridge, making the Pier

7 expansion joint similar to the Pier 4 expansion joint. It was assumed that the damage to Pier 7 was repaired and the section properties of all other members were returned to their as-built values.

6.4.5 Modal Assessment

A modal analysis was performed on each of the structural configurations in order to compare the accelerations that actually acted on the structure against the ones of the NZS1170.5 [2004] [21] response spectra and see the level of the demand on the code scale. The response spectra were formed based on the motions of both Darfield and Christchurch earthquakes recorded at the nearest seismic station, the Catholic Cathedral College one (CCCC). The code response spectra was determined for the bridge site for a 1/500 year earthquake.

The natural period of the structure is between 0.11 and 0.236 s depending on the section as well as on the configuration of the model. In fact seismic gaps in the bridge allowed the eastern section to act independently (disregarding pounding) from the two western sections. The results from the modal analysis are shown in Table 6.2. In the report published by Opus International on damage assessment and repair of the bridge, it was stated that using Rayleigh's method the natural period of the bridge was found to be 0.6s which displays some differences from that found from this analysis.

Table 6.2. ***Natural periods of the structure***

	Undamaged	**Damaged**	**Repaired**
Main Section	0.187s	0.236s	0.134s
Eastern Section	0.131s	0.186s	0.110s

The natural period values provided by modal analysis, give a spectral acceleration, based on the GNS data from the nearby Catholic Cathedral College (CCCC), of 0.5g – 0.7g. The spectral acceleration chart in Figure 6.16 show that both the earthquake demands do not exceed the NZS1170 design spectral values. This would lead us to expect the structure to have a good dynamic response to the earthquake, even if the conclusion needs to be dampened a little since the bridge was built according to different standards. Since in the reality the structure became more inelastic, it would be expected that its natural period will extend, shifting its motion into the 0.3s to 0.7s region, where spectral accelerations are in the order of 0.9g to 1.1g.

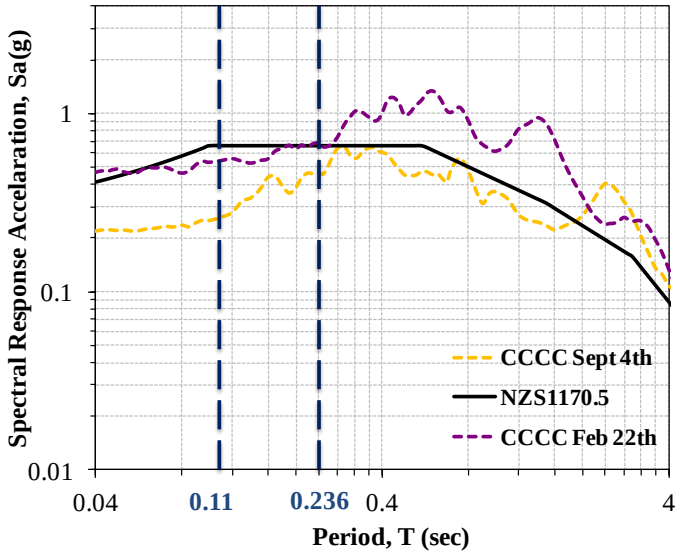

Figure 6.16. ***Site Response for Moorhouse Overpass for the fundamental periods of the structure, depending on the model and on the section, with Darfield and Lyttelton earthquake records.***

6.4.6 Nonlinear Static Push Over Analysis

Pushover analyses were undertaken on the structure in its undamaged and repaired condition as shown in Figure 6.17 and Figure 6.18. From these figures it can be seen that repairs made to strengthen the structure following the February 2011 event have a significant influence on the level of deformation.

From pushover analyses, piers 6 and 7 were identified as having the critical response. In the undamaged condition, the failure mechanism was through shear in pier 7, the ultimate lateral load was found to be 1.34g ($1.34w_d$) and occurred at a displacement of 72.6mm. This is over three times greater than the maximum displacement found using time-history analysis which is attributed to the monotonic loading applied in analysing the structure. Repeated inelastic cyclic behaviour induces increased degradation of strength in the model used for these analyses which would have occurred in the time-history analysis but not the pushover analysis.

Within Figure 6.17 undamaged pushover analysis is accompanied by pushover analysis of the repaired structure. Inclusion of steel cross-bracing greatly increased the repaired structure's stiffness which can be seen by the relationship between displacement at pier 7 where bracing is located. Inclusion of bracing induces a change in location of the ultimate failure mechanism to pier 6, one of the fixed base piers in the central section of the bridge. Failure occurs at over 3.0g ($3.0w_d$) due to

shear in the pier frame legs. While shear is not a desirable failure mechanism, failure occurs far above any current design levels.

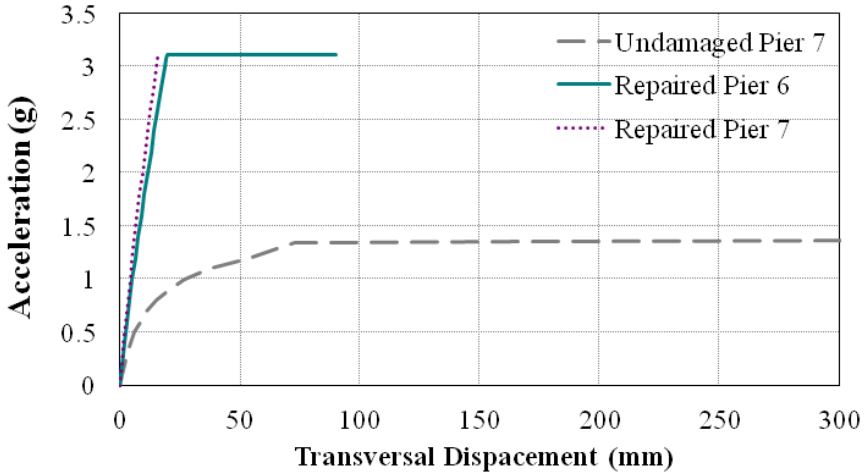

Figure 6.17. ***Pushover analysis of undamaged and repaired condition, investigating transversal displacement of Piers 6 and 7.***

Figure 6.18 shows the transversal displacement profile of the structure under various levels of loading. It can be seen that the inclusion of cross-bracing units tied the structure together giving a more symmetric profile with only a minor difference in deformation at pier 7. The inclusion of cross bracing also stiffened and strengthened the structure. Using modal analysis (Table 6.2) it can be seen that this in turn decreased the natural period of the structure which might be expected to increase accelerations, though in NZS1170.5 [21] the structure remains in the plateau region of the design spectra, thus having a minimal effect on design base shear.

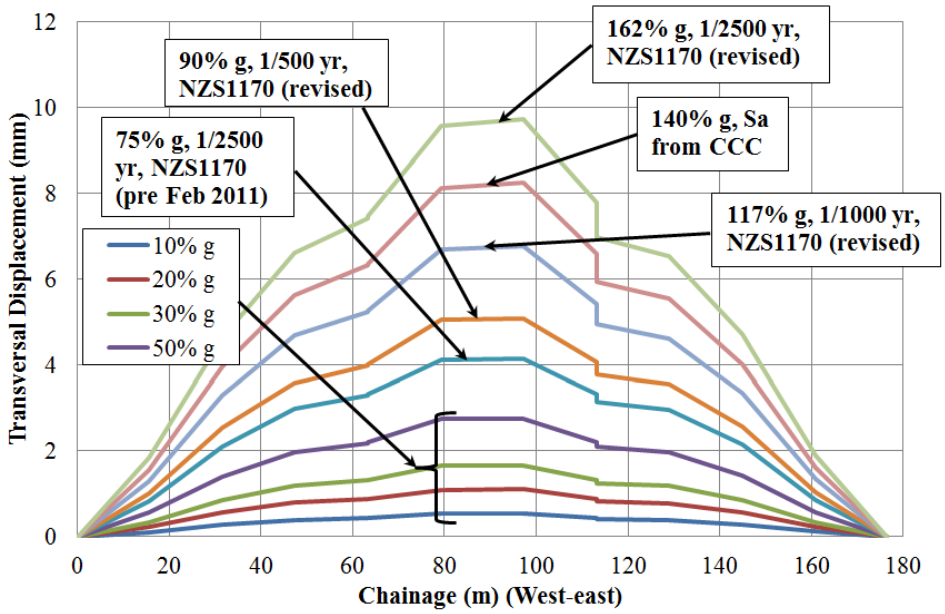

Figure 6.18. ***Pushover analysis on the structure in its repaired condition displacement in the transversal direction.***

6.4.7 Nonlinear Time History Analyses

The ground motions used for analysis were recorded at Catholic Cathedral College (Site CCCC) which is located 700 meters east of Moorhouse Avenue Overbridge. A N64E, a N26W and a vertical component were recorded during each seismic event. A summary of peak ground accelerations from the Darfield and Christchurch earthquakes are given in Table 6.3. As can been seen from the table, the lateral components of Christchurch PGA were two times of the Darfield ones while the vertical component was approximately four times. Refer to APPENDIX C for of the accelerograms of the earthquakes in each component.

Table 6.3. ***Comparison of peak ground accelerations as measured at site CCCC for the Darfield and Lyttelton earthquakes (geometric mean of horizontal PGAs)***

Event	M_w	PGA		
		N26E	N64W	Vertical
Darfield, September 4, 2010	7.1	0.195g	0.234g	0.200g
Lyttelton, February 22, 2011	6.2	0.384g	0.479g	0.812g

Table 6.4 gives a summary of results from the analysis showing the peak displacement, drift and shear force that occurred at Pier 7. Pier 7 was chosen for comparison as it was the pier that underwent the largest deformations in the As-Built models and is also the pier that exhibited the most damage in the detailed damage assessment. Figure 6.20 shows the peak displacement profiles of each model.

Table 6.4. Summary of results obtained from Time Hystory Analyses for the Pier 7

Earthquake	Model	Peak Transversal Displacement [mm]	Peak Drift [%]	Peak Shear Force [kN]
Darfield	As Built	5.6	0.13	340
Christchurch	As Built*	9.3	0.22	529
	Repaired	2.6	0.062	82
	FRP Retrofit	10.3	0.24	514
	Tie-Bolt Retrofit	6.3	0.15	364

** Analysis was terminated due to Shear Failure.*

Shear failure of Pier 7 occurred in the As-Built model after ~14 s when subjected to the Christchurch earthquake as expected (Figure 6.19). The failure of Pier 7 during the analysis meant that the full analysis could not be carried out, meaning the true peak displacement and shear force of the As-Built model may not have been obtained. No failure occurred in any of the other tests, indicating that the repair and retrofit methods were effective in preventing failure of the bridge.

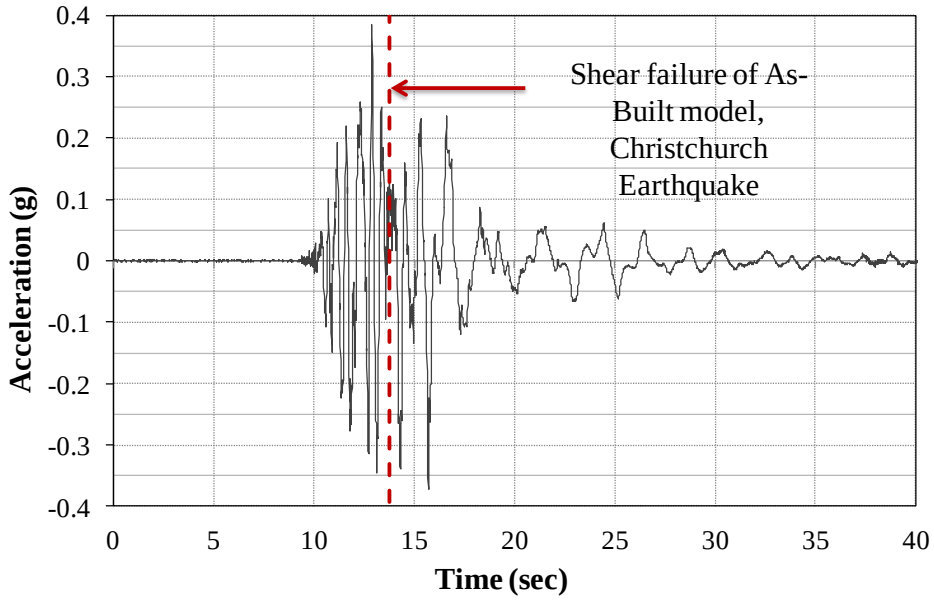

Figure 6.19. ***Ground Motion measured at Catholic Cathedral College (CCCC) with the indication of the instant in which the shear failure happened according to the numerical analyses.***

The displacement profiles show a larger peak displacement in the south direction than the north direction which is consistent with the damage to the west abutment in which spalling occurred on the southern side of the abutment, but not the northern side (Figure 6.20).

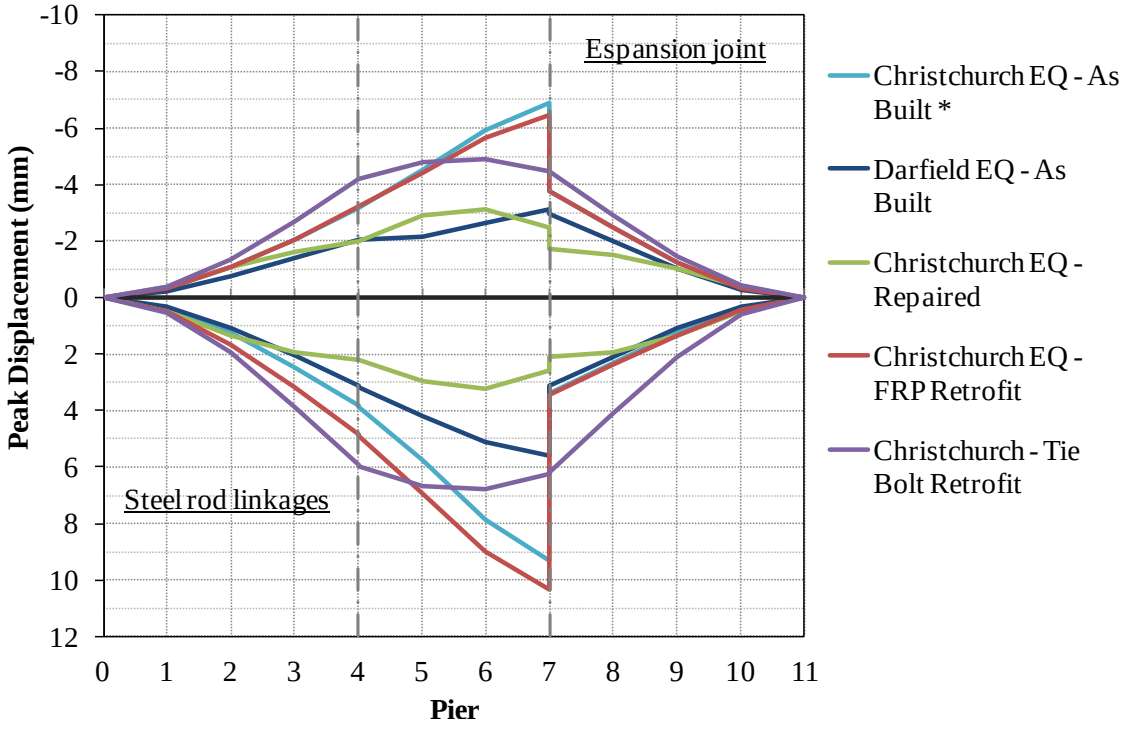

Figure 6.20. ***Displacement profile of each model when subjected to CCCC records.***

It can be seen that the peak displacement and shear force of the As-Built model during the Christchurch earthquake were approximately 1.6 times those that occurred during the Darfield earthquake.

The repaired model exhibited significantly lower peak displacements than any of the other models even though the stiffness of the piers was reduced by 60% to account for cracking. The peak shear force in Pier 7 after repair was reduced from 529 KN in the As-Built model to 82 KN in the Repaired model, indicating that the method of repair is effective in limiting the shear demand in Pier 7, and hence aiding in the prevention of further shear damage in subsequent earthquakes.

The FRP retrofit method resulted in a slight reduction in shear demand in Pier 7 although the difference in shear force is small. The FRP retrofit method gave a higher peak displacement than the As-Built model but this is due to the fact that the As-Built analysis was prematurely terminated due to shear failure. It would be expected that the FRP Retrofit model would have a slightly lower peak displacement than the As-Built model due to the increase in stiffness of Pier 7 associated with the addition of FRP material. The peak shear force of 514 KN gives an indication of the design shear force that would be used in the design of the FRP retrofit system.

The analysis indicates that the Tie-Bolt Retrofit method is effective in reducing both the peak lateral displacement and peak shear force in Pier 7. The Tie-Bolt Retrofit model caused an increase in peak displacement in almost all of the other piers although the increases were relatively insignificant when compared with the reduction in peak displacement of Pier 7. The maximum increase in peak displacement, when compared with the other models, was about 1 mm occurring at Pier 4. The peak displacement and shear force exhibited by the Tie-Bolt Retrofit model when subjected to the Christchurch earthquake was similar to the values observed in the As-Built model when subjected to the Darfield earthquake. No shear failure occurred in the bridge during the analysis of the Tie-Bolt Retrofit model indicating that after repair of Pier 7, further shear strengthening may not be required.

6.5 Conclusion

The Moorhouse Avenue Overbridge was heavily damaged in the last earthquake and series of following aftershocks on February 22nd 2011. The most severe damaged was situated at the eastern end of the central bridge section where ‘split’ piers straddling an expansion joint buckled in the lower sections due to heavy shear induced cracking. Damage was focused at this position due to the non-symmetric layout of the structure caused by tying of the western expansion joint. Less critical damage was also observed in other sections of the structure in the form of pounding, spalling and buckling of some reinforcing bars within secondary structural components. The overbridge was closed to traffic for five weeks following the February event while repairs and strengthening works were implemented. Initial works focused on supporting Pier 7 under gravity loads and were followed by instalment of cross-bracing steel section to take lateral loads which upon installation allowed for the bridge to be reopened to traffic.

Modal, time-history and push-over analyses were run on the bridge. The natural period of the undamaged structure was found to be 0.187 seconds, once repaired this reduced to 0.134 seconds. This corresponds to spectral acceleration of the order of 0.6g to 0.7g based on the February event ground motion record, and this values match quite well design spectral accelerations in that range.

Ground motions recorded from the station next to the site in the February and September events were used in a non-linear time-history analysis of the structure in five conditions, including as built, damaged and retrofit model with two different solutions.

When the analysis was run on the 'as built' condition, shear failure occurred at the western piers in the first few seconds of strong ground motion, matching the damaged witnessed to the structure following the February events. So numerical analysis provided results that were consistent with the observed damage. An analysis was re-run including the 'repaired' condition with strengthening implemented. This showed a large decrease of member loads throughout the structure, with addition of cross-bracing causing a significant increase of stiffness in the 'split' piers. This in turn reduced transversal displacements by 70%. Similar effects were found from the push over analysis of the structure where under the current 1/2500 year event loading, inclusion of cross-bracing reduced the displacement from over 100 mm to just under 10mm at Pier 7. Based on the pushover analysis carried out, in the event of a severe earthquake similar to the February 22nd 2011 event, the repaired structure would perform adequately. This is on the provision that the additional bracing and strengthening units which have been installed are capable of acting in unison with the existing structure.

FRP retrofit and Tie-Bolt retrofit methods were also investigated using the numerical model. The results indicate that the Tie-Bolt retrofit method is the most effective, with the method causing reductions in peak displacement and shear demand in the bridge.

A case study on the Moorhouse Avenue overbridge was then given which included a description of the structure, a detailed damage analysis and the results of a numerical analysis. The main damage to the Moorhouse Avenue overbridge was found to be shear failure and secondary buckling of Pier 7. The numerical analysis provided results that were consistent with the observed damage. FRP retrofit and Tie-Bolt retrofit methods were investigated using the numerical model. The results indicate that the Tie-Bolt retrofit method is the most effective, with the method causing reductions in peak displacement and shear demand in the bridge.

7 CONCLUSION

The work presented gathers some considerations related to the assessment of the damage of the bridges in Christchurch after Darfield and Lyttelton Earthquake, focusing the attention in particular on the last event.

The global overview of damage showed that overall bridge structures performed well during the 2010 and 2011 Canterbury earthquakes, confirming the design expectations. The robustness of Christchurch City Council road bridges built in the 1940s and 50s without any seismic design criteria certainly helped to sustain earthquake loadings comparable or higher than the current design levels. However, the significant damage to the approaches due to lateral spreading of the riverbanks caused traffic disruption which should be mitigated through possible low-damage approach solutions. More importantly, utilities/pipes which are commonly carried over bridges sustained severe damage due to a lack of a design-integrated approach.

In order to quantify the damage in Christchurch area providing thus a better overview of the bridges condition after the two last earthquakes, the database developed by University of Canterbury collected the field observation from the inspection conducted by the authorities. This unbiased statistical tool for assessing the bridges performance confirmed that the seismic behaviour was acceptable according to typical seismic codes, although in the last event was worse than the previous one in September. In statistical terms, the percentage of moderately and severely damaged bridges increased from 8% after September to 38.6%. Making a distinction according to the structural form, steel, cast-in-situ concrete, and precast concrete, they all performed to a similar standard. As expected masonry bridges did not perform well, with 80% of them experiencing some type of damage in the last earthquake. Surprisingly, timber bridges, for the most part pedestrian, performed better than both steel and concrete, thanks to the lightness of this material. Differences about the consequences of the two earthquakes are not only quantitative, but they concern also the cause of the damage: during the Darfield earthquake the main reason of damage was the liquefaction, while in the last event also the ground motion, stronger than the previous one, had an important influence on the performance of the structures. This was also confirmed by numerical analyses conducted on three bridges of the entire stock of the Database.

In particular for Port Hills Overpass, even if the general performance was satisfactory, plastic hinges developed at the base of the central piers. Non-linear time history analyses showed that the cause of the damage was the closeness of the bridge to the February 22nd earthquake's epicentre.

In fact, when ground motion records from HVSC station amplified by site topographic effects were applied to the structure, the bridge response well matched the one observed during the inspections on the field. The significant vertical component affected the ground motion: the transversal displacement of the deck, which varied according to the stiffness variation of the piers. Obviously also the geometry and the restrains played an important role. As expected for a precast concrete bridge, the connection next to the abutments cannot be considered fully fixed, since the response of the bridge is between that one of the two modelling considered configurations, i.e. fully fixed abutments and pinned restrain about the vertical axis.

With regard to the geometry, its influence is even more clear if we take a look at the performance of Horotane Valley Overpass. Indeed although the two bridges are close, the latter, short and thus very stiff, did not suffer any damage due to the ground motion. This was also confirmed by the numerical analyses. Results from time history displacement analysis proved that the slope failure of the approach was the main cause of the shear rupture of the retrofit bolts, much more stiffer than the existing ones and so more loaded. For this reason, even if the performance of the retrofit works was not satisfactory, its presence prevented the existing rods from yielding and so the possibility of pounding between the deck and the abutments.

Retrofit works would have prevented also the shear failure, due to the ground shaking, occurred at the western piers of Moorhouse Ave Overbridge. The "repaired" condition with addition of cross-bracing, which cause a significant increase of stiffness in the 'split' piers, showed a large decrease of member loads throughout the structure,. This in turn reduced transversal displacements by 70%.

Further objectives of the research

Satisfactory results have been achieved at this stage of the research. Nevertheless in pursuance of this work, the need to improve the accuracy of the tools used has arisen and objective of development in this sense can be identified.
First of all, considering the global performance of bridges in Christchurch, even if life safety of bridges is still the primary scope within current design standards, however further advanced technology should be implemented to preserve not only the integrity of the structure, but also of the foundations/approaches. New Zealand Standards, as well as overseas codes are deficient in terms of the above mentioned aspects and further research is needed.
In regard to the numerical assessment, it has been already presented how the vertical accelerations have considerably affected the response of some bridges. The analyses could take into account the change in the stiffness of elements, but not the ductility variation demand. It is very important therefore to implement in Ruaumoko 3D lumped plasticity models of interaction between the moment and the axial force (M-N) and the moment and the shear force (V-M), in order to improve the residual capacity assessment of bridges.
Detailed analysis of the retrofit linkages can be one of the next steps to have a more complete picture of the performance and to estimate their integrity during a seismic event. To assess their actual beneficial contribution, a comparison between the situations with and without the retrofit works could be useful.
On a large scale, the use of the Database in combination with the software platform MAEviz allowed to realize that further research is required to improve the reliability and robustness of the

outcome, in particular if used for actual prediction of a future scenario. In this sense the Natural Hazard Research group of the University of Canterbury is working to provide hazard and fragility models specific for New Zealand. They will replace the US fragility curves currently used for the risk assessment analyses. Moreover, specifically for bridges, it is worthwhile the development of fragility curves able to relate the level of liquefaction hazard with the probability of reaching the damage. Finally the inclusion of social and economic effects due to structural damage into MAEviz is another important challenge.

8 REFERENCES

1. Chung, R., et al., *The January 17, 1995 Hyogoken-Nanbu (Kobe) Earthquake.* NIST Special Publication 901, July 1996: p. 544.
2. EERI, *Northridge Earthquake Reconnaissance Report* Earthquake Spectra, Feb. 1995. Special Supplement to Vol. 11: p. 116.
3. EERI, *Loma Prieta Earthquake Reconnaissance Report.* Earthquake Spectra, May 1990. Special Supplement to Vol. 6: p. 448.
4. EERI, *Costa Rica earthquake reconnaissance report.* Earthquake Spectra, Oct. 1991. Vol. 11: p. 127.
5. Iwasaki, T., Penzien, J., and Clough, R., *Literature Survey-Seismic Effects on Highway Bridges*, in *Earthquake Engineering Research Report No. 72-11*Nov 1972, University of California: Berkeley. p. 397.
6. Fung, G.G., Lebeau,R. J., Klein, E. D., Belvedere, J., and Goldschmidt, A. F. , *Field Investigation of Bridge Damage in the San Fernando Earthquake*, 1971: Sacramento, California. p. 209.
7. Priestley, M.J.N., Seible,F., Calvi, G. M., *Seismic design and retrofit of bridges*1996, Hoboken, United States of America: John Wiley & Sons, Inc.
8. *Seismic design and retrofit - structural solutions.* Fib Bulletin No. 39, 2007.
9. Hsu, Y.T., Fu, C. C. , *Study of Damaged Wushi Bridge in Taiwan 921 Earthquake.* Pract. Periodical on Struct. Des. and Constr., November 2000. Vol. 5(Issue 4): p. 166-171.
10. Bruneau, M., *Performance of steel bridges during the 1995 Hyogoken–Nanbu (Kobe, Japan) earthquake—a North American perspective.* Engineering Structures, 1998. Vol. 20, No. 12: p. 1063–1078.
11. Zhiqiang, W., and Lee, G. C. , *A comparative study of bridge damage due to the Wenchuan, Northridge, Loma Prieta and San Fernando earthquakes.* Earthquake Engineering And Engineering Vibration, June 2009. Vol. 8, No. 2: p. 251–261.
12. Chai, Y.H., Priestley, M. J. N. and Seible, F. , *Seismic Retrofit of Circular Bridge Columns for Enanched Flexural Performance.* ACI Structural Journal, Sept./ Oct. 1991. Vol. 88 No. 5: p. 572-584.

13. Priestley, M.J.N., F. Seible, and J. MacRae, *The Kobe Earthquake of January 17, 1995: Initial Impressions from a Quick Reconnaissance*, in *Structural System Research Project*Febr. 1995, University of California: San Diego. p. 71.

14. Kawashima, K., Ichimasu, H. and Ohuchi, H. . *Retrofitting*. in *Proceedings, International Workshop on Seismic Design and Retrofitting of Reinforced Concrete Bridges*. Apr. 1991. Bormio, Italy.

15. F., P.W., *Performance of Bridges during San Fernando Earthquake*. PCI Journal July - August 1972.

16. Priestley, M.J.N., Seible, F., and Uang, C. M., *The Northridge Earthquake of January 17, 1994: Damage Analysis of Selected Freeway Bridges*, in *Structural System Reasearch Project, Report SSRP-94/06*Feb. 1994, University of California: San Diego. p. 260.

17. Palermo, A., Le Heux, M., Bruneau, M., Anagnostopoulou, M., Wotherspoon, L., Hogan, L., *Preliminary findings on performance of bridges in the 2010 Darfield earthquake*. Bulletin of the New Zealand Society for Earthquake Engineering, 2010. Vol. 43 No 4: p. 412-420.

18. Palermo, A., Wotherspoon, L., Hogan, L., Kivell, A., Yashinsky, M., Bruneau, M., *Preliminary findings on performance of bridges in the 2011 Christchurch earthquake*, in *Reconnaissance report*2011.

19. Cousins, J., & McVerry, G. H., *Overview of Strong Motion Data from the Darfield Earthquake*. Bulletin of the New Zealand Society for Earthquake Engineering, 2010. Vol. 43, No. 4: p. 222-227.

20. Holden, C., Beavan, J., Fry, B., Reyners, M., Ristau, J., Van Dissen, R., et al. *Preliminary source model of the Mw 7.1 Darfield earthquake from geological, geodetic and seismic data*. in *Proceedings of the Ninth Pacific Conference on Earthquake Engineering*. 2011. Auckland, New Zealand.

21. NZS1170, *Structural design actions*, in *Standards*2004: New Zealand.

22. Berrill, J., Yasuda, S., *Liquefaction and pile foundations: some issues*. Journal of Earthquake Engineering, 2002. Vol. 6(Special Issue): p. 1-41.

23. Akiyama, M., Frangopol, D. M. *On life-cycle reliability under earthquake excitations of corroded reinforced concrete structures*. in *Proceedings of the 2nd International Symposium on Life-Cycle Civil Engineering*. October, 27-31, 2010 Taipei, Taiwan.

24. Biondini, F., Palermo, A., Toniolo, G., *Seismic performance of concrete structures exposed to corrosion: case studies of low-rise precast buildings. Structure and Infrastructure Engineering*First published on 01 April 2010.

25. Zealand, T.N., *Manual for seismic screening of bridges, SM110*1998, Wellington, New Zealand.

26. Chapman, H.E., Lauder, M. K., Wood, J. *Seismic assessment and retrofitting of New Zealand state highway Bridges*. in *Proc. of the New Zealand Society Earthquake Engineering Conference (NZEES)*. March, 11-13, 2005. Wairakei, New Zealand.

27. Le Heux, M., Palermo, A., Mackenzie, J. R. *Darfield earthquake 2010 - Lateral spreading actions on the Dallington pedestrian bridge*. in *Proc. of the Ninth Pacific Conference on Earthquake Engineering - Building an Earthquake-Resilient Society (PCEE)*. April, 14-16, 2011. Auckland, New Zealand.

28. Palermo, A., Mashal, M. *Accelerated bridge construction (ABC) in earthquake prone areas, international trends and New Zealand needs*. in *Proc. of the New Zealand Concrete Society Conference (NZCSC)*. August, 7-8, 2011. Rotorua, New Zealand.

29. Zealand, T.N., *New Zealand Bridge Design Manual, second edition*, 2004.

30. Kam, W.Y., Pampanin, S. and E. K., *Seosmic Performance of Reinforced Concrete Buildings in the 22 February Christchurch (Lyttelton) Earthquake.* Bullettin of the New Zealand Society for Earthquake Engineering, 2011. Vol. 44: p. 239-278.

31. Clifton, C., Bruneau, M., and MacRae, G., *Steel Structures Damage from the Christchurch Earthquake Series of 2010 and 2011.* Bulletin of the New Zealand Society for Earthquake Engineering, 2011. Vol. 44: p. 297-318.

32. Buchanan, A., Carradin, D., and Jordan, J., *Performance of Engineering Timber Structures in the Canterbury Earthquakes.* Bulletin of the New Zealand Society for Earthquake Engineering, 2011. Vol. 44: p. 394-401.

33. Palermo, A., Wotherspoon, L., Wood, J., Chapman, H., Scott, A., Hogan, L., Kivell, A., Camnasio, E., Yashinsky, M., Bruneau, M., and Chouw, N., *Lessons Learnt from 2011 Chrischurch Earthquakes: Analysis and Assessment of Bridges.* Bulletin of the New Zealand Society for Earthquake Engineering, 2011. Vol. 44 p. 319-333.

34. Giovinazzi, S., Wilson, T., Davis, C., Bristow, D., Gallagher, M., Scholfield, A., Villemure, M., Eidinger, J., and Tang, A., *Lfelines Performance and Management Following the 22 February 2011 Christchurch Earthquake, New Zealand: Highlights of Resilience.* Bulletin of the New Zealand Society for Earthquake Engineering, 2011. Vol. 44 p. 402-417.

35. Kam, W.Y., Pampanin, S., *General Performance of Buildings in Christchurch CBD: a contestual report prepared for DBH Expert Panel.*, 2011, University of Canterbury: Christchurch, New Zealand.

36. Cubrinovsky, M., Bradley, B., Wotherspoon, L., Green, R., Bray, J., Wood, C., Pender, M., Allen, J., Bradshaw, RA., Rix, G., Taylor, M., Robinson, K., Henderson, D., Giorgini, S., Ma, K., Winkley, A., Zupan, J., O'Rourke, T., DePascale, G., and Wells, D., *Geotechnical Aspects of the 22 February 2011 Christchurch Earthquake*. Bulletin of the New Zealand Society for Earthquake Engineering, 2011. Vol.44: p. 205-226.

37. GeoNet. *GeoNet Strong Motion Database.* http://www.geonet.org.nz/earthquake/. 2012.

38. Nielson, B.G., and DesRoches, R., *Seismic fragility methodology for highway bridges using a component level approach.* Oct. 2006.

39. Padgett, J.E., and DesRoches, R., *Bridge Functionality Relationships for Improved Seismic Risk Assessment of Transportation Networks.* Sept. 2006.

40. Carr, A.J., *RUAUMOKO Program for Inelastic Dynamic Analysis*2008, Department of Civil Engineering, Christchurch, New Zealand.

41. Motejo, L., Kowalsky, M., *CUMBIA; Set of codes for the analysis of reinforced concrete members*2007, North Carolina: North Carolina State University.

42. Carr, A.J., *Structural Analysis Course Notes*, 2008: New Zealand: University of Canterbury.

43. Kulhawy, F., and Mayne, P., *Manual on Estimating Soil Properties for Foundation Design*, in *Report No. EL-6800*1990, Electric Power Research Institute: Palo Alto, CA.

44. Bresler, B., *Design Criteria for Reinforced Columns Under Axial Load and Biaxial Bending.* ACI Journal, 1960. Vol. 32 (5): p. 481-490.

45. Carr, A., *Ruaumoko Manual*2010, Christchurch, University of Canterbury.

46. Campbell, A., *New Seismic Design Methods: N2 Method and Comparison with Force Based Design*, in *Department of Civil and Natural Resources Engineering*, University of Canterbury: Christchurch, New Zealand.

47. Isaković, T., Fischinger, M., *Applicability of Pushover Methods to the Seismic Analysis of an RC Bridge Experimentally Tested on Three Shake Tables.* Journal of Earthquake Engineering, 2011. Vol. 15: p. 303-320.

48. Isakovic, T., Pompeyo, M., Lazaro, N., and Fischinger, M., *Applicability of pushover methods for the seismic analysis of single-column bent viaducts.* EARTHQUAKE ENGINEERING AND STRUCTURAL DYNAMICS, 2008. Vol. 37: p. 1185–1202.

49. Magliulo, G., Cosenza, E., *Lo Scaling di Set di Accelerogrammi per la Spettrocompatibilità secondo Normativa.*

50. 1998-1:2005, U.E., *Parte 1: Regole generali, azioni sismiche e regole per gli edifici*, 2005.

51. Richards, R., and Elms, D. G., *Seismic Behaviour of Retaining Walls and Bridge Abutments* in *Report 77-10*1977, Department of Civil Engineering, University of Canterbury: Christchurch, New Zealand

52. Newmark, N.M., *Effect of Earthquakes on Dams and Eambarkments.* Geotchnique, 1965. Vol.15, No. 2: p. 139-160.

53. WSDOT, *Geotechnical Design Manual*, in *Chapter 6: Seismic Design*Jan 2010. p. 54-55.

54. Bentz, E., and Collins, M. P., *Response-2000 User Manual*2001.

55. Khalifa, A., Gold, W.J., Nanni, A., Aziz M.I., A., *Contribution of Externally Bonded FRP to Shear Capacity of Flexural Members.* ASCE-Journal of Composites for Construction, 1998. Vol. 2, No.4: p. 195- 203.

56. Bentz, E.C., Vecchio, F. J., and Collins, M. P., *Simplified Modified Compression Field Theory for Calculating Shear Strength of Reinforced Concrete Elements.* ACI Structural Journal/July-August 2006: p. 614-624.

57. Bentz, E.C., Massam, L., and Collins, M. P., *Shear Strength of Large Concrete Members with FRP Reinforcement.* Journal of Composites for Construction, Nov.- Dec. 2010: p. 637-646.

58. Campbell, A., *Damage Assessment of Moorhouse Avenue Overbridge*, 2011.

59. Galal, K., and El-Sokkary, H., *Analytical Evaluation of Seismic Performance of RC Frames Rehabilitated Using FRP for Increased Ductility of Members.* Journal of Performance of Constructed Facilities, Sept/ Oct 2008: p. 276-288.

60. Lee, D.H., and Elnashai, A. S., Fellow, ASCE, *Seismic Analysis of RC Bridge Columns with Flexure-Shear Interaction.* Journal of Earthquake Engineering, May 2001: p. 546-553.

61. Priestley, M.J., Verma, R., and Xiao, Y., *Seismic Shear Strength of Reinforced Concrete Columns.* Journal of Structural Engineering, 1994. Vol.120: p. 2310-2329.

62. Roy, N., Paultre, P., and Proulx, J., *Performance-based seismic retrofit of a bridge bent: Design and experimental validation.* NRC Research Press, 2010.

63. Segou, M., Kalkan, E., *Ground Motion Attenuation during M7.1 Darfield and M6.3 Christchurch (New Zealand) Earthquakes and Performance of Global Predictive Models*, 2011.

64. Sezen, H., and Chowdhury, T., *Hysteretic Model for Reinforced Concrete Columns Including the Effect of Shear and Axial Load Failure.* Journal of Sructural Engineering, Feb. 2009: p. 139-146.

65. Zararis, P.D., *Concrete Shear Failure in Reinforced-Concrete Elements.* Journal of Structural Engineering, 1996: p. 1006-1015.

66. NZS3101, *Concrete Structures Standard. Part 1: The Design of Concrete Structures*, 2006: New Zealand: Concrete Design Committee. p. 3101.

67. NZTA, *Last section of state highway open in Christchurch*2011, March 4: Retrieved September 2011, from New Zealand Tranpsort Agency; Media Centre: http://www.nzta.govt.nz/about/media/releases/1110/news.html.

68. Wood J., C.H., *Performance of New Zealand State Highway Bridges in the Darfield and Christchurch Earthquakes*, in *ABC Bridge Conference*2011: Sydney 31st Oct - 5th Nov.

Appendix A: Drawings of Case Study Bridges

- Port Hills Overpass
- Horotane Valley Overpass
- Moorhouse Avenue Overbridge

A.1 Port Hills Overpass

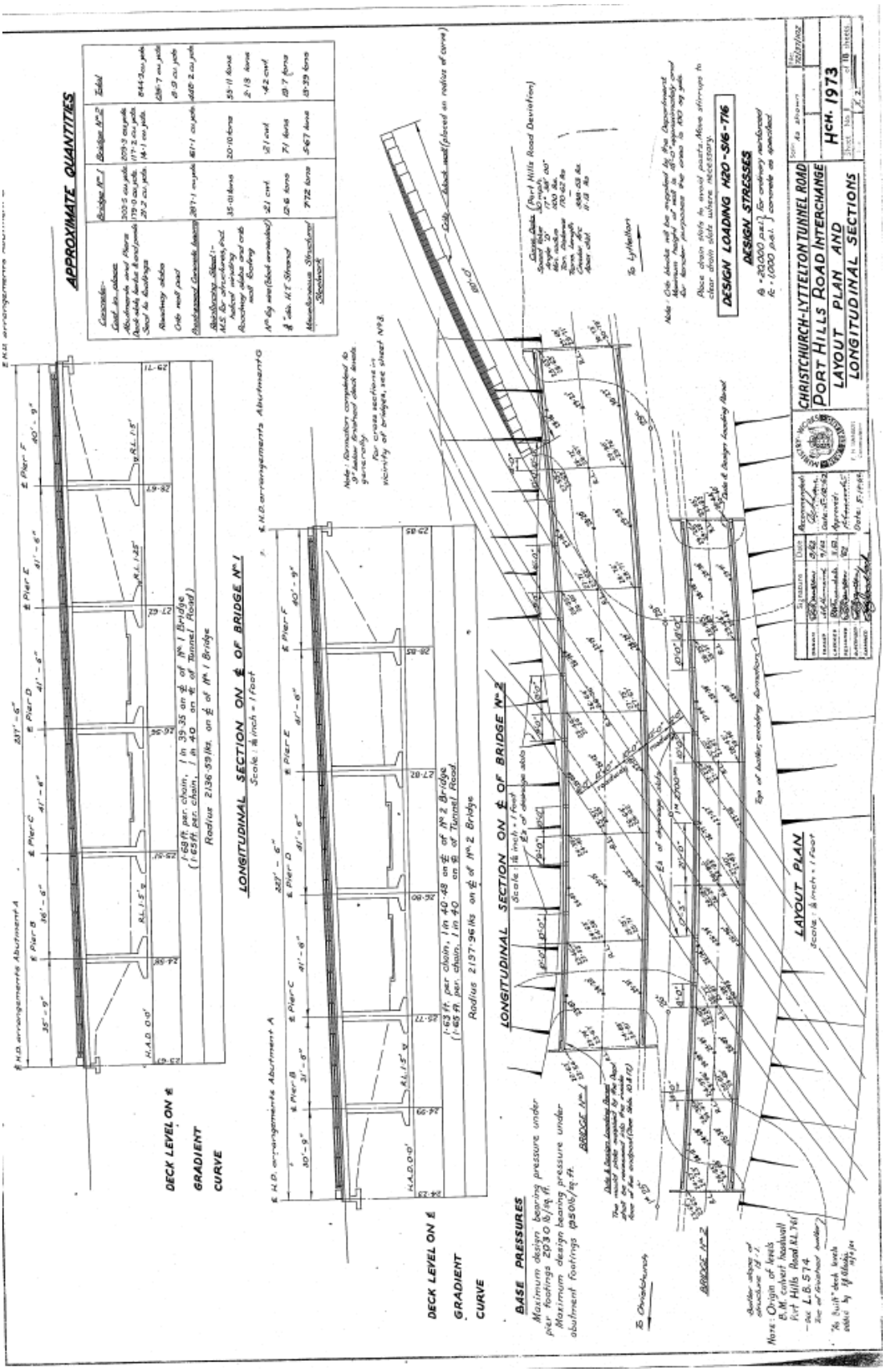

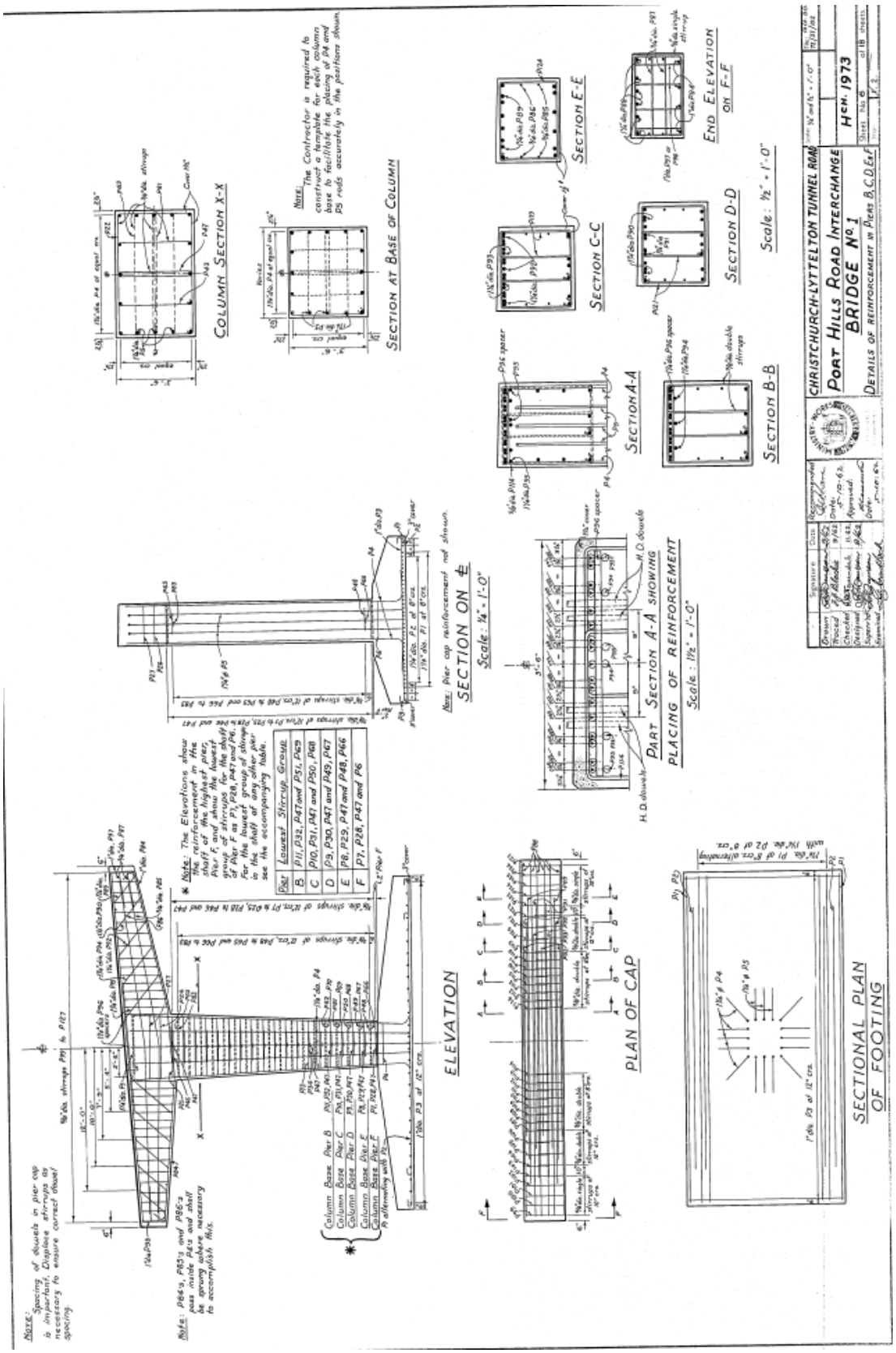
CHRISTCHURCH-LYTTELTON TUNNEL ROAD
PORT HILLS ROAD INTERCHANGE
BRIDGE No. 1
DETAILS OF REINFORCEMENT IN PIERS B, C, D, E & F
HCH. 1973
COLUMN SECTION X-X
SECTION AT BASE OF COLUMN
SECTION E-E
SECTION C-C
SECTION A-A
SECTION B-B
SECTION D-D
END ELEVATION ON F-F
SECTION ON ℄
Scale: ¾" = 1'-0"
PART SECTION A-A SHOWING PLACING OF REINFORCEMENT
Scale: 1½" = 1'-0"
ELEVATION
PLAN OF CAP
SECTIONAL PLAN OF FOOTING
Note: Pier cap reinforcement not shown.
Note: Spacing of dowels in pier cap is important. Displace stirrups as necessary to ensure correct dowel spacing
Note: P84's, P85's and P86's pass inside P4's and shall be sprung where necessary to accomplish this.
Note: The Elevations show the reinforcement in the shaft of the highest pier. Pier F and show the lowest group of stirrups for the shaft of Pier F as P1, P28, P47 and P6. For the lowest group of stirrups in the shaft of any other pier see the accompanying table.
Note: The Contractor is required to construct a template for each column base to facilitate the placing of P4 and P5 rods accurately in the positions shown.
Pier | Lowest Stirrup Group
B | P11, P32, P47 and P51, P69
C | P10, P31, P47 and P50, P68
D | P9, P30, P47 and P49, P67
E | P8, P29, P47 and P48, P66
F | P7, P28, P47 and P6

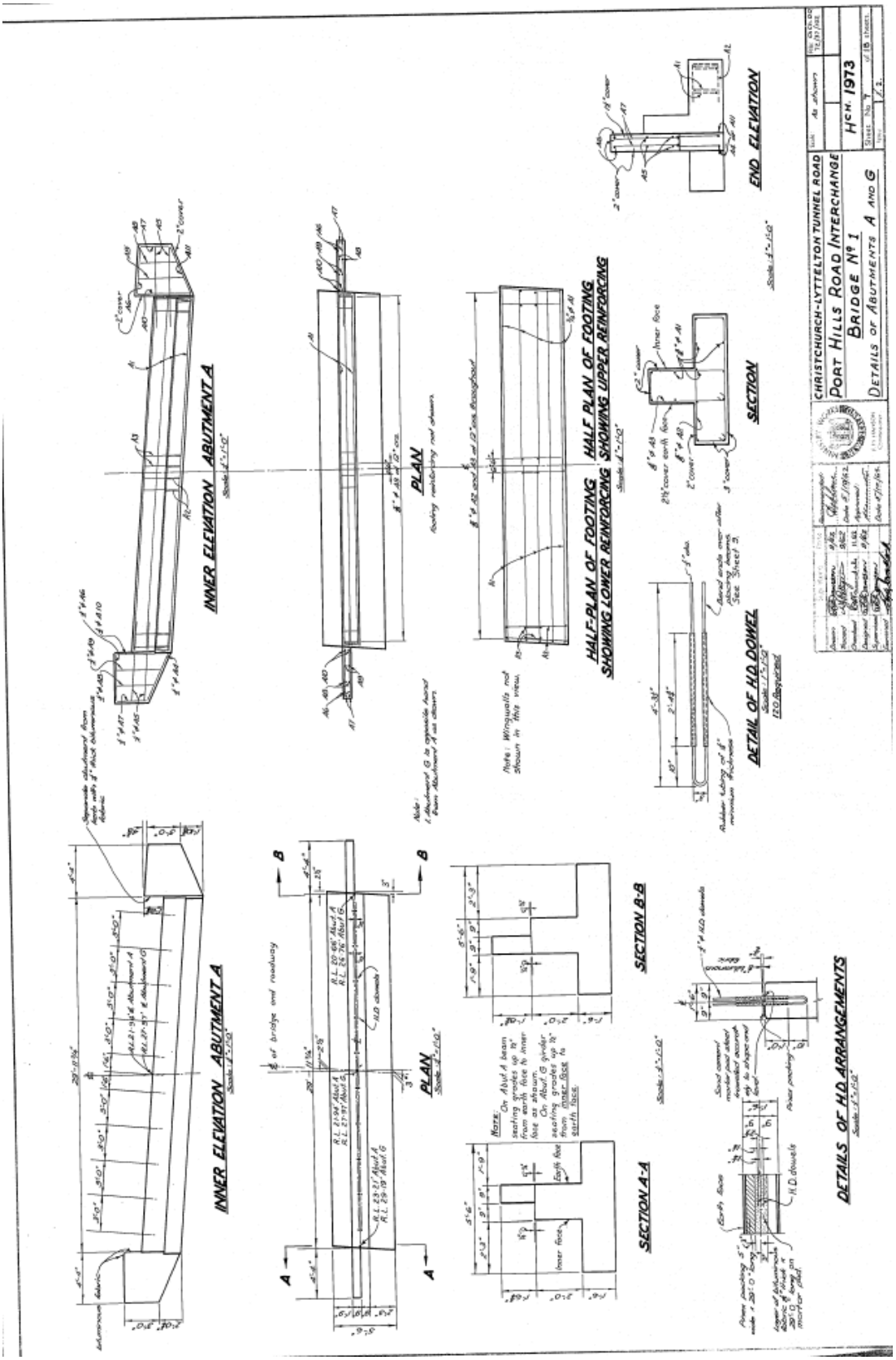
INNER ELEVATION ABUTMENT A
PLAN
HALF PLAN OF FOOTING SHOWING LOWER REINFORCING
HALF PLAN OF FOOTING SHOWING UPPER REINFORCING
END ELEVATION
SECTION
DETAIL OF H.D. DOWEL
INNER ELEVATION ABUTMENT A
PLAN
SECTION A-A
SECTION B-B
DETAILS OF H.D. ARRANGEMENTS
CHRISTCHURCH-LYTTELTON TUNNEL ROAD
PORT HILLS ROAD INTERCHANGE
BRIDGE Nº 1
DETAILS OF ABUTMENTS A AND G
MCH. 1973

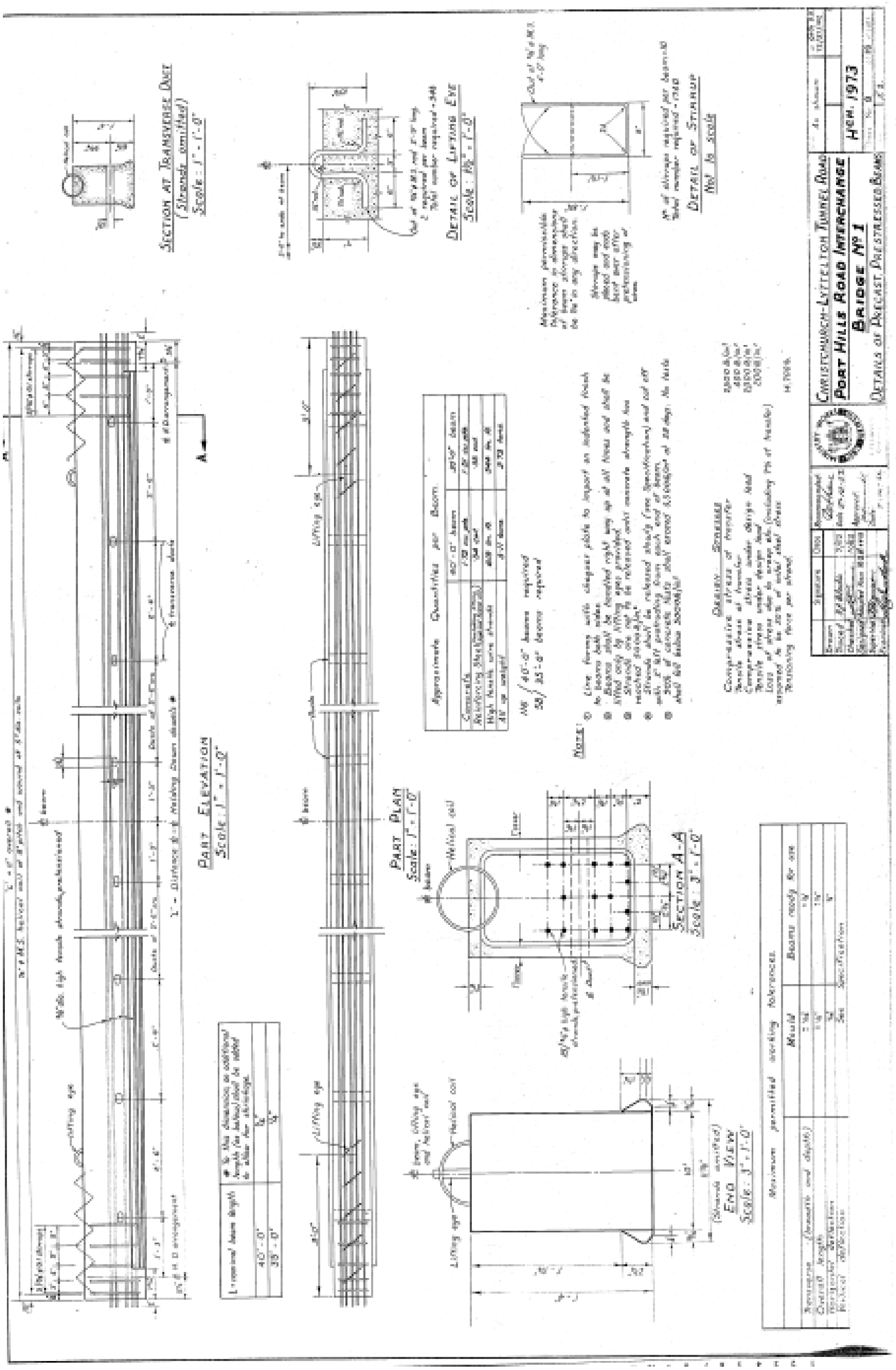
PART ELEVATION
PART PLAN
SECTION A-A
END VIEW
SECTION AT TRANSVERSE DUCT
DETAIL OF LIFTING EYE
DETAIL OF STIRRUP
Not to scale
CHRISTCHURCH-LYTTELTON TUNNEL ROAD
PORT HILLS ROAD INTERCHANGE
BRIDGE No 1
DETAILS OF PRECAST PRESTRESSED BEAMS

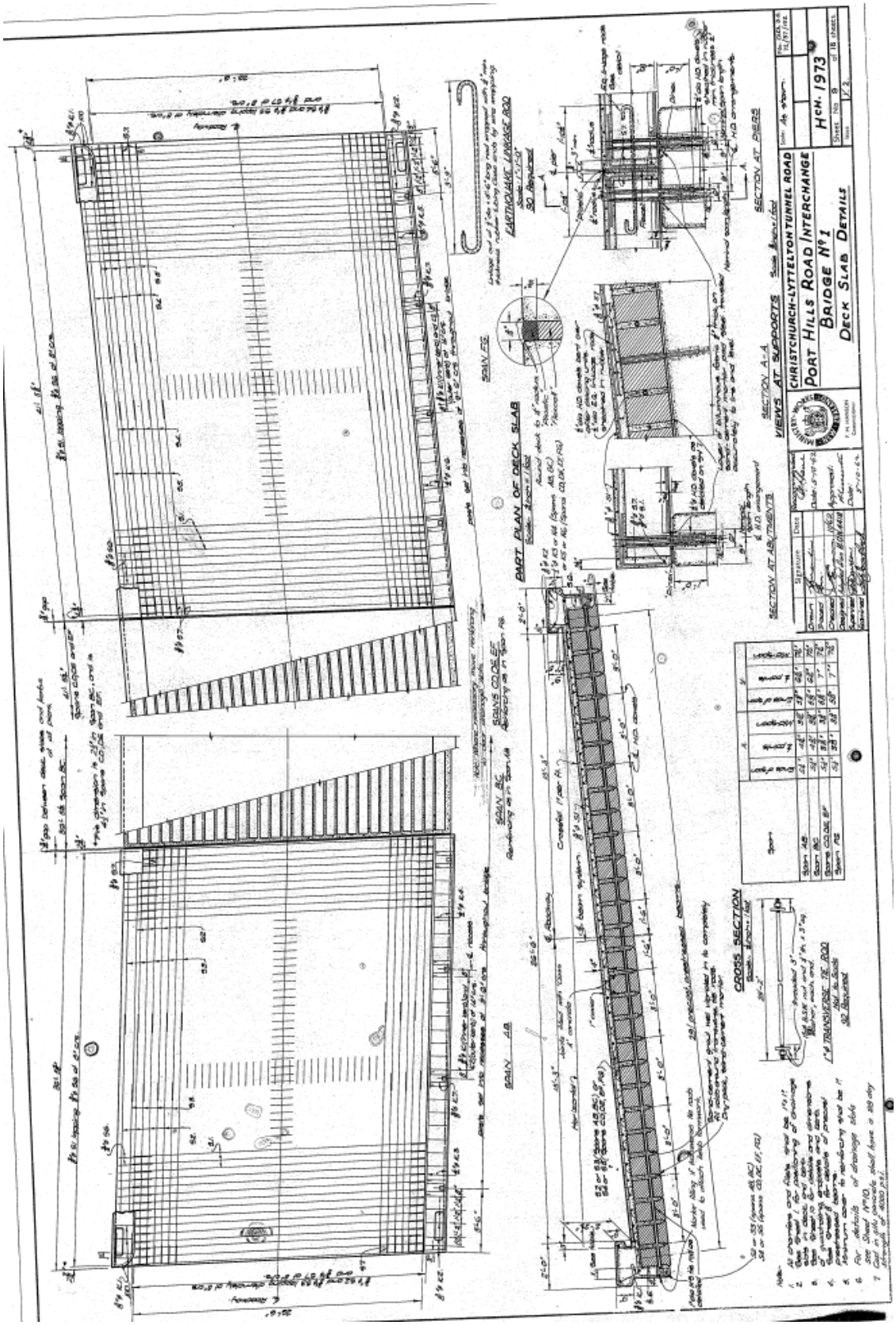
CHRISTCHURCH-LYTTELTON TUNNEL ROAD
PORT HILLS ROAD INTERCHANGE
BRIDGE No 1
DECK SLAB DETAILS
HCH. 1973
PLAN OF DECK SLAB
CROSS SECTION
SECTION AT ABUTMENTS
SECTION AT PIERS
VIEWS AT SUPPORTS
EARTHQUAKE LINKAGE ROD

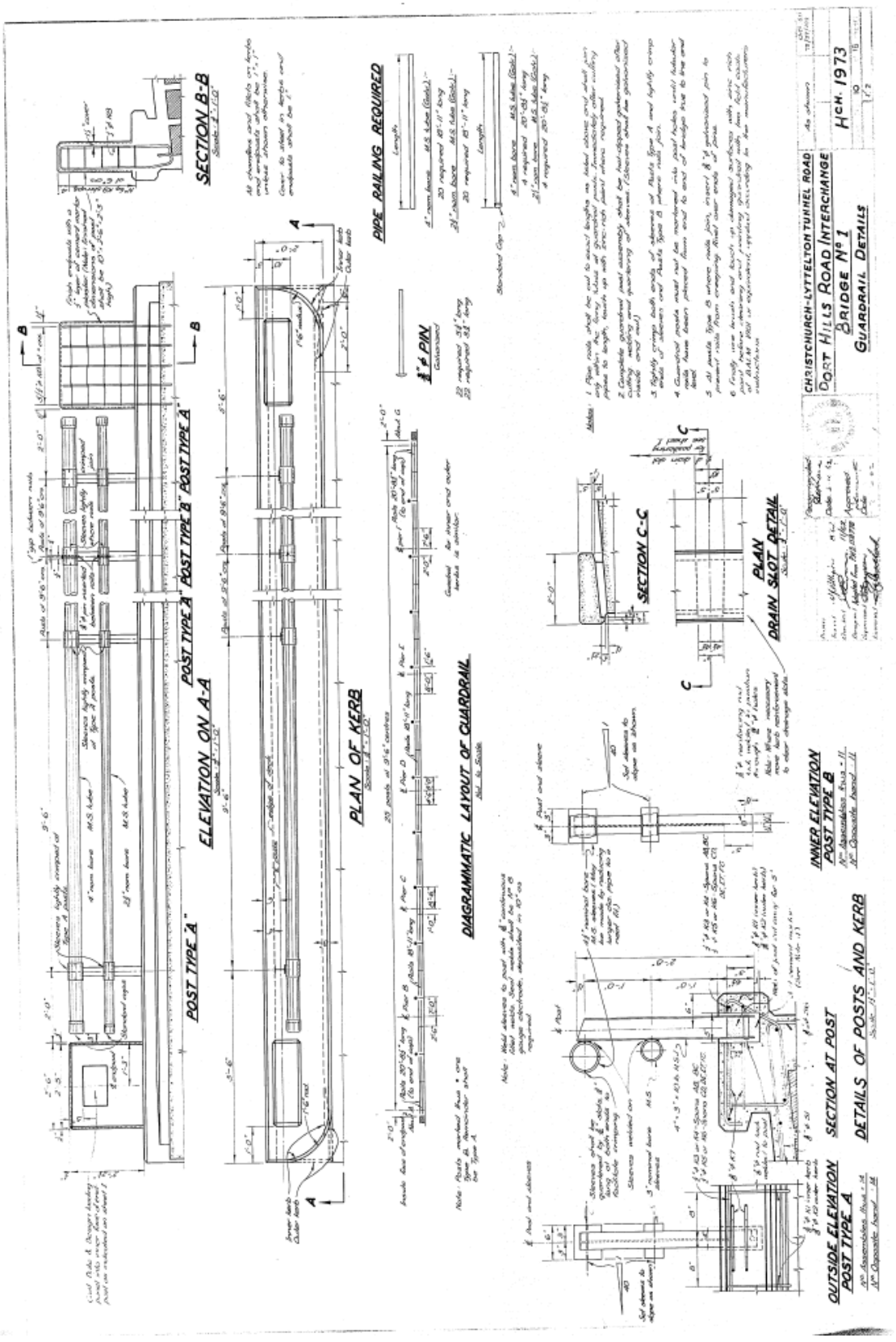
SECTION B-B
ELEVATION ON A-A
POST TYPE 'A'
POST TYPE 'B'
PLAN OF KERB
PIPE RAILING REQUIRED
DIAGRAMMATIC LAYOUT OF GUARDRAIL
SECTION C-C
PLAN
DRAIN SLOT DETAIL
OUTSIDE ELEVATION
POST TYPE A
SECTION AT POST
DETAILS OF POSTS AND KERB
INNER ELEVATION
POST TYPE B
CHRISTCHURCH-LYTTELTON TUNNEL ROAD
PORT HILLS ROAD INTERCHANGE
BRIDGE No 1
GUARDRAIL DETAILS
MCH. 1973

A.2 Horotane Valley Overpass

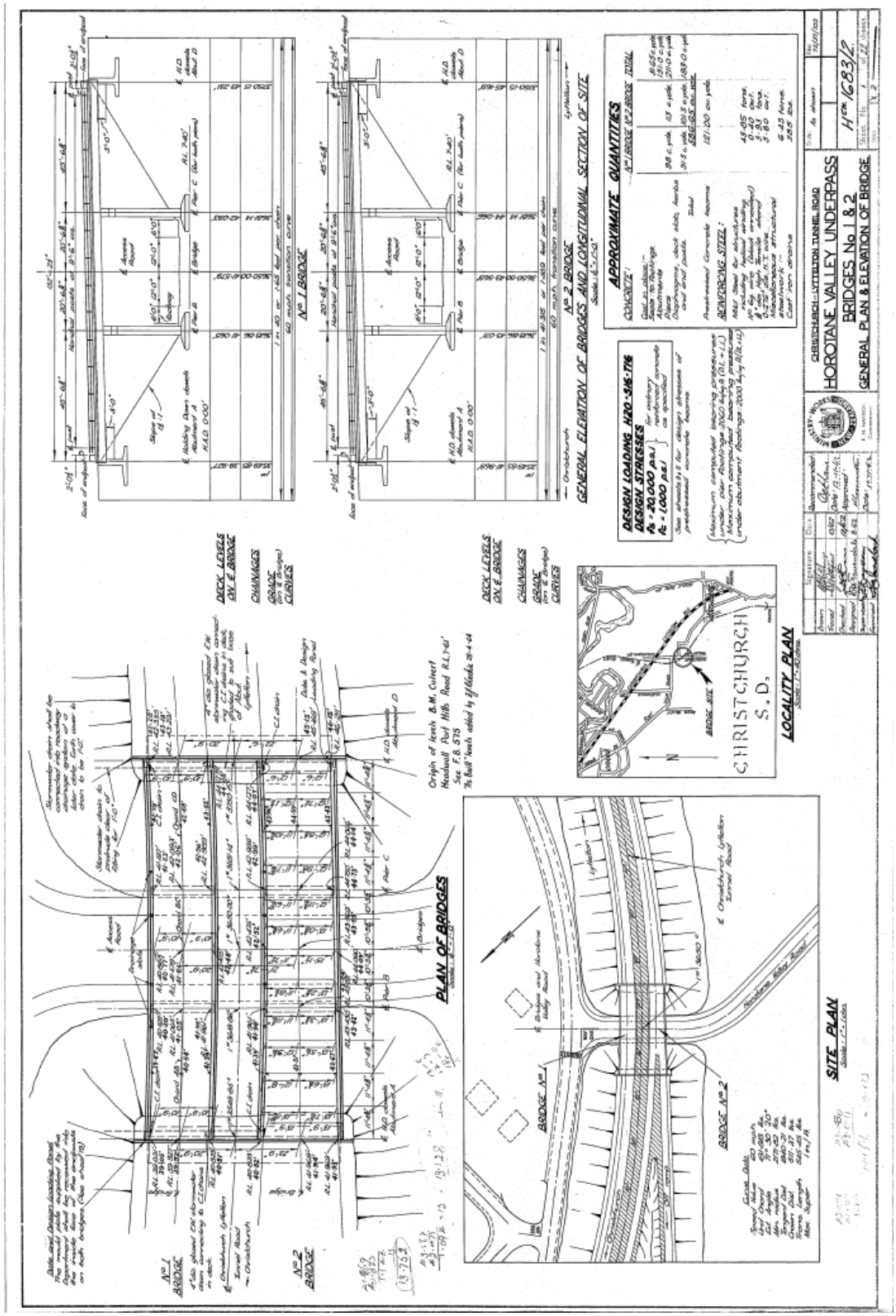

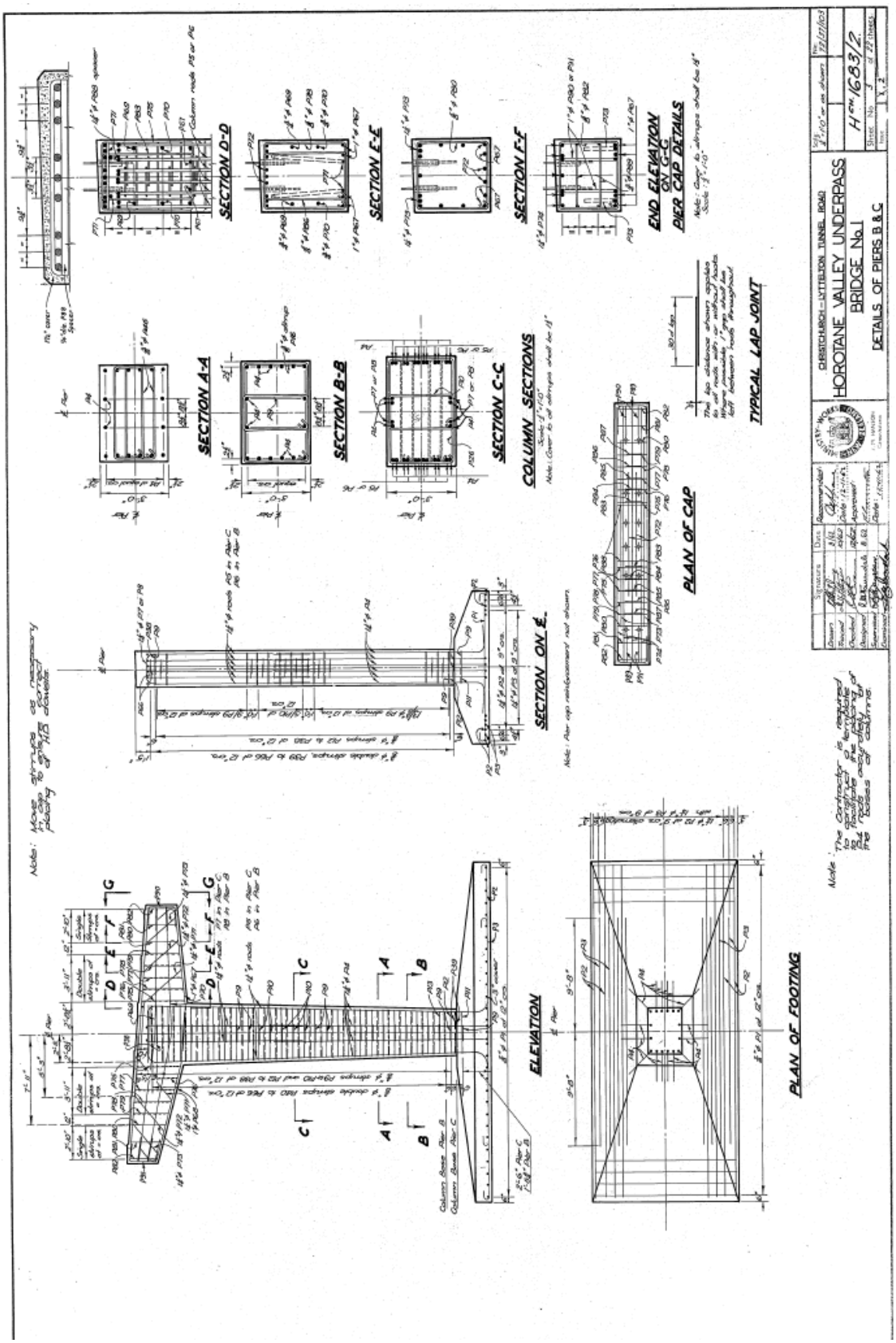
HOROTANE VALLEY UNDERPASS
BRIDGE No.1
DETAILS OF PIERS B & C
H 6W 1683/2
SECTION A-A
SECTION B-B
SECTION C-C
SECTION D-D
SECTION E-E
SECTION F-F
COLUMN SECTIONS
END ELEVATION ON C-C
PIER CAP DETAILS
TYPICAL LAP JOINT
PLAN OF CAP
SECTION ON E
ELEVATION
PLAN OF FOOTING

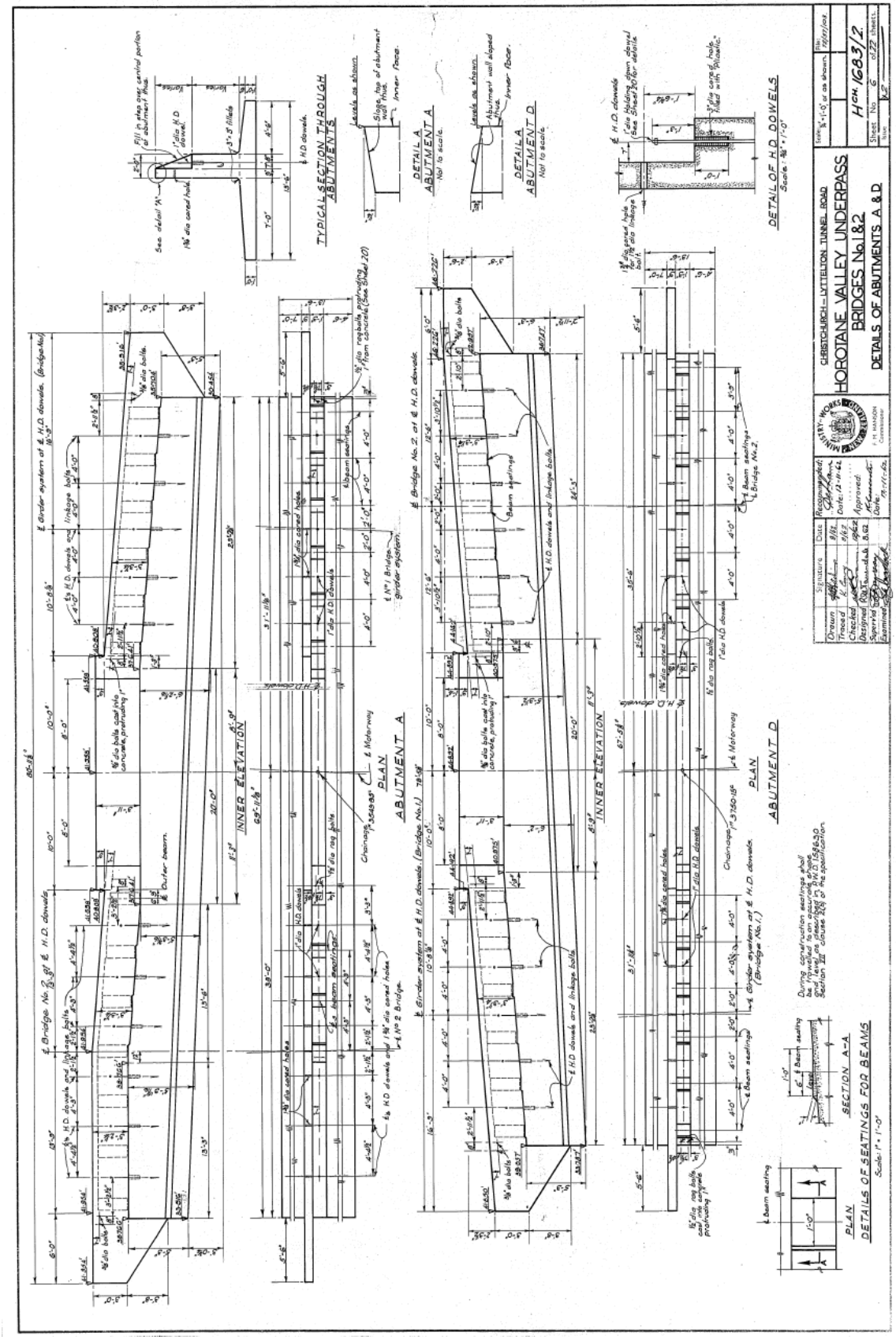
HOROTANE VALLEY UNDERPASS
BRIDGES No.1&2
DETAILS OF ABUTMENTS A & D
CHRISTCHURCH — LYTTELTON TUNNEL ROAD
HGH 1683/2
TYPICAL SECTION THROUGH ABUTMENTS
DETAIL A ABUTMENT A
DETAIL A ABUTMENT D
DETAIL OF H.D. DOWELS
INNER ELEVATION
PLAN ABUTMENT A
PLAN ABUTMENT D
SECTION A-A
PLAN DETAILS OF SEATINGS FOR BEAMS

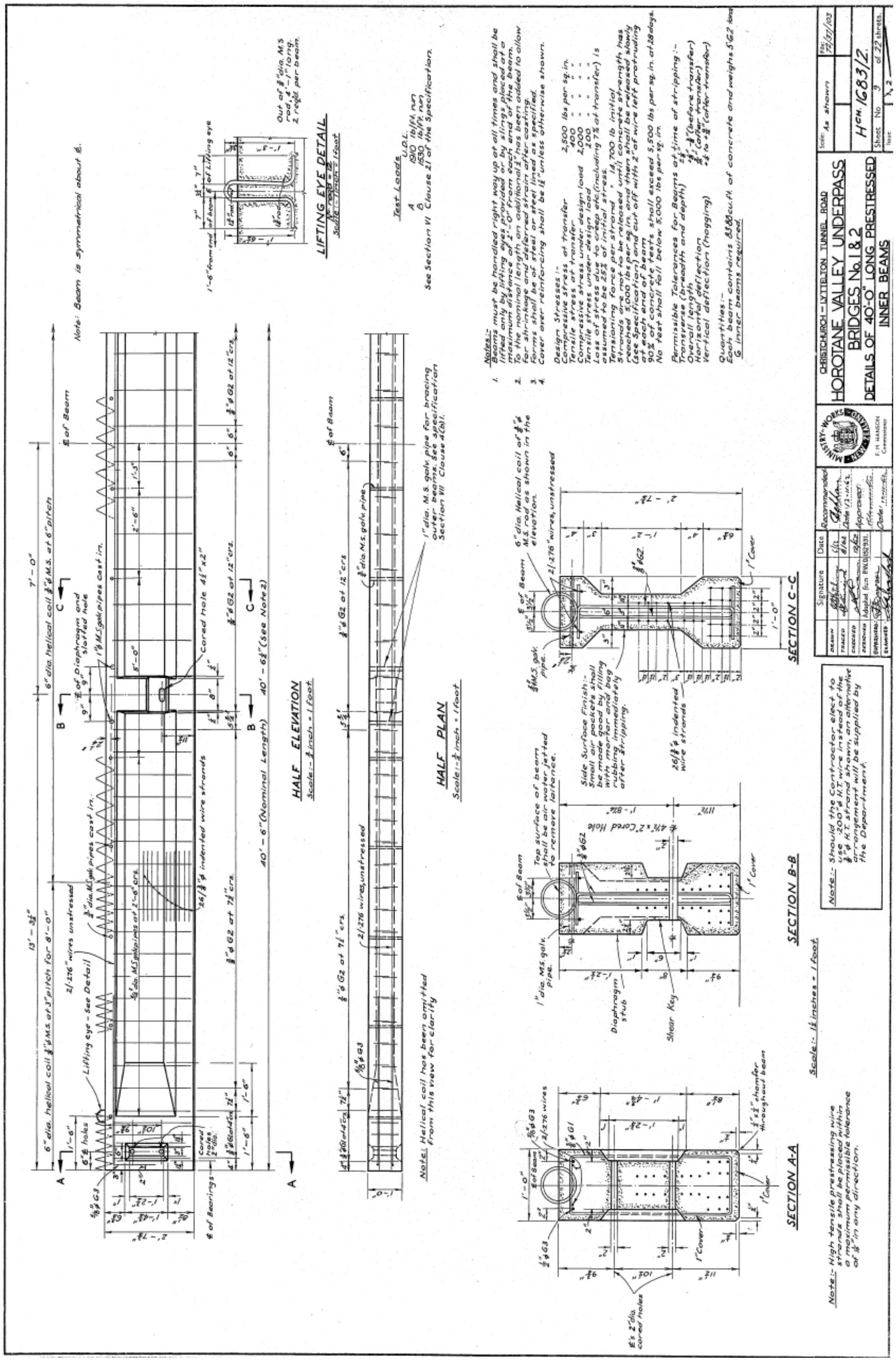
CHRISTCHURCH – LYTTELTON TUNNEL ROAD
HOROTANE VALLEY UNDERPASS
BRIDGES No. 1 & 2
DETAILS OF 40'-0" LONG PRESTRESSED
INNER BEAMS
MINISTRY OF WORKS NEW ZEALAND
HALF ELEVATION
HALF PLAN
SECTION A-A
SECTION B-B
SECTION C-C
LIFTING EYE DETAIL
Note: Beam is symmetrical about ℄.
Note: Helical coil has been omitted from this view for clarity
Notes:-
Design Stresses:-
Permissible Tolerances for Beams at time of stripping:-
Quantities:-
Test Loads
As shown
Hᶜᴴ 1683/2

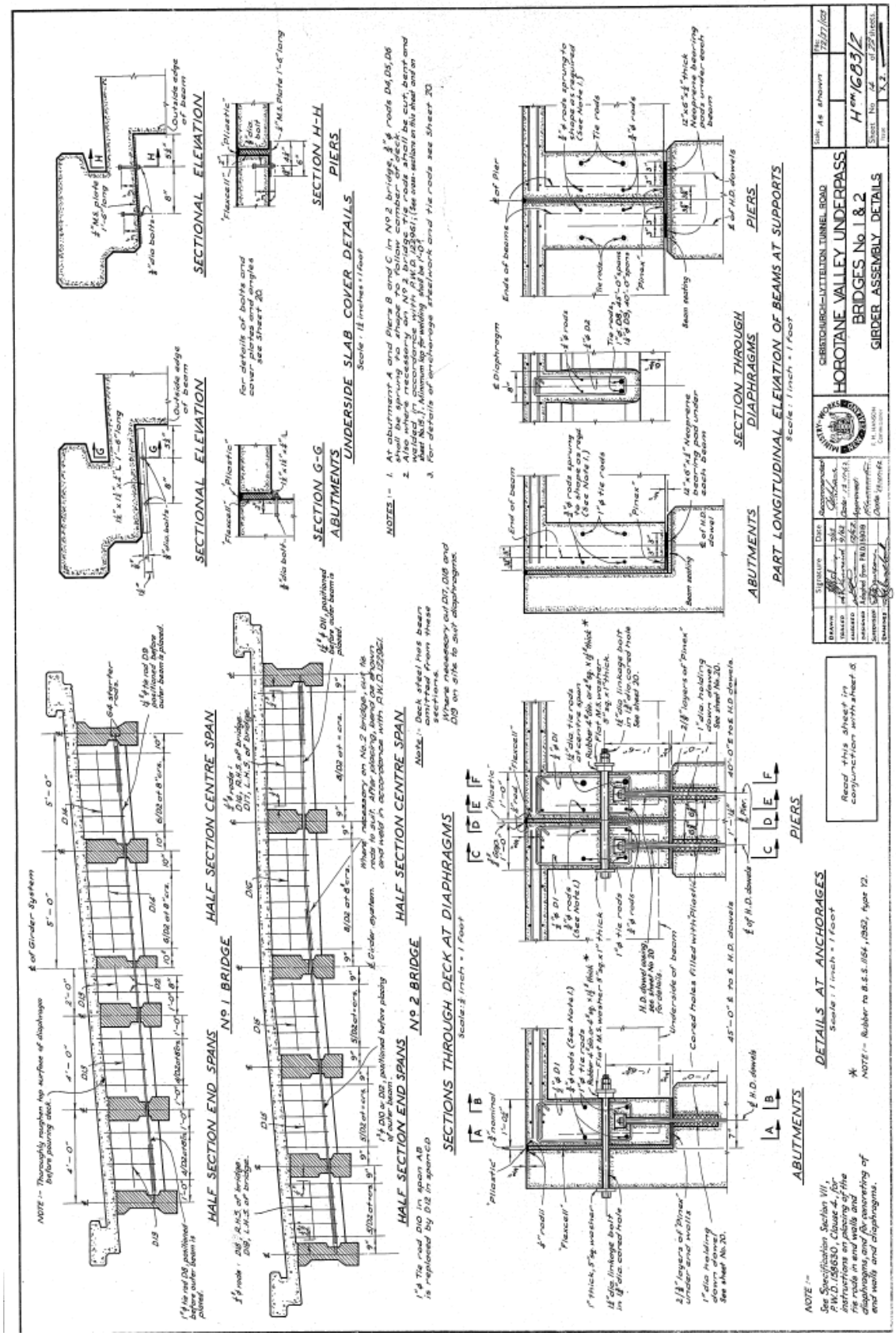
HALF SECTION END SPANS
No 1 BRIDGE
HALF SECTION CENTRE SPAN
HALF SECTION END SPANS
No 2 BRIDGE
HALF SECTION CENTRE SPAN
SECTIONS THROUGH DECK AT DIAPHRAGMS
ABUTMENTS
PIERS
DETAILS AT ANCHORAGES
SECTIONAL ELEVATION
SECTIONAL ELEVATION
SECTION G-G
ABUTMENTS
SECTION H-H
PIERS
UNDERSIDE SLAB COVER DETAILS
SECTION THROUGH DIAPHRAGMS
ABUTMENTS
PIERS
PART LONGITUDINAL ELEVATION OF BEAMS AT SUPPORTS
CHRISTCHURCH-LYTTELTON TUNNEL ROAD
HOROTANE VALLEY UNDERPASS
BRIDGES No 1 & 2
GIRDER ASSEMBLY DETAILS
H cm/683/2

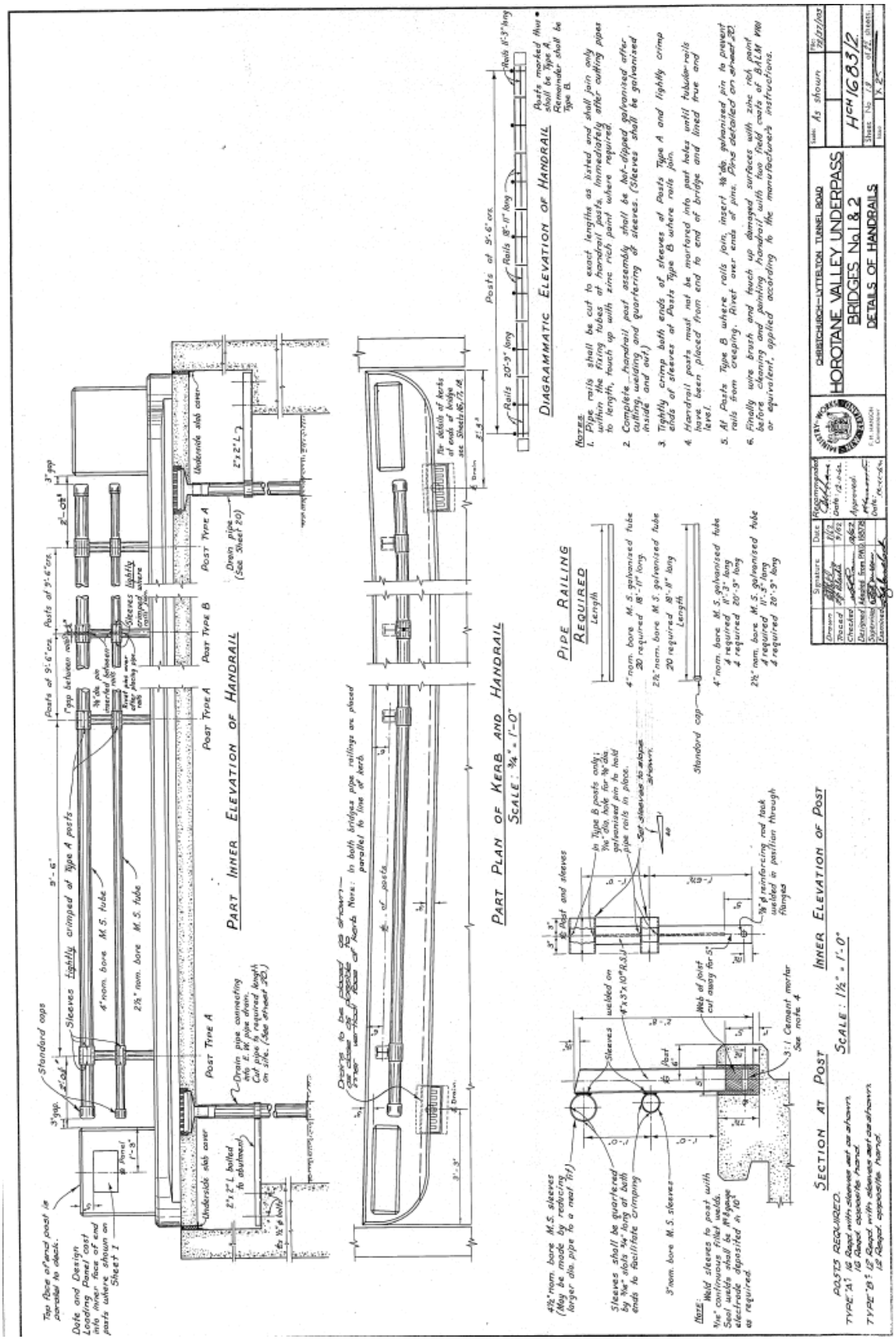
PART INNER ELEVATION OF HANDRAIL
PART PLAN OF KERB AND HANDRAIL
SCALE: ¾" = 1'-0"
DIAGRAMMATIC ELEVATION OF HANDRAIL
PIPE RAILING REQUIRED
SECTION AT POST
INNER ELEVATION OF POST
SCALE: 1½" = 1'-0"
Notes
1. Pipe rails shall be cut to exact lengths as listed and shall join only within the fixing tubes at handrail posts. Intermediately after cutting pipes to length, touch up with zinc rich paint where required.
2. Complete handrail post assembly shall be hot-dipped galvanised after cutting, welding and quartering of sleeves. (Sleeves shall be galvanised inside and out.)
3. Tightly crimp both ends of sleeves at Posts Type A and tightly crimp ends of sleeves at Posts Type B where rails join.
4. Handrail posts must not be marred into past holes until tubular rails have been placed from end to end of bridge and lined true and level.
5. At Posts Type B where rails join, insert ⅜" dia galvanised pin to prevent rails from creeping. Rivet over ends of pins. Pins detailed on sheet 2/2.
6. Finally wire brush and touch up damaged surfaces with zinc rich paint or equivalent, applied according to the manufacturer's instructions.
POSTS REQUIRED.
TYPE 'A' 16 Reqd with sleeves set as shown
16 Reqd opposite hand
TYPE 'B' 12 Reqd with sleeves set as shown
12 Reqd opposite hand
Signature Date
Drawn 10/2
Traced 9/82
Checked
Designed Marked from PWD 16578
Submitted
Approved
Date
Recommended
Date
CHRISTCHURCH—LYTTELTON TUNNEL ROAD
HOROTANE VALLEY UNDERPASS
BRIDGES No1 & 2
DETAILS OF HANDRAILS
Scale As shown
Sheet No 1/2 of 2 Sheets
HCH 1683/2

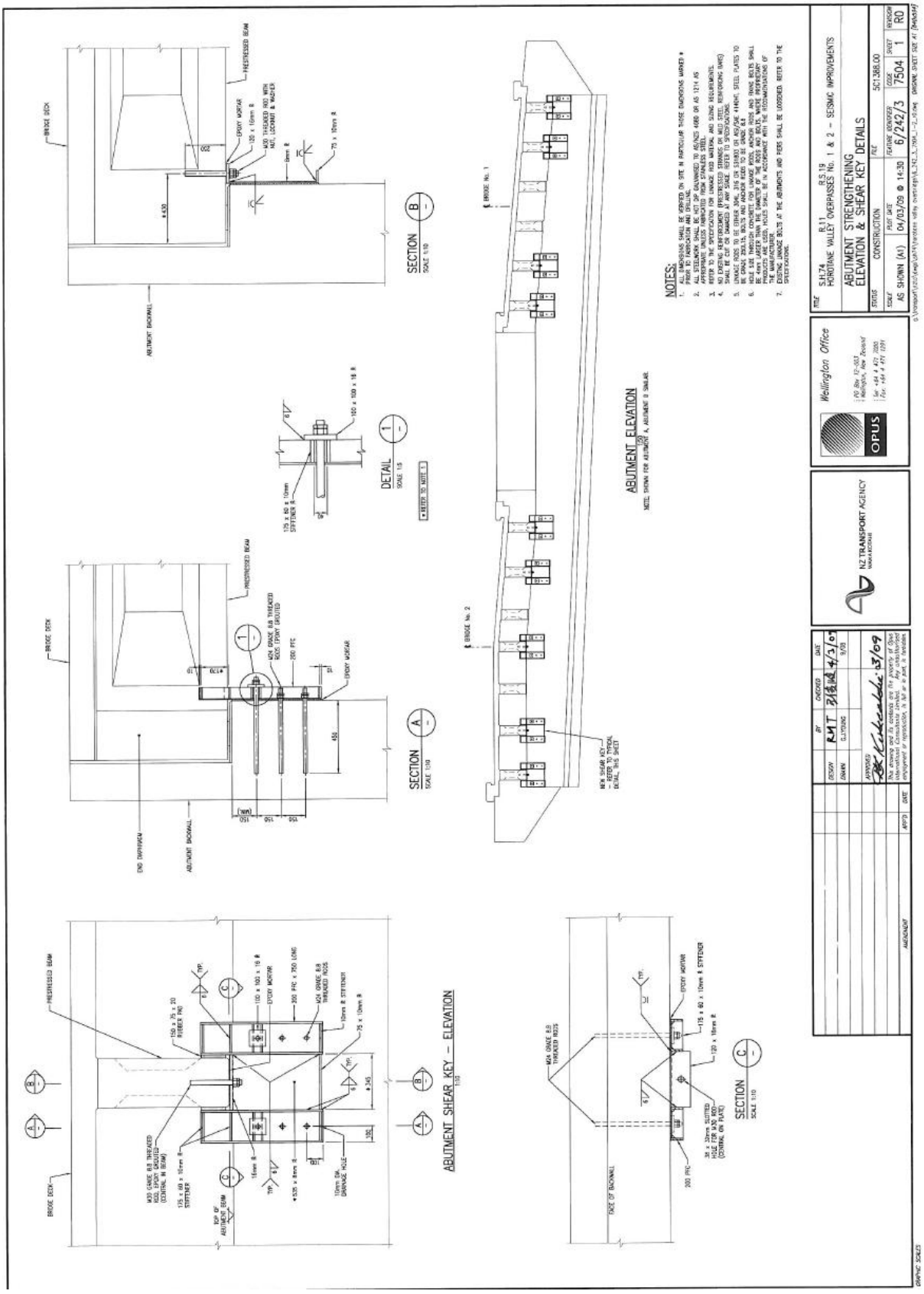
NOTES:
ABUTMENT ELEVATION
ABUTMENT SHEAR KEY – ELEVATION
SECTION
DETAIL
Wellington Office
OPUS
NZ TRANSPORT AGENCY
ABUTMENT STRENGTHENING
ELEVATION & SHEAR KEY DETAILS
S.H.74 HOROTANE VALLEY OVERPASSES No. 1 & 2 – SEISMIC IMPROVEMENTS
R.11 R.S.19
SCT.388.00
CONSTRUCTION
AS SHOWN (A1)
04/03/09 @ 14:30
6/242/3
7504
R0

A.3 Moorhouse Avenue Overbridge

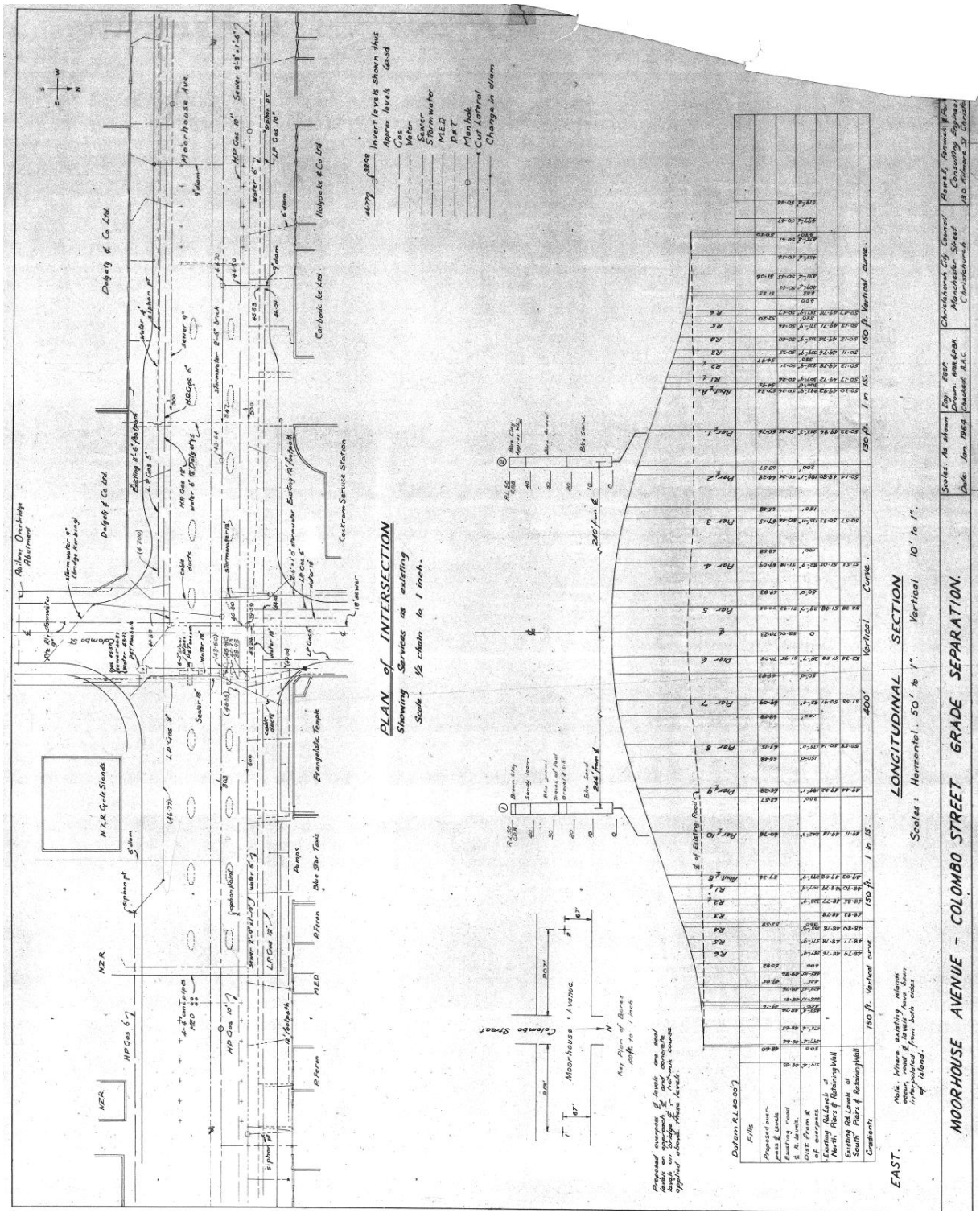

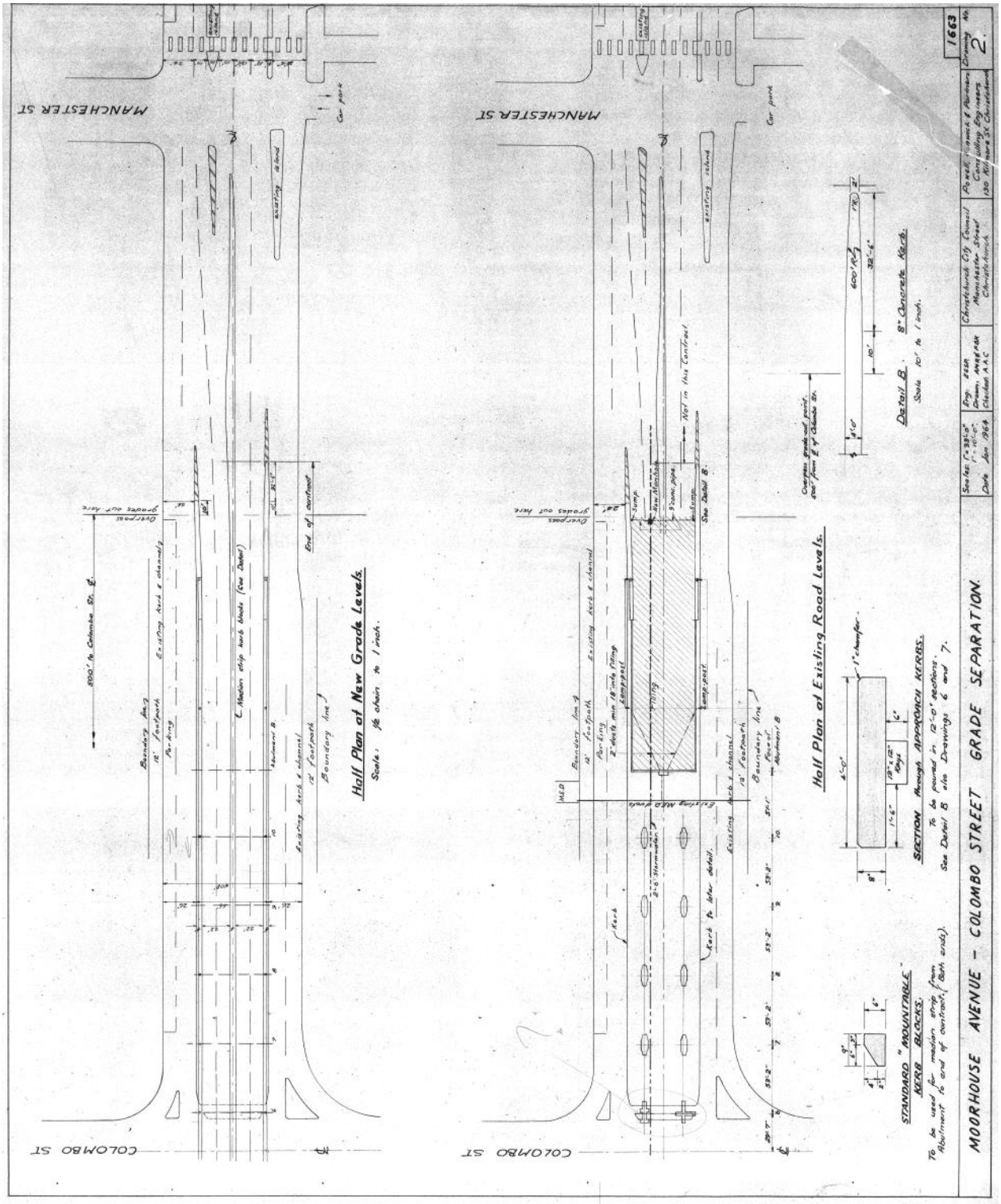
MANCHESTER ST
COLOMBO ST
Half Plan of New Grade Levels.
Scale: ½ chain to 1 inch.
Half Plan of Existing Road Levels.
Detail B. 8" Concrete Kerb.
Scale 10" to 1 inch.
SECTION through APPROACH KERBS.
STANDARD "MOUNTABLE" KERB BLOCKS.
MOORHOUSE AVENUE - COLOMBO STREET GRADE SEPARATION.
1663
Drawing No. 2.

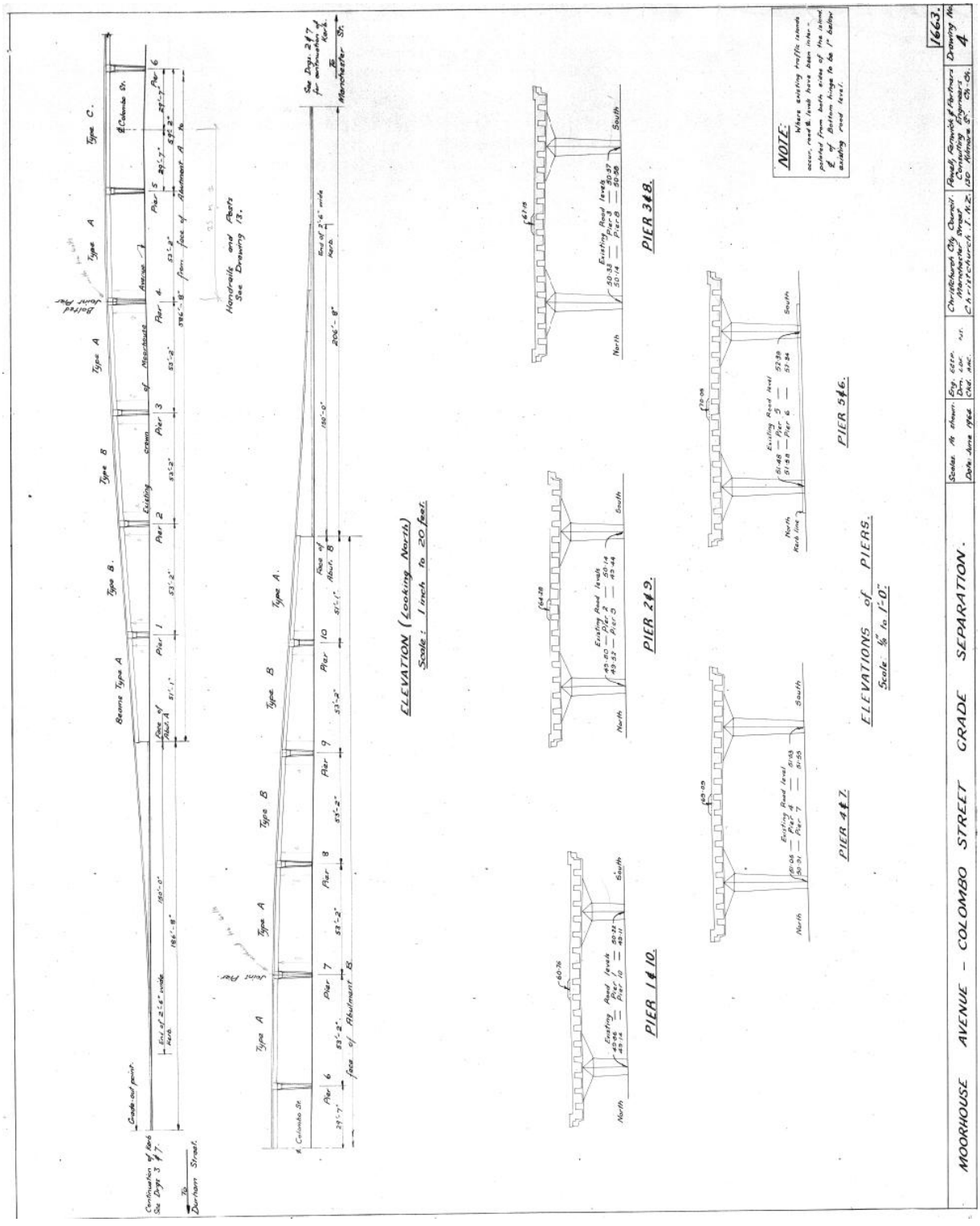
MOORHOUSE AVENUE - COLOMBO STREET GRADE SEPARATION.
ELEVATION (Looking North)
Scale: 1 inch to 20 feet.
ELEVATIONS of PIERS.
Scale: ½" to 1'-0"
PIER 1 & 10.
PIER 2 & 9.
PIER 3 & 8.
PIER 4 & 7.
PIER 5 & 6.
NOTE:
Where existing traffic islands occur, road & kerb have been interpolated from both sides of the island & of Bottom kerbs to be 1" below existing road level.
Christchurch City Council Manchester Street CHRISTCHURCH, N.Z.
Powell, Fenwick & Partners Consulting Engineers 150 Kilmore St. CHCH.
Drawing No 4
1663.

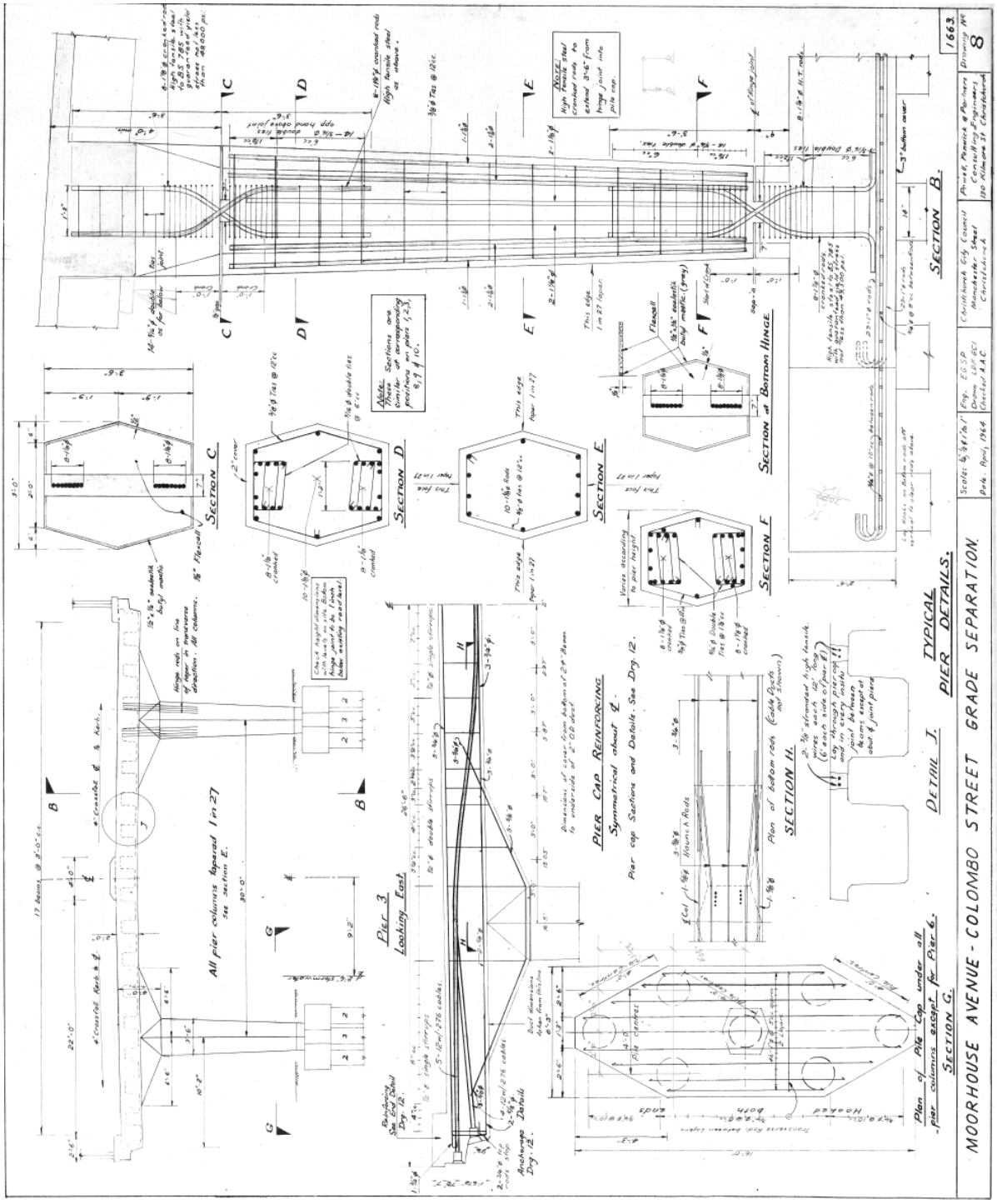
MOORHOUSE AVENUE - COLOMBO STREET GRADE SEPARATION
TYPICAL PIER DETAILS.
SECTION B.
SECTION C.
SECTION D
SECTION E
SECTION F
SECTION at BOTTOM HINGE
DETAIL J.
Pier 3 Looking East
PIER CAP REINFORCING
Symmetrical about ℄.
SECTION H.
Plan of Pile Cap under all pier columns except for Pier 6.
SECTION G.
All pier columns Spaced 1 in 27
Christchurch City Council
Christchurch
Drawing No 8
1663

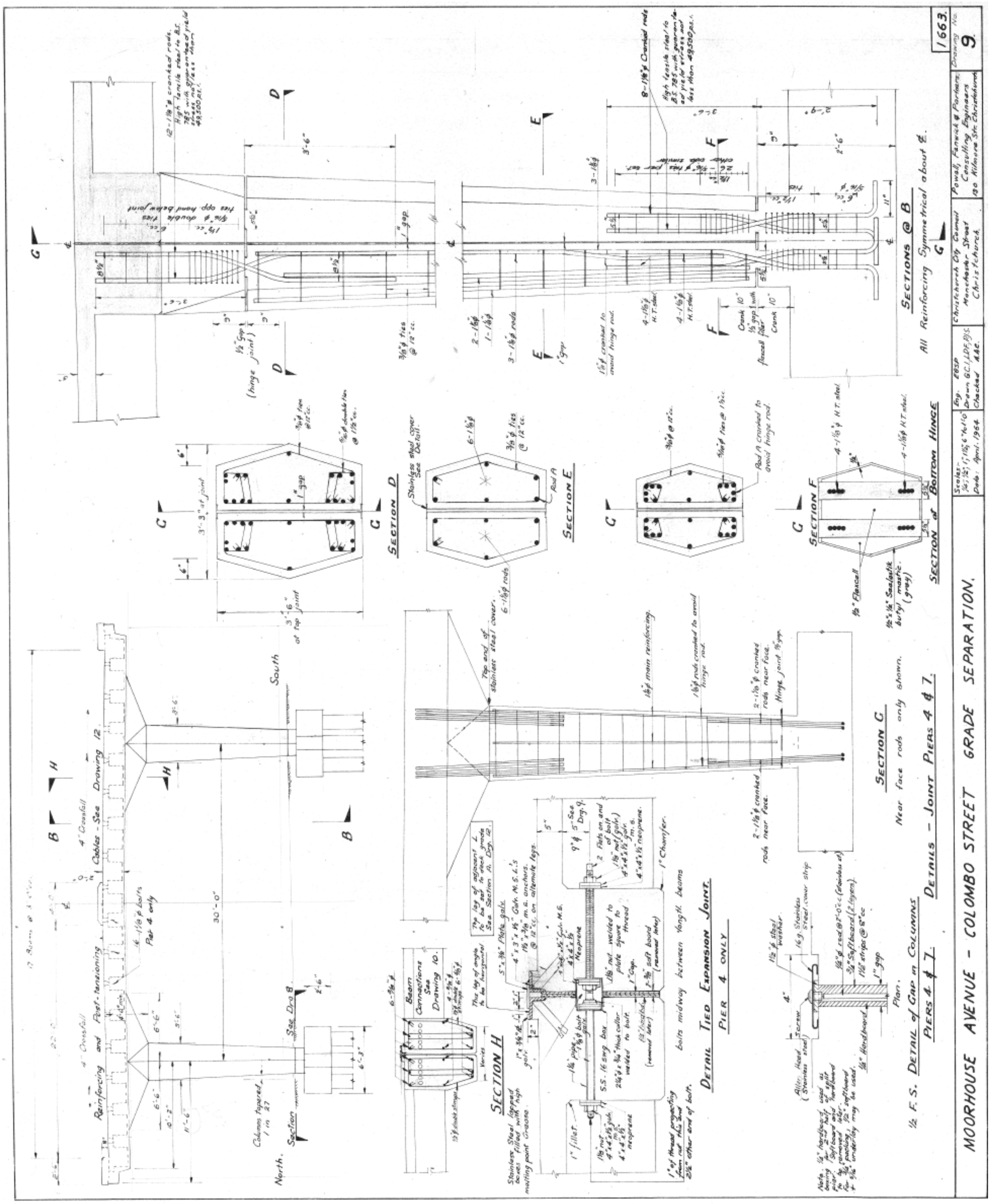
MOORHOUSE AVENUE - COLOMBO STREET GRADE SEPARATION.
SECTIONS @ B
All Reinforcing Symmetrical about ℄.
SECTION D
SECTION E
SECTION F
SECTION of BOTTOM HINGE
SECTION G
Near face rods only shown.
DETAILS - JOINT PIERS 4 & 7.
SECTION H
DETAIL TIED EXPANSION JOINT.
PIER 4 ONLY
½ F. S. DETAIL of GAP in COLUMNS
PIERS 4 & 7.
North.
South
Section
1663
9

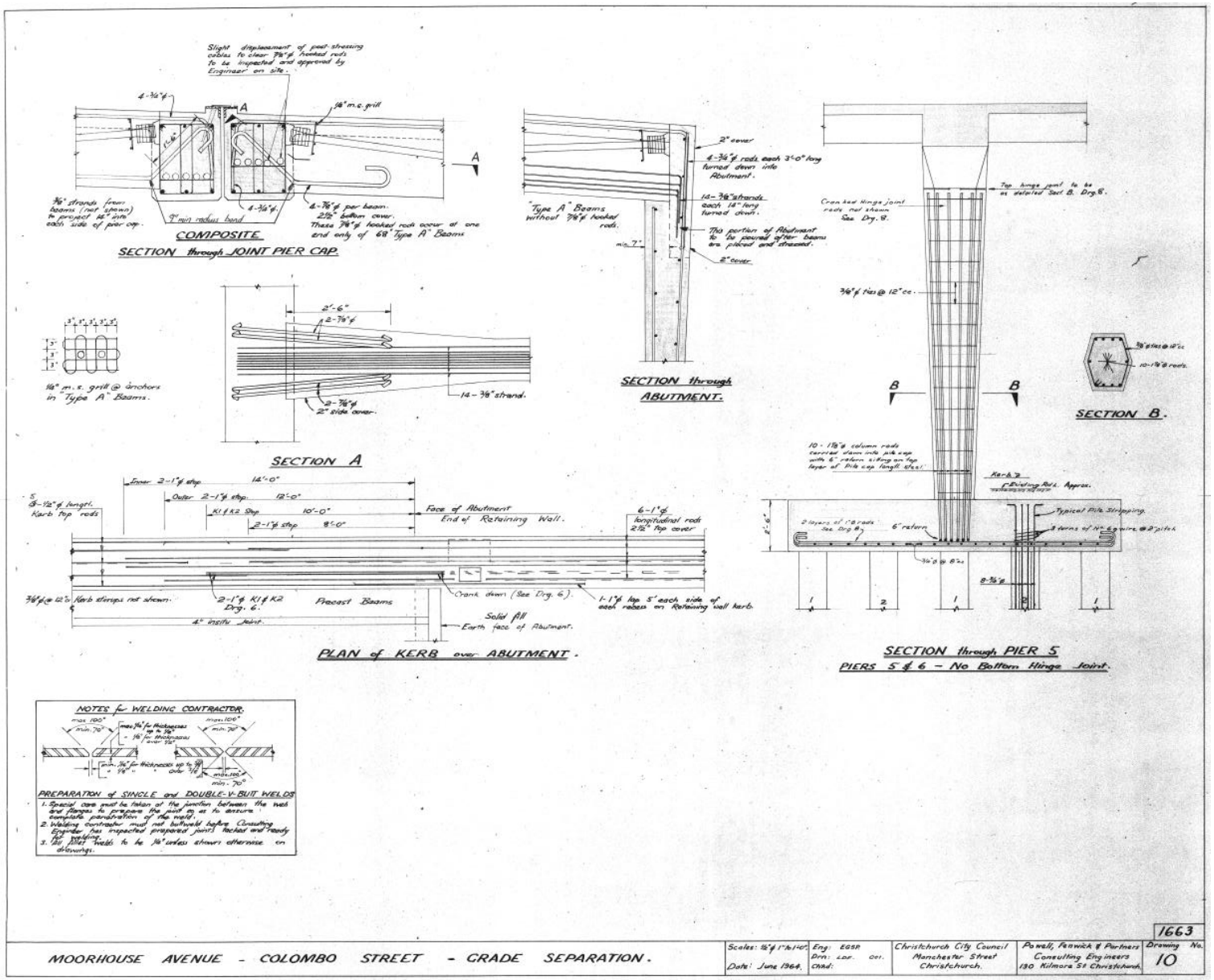

1663

MOORHOUSE AVENUE - COLOMBO STREET - GRADE SEPARATION.	Scales: ½" = 1'-0" 1"=40' Date: June 1964.	Eng: EASH Drn: LAR. ccl. Chkd:	Christchurch City Council Manchester Street Christchurch.	Powell, Fenwick & Partners Consulting Engineers 130 Kilmore St Christchurch.	Drawing No. 10

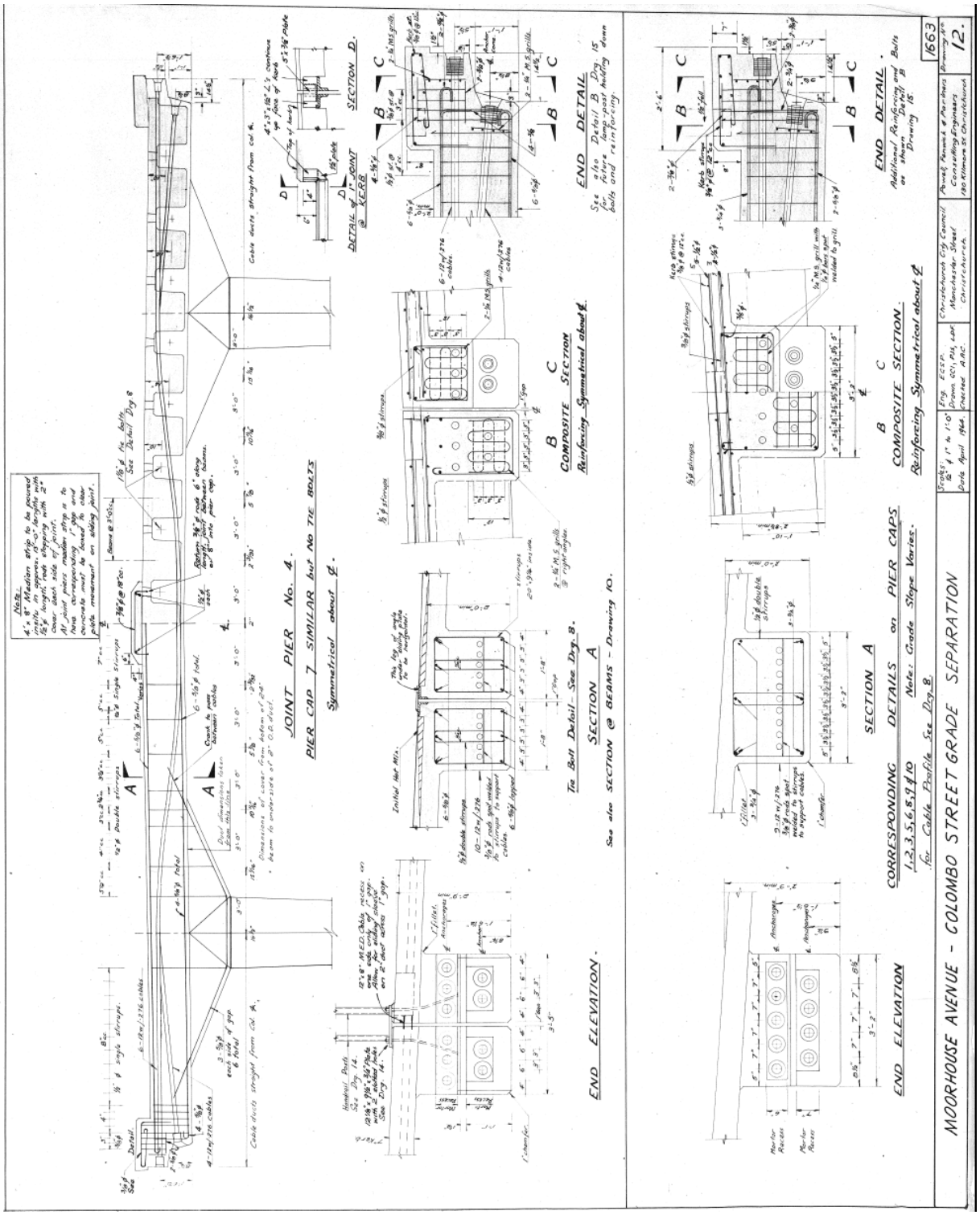
MOORHOUSE AVENUE - COLOMBO STREET GRADE SEPARATION
PIER CAP 7 SIMILAR but NO TIE BOLTS
Symmetrical about ℄.
JOINT PIER No. 4.
END ELEVATION.
SECTION A
SECTION B C
COMPOSITE SECTION
Reinforcing Symmetrical about ℄.
END DETAIL.
CORRESPONDING DETAILS on PIER CAPS 1,2,3,5,6,9 & 10
Note: Grade Slope Varies.
for Cable Profile See Dwg 8.
Scale: ½" = 1'0" Eng. E.E.P.
Date April 1964. Checked A.N.C.
Christchurch City Council
Parkes, Nowack & Partners
Consulting Engineers
Manchester Street
Christchurch.
1663
12.

Appendix B: Numerical Data for the Analyses

- Calculation of Loading of Port Hills Overpass
- Calculation of Yielding Moments of Port Hills Overpass
- Calculation of Loading of Horotane Valley Overpass
- Calculation of Yielding Moments of Horotane Valley Overpass
- Pier Dimensions of Moorhouse Avenue Overbridge
- Section Properties of Moorhouse Avenue Overbridge
- Calculation of Loading of Moorhouse Avenue Overbridge

B.1 Calculation of Loading of Port Hills Overpass

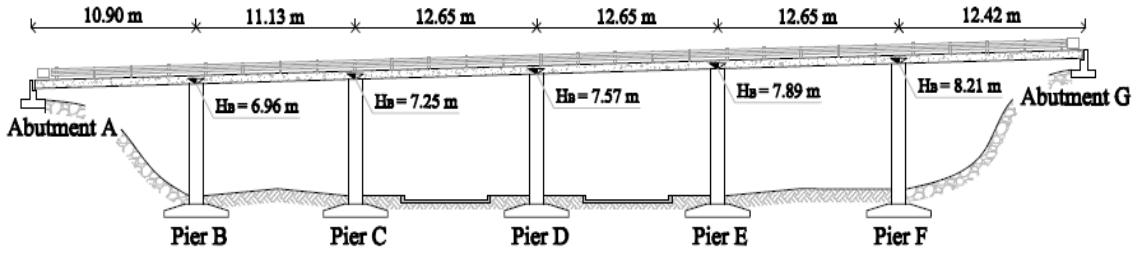

SELF WEIGHTS

TOTAL VOLUME	**[m^3]**	**TOTAL MASS**	**[kg]**	**TOTAL FORCE**	**[kN]**
Tot Vol. Pier B_{CAP}	10.39	Tot Mass Pier B_{CAP}:	24935	Tot Force Pier B_{CAP}:	244.61
Tot Vol. Pier B_{PIER}	6.72	Tot Mass Pier B_{PIER}:	16127.5	Tot Force Pier B_{PIER}:	158.21
Tot. Vol. Pier B:	**17.11**	**Tot. Mass Pier B:**	**41062.52**	**Tot. Force Pier B:**	**402.82**
Tot Vol. Pier C_{CAP}	10.39	Tot Mass Pier C_{CAP}:	24935	Tot Force Pier C_{CAP}:	244.61
Tot Vol. Pier C_{PIER}	7.09	Tot Mass Pier C_{PIER}:	17015.9	Tot Force Pier C_{PIER}:	166.93
Tot. Vol. Pier C:	**17.48**	**Tot. Mass Pier C:**	**41950.92**	**Tot. Force Pier C:**	**411.54**
Tot Vol. Pier D_{CAP}	10.39	Tot Mass Pier D_{CAP}:	24935	Tot Force Pier D_{CAP}:	244.61
Tot Vol. Pier D_{PIER}	7.52	Tot Mass Pier D_{PIER}:	18041.3	Tot Force Pier D_{PIER}:	176.99
Tot. Vol. Pier D:	**17.91**	**Tot. Mass Pier D:**	**42976.30**	**Tot. Force Pier D:**	**421.60**
Tot Vol. Pier E_{CAP}	10.39	Tot Mass Pier E_{CAP}:	24935	Tot Force Pier E_{CAP}:	244.61
Tot Vol. Pier E_{PIER}	8.02	Tot Mass Pier E_{PIER}:	19245.9	Tot Force Pier E_{PIER}:	188.80
Tot. Vol. Pier E:	**18.41**	**Tot. Mass Pier E:**	**44180.89**	**Tot. Force Pier E:**	**433.41**
Tot Vol. Pier F_{CAP}	10.39	Tot Mass Pier F_{CAP}:	24935	Tot Force Pier F_{CAP}:	244.61
Tot Vol. Pier F_{PIER}	8.32	Tot Mass Pier F_{PIER}:	19965.2	Tot Force Pier F_{PIER}:	195.86
Tot. Vol. Pier F:	**18.71**	**Tot. Mass Pier F:**	**44900.14**	**Tot. Force Pier F:**	**440.47**
		Tot Mass Beams:	519100	Tot Force Beams:	5087.18
Tot Vol. Slab:	127.70	Tot Mass Slab:	306481.95	Tot Force Slab:	3003.52
		Tot. Mass Deck:	**825581.95**	**Tot. Force Deck:**	**8090.70**
Tot. Vol. Abutments:	**20.60**	**Tot. Mass Abutments:**	**49434.84**	**Tot. Force Abutments:**	**484.46**

DEAD LOADINGS

Φ_{pipe} [in]	Weight [kg/m]
4"	4.64
2.5"	2.87
Total Weight (x2) [kg/m]	**15.01**
Total Weight (x2) [kN/m]	**0.15**

B.2 Calculation of Yielding Moments of Port Hills Overpass

	Design Properties				Actual Properties			
	BASE		TOP		BASE		TOP	
PIER B	N_{Ed} [kNm]	1633.05	N_{Ed} [kNm]	1475.25	N_{Ed} [kNm]	1633.05	N_{Ed} [kNm]	1475.25
	I_{yy} [m^4]	0.041	I_{yy} [m^4]	0.042	I_{yy} [m^4]	0.035	I_{yy} [m^4]	0.036
	I_{zz} [m^4]	0.058	I_{zz} [m^4]	0.109	I_{zz} [m^4]	0.050	I_{zz} [m^4]	0.093
	M_{yy} [kNm]	2584.66	M_{yy} [kNm]	2557.39	M_{yy} [kNm]	2678.72	M_{yy} [kNm]	2637.71
	M_{zz} [kNm]	3083.60	M_{zz} [kNm]	4119.54	M_{zz} [kNm]	3164.69	M_{zz} [kNm]	4206.07
	Hinge Length L_p [m]				0.58			
PIER C	N_{Ed} [kNm]	1739.70	N_{Ed} [kNm]	1573.19	N_{Ed} [kNm]	1739.70	N_{Ed} [kNm]	1573.19
	I_{yy} [m^4]	0.041	I_{yy} [m^4]	0.043	I_{yy} [m^4]	0.036	I_{yy} [m^4]	0.036
	I_{zz} [m^4]	0.056	I_{zz} [m^4]	0.111	I_{zz} [m^4]	0.049	I_{zz} [m^4]	0.094
	M_{yy} [kNm]	2613.43	M_{yy} [kNm]	2604.49	M_{yy} [kNm]	2687.93	M_{yy} [kNm]	2693.67
	M_{zz} [kNm]	3036.88	M_{zz} [kNm]	4181.14	M_{zz} [kNm]	3179.02	M_{zz} [kNm]	4299.00
	Hinge Length L_p [m]				0.60			
PIER D	N_{Ed} [kNm]	1834.91	N_{Ed} [kNm]	1658.36	N_{Ed} [kNm]	1834.91	N_{Ed} [kNm]	1658.36
	I_{yy} [m^4]	0.041	I_{yy} [m^4]	0.044	I_{yy} [m^4]	0.03637	I_{yy} [m^4]	0.038505
	I_{zz} [m^4]	0.053	I_{zz} [m^4]	0.112	I_{zz} [m^4]	0.047189	I_{zz} [m^4]	0.094811
	M_{yy} [kNm]	2606.1	M_{yy} [kNm]	2641.40	M_{yy} [kNm]	2759.29	M_{yy} [kNm]	2732.12
	M_{zz} [kNm]	3032.28	M_{zz} [kNm]	4235.53	M_{zz} [kNm]	3139.78	M_{zz} [kNm]	4265.11
	Hinge Length L_p [m]				0.62			
PIER E	N_{Ed} [kNm]	1846.72	N_{Ed} [kNm]	1658.36	N_{Ed} [kNm]	1846.72	N_{Ed} [kNm]	1658.36
	I_{yy} [m^4]	0.041	I_{yy} [m^4]	0.044	I_{yy} [m^4]	0.036	I_{yy} [m^4]	0.038
	I_{zz} [m^4]	0.050	I_{zz} [m^4]	0.112	I_{zz} [m^4]	0.043	I_{zz} [m^4]	0.095
	M_{yy} [kNm]	2658.39	M_{yy} [kNm]	2641.40	M_{yy} [kNm]	2761.55	M_{yy} [kNm]	2732.12
	M_{zz} [kNm]	2924.31	M_{zz} [kNm]	4235.53	M_{zz} [kNm]	3040.30	M_{zz} [kNm]	4265.11

	Hinge Length L_p [m]				0.66			
PIER F	N_{Ed} [kNm]	1840.99	N_{Ed} [kNm]	1645.58	N_{Ed} [kNm]	1840.99	N_{Ed} [kNm]	1645.58
	I_{yy} [m^4]	0.040	I_{yy} [m^4]	0.044	I_{yy} [m^4]	0.035	I_{yy} [m^4]	0.038
	I_{zz} [m^4]	0.047	I_{zz} [m^4]	0.112	I_{zz} [m^4]	0.041	I_{zz} [m^4]	0.098
	M_{yy} [kNm]	2633.09	M_{yy} [kNm]	2638.27	M_{yy} [kNm]	2753.08	M_{yy} [kNm]	2728.37
	M_{zz} [kNm]	2829.84	M_{zz} [kNm]	4231.60	M_{zz} [kNm]	2965.53	M_{zz} [kNm]	4246.50
	Hinge Length L_p [m]				0.67			

B.3 Calculation of Loading of Horotane Valley Overpass

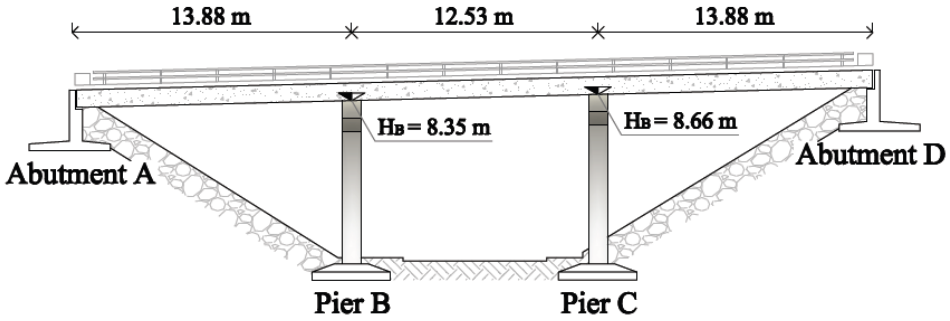

SELF WEIGHTS

TOTAL VOLUME	**[m^3]**	**TOTAL MASS**	**[kg]**	**TOTAL FORCE**	**[kN]**
Tot Vol. Pier B $_{CAP}$	5.52	Tot Mass Pier B $_{CAP}$:	13251.81	Tot Force Pier B $_{CAP}$:	130
Tot Vol. Pier B $_{PIER}$	9.21	Tot Mass Pier B $_{PIER}$:	22093.68	Tot Force Pier B $_{PIER}$:	216.74
Tot Vol. Pier B:	**14.73**	**Tot Mass Pier B:**	**35345.50**	**Tot Force Pier B:**	**346.74**
Tot Vol. Pier C $_{CAP}$	5.52	Tot Mass Pier C $_{CAP}$:	13251.81	Tot Force Pier C $_{CAP}$:	130.00
Tot Vol. Pier C $_{PIER}$	9.57	Tot Mass Pier C $_{PIER}$:	22973.58	Tot Force Pier C $_{PIER}$:	225.37
Tot Vol. Pier C:	**15.09**	**Tot Mass Pier C:**	**36225.39**	**Tot Force Pier C:**	**355.37**
		Tot Mass Beams:	103220	Tot Force Beams:	1012.59
Tot Vol. Slab:	55.92	Tot Mass Slab:	134219.66	Tot Force Slab:	1316.69
		Tot Mass Deck:	**237439.66**	**Tot Force Deck:**	**2329.28**
Tot Vol. Abutments:	**123.93**	**Tot Mass Abutments:**	**297428.14**	**Tot Force Abutments:**	**2917.77**

B.4 Calculation of Yielding Moments of Horotane Valley Overpass

	Design Properties				Actual Properties			
	BASE		**TOP**		**BASE**		**TOP**	
PIER B	N_{Ed} [kNm]	1086.07	N_{Ed} [kNm]	739.33	N_{Ed} [kNm]	1086.07	N_{Ed} [kNm]	739.33
	I_{yy} [m^4]	0.025	I_{yy} [m^4]	0.025	I_{yy} [m^4]	0.020	I_{yy} [m^4]	0.019
	I_{zz} [m^4]	0.055	I_{zz} [m^4]	0.091	I_{zz} [m^4]	0.043	I_{zz} [m^4]	0.070
	M_{yy} [kNm]	1937.58	M_{yy} [kNm]	1862.21	M_{yy} [kNm]	2021.81	M_{yy} [kNm]	1930.37
	M_{zz} [kNm]	2787.53	M_{zz} [kNm]	3379.19	M_{zz} [kNm]	2834.06	M_{zz} [kNm]	3463.45
	Hinge Length L_p [m]				0.80			
PIER C	N_{Ed} [kNm]	1094.70	N_{Ed} [kNm]	739.33	N_{Ed} [kNm]	1094.70	N_{Ed} [kNm]	739.33
	I_{yy} [m^4]	0.025	I_{yy} [m^4]	0.025	I_{yy} [m^4]	0.020	I_{yy} [m^4]	0.019
	I_{zz} [m^4]	0.053	I_{zz} [m^4]	0.091	I_{zz} [m^4]	0.042	I_{zz} [m^4]	0.070
	M_{yy} [kNm]	1960.52	M_{yy} [kNm]	1862.21	M_{yy} [kNm]	2011.18	M_{yy} [kNm]	1930.37
	M_{zz} [kNm]	2768.56	M_{zz} [kNm]	3379.19	M_{zz} [kNm]	2799.24	M_{zz} [kNm]	3463.45
	Hinge Length L_p [m]				0.82			

B.5 Pier Dimensions of Moorhouse Avenue Overbridge

	Elevation			Pier Height (ft)		Section Depth					Section Width	
						N		S		Average	dim a	dim b
	Deck	N	S	N	S	Top	Bottom	Top	Bottom	Bottom (mm)	Bottom	Bottom
Pier 1	60.76	49.86	50.22	6.9	6.54	1067	911.21	1067	919.34	904.95	761.78	457.28
Pier 2	64.28	49.8	50.15	10.48	10.13	1067	830.38	1067	838.29	828.75	680.84	376.34
Pier 3	67.15	50.33	50.57	12.82	12.58	1067	777.55	1067	782.97	779.25	626.76	322.26
Pier 4	69.09	51.05	51.53	14.04	13.56	1067	750.01	1067	760.84	751.64	327.21	174.21
Pier 5	70.05	51.48	52.38	14.57	13.67	1067	738.04	1067	758.36		594.70	290.20
Pier 6	70.05	51.58	52.34	14.47	13.71	1067	740.30	1067	757.46		595.38	290.88
Pier 7	69.09	50.91	51.55	14.18	13.54	1067	746.85	1067	761.30		326.54	173.54
Pier 8	67.15	50.14	50.58	13.01	12.57	1067	773.26	1067	783.20	779.25	624.73	320.23
Pier 9	64.28	49.52	49.44	10.76	10.84	1067	824.06	1067	822.26	828.75	669.66	365.16
Pier 10	60.76	49.14	49.11	7.62	7.65	1067	894.96	1067	894.28	904.95	741.12	436.62

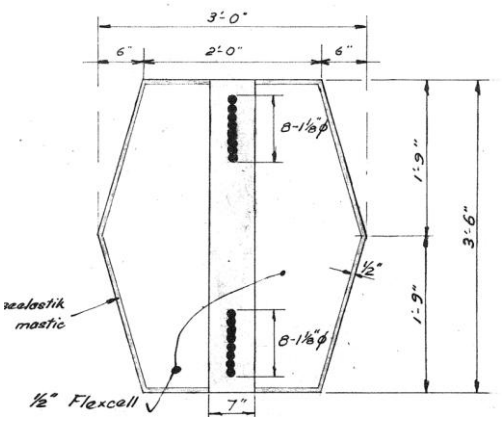

B.6 Section Properties of Moorhouse Avenue Overbridge

	Top					Bottom					Average				
	I_{lat} (mm^4)	I_{long} (mm^4)	A (mm^2)	S_{lat} (mm)	S_{long} (mm)	I_{lat} (mm^4)	I_{long} (mm^4)	A (mm^2)	S_{lat} (mm)	S_{long} (mm)	I_{lat} (mm^4)	I_{long} (mm^4)	A (mm^2)	S_{lat} (mm)	S_{long} (mm)
Pier 1	7.72E+10	4.38E+10	8.13E+05	483	201	3.77E+10	1.90E+10	5.84E+05	401	139	5.75E+10	3.14E+10	6.99E+05	442	170
Pier 2	7.72E+10	4.38E+10	8.13E+05	483	201	2.57E+10	1.20E+10	4.76E+05	363	117	5.15E+10	2.79E+10	6.44E+05	423	159
Pier 3	7.72E+10	4.38E+10	8.13E+05	483	201	1.93E+10	8.70E+09	4.00E+05	340	105	4.82E+10	2.63E+10	6.07E+05	411.5	153
Pier 4	4.12E+10	7.03E+09	4.59E+05	483	279	9.31E+09	1.36E+09	2.14E+05	330	119	2.52E+10	4.20E+09	3.36E+05	406.5	199
Pier 5	7.72E+10	4.38E+10	8.13E+05	483	201	1.65E+10	7.03E+09	3.75E+05	325	104	4.69E+10	2.54E+10	5.94E+05	404	152.5
Pier 6	7.72E+10	4.38E+10	8.13E+05	483	201	1.65E+10	7.03E+09	3.75E+05	325	104	4.69E+10	2.54E+10	5.94E+05	404	152.5
Pier 7	4.12E+10	7.03E+09	4.59E+05	483	279	9.31E+09	1.36E+09	2.14E+05	330	119	2.52E+10	4.20E+09	3.36E+05	406.5	199
Pier 8	7.72E+10	4.38E+10	8.13E+05	483	201	1.93E+10	8.70E+09	4.00E+05	340	105	4.82E+10	2.63E+10	6.07E+05	411.5	153
Pier 9	7.72E+10	4.38E+10	8.13E+05	483	201	2.57E+10	1.20E+10	4.76E+05	363	117	5.15E+10	2.79E+10	6.44E+05	423	159
Pier 10	7.72E+10	4.38E+10	8.13E+05	483	201	3.77E+10	1.90E+10	5.84E+05	401	139	5.75E+10	3.14E+10	6.99E+05	442	170

	Top		Bottom		Average	
	Lat	Long	Lat	Long	Lat	Long
	V_y	V_y	V_y	V_y	V_y	V_y
Pier 1	1124	868.1	755	536	939.5	702.05
Pier 2	1124	868.1	604.6	464.1	864.3	666.1
Pier 3	1124	868.1	544.4	417.2	834.2	642.65
Pier 4	598.1	417.9	367.9	231.3	483	324.6
Pier 5	1124	868.1	508.9	392.5	816.45	630.3
Pier 6	1124	868.1	508.9	392.5	816.45	630.3
Pier 7	598.1	417.9	367.9	231.3	483	324.6
Pier 8	1124	868.1	544.4	417.2	834.2	642.65
Pier 9	1124	868.1	604.6	464.1	864.3	666.1
Pier 10	1124	868.1	755	536	939.5	702.05

B.7 Calculation of Loading of Moorhouse Avenue Overbridge

Deck

Cross sectional area		Mass	Weight
mm^2	m^2	kg/m	kN/m
5326800	5.3268	12784.32	125.4142

Pier Cap

Volume		Mass	Weight
mm^3	m^3	kg	kN
1.1E+09	1.098	2635.2	25.85131

Piers

	Volume		Mass	Weight	Trib length		total kN/pier	per column
Pier	mm^3	m^3	kg	kN	ft	m	kN	kN
Pier 1	7.74E+08	0.77	1857.563	18.22	52.15	15.89	2081.65	1040.82
Pier 2	1.14E+09	1.14	2746.208	26.94	53.2	16.22	2139.22	1069.61
Pier 3	1.37E+09	1.37	3296.664	32.34	53.2	16.22	2150.02	1075.01
Pier 4	8.36E+08	0.84	2006.503	19.68	26.6	8.11	1107.89	553.94
Pier 5	1.51E+09	1.51	3632.473	35.63	56.2	17.13	2271.29	1135.64
Pier 6	1.51E+09	1.51	3624.755	35.56	56.2	17.13	2271.14	1135.57
Pier 7	8.4E+08	0.84	2015.227	19.77	26.6	8.11	1108.06	554.03
Pier 8	1.38E+09	1.38	3320.027	32.57	53.2	16.22	2150.48	1075.24
Pier 9	1.2E+09	1.20	2878.122	28.23	53.2	16.22	2141.81	1070.90
Pier 10	8.79E+08	0.88	2110.491	20.70	52.15	15.90	2086.61	1043.30

Appendix C: Accelerograms

- Christchurch Cashmere Hight School, CMHS (Lyttelton Records)
- Catholic Cathedral College, CCCC (Lyttelton Records)
- Heathcote Valley Primary School, HVSC (Lyttelton Records)
- Catholic Cathedral College, CCCC (Darfield Records)
- Heathcote Valley Primary School, HVSC (Darfield Records)
- Scaled Californian Earthquake

C.1 Christchurch Cashmere High School, CMHS (Lyttelton Records)

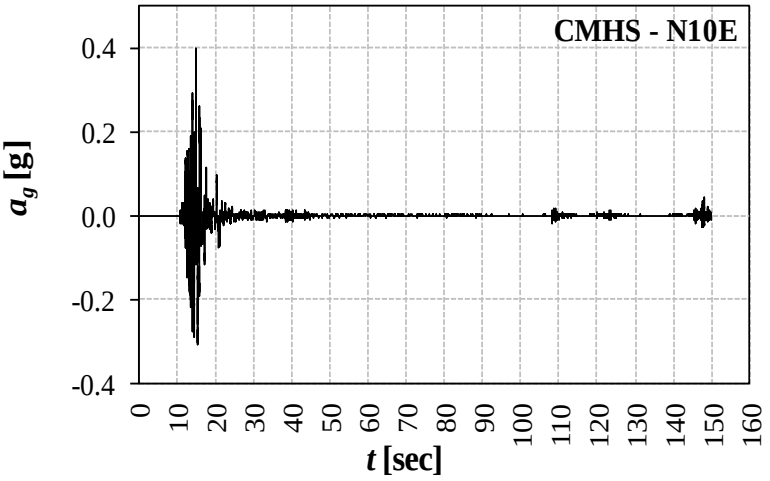

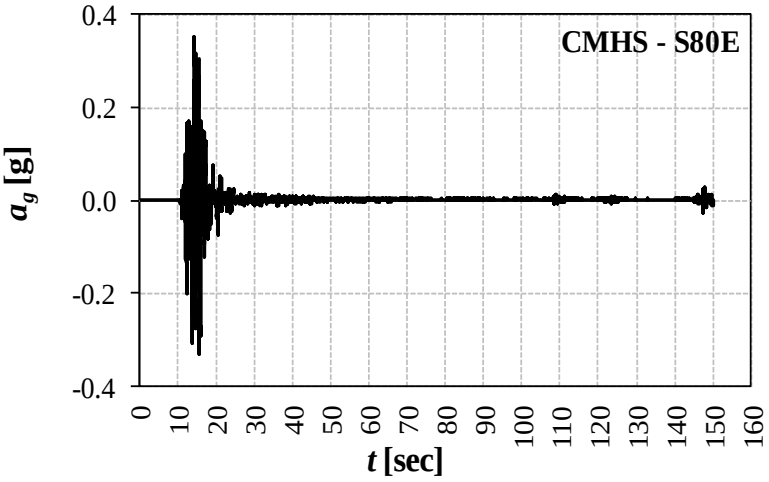

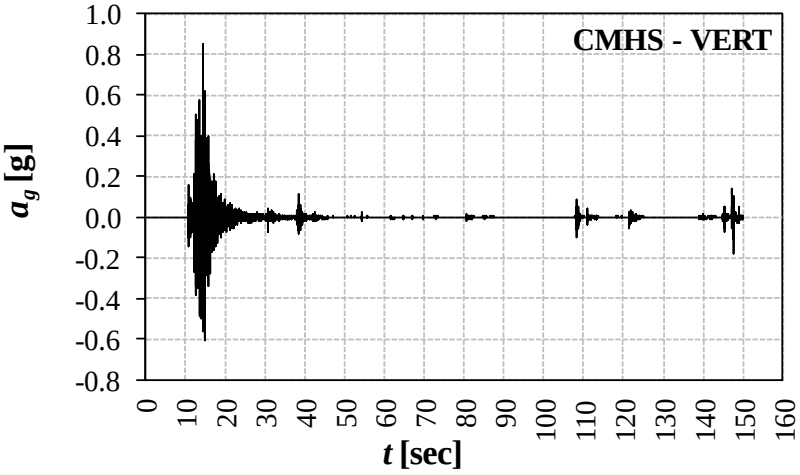

C.2 Catholic Cathedral College, CCCC (Lyttelton Records)

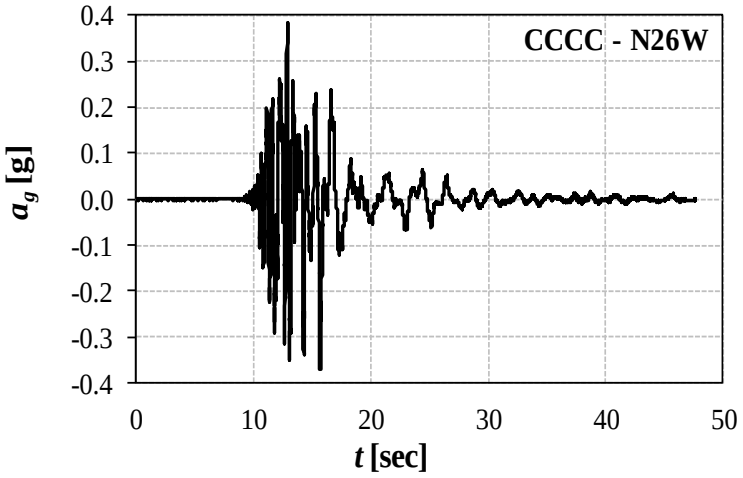

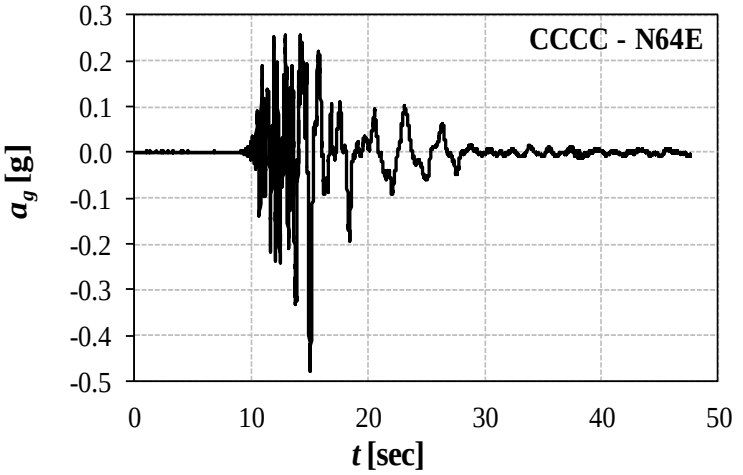

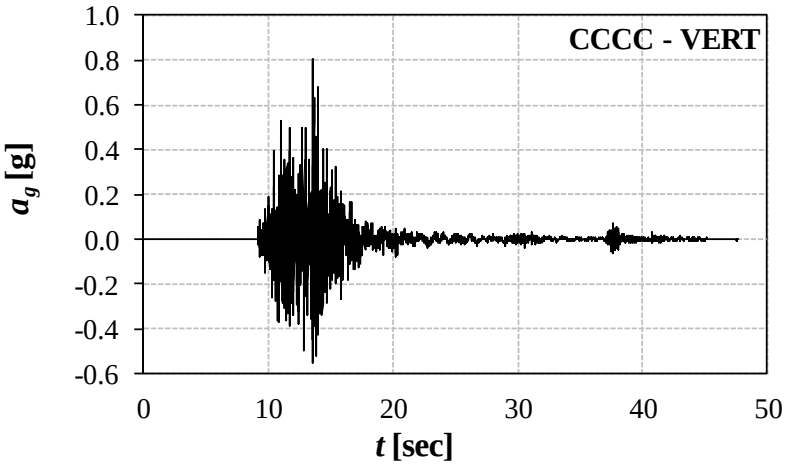

C.3 Heathcote Valley Primary School, HVSC (Lyttelton Records)

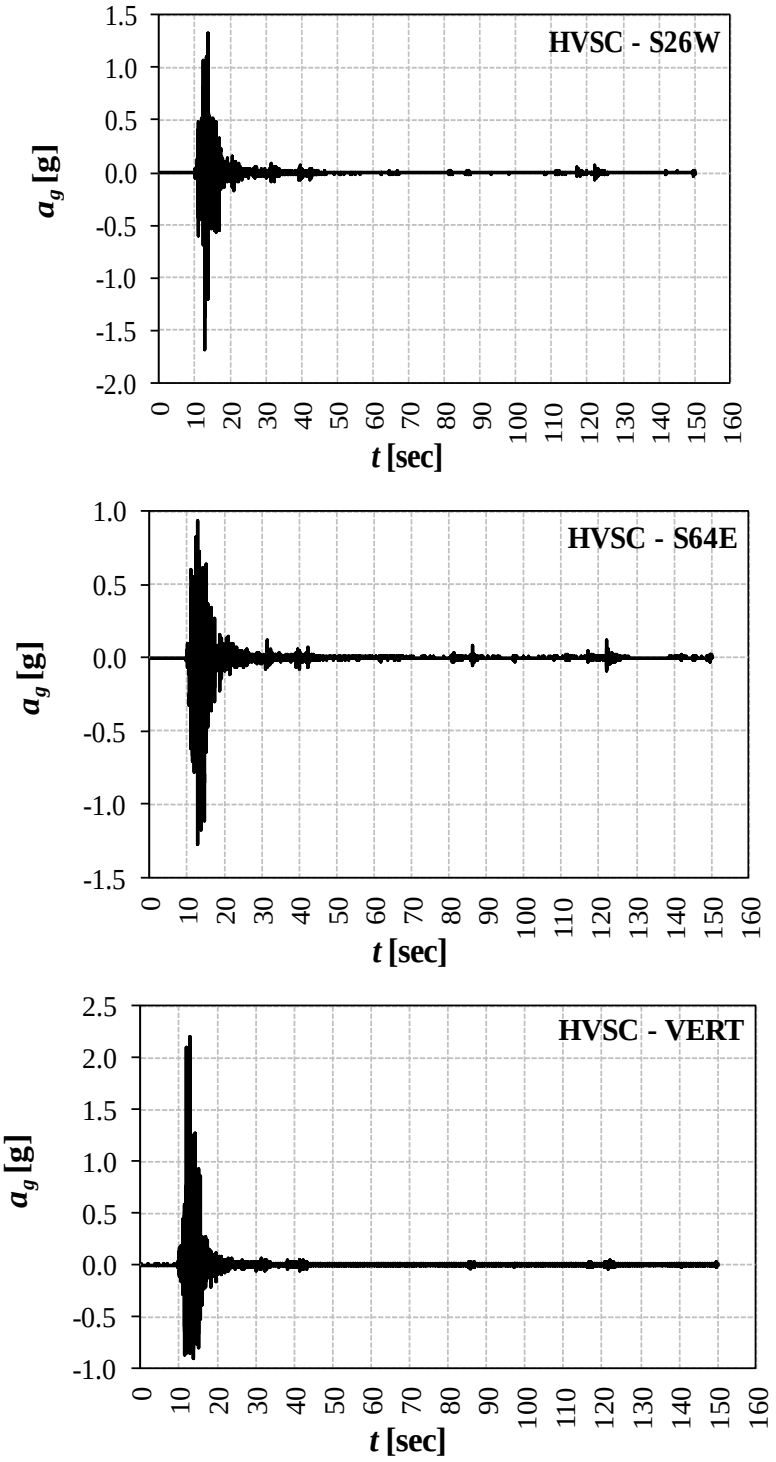

C.4 Catholic Cathedral College, CCCC (Darfield Records)

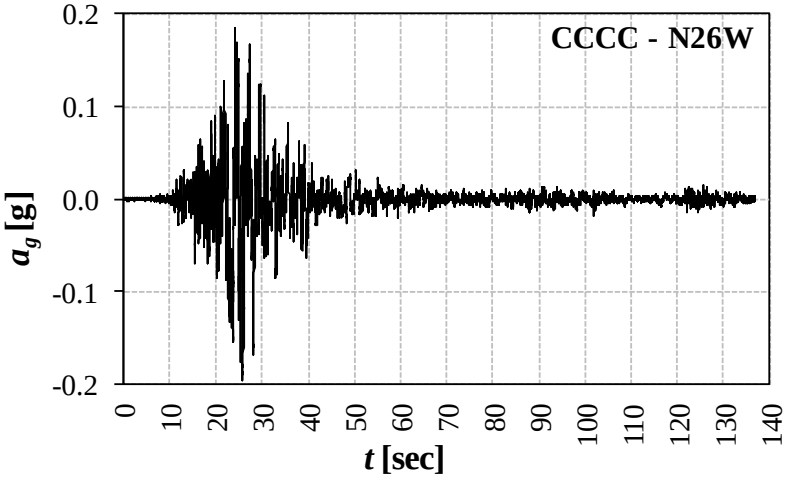

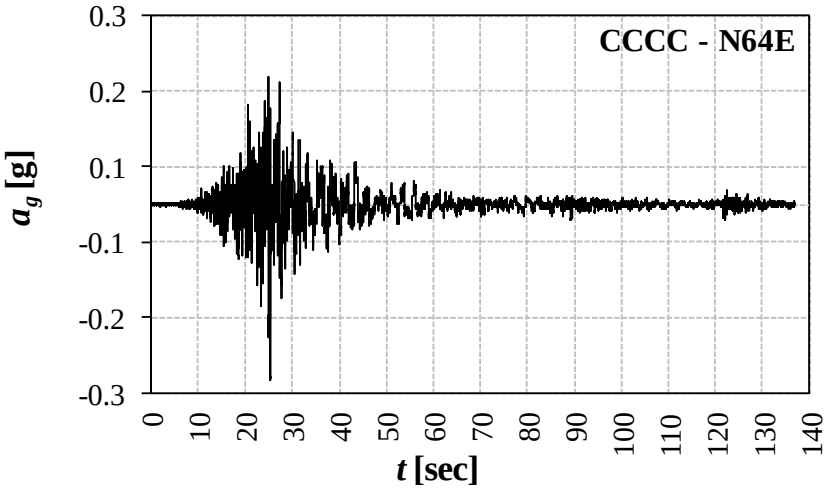

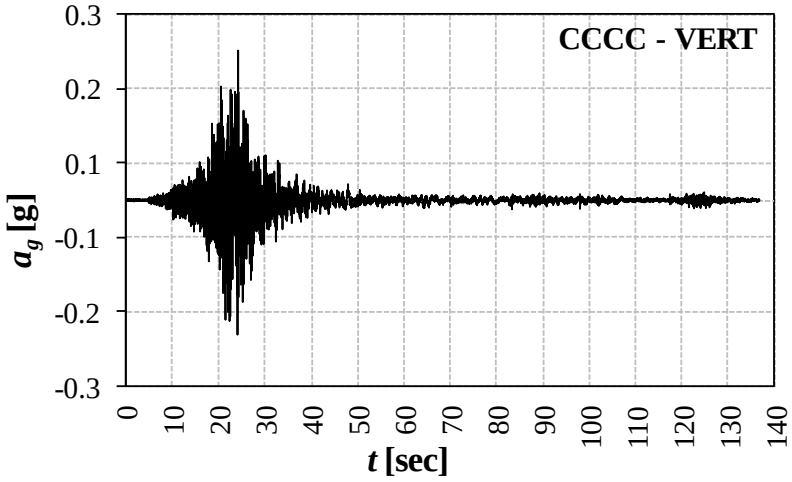

C.5 Heathcote Valley Primary School, HVSC (Darfield Records)

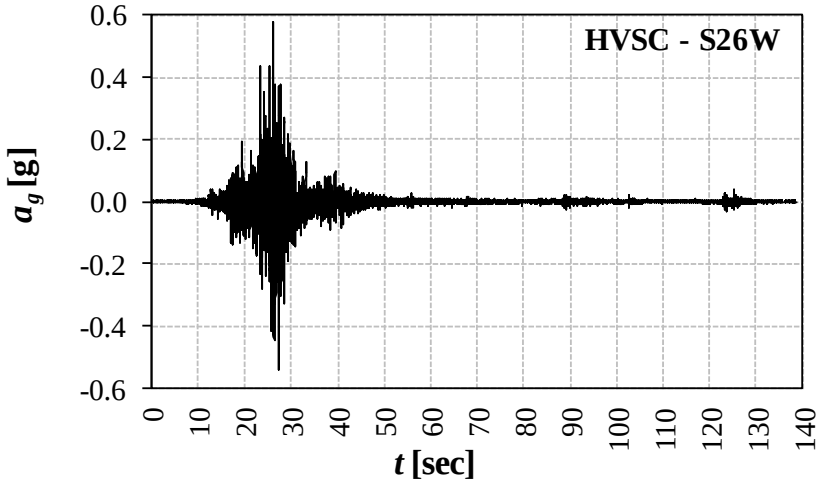

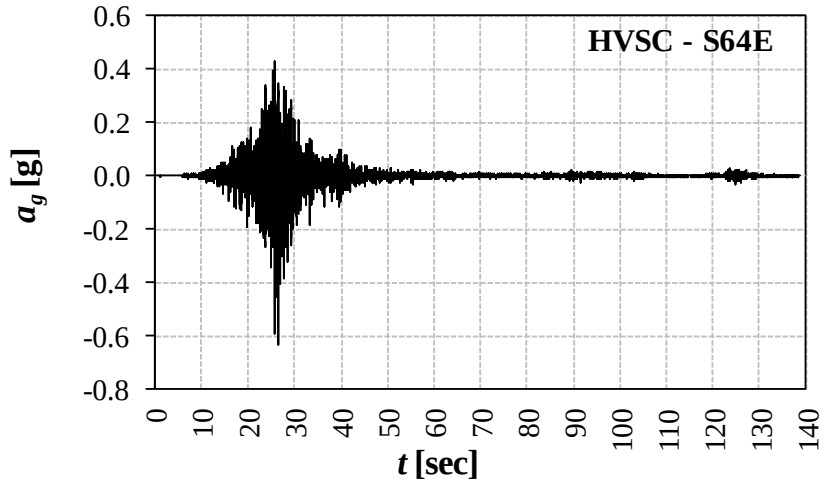

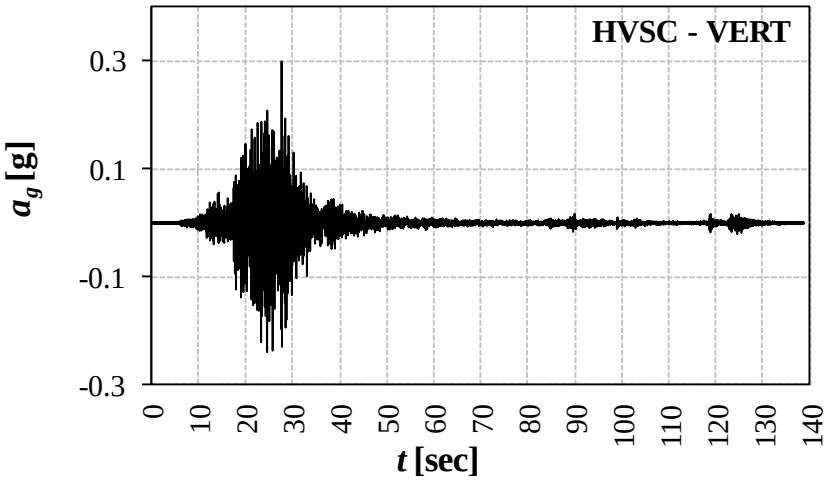

C.6 Scaled Californian Earthquakes

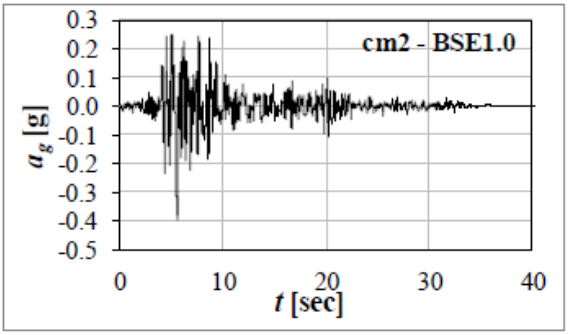

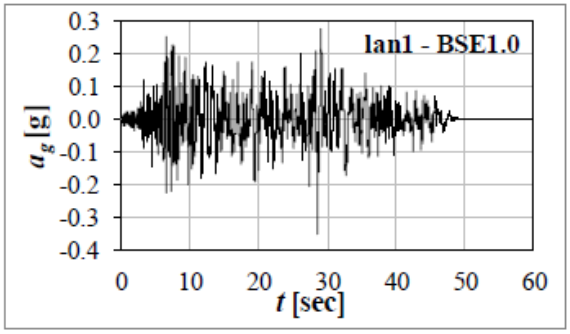

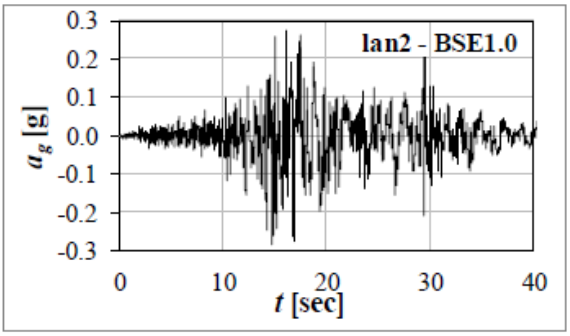

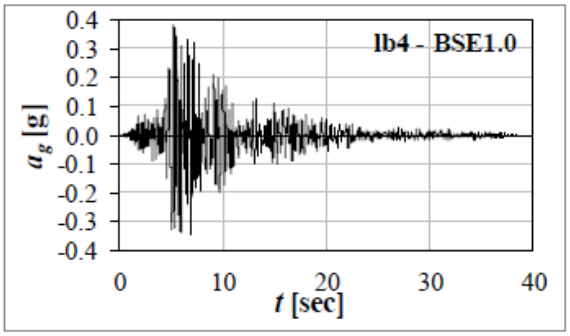

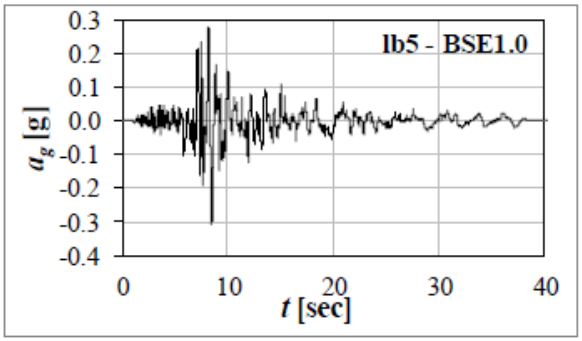

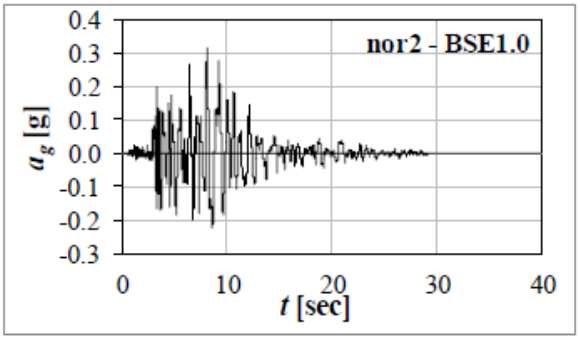

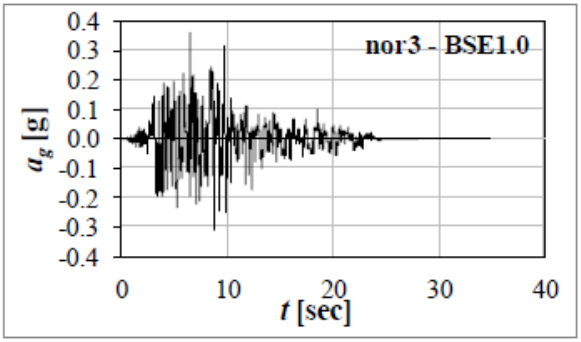

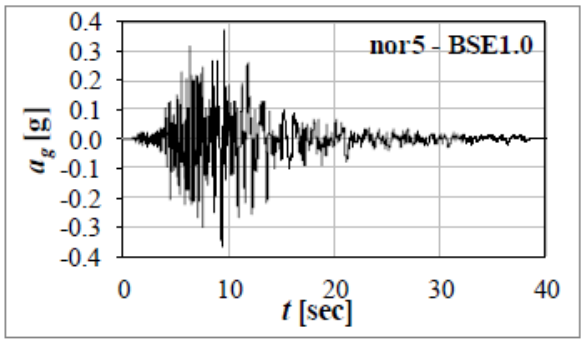

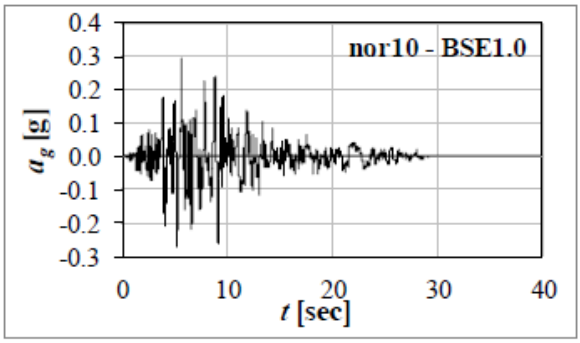
nor10 - BSE1.0
a_g [g]
0.4
0.3
0.2
0.1
0.0
-0.1
-0.2
-0.3
0
10
20
30
40
t [sec]

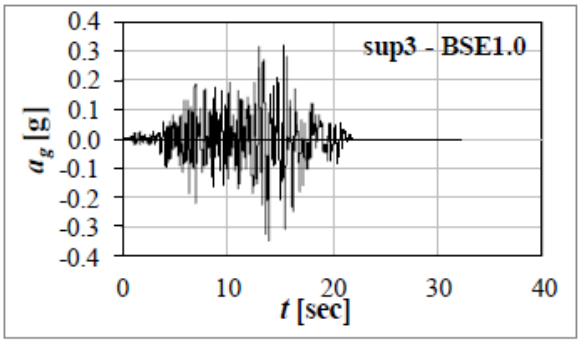
sup3 - BSE1.0
a_g [g]
0.4
0.3
0.2
0.1
0.0
-0.1
-0.2
-0.3
-0.4
0
10
20
30
40
t [sec]